# Stochastic Analysis of Sorption and Biodegradation in Three-Dimensionally Heterogeneous Aquifers

by

**Fernando Miralles-Wilhelm**

Ingeniero Mecanico, Universidad Simon Bolívar. 1987
M.S. in Engineering, University of California, Irvine. 1989

Submitted to the Department of Civil and Environmental Engineering
in partial fulfillment of the requirements for the degree of

Doctor of Philosophy

at the

MASSACHUSETTS INSTITUTE OF TECHNOLOGY

February 1993



Author .....
Department of Civil and Environmental Engineering
February, 1993

Certified by. .....
Lynn W. Gelhar
Professor of Civil and Environmental Engineering
Thesis Supervisor

Accepted by .... .....
Ole S. Madsen
Chairman, Departmental Committee on Graduate Studies

# Stochastic Analysis of Sorption and Biodegradation in Three-Dimensionally Heterogeneous Aquifers

by

**Fernando Miralles-Wilhelm**

Ingeniero Mecanico, Universidad Simon Bolívar, 1987

M.S. in Engineering, University of California, Irvine, 1989

Submitted to the Department of Civil and Environmental Engineering
on February, 1993, in partial fulfillment of the
requirements for the degree of
Doctor of Philosophy

## Abstract

This thesis presents an analysis of the processes of sorption and biodegradation in groundwater, incorporating the effects of natural aquifer heterogeneity. This analytical treatment is developed using a stochastic methodology that conceives the spatially variable hydrogeologic, chemical and microbiological processes as being random. Within this theoretical framework, features of the field scale characteristics of plume sorption and biodegradation are explored. The influence of intragrain diffusion and sorption on plume retardation, dispersion and skewness is quantified in relation to the influence of natural aquifer variability. The time dependence of the effective retardation factor, longitudinal macrodispersivity and skewness coefficient for reactive solutes at a field scale is explained in terms of aquifer heterogeneities. Nonlinear sorption isotherm effects are found to play an important role on the amount of sorbed solute in a real field case. For the problem of biodegradation in groundwater, the hypothesis of an established microbial population at steady state was found to be adequate for the purposes of modeling the decay of a contaminant solute under oxygen-limiting conditions in the aquifer. Longitudinal macrodispersivities for the contaminant and dissolved oxygen differed significantly, and were found to be considerably affected by biodegradation. A calculation example of biodegradation enhancement by supplying oxygen to the aquifer is presented using a lumped parameter formulation. The limitations and impact of the presented approach are discussed regarding data collection guidance and modeling of multicomponent transport and transformation in three dimensionally heterogeneous porous media.

Thesis Supervisor: Lynn W. Gelhar
Title: Professor of Civil and Environmental Engineering

# Acknowledgments

The research work presented in this thesis was supported in part by the American Petroleum Institute project API GW-14-360-8 entitled *Modeling Oxygen-Transport Limited Biodegradation in Groundwater*, the National Science Foundation grant number CES-8814615 entitled *Stochastic Analysis of Large-Scale Transport Processes in Aquifers*, and the NIEHS grant number ESO-4675, entitled *Field-Scale Contaminant Attenuation Processes in the Aberjona Watershed* administered through the *M.I.T. Superfund Basic Research Program.*

Many people are to be thanked when you finally complete a doctoral thesis. I sincerely hope I can include most of them here, and I really apologize in advance if I leave anyone out.

To my thesis advisor, Professor Lynn W. Gelhar, for providing insightful and stimulating guidance of this research, for his support and motivation, but most important, for his friendship. That perhaps the most important mission of a scientist is not to come up with the right answers, but to come up with the right questions is a whole deal of learning just by itself. Without his invaluable advice and knowledge, this work would have not been possible.

To Professors Phil M. Gschwend, Lee R. Krumholz and Dennis B. McLaughlin for suggesting alternative angles and approaches for my research, both as teachers in the classroom, and as members of my thesis committee. Thanks go to them for their time, patience and useful input during all stages of this work.

Deep expressions of gratitude go to Professor Ignacio Rodríguez-Iturbe. His continuous demonstrations of sincere friendship and support through the years we have known each other have provided me with an example to follow, the one I will never be able to thank him enough for.

I would also like to thank Pat Dixon, our Assistant Director here in the Lab, for allowing me not to worry about the details (especially those financial!!!) of my graduate education here at MIT. She has to be commended for being a friend, and for being successful in making this lab a warm and human place to work in. Thanks

to Kathy Perez-Dewey for her always happy attitude that certainly makes things run much smoother in our research group.

Ramon Herrera, my countryman and friend, was an immense source of computer related wisdom, something I have very little of. He was always there when I needed help with sometimes trivial problems. Thank you very much...

To my fellow students at Parsons Lab, for sharing moments and experiences, thank you all. I would specially like to mention Vivek Kapoor, for being my 'research buddy', providing a lot of useful insight into this investigation, and for sharing a lot of thoughts on life, mathematics and stochastic subsurface hydrology. To Hari Rajaram, Nadia Dimou and Shawn Morrissey for always being there to help or just to talk during my days here at MIT. To the 'tennis bunch': John Durant, Glenn Moglen, Kevin Johnson and Paolo Sammarco, for helping me keep my priorities straight, never to forget that tennis always comes first!!!

My parents, my brother and my two sisters were always there with the moral support you can't get enough of. When I look back on the years, they have been there for me, with the encouragement and advice to keep me going. Family is invaluable, believe me...

And finally my soulmate, the love of my life, my best friend: my beautiful wife Monica. It is she who deserves the credit for making this trip the most enjoyable. Day by day, getting her support, her love and stimulation, was the fuel that got me to this stage, and that I know will take me to others as exciting and important. I just hope I can someday be able to give her as much as she has given me to this day.

# Contents

# List of Figures

# List of Tables

# Chapter 1

# Introduction

Groundwater contamination by pollutants released from spills, waste disposal facilities, pesticide and fertilizer applications in soils, landfills and many other sources has been realized to be a serious environmental, economic and political problem throughout the world in the past few years. Although some of these pollution sources have begun to be controlled and regulated, many others remain even to be discovered, and the effects of a significant number those groundwater contamination events that have taken place in the past are reaching people every day through their water supplies. Multimillion dollar funds have been established in an attempt to clean up subsurface contaminated sites, and a large part of these efforts has been directed towards research and development of environmental remediation alternatives.

A large number of contaminating agents are chemically and/or biologically reactive in the subsurface. Understanding the way by which these chemicals migrate and react in aquifer environments is becoming one of the most active areas of research within the environmental field. Of particular importance, because of their abundance, are those compounds that have a tendency to sorb onto solid surfaces and those that can be biodegradable under certain environmental conditions. One of the limitations to this understanding is the natural intrinsic heterogeneity of aquifer environments, which is in itself a major source of uncertainty. This uncertainty is reflected in the way contaminants are transported, sorbed and biodegraded in the soil and groundwater. Trying to conjugate this aquifer natural heterogeneity with chemical and microbio-

logical processes is by no means an easy task. It requires research across disciplinary boundaries, trying to capture and identify the most important features of the problem, and produce some knowledge that may actually be used in field applications. This work represents an effort in pursuing this line of investigation.

At the same time, questions regarding the specific mechanisms by which sorption and biodegradation take place in aquifer environments at a field scale are posed in recent literature. Experimental findings and interpretations are overwhelmed by the immense number of factors involved, many of them difficult to isolate and understand. This is where mathematical modeling can become a useful tool in identifying factors and parameters that control these occuring processes, contributing to understand them and gaining an insight into further experimental efforts.

This thesis presents a mathematical development of the processes of sorption and biodegradation in the subsurface which takes into consideration the heterogeneous nature and three-dimensionality of aquifers. Heterogeneity of hydrologic, chemical and microbiological parameters is treated using a stochastic analysis that essentially conceives these processes as being random. Through this analytical methodology, some of the features of the sorption and biodegradation mechanisms in the subsurface are explored and brought to attention. Focus is placed on deriving field scale transport and transformation coefficients that incorporate the variability in the different parameters involved, and that can be used as a modeling tool for predictive purposes.

For organizational purposes, this thesis has been structured into two main parts: Part I is a study of the process of field scale sorption in groundwater. Part II deals with modeling biodegradation of contaminants in aquifers under limiting environmental conditions, with a particular emphasis on dissolved oxygen limitations in aerobic environments. Each of these parts consists of two Chapters that explore different aspects within each basic problem.

Chapter 2 presents an analysis of the influence of intragrain diffusion and sorption processes on the field scale characteristics of reactive plumes. This is a problem that has raised considerable attention lately in the interpretation of nonequilibrium sorp-

tion experimental results [Wood *et al*, 1990, Ball and Roberts, 1991]. A stochastic treatment of this problem is developed under the assumption that there is a diffusional transport process and subsequent sorption that occurs between regions of mobile and stagnant water associated with the groundwater flow and grain interiors, respectively. This transport mechanism can result in additional retardation, dispersion and asymmetry of the reactive solute under consideration [Valocchi, 1988, 1989]. An analysis of these processes that incorporates the variability of the aquifer material at scales much greater than the typical grain or aggregate sizes is developed to understand the influence of intragrain diffusion and sorption on the field scale applicable coefficients of retardation, dispersion and skewness, and the interaction of the different physical and chemical factors at a field scale.

Further analysis of the transient characteristics of the sorption process is the subject of Chapter 3. The slow diffusional transport mechanism into zones of water immobilization represents a limiting factor for the sorption reaction, which then results in a time dependence of the retardation factor of the contaminant solute under consideration. Heterogeneities in the aquifer material can also be responsible for transient effects of plume behavior [Gelhar, 1987, Dagan, 1988, Naff, 1990]. An analysis aimed at sorting out these effects and underlining their relative importance is developed, and results are presented for two actual contaminated sites. The limitations in comparing experimental results with the analysis presented is discussed in light of data availability and quality.

Chapter 4 is a development of a two-component analytical model with an application to oxygen-limited biodegradation with the assumption of an established microbial population at steady state. Biodegradation of contaminants by natural populations of microorganisms represents one of the primary mechanisms by which petroleum derivatives and other anthropogenic pollutants can be eliminated from the environment. Many of the organic pollutants entering the groundwater from leaking tanks, spills and other sources are potentially biodegradable, yet the persistence of many of these compounds in the subsurface indicates that some factor or group of factors must be limiting the biodegradation process. One of these key factors appears to be the

lack of an electron acceptor such as oxygen. Laboratory and field observations cited in Brookman *et al.* [1985], Patrick and Barker [1986] and Wilson *et al.* [1987] suggest the natural biodegradation process is sensitive to the availability of dissolved oxygen in the aquifer, and, in addition, that the process is spatially variable. Therefore, a realistic approach to this problem must consider the natural heterogeneity of aquifer hydraulic properties as it influences the transport of oxygen, as well as chemical and biological heterogeneity which is likely to affect biodegradation rates. In addition, one must consider the possibility that there is a significant interaction between physical transport and chemical/biological transformations. The analysis of the field scale effects of dissolved oxygen limitations and parameter interactions are the essence of this Chapter. Results are presented and discussed for two field contaminated sites.

In order to study the effects of microbial growth on the field scale process of biodegradation, the assumption of the steady state condition for the microbial population is relaxed in Chapter 5. The effects of transient microbial growth dynamics are incorporated into the predictions for the field scale transport and transformation coefficients, and an evaluation of the assumption of steady state in the microorganisms is presented. Application examples for field scale predictions of plume characteristics under a biodegradation process are posed through the development of a lumped parameter model that provides estimates of contaminant mass loss, retardation and dispersion rates considering parameter heterogeneity. These results are discussed in the context of groundwater bioremediation enhancement through supply of dissolved oxygen.

Finally, Chapter 6 presents a brief summary and discusses the impact of this research, along with the limitations of the stochastic approach, and recommendations for modeling practitioners, experimentalists, and those not familiarized with stochastic theories.

# Part I

# Effects of heterogeneities on field-scale sorption in groundwater

# Chapter 2

# Analysis of intragrain diffusion and sorption in heterogeneous aquifers

## 2.1 Introduction

The following sections present a theoretical development for mass exchange between the aqueous and solid phases of a reactive solute in the subsurface. A better understanding of the mechanisms of sorption onto the solid phase in the aquifer, solute movement and dispersion and plume asymmetry through an analysis of the different processes involved are the focus of this chapter.

Sorption of reactive solutes in groundwater is usually described using equilibrium sorption isotherms. Perhaps the simplest description is the assumption of a linear reversible equilibrium relationship between the amount of chemical in the sorbed and solution phases [Schwarzenbach and Westall, 1981]. However, its been reported that the symmetric forms of breakthrough responses predicted using models making the simplification of a constant retardation factor do not agree with experimental observations [Curtis *et al.*, 1986]. In this article, the authors suggest nonlinear equilibrium sorption and intragrain diffusion rate limitations as possible explanations for reactive plume behavior. Because it is very complicated to determine which of these processes

controls in actual field situations, or if they are indeed the cause of experimental observations, modeling can serve as a guide in assessing the scenarios where these mechanisms are controlling factors in the sorption process in aquifers.

In groundwater transport, the effects of diffusion of the contaminant to and from regions of water immobilization have been extensively studied by chemical engineers, environmental engineers and earth scientists [Skopp and Warrick, 1974, van Genuchten and Wierenga, 1976, Goltz and Roberts, 1986]. Where natural soils are involved, the nature of the immobile regions is poorly understood, and the diffusive mechanism difficult to isolate and understand. It is clear, however, that the influence of diffusive rate limitations will be most important where the rate of contaminant uptake and release by immobile regions is low relative to the rates of advective transport and hydrodynamic dispersion. Where transfer rates are sufficiently slow, large effects on transport can be anticipated, such as a time-dependence of the retardation factor due to intragrain sorption [Brusseau, 1991].

Natural heterogeneity has also been proposed as an explanation for observed field scale behavior of passive and reactive plumes [Gelhar *et al.*, 1979, Dagan, 1982, 1984, 1988, Gelhar and Axness, 1983, Sposito and Barry, 1987]. Investigations of plume retardation and dispersion due to heterogeneity have been developed using stochastic theories that incorporate the natural variability of aquifer material into the governing transport equation for a reactive solute [Garabedian *et al.*, 1988, Valocchi, 1989, Cvetkovic and Shapiro, 1990]. This mathematical approach is used here to explore the influence of the different physical processes involved on reactive solute transport.

Important effects of sorption on plume dispersion rates have also been observed in the field. Garabedian *et al.* [1988] use the linear equilibrium approximation for low concentrations and find that the distribution and movement of a reactive solute is strongly affected by adsorption to aquifer sediments. Their results show an order of magnitude increase in the longitudinal macrodispersion with respect to a conservative solute. A theoretical explanation for this increase in dispersion is provided on the basis of stochastic analysis. This increase in dispersion is explained by Wood *et al.* [1990] as a result of mass transfer limitations associated with diffusion into and out

of the porous interiors of rock grains. However, the numerical simulations of Burr [1992] find no apparent effect of intragrain diffusion on the field scale characteristics of a reactive plume in a three dimensional heterogenous porous medium. The potential significance of mass transfer limitations in field-scale transport is thus clear, but questions still remain about the most important domains of diffusion in natural environments. Distinction between large scale rate limitations, as caused, for example, by sorbing layers of low permeability, and smaller scale (grain) rate limitations can be very difficult, and laboratory and field studies can improve attempts to build more realistic models for sorptive mass exchange.

Finding an explanation for the asymmetry of reactive tracer plumes is also an objective of this study. Experimental breakthrough curves exhibit non-sigmoid profiles, commonly termed tailing. Tailing may be attributable to the slow diffusion of contaminant into zones of immobile water. In the recent literature on the subject, most authors have recognized the importance of diffusive mass transfer limitations in the fate of organic contaminants in groundwater [Roberts *et al.*, 1986, Curtis *et al.*, 1986, Goltz and Roberts, 1986, Wu and Gschwend, 1986, Brusseau and Rao, 1989]. Gelhar *et al.* [1979] use a stochastic approach to incorporate the effects of natural aquifer heterogeneities on nonreactive solute transport. Their theoretical results show that these heterogeneities cause plume skewness, even in the absence of soil matrix diffusion.

In this chapter, the question of the mechanisms explaining plume retardation, increased dispersion rates and plume asymmetry is addressed. Focus is placed on the effects of intragrain diffusion and sorption on the long time behavior of solute plumes. A set of governing equations obtained by first principles is proposed and a stochastic treatment of these transport equations is developed in order to address the issues explained above. The goal is to be able to define the importance of the competing physical and chemical processes that take place in subsurface sorption.

## 2.2 Methodology of solution

In this section, a set of differential equations governing solute transport are developed considering diffusion to and from regions of water immobilization, along with an instantaneous sorption process characterized by a linear isotherm. An analysis for nonlinear isotherm effects is also developed and discussed later in Chapter 3.

### 2.2.1 Governing equations

The equations governing transport in a two-component system consisting of a contaminant solute in mobile and immobile zones, with a diffusional exchange between these zones characterized by a first order mass transfer coefficient is presented here. The solute sorption process is modeled as a pore diffusion process into intragrain regions, as interpreted by Wood *et al.* [1990], or as diffusion into strongly sorbing zones of immobile water as in Goltz and Roberts [1986]. This yields the the transport equation for an organic substrate undergoing advection, dispersion, equilibrium linear sorption to the soil particle surfaces and diffusion to immobile water zones:

$$\frac{\partial S}{\partial t} + \frac{\partial (v_i S)}{\partial x_i} = \frac{\partial}{\partial x_i} D_{ij} \frac{\partial S}{\partial x_j} - \frac{\rho K_d}{n} \frac{\partial S}{\partial t} - \frac{\omega}{n}(S - \Omega) \tag{2.1}$$

Here, $S$ is the aqueous concentration of the solute (mass of solute per unit volume of mobile water), $\Omega$ is the average concentration in the immobile water zone (mass of solute per unit volume of immobile water), $v_i$ is the local groundwater velocity field, $D_{ij}$ is the local dispersion coefficient, $\rho$ is the bulk density of the aquifer medium and $n$ is the mobile porosity (volume of mobile water per unit bulk volume). Sorption is assumed to occur according to an equilibrium partitioning characterized by a distribution coefficient $K_d$. A first-order rate formulation using a transfer coefficient $\omega$ is adopted to account for the diffusion of contaminant between the mobile and immobile water zones [Skopp and Warrick, 1974, Van Genuchten, 1975, Goltz and Roberts, 1986].

For the solute in the immobile water zone, with a volumetric water content given through the immobile or intragrain porosity $\tilde{n}$ (volume of immobile water per unit

bulk volume) and a bulk density $\tilde{\rho}$, equilibrium sorption characterized by a distribution coefficient $\tilde{K}_d$ occurs onto the solid phase in the zone. Since the water in this zone is motionless, and no concentration gradients are assumed ($\Omega$ is an averaged concentration) within the zone, the governing equation for $\Omega$ is written as:

$$\frac{\partial \Omega}{\partial t} = -\frac{\rho \tilde{K}_d}{\tilde{n}} \frac{\partial \Omega}{\partial t} + \frac{\omega}{\tilde{n}}(S - \Omega) \tag{2.2}$$

Retardation factors for the mobile and immobile zones can be defined as [Freeze and Cherry, 1979]:

$$R = 1 + \frac{\rho K_d}{n} \tag{2.3}$$

$$\Gamma = 1 + \frac{\tilde{\rho} \tilde{K}_d}{\tilde{n}} \tag{2.4}$$

In order to develop a more general analysis of this two-component system the transfer coefficients for the components are allowed to be different. In this way, the starting governing equations can be rewritten as:

$$R\frac{\partial S}{\partial t} + \frac{\partial (v_i S)}{\partial x_i} = \frac{\partial}{\partial x_i} D_{ij} \frac{\partial S}{\partial x_j} - \omega_1 (S - \Omega) \tag{2.5}$$

$$\Gamma \frac{\partial \Omega}{\partial t} = \omega_2 (S - \Omega) \tag{2.6}$$

This set of differential equations can be used, for example, to model first order sorption kinetics [Valocchi, 1988, 1989], where the different rates of transfer represent the forward and backward reaction rates. It can also be used to model intragrain diffusion limitations by taking the transfer parameters to be related by the ratio of the immobile to mobile porosity, according to equations (2.1) and (2.2).

### 2.2.2 Random fields

#### Hydrologic Processes

The aquifer hydraulic conductivity is typically found to be log-normally distributed. In order to describe its variation as a function of the position vector $\mathbf{x}$, it is convenient to introduce the variable:

$$f(\mathbf{x}) = lnK(\mathbf{x}) \tag{2.7}$$

where $K(\mathbf{x})$ is the hydraulic conductivity; $f(\mathbf{x})$ can be expressed as the sum of its ensemble mean $\bar{f}$ and a perturbation $f'$.

$$f = \bar{f} + f' \tag{2.8}$$

The variations represented by $f'$ are described by a three-dimensional statistically anisotropic exponential autocovariance function with spectrum [Gelhar and Axness, 1983]:

$$S_{ff} = \frac{\sigma_f^2 \lambda_1 \lambda_2 \lambda_3}{\pi^2[1 + (k_1\lambda_1)^2 + (k_2\lambda_2)^2 + (k_3\lambda_3)^2]^2} \tag{2.9}$$

In this expression, $\lambda_i$ is the correlation length in the *ith* direction, $\sigma_f^2$ is the variance of the $lnK$ field, and $\mathbf{k} = (k_1, k_2, k_3)$ is the wave number vector.

#### Geochemical processes

In this analysis, the processes of sorption and intragrain diffusion are modeled as random fields. For the sorption processes in the immobile and mobile zones, we have,

$$R = \bar{R} + R' \tag{2.10}$$

$$\Gamma = \bar{\Gamma} + \Gamma' \tag{2.11}$$

Following the approach described in Garabedian *et al.* [1988], these random fields

are assumed to be linearly correlated with the $lnK$ process. Ball and Roberts [1991] present results for intragrain diffusion rates $\omega$ which show an imperfect correlation with grain size (grain size has been found to be correlated with $lnK$). This analysis accounts for either perfect, imperfect, or no correlation of the random fields for retardation and intragrain diffusion with $f = lnK$.

$$\Gamma = a_1 + b_1 f + g_1 \tag{2.12}$$

$$R = a_2 + b_2 f + g_2 \tag{2.13}$$

with means given by:

$$\bar{\Gamma} = a_1 + b_1 \bar{f} \tag{2.14}$$

$$\bar{R} = a_2 + b_2 \bar{f} \tag{2.15}$$

and perturbations,

$$\Gamma' = b_1 f' + g_1 \tag{2.16}$$

$$R' = b_2 f' + g_2 \tag{2.17}$$

Similarly, the solute transfer between the mobile and immobile zones is modeled as a stochastic process given by the following equations:

$$\omega_1 = \bar{\omega}_1 + \omega_1' \tag{2.18}$$

$$\omega_2 = \bar{\omega}_2 + \omega_2' \tag{2.19}$$

and,

$$\omega_1 = a_3 + b_3 f + g_3 \tag{2.20}$$

$$\omega_2 = a_4 + b_4 f + g_4 \tag{2.21}$$

The means and perturbations of these processes then follow:

$$\bar{\omega}_1 = a_3 + b_3 \bar{f} \tag{2.22}$$

$$\bar{\omega}_2 = a_4 + b_4 \bar{f} \tag{2.23}$$

$$\omega_1' = b_3 f' + g_3 \tag{2.24}$$

$$\omega_2' = b_4 f' + g_4 \tag{2.25}$$

The coefficients $a_i, b_i$ are the intercepts and slopes of the assumed linear correlations with $f = lnK$. Uncorrelated residuals $g_i$ are introduced in the analysis to include the possibility that these correlations are not perfect.

### Transport variables

The flow field and component concentrations are also represented as stochastic processes, with ensemble means and perturbations,

$$v_i = \bar{v}_i + v_i' \tag{2.26}$$

$$S = \bar{S} + S' \tag{2.27}$$

$$\Omega = \bar{\Omega} + \Omega' \tag{2.28}$$

### 2.2.3 Development of spectral equations

Assuming uni-directional mean flow, the coordinate system $x_i$ is aligned such that the $x_1$ direction is along the direction of the mean flow:

$$\bar{v_1} = v; \quad \bar{v_2} = \bar{v_3} = 0$$

The local dispersion tensor is approximated in the form [Naff, 1978]:

$$D_{ij} = \begin{bmatrix} \alpha_L v & 0 & 0 \\ 0 & \alpha_T v & 0 \\ 0 & 0 & \alpha_T v \end{bmatrix} \tag{2.29}$$

where $\alpha_L$ is the local longitudinal dispersivity and $\alpha_T$ is the local transverse dispersivity.

The mean and perturbation decompositions for all random fields are substituted in the transport equations for the solute in the mobile and immobile zones, equations (2.1) and (2.2). Expanding these terms and taking expectations of the equations yields:

$$\bar{R}\frac{\partial \bar{S}}{\partial t} + v\frac{\partial \bar{S}}{\partial x_1} + \frac{\partial}{\partial t}\overline{R'S'} + \frac{\partial}{\partial x_i}\overline{v_i'S'} = D_{ij}\frac{\partial^2 \bar{S}}{\partial x_i \partial x_j} - \bar{\omega_1}(\bar{S} - \bar{\Omega}) - \overline{\omega_1'(S' - \Omega')} \tag{2.30}$$

$$\bar{\Gamma}\frac{\partial \bar{\Omega}}{\partial t} + \frac{\partial}{\partial t}\overline{\Gamma'\Omega'} = \bar{\omega_2}(\bar{S} - \bar{\Omega}) + \overline{\omega_2'(S' - \Omega')} \tag{2.31}$$

By subtracting these mean transport equations from equations (2.1) and (2.2), transport equations for the perturbation quantities $S'$ and $\Omega'$ are obtained. These are:

$$R'\frac{\partial \bar{S}}{\partial t} + \bar{R}\frac{\partial S'}{\partial t} + \bar{v_i}\frac{\partial S'}{\partial x_i} + v_i'\frac{\partial \bar{S}}{\partial x_i} = \frac{\partial}{\partial x_i}D_{ij}\frac{\partial S'}{\partial x_j} - \omega_1'(\bar{S} - \bar{\Omega}') - \bar{\omega_1}(S' - \Omega') \tag{2.32}$$

$$\Gamma' \frac{\partial \bar{\Omega}}{\partial t} + \bar{\Gamma} \frac{\partial \Omega'}{\partial t} = \omega_2'(\bar{S} - \bar{\Omega}') - \bar{\omega}_2(S' - \Omega') \tag{2.33}$$

Following the approach in Garabedian *et al.* [1988], a system of moving coordinates following the solute plume is introduced to describe the changes in the means and perturbations of the concentrations in time.

$$\zeta_1 = x_1 - \frac{vt}{R_S}; \zeta_2 = x_2; \zeta_3 = x_3 \tag{2.34}$$

This system of coordinates introduces the effective retardation factor $R_S$ and it defines it as the effective value of plume retardation with respect to the displacement of a conservative solute plume. Also note that,

$$\left(\frac{\partial}{\partial x_1}\right) = \left(\frac{\partial}{\partial \zeta_1}\right) \tag{2.35}$$

$$\left(\frac{\partial}{\partial t}\right)_x = \left(\frac{\partial}{\partial t}\right)_\zeta - \frac{v}{R_S}\frac{\partial}{\partial \zeta_1} \tag{2.36}$$

In this coordinate system, the transport equations for the mean and perturbation of the solute concentration in the mobile zone are changed to:

$$\bar{R}\left(\frac{\partial \bar{S}}{\partial t} - \frac{v}{R_S}\frac{\partial \bar{S}}{\partial \zeta_1}\right) + \frac{\partial}{\partial t}\overline{R'S'} - \frac{v_i}{R_S}\frac{\partial}{\partial \zeta_i}\overline{R'S'} + v\frac{\partial \bar{S}}{\partial \zeta_1} + \frac{\partial}{\partial \zeta_i}\overline{v_i'S'} =$$

$$\frac{\partial}{\partial \zeta_i} D_{ij}\frac{\partial \bar{S}}{\partial \zeta_j} - \bar{\omega}_1(\bar{S} - \bar{\Omega}) - \overline{\omega_1'(S' - \Omega')} \tag{2.37}$$

$$R'(\frac{\partial \bar{S}}{\partial t} - \frac{v}{R_S}\frac{\partial \bar{S}}{\partial \zeta_1}) + \bar{R}(\frac{\partial S'}{\partial t} - \frac{v}{R_S}\frac{\partial S'}{\partial \zeta_1}) + v\frac{\partial S'}{\partial \zeta_1} + v_i'\frac{\partial \bar{S}}{\partial \zeta_i} =$$

$$\frac{\partial}{\partial \zeta_i} D_{ij}\frac{\partial S'}{\partial \zeta_j} - -\omega_1'(\bar{S} - \bar{\Omega}') - \bar{\omega}_1(S' - \Omega') \tag{2.38}$$

Field-scale effects have been predicted by calculating the second-order cross correlation terms that appear in the mean transport equations for conservative and reactive

solutes [Gelhar and Axness, 1983; Garabedian *et al.*, 1988; Welty and Gelhar, 1991]. In this case, these second order terms involve correlations between perturbations in flow and concentrations, sorption and concentrations, and mass transfer coefficient and concentrations. The calculation of these terms involves solving the partial differential equations of the perturbation equations. The use of a spectral approach has been used successfully to analyze these equations. This approach is based on the introduction of Fourier-Stieltjes Representations (FSR) and the Spectral Representation Theorem (SRT) [Lumley and Panofsky, 1964]. In this stochastic treatment, the random perturbations are assumed to be statistically homogeneous, with the premise that the field scale under consideration is much larger than the correlation scales of these random processes. The perturbed quantities are then represented as:

$$S' = \int_{-\infty}^{\infty} e^{i\mathbf{k}.\mathbf{x}} dZ_S(\mathbf{k}) \tag{2.39}$$

$$v_i' = \int_{-\infty}^{\infty} e^{i\mathbf{k}.\mathbf{x}} dZ_{v_i}(\mathbf{k}) \tag{2.40}$$

$$R' = \int_{-\infty}^{\infty} e^{i\mathbf{k}.\mathbf{x}} dZ_R(\mathbf{k}) \tag{2.41}$$

$$\Gamma' = \int_{-\infty}^{\infty} e^{i\mathbf{k}.\mathbf{x}} dZ_\Gamma(\mathbf{k}) \tag{2.42}$$

$$\omega_1' = \int_{-\infty}^{\infty} e^{i\mathbf{k}.\mathbf{x}} dZ_{\omega_1}(\mathbf{k}) \tag{2.43}$$

$$\omega_2' = \int_{-\infty}^{\infty} e^{i\mathbf{k}.\mathbf{x}} dZ_{\omega_2}(\mathbf{k}) \tag{2.44}$$

Here, the integration is carried over three-dimensional wave number space. In spectral space, the perturbation equations are transformed to:

$$\bar{R}\frac{\partial dZ_S}{\partial t} + dZ_R\left(\frac{\partial \bar{S}}{\partial t} - \frac{v}{R_S}\frac{\partial \bar{S}}{\partial \zeta_1}\right) + ivk_1 dZ_S - \frac{\partial \bar{S}}{\partial \zeta_i} dZ_{v_i} = -D_{ij}k_i k_j dZ_S$$

$$- dZ_{\omega_1}(\bar{S} - \bar{\Omega}) - \bar{\omega_1}(dZ_S - dZ_\Omega) \tag{2.45}$$

$$\bar{\Omega}\frac{\partial dZ_\Omega}{\partial t} + dZ_\Gamma\frac{\partial \bar{\Omega}}{\partial t} = dZ_{\omega_2}(\bar{S} - \bar{\Omega}) + \bar{\omega_2}(dZ_S - dZ_\Omega) \tag{2.46}$$

where

$$G_i = -\frac{\partial \bar{S}}{\partial \zeta_i} \tag{2.47}$$

This is a set of ordinary differential equations with time as the independent variable. The primary interest is to obtain the behavior of the concentration profiles at large times, where changes of the concentrations are negligible (time derivative terms can be dropped). Since there is mass transfer between the mobile and immobile zones,*i.e.*, the concentrations are undergoing a growth-decay process, it is necessary to follow the concentrations in time, as it was done in space by transforming into the moving coordinate system. This is achieved by scaling the concentration spectral amplitudes $dZ_S$ and $dZ_\Omega$ according to the following (see Appendix B):

$$dZ_S = dZ_{\bar{S}}exp\left(-\int_0^t \frac{\omega_{1e}}{\bar{R}}dt'\right) + \int_0^t \frac{\omega_{1e}}{\bar{R}}dZ_\Omega exp\left(-\int_{t'}^t \frac{\omega_{1e}}{\bar{R}}dt''\right)dt' \tag{2.48}$$

$$dZ_\Omega = dZ_{\bar{\Omega}}exp\left(-\int_0^t \frac{\omega_{2e}}{\bar{\Gamma}}dt'\right) + \int_0^t \frac{\omega_{2e}}{\bar{\Gamma}}dZ_S exp\left(-\int_{t'}^t \frac{\omega_{2e}}{\bar{\Gamma}}dt''\right)dt' \tag{2.49}$$

This scaling gives the spectral amplitudes $dZ_S$ and $dZ_\Omega$ in terms of spectral amplitudes for the non-decaying quantities $dZ_{\bar{S}}$ and $dZ_{\bar{\Omega}}$, and it defines the effective mass transfer rates $\omega_{1e}$ and $\omega_{2e}$. These effective parameters become important factors in determining the effect of intragrain diffusion on the field scale characteristics of solute plumes. The perturbation equations are now transformed to:

$$\bar{R}\frac{\partial dZ_{\bar{S}}}{\partial t}exp\left(-\int_0^t \frac{\omega_{1e}}{\bar{R}}dt'\right) + (ivk_1 + D_{ij}k_ik_j + \bar{\omega_1} - \omega_{1e})dZ_S + dZ_R(\frac{\partial \bar{S}}{\partial t} + \frac{v}{R_S}G_1)$$

$$-G_j dZ_{v_j} = (\bar{\omega}_1 - \omega_{1e})dZ_\Omega - (\bar{S} - \bar{\Omega})dZ_{\omega_1} \tag{2.50}$$

$$\bar{\Gamma}\frac{\partial dZ_\Omega}{\partial t} exp\left(-\int_0^t \frac{\omega_{1e}}{\bar{\Gamma}} dt'\right) - (\bar{\omega}_2 - \omega_{2e})dZ_S + dZ_\Gamma \frac{\partial \bar{\Omega}}{\partial t} + (\bar{\omega}_2 - \omega_{2e})dZ_\Omega - (\bar{S} - \bar{\Omega})dZ_{\omega_2} = 0 \tag{2.51}$$

Now, time derivative changes of the non-decaying quantities can be neglected so that a system of algebraic equations result:

$$(ivk_1 + D_{ij}k_ik_j + \bar{\omega}_1 - \omega_{1e})dZ_S - (\bar{\omega}_1 - \omega_{1e})dZ_\Omega + dZ_R(\frac{\partial \bar{S}}{\partial t} + \frac{v}{R_S}G_1) - G_j dZ_{v_j} + (\bar{S} - \bar{\Omega})dZ_{\omega_1} = 0 \tag{2.52}$$

$$-(\bar{\omega}_2 - \omega_{2e})dZ_S + (\bar{\omega}_2 - \omega_{2e})dZ_\Omega + dZ_\Gamma \frac{\partial \bar{\Omega}}{\partial t} - (\bar{S} - \bar{\Omega})dZ_{\omega_2} = 0 \tag{2.53}$$

The solution to this system of equations gives expressions for the spectral amplitudes $dZ_S$ and $dZ_\Omega$:

$$dZ_S = \frac{1}{\beta}\left[G_i dZ_{v_i} - (\frac{\partial S}{\partial t} + \frac{v}{R_S}G_1)dZ_R - (\bar{S} - \bar{\Omega})dZ_{\omega_1} + \frac{\bar{\omega}_1 - \omega_{1e}}{\bar{\omega}_2 - \omega_{2e}}\left((\bar{S} - \bar{\Omega})dZ_{\omega_2} - \frac{\partial \Omega}{\partial t}dZ_\Gamma\right)\right] \tag{2.54}$$

$$dZ_\Omega = \frac{1}{\beta}\left[G_i dZ_{v_i} - (\frac{\partial S}{\partial t} + \frac{v}{R_S}G_1)dZ_R - (\bar{S} - \bar{\Omega})dZ_{\omega_1}\right] + \frac{(\bar{S} - \bar{\Omega})dZ_{\omega_2} - \frac{\partial \Omega}{\partial t}dZ_\Gamma}{\bar{\omega}_2 - \omega_{2e}}(1 + \frac{\bar{\omega}_1 - \omega_{1e}}{\beta}) \tag{2.55}$$

where,

$$\beta = ivk_1 + D_{ij}k_ik_j \tag{2.56}$$

The field scale transfer coefficients can be obtained by finding expressions for the second-order correlations that appear in the mean equations (2.37) and (2.31). These correlations can be found using the Spectral Representation Theorem [Lumley and

Panofsky, 1964] as:

$$\overline{R'S'} = \int_{-\infty}^{\infty} S_{RS} d\mathbf{k} = \int_{-\infty}^{\infty} E[dZ_R dZ_S^*] \tag{2.57}$$

$$\overline{v_i' S'} = \int_{-\infty}^{\infty} S_{v_i S} d\mathbf{k} = \int_{-\infty}^{\infty} E[dZ_{v_i} dZ_S^*] \tag{2.58}$$

$$\overline{\omega_1'(S' - \Omega')} = \int_{-\infty}^{\infty} S_{\omega_1(S-\Omega)} d\mathbf{k} = \int_{-\infty}^{\infty} E[dZ_{\omega_1}(dZ_S^* - dZ_\Omega^*] \tag{2.59}$$

$$\overline{\omega_2'(S' - \Omega')} = \int_{-\infty}^{\infty} S_{\omega_2(S-\Omega)} d\mathbf{k} = \int_{-\infty}^{\infty} E[dZ_{\omega_2}(dZ_S^* - dZ_\Omega^*] \tag{2.60}$$

In these expressions the (*) stands for the complex conjugate of the given quantity. The spectral amplitudes $dZ_\Gamma$, $dZ_R$, $dZ_{\omega_1}$ and $dZ_{\omega_2}$ are directly related to the spectral amplitude of the log-conductivity perturbations $dZ_f$. Following Gelhar and Axness [1983], a relation between the flow velocity and hydraulic conductivity perturbations is found as:

$$dZ_{v_i} = \frac{K_l}{n}(J_i - J_j \frac{k_i k_j}{k^2}) dZ_f \tag{2.61}$$

Here, $K_l = exp(E[lnK])$, $n$ is the soil porosity and $J_i$ is the mean hydraulic gradient in the $x_i$ direction.

The spectral amplitudes for retardation and transfer coefficients are related to the amplitude $dZ_f$ by:

$$dZ_\Gamma = b_1 dZ_f + dZ_{g_1} \tag{2.62}$$

$$dZ_R = b_2 dZ_f + dZ_{g_2} \tag{2.63}$$

$$dZ_{\omega_1} = b_3 dZ_f + dZ_{g_3} \tag{2.64}$$

$$dZ_{\omega_2} = b_4 dZ_f + dZ_{g_4} \tag{2.65}$$

The autocovariance function of the residuals $g_i$, $i = 1,2,3,4$ appears in some of these second-order correlation terms. These residuals are assumed to have a negative exponential autocovariance function with spectra:

$$S_{g_i g_i} = \frac{\sigma_{g_i}^2 \lambda_{gi1} \lambda_{gi2} \lambda_{gi3}}{\pi^2 (1 + \lambda_{gi1}^2 k_1^2 + \lambda_{gi2}^2 k_2^2 + \lambda_{gi3}^2 k_3^2)^2} \tag{2.66}$$

with no summation on the index $i$. No correlations are assumed between residuals of different quantities, *i.e.*, $S_{g_i g_j} = 0$ if $i \neq j$.

In the calculation of these second-order correlations, a number of integral expressions must be evaluated. These integral expressions are identical to those that appear in Gelhar and Axness [1983] for the analysis of conservative solute macrodispersion. The assumption of negligible local dispersion (compared to the magnitude of macrodispersion) is introduced to obtain the second-order correlations related to decay, equations (2.59) and (2.60). These are found to be given by:

$$\begin{aligned} \overline{\omega_1'(S' - \Omega')} &= \left[ \frac{b_1 b_3}{\bar{\omega}_2 - \omega_{2e}} \frac{\partial \bar{\Omega}}{\partial t} - \frac{b_3 b_4 (\bar{S} - \bar{\Omega})}{\bar{\omega}_2 - \omega_{2e}} \right] \int_{-\infty}^{\infty} S_{ff}(\mathbf{k}) d\mathbf{k} \\ &= \left[ \frac{b_1 b_3}{\bar{\omega}_2 - \omega_{2e}} \frac{\partial \bar{\Omega}}{\partial t} - \frac{b_3 b_4 (\bar{S} - \bar{\Omega})}{\bar{\omega}_2 - \omega_{2e}} \right] \sigma_f^2 \end{aligned} \tag{2.67}$$

$$\begin{aligned} \overline{\omega_2'(S' - \Omega')} &= \left[ \frac{b_1 b_4}{\bar{\omega}_2 - \omega_{2e}} \frac{\partial \bar{\Omega}}{\partial t} - \frac{b_4^2 (\bar{S} - \bar{\Omega})}{\bar{\omega}_2 - \omega_{2e}} \right] \int_{-\infty}^{\infty} S_{ff}(\mathbf{k}) d\mathbf{k} - \frac{(\bar{S} - \bar{\Omega})}{\bar{\omega}_2 - \omega_{2e}} \int_{-\infty}^{\infty} S_{g_4 g_4}(\mathbf{k}) d\mathbf{k} \\ &= \left[ \frac{b_1 b_4}{\bar{\omega}_2 - \omega_{2e}} \frac{\partial \bar{\Omega}}{\partial t} - \frac{(b_4^2 \sigma_f^2 + \sigma_{g_4}^2)(\bar{S} - \bar{\Omega})}{\bar{\omega}_2 - \omega_{2e}} \right] \end{aligned} \tag{2.68}$$

### 2.2.4 Effective transfer coefficients and immobile zone retardation factor

The effective transfer coefficients defined in the scaling procedure can now be found by grouping together the terms in the mean equations that correspond to mass transfer processes (zeroth-order derivative terms). In this case, in the mean equation for the solute in the mobile zone (2.37), one can write:

$$-\omega_{1e}(\bar{S}-\bar{\Omega}) = -\bar{\omega}_1(\bar{S}-\bar{\Omega}) + \frac{b_3 b_4(\bar{S}-\bar{\Omega})}{\bar{\omega}_2-\omega_{2e}}\sigma_f^2$$

from which the effective transfer coefficient in the mobile zone is found to be:

$$\omega_{1e} = \bar{\omega}_1 - \frac{b_3 b_4}{\bar{\omega}_2-\omega_{2e}}\sigma_f^2 \tag{2.69}$$

Similarly, in the mean equation for the soulte in the immobile zone,

$$\omega_{2e}(\bar{S}-\bar{\Omega}) = \bar{\omega}_2(\bar{S}-\bar{\Omega}) - \frac{(b_4^2\sigma_f^2+\sigma_{g_4}^2)(\bar{S}-\bar{\Omega})}{\bar{\omega}_2-\omega_{2e}}$$

so,

$$\bar{\omega}_2-\omega_{2e} = \frac{b_4^2\sigma_f^2+\sigma_{g_4}^2}{\bar{\omega}_2-\omega_{2e}} = \frac{\sigma_{\omega_2}^2}{\bar{\omega}_2-\omega_{2e}}$$

which results in the expression:

$$\omega_{2e} = \bar{\omega}_2 - \sigma_{\omega_2} \tag{2.70}$$

Note that a double solution exists for the parameter $\omega_{2e}$. However, choosing one of the solutions over the other is irrelevant to the analysis that follows, since the variance $\sigma_{\omega_2}^2$ is the value that appears in subsequent calculations. Also note that in order to obtain the parameter $\omega_{1e}$, $\omega_{2e}$ must be found previously.

The other effective parameter of interest in the mean equation for the solute in the immobile zones is the effective retardation factor, $\Gamma_e$, defined as the coefficient of

the storage term in the transport equation for $\bar{\Omega}$. Grouping out the storage terms at large times in equation (2.31), one can show that:

$$\Gamma_e = \bar{\Gamma} - \frac{b_1 b_4}{\bar{\omega}_2 - \omega_{2e}} \sigma_f^2 \tag{2.71}$$

Now that these parameters have been found, the mean equations can be rewritten as:

$$\bar{R}\left(\frac{\partial \bar{S}}{\partial t} - \frac{v}{R_S}\frac{\partial \bar{S}}{\partial \zeta_1}\right) + \frac{\partial}{\partial t}\overline{R'S'} - \frac{v_i}{R_S}\frac{\partial}{\partial \zeta_i}\overline{R'S'} + v\frac{\partial \bar{S}}{\partial \zeta_1} + \frac{\partial}{\partial \zeta_i}\overline{v_i'S'} = \frac{\partial}{\partial \zeta_i} D_{ij}\frac{\partial \bar{S}}{\partial \zeta_j} - \omega_{1e}(\bar{S} - \bar{\Omega}) \tag{2.72}$$

$$\Gamma_e \frac{\partial \bar{\Omega}}{\partial t} = \omega_{2e}(\bar{S} - \bar{\Omega}) \tag{2.73}$$

### 2.2.5 Field-scale coefficients

In a field situation, where measurements of sorption, dispersion and skewness are made, it is very unlikely that it is possible to distinguish between mobile and immobile zone processes. What is actually measured is the amount of total sorption, dispersion and tailing that occurs, but how these processes are distributed between zones of relatively high and low mobility of water can be very difficult to determine. In laboratory batch experiments, a significant amount of sorption has been attributed to intragrain processes [Wood *et al.*, 1990, Ball and Roberts, 1991], but laboratory measurements are hindered given the difficulty to isolate these processes when considered separately.

Given the simplicity of the mean transport equation (2.73) for the solute in the immobile zones, is possible to solve it as a function of the mean concentration in the mobile zone and substitute back into equation (2.72) to obtain a single component model, that is able to represent the total amount of sorption, dispersion and tailing that occurs at a field scale. Rewriting (2.73) as:

$$\frac{\partial \bar{\Omega}}{\partial t} + \frac{\omega_{2e}}{\Gamma_e}\bar{\Omega} = \frac{\omega_{2e}}{\Gamma_e}S \tag{2.74}$$

The solution to this linear, first-order differential equation is:

$$\bar{\Omega} = \int_0^t \frac{\omega_{2e}}{\Gamma_e} S(\mathbf{x},t)\ exp\left[-\frac{\omega_{2e}}{\Gamma_e}(t-\tau)\right] d\tau \tag{2.75}$$

Substituting the latter expression into equation (2.72) would result in an integro-differential equation that cannot be solved without some approximate methodology. Since the $\bar{\Omega}$ profile results from exponentially weighted values of the mean concentration $\bar{S}$, a suitable approximation to evaluate this expression is to expand the $\bar{S}$ profile in time around $\tau = t$.

$$\bar{S}(\mathbf{x},t) = \bar{S}(\mathbf{x},\tau) + \left(\frac{\partial \bar{S}}{\partial \tau}\right)_{\tau=t}(\tau - t) + \left(\frac{\partial^2 \bar{S}}{\partial^{\cdots 2}}\right)_{\tau=t}(\tau - t)^2 \tag{2.76}$$

An approximate solution can be written for $\bar{\Omega}$:

$$\bar{\Omega} = \frac{\omega_{2e}}{\Gamma_e}\left[\bar{S}(\mathbf{x},t)\int_0^t exp\left[-\frac{\omega_{2e}}{\Gamma_e}(t-\tau)\right] d\tau + \left(\frac{\partial \bar{S}}{\partial t}\right)\int_0^t (\tau - t) exp\left[-\frac{\omega_{2e}}{\Gamma_e}(t-\tau)\right] d\tau + \ldots\right] \tag{2.77}$$

Once the integrations over $\tau$ are evaluated, this solution is expressed as:

$$\bar{\Omega} = \bar{S}\left[1 - exp(-\frac{\omega_{2e}t}{\Gamma_e})\right] + \left(\frac{\partial \bar{S}}{\partial t}\right)\frac{\Gamma_e}{\omega_{2e}}\left[(1 + \frac{\omega_{2e}t}{\Gamma_e})exp(-\frac{\omega_{2e}t}{\Gamma_e}) - 1\right]$$

$$+ \left(\frac{\partial^2 \bar{S}}{\partial t^2}\right)\left(\frac{\Gamma_e}{\omega_{2e}}\right)^2\left[2 + \left(\frac{\omega_{2e}^2 t^2}{\Gamma_e^2} - 2\frac{\omega_{2e}t}{\Gamma_e} - 2\right) exp(-\frac{\omega_{2e}t}{\Gamma_e})\right] + \ldots \tag{2.78}$$

This analysis for the solute concentration in the immobile zone yields a time scale given by $\frac{\Gamma_e}{\omega_{2e}}$. This is the time scale at which transient effects must be considered in intragrain diffusion/sorption processes, and it is equivalent to the time scale observed in laboratory batch experiments such as those reported in Wu and Gschwend [1986] and Ball and Roberts [1991], as indicated by the analysis shown in Appendix C. However, for now, focus is placed on the large-time behavior $t >> \frac{\Gamma_e}{\omega_{2e}}$ of the field

scale coefficients. At large times,

$$\bar{S} - \bar{\Omega} = \frac{\Gamma_e}{\omega_{2e}} \frac{\partial \bar{S}}{\partial t} - 2\frac{\Gamma_e^2}{\omega_{2e}^2} \frac{\partial^2 \bar{S}}{\partial t^2} + \ldots \tag{2.79}$$

In order to replace this expression in the mean transport equation for the solute in the immobile zone, time derivatives must be expressed in the moving coordinate system, so that:

$$\bar{S} - \bar{\Omega} = \frac{\Gamma_e}{\omega_{2e}} \left( \frac{\partial \bar{S}}{\partial t} + \frac{vG_1}{R_S} \right) - 2\frac{\Gamma_e^2}{\omega_{2e}^2} \left( \frac{\partial^2 \bar{S}}{\partial t^2} + 2\frac{v}{R_S} \frac{\partial G_1}{\partial t} + \frac{v^2}{R_S^2} \frac{\partial^2 \bar{S}}{\partial \zeta_1^2} \right) \tag{2.80}$$

The latter expression must be used in conjunction with equation (2.72) to determine the field scale coeffcients of retardation dispersion and plume asymmetry. Before this can be done, the two remaining correlations in equation (2.72) must be evaluated. Recalling equations (2.57) and (2.58) we have,

$$\overline{R'S'} = G_1 I_1 - \left( \frac{\partial \bar{S}}{\partial t} + \frac{v}{R_S} G_1 \right) I_3 - (\bar{S} - \bar{\Omega}) I_5 \tag{2.81}$$

$$\overline{v_i' S'} = G_1 I_2 - \left( \frac{\partial \bar{S}}{\partial t} + \frac{v}{R_S} G_1 \right) I_1 - (\bar{S} - \bar{\Omega}) I_4 \tag{2.82}$$

where the integral expressions $I_j$ are identical to those evaluated in Garabedian *et al.* [1988] for reactive solute macrodispersion. These are given by the following expressions:

$$I_1 = \int_{-\infty}^{\infty} \frac{E[dZ_{v_i} dZ_R^*]}{\beta} = \int_{-\infty}^{\infty} \frac{S_{Rv_i}}{\beta} d\mathbf{k} = b_2 \frac{\sigma_f^2 \lambda_1}{\gamma} \tag{2.83}$$

$$I_2 = \int_{-\infty}^{\infty} \frac{E[dZ_{v_i} dZ_{v_j}^*]}{\beta} = \int_{-\infty}^{\infty} \frac{S_{v_i v_j}}{\beta} d\mathbf{k} = \frac{\sigma_f^2 \lambda_1}{\gamma^2} v \tag{2.84}$$

$$I_3 = \int_{-\infty}^{\infty} \frac{E[dZ_R dZ_R^*]}{\beta} = \int_{-\infty}^{\infty} \frac{S_{RR}}{\beta} d\mathbf{k} = (b_2^2 \sigma_f^2 + \sigma_{g_2}^2) \frac{\lambda_1}{v} \tag{2.85}$$

$$I_4 = \int_{-\infty}^{\infty} \frac{E[dZ_{v_i} dZ^*_{\omega_1}]}{\beta} - \frac{\bar{\omega}_1 - \omega_{1e}}{\bar{\omega}_2 - \omega_{2e}} \int_{-\infty}^{\infty} \frac{E[dZ_{v_i} dZ^*_{\omega_2}]}{\beta} = \int_{-\infty}^{\infty} \frac{S_{\omega_1 v_i}}{\beta} d\mathbf{k} - \frac{\bar{\omega}_1 - \omega_{1e}}{\bar{\omega}_2 - \omega_{2e}} \int_{-\infty}^{\infty} \frac{S_{\omega_2 v_i}}{\beta} d\mathbf{k}$$

$$= \left( b_3 - \frac{\bar{\omega}_1 - \omega_{1e}}{\bar{\omega}_2 - \omega_{2e}} b_4 \right) \frac{\sigma_f^2 \lambda_1}{\gamma} \tag{2.86}$$

$$I_5 = \int_{-\infty}^{\infty} \frac{E[dZ_R dZ^*_{\omega_1}]}{\beta} - \frac{\bar{\omega}_1 - \omega_{1e}}{\bar{\omega}_2 - \omega_{2e}} \int_{-\infty}^{\infty} \frac{E[dZ_R dZ^*_{\omega_2}]}{\beta} = \int_{-\infty}^{\infty} \frac{S_{\omega_1 R}}{\beta} d\mathbf{k} - \frac{\bar{\omega}_1 - \omega_{1e}}{\bar{\omega}_2 - \omega_{2e}} \int_{-\infty}^{\infty} \frac{S_{\omega_2 R}}{\beta} d\mathbf{k}$$

$$\left( b_2 b_3 - \frac{\bar{\omega}_1 - \omega_{1e}}{\bar{\omega}_2 - \omega_{2e}} b_2 b_4 \right) \frac{\sigma_f^2 \lambda_1}{v} \tag{2.87}$$

In these expressions, the flow factor $\gamma$ is defined as:

$$\gamma = \frac{nv}{K_l J_1} \tag{2.88}$$

**Effective retardation factor**

The advection terms (first-order spatial derivatives of concentration) that appear in the mean transport equation can be grouped together to obtain the effective retardation factor $R_S$. In the moving coordinate system, no advective terms must result, so the coefficient of these terms must be equal to zero. This means,

$$v \left( 1 - \frac{\bar{R}}{R_S} \right) - \omega_{1e} \frac{\Gamma_e}{\omega_{2e}} \frac{v}{R_S} = 0$$

from which the effective retardation factor is found to be:

$$R_J = \bar{R} + \frac{\omega_{1e}}{\omega_{2e}} \Gamma_e \tag{2.89}$$

This means that the bulk, effective retardation factor, is the result of adding two sorption processes: the external (mobile) retardation and the internal (immobile) retardation, accounting for the difference between the effective transfer factors in the two zones due to aquifer heterogeneities. Notice that in the case of no spatial

heterogeneity of the parameters, the value of the effective retardation factor is the one given by the total retardation calculated in batch experiments (see Appendix C).

### Longitudinal macrodispersivity

Second-order spatial derivative terms can be also grouped together to define the longitudinal component of the macrodispersivity tensor. In this case, the macrodispersivity is defined by the expression:

$$vA_{11}\frac{\partial \bar{S}}{\partial \zeta_1^2} = 2\frac{\omega_{1e}v^2}{\omega_{2e}^2}\frac{\Gamma_e^2}{R_S^2}\frac{\partial \bar{S}}{\partial \zeta_1^2} + \frac{v}{R_S}\frac{\partial}{\partial \zeta_1}\left[I_1G_1 - \frac{v}{R_S}I_3G_1 - \frac{v}{\omega_{2e}}\frac{\Gamma_e}{R_S}I_5G_1\right]$$

$$-\frac{\partial}{\partial \zeta_1}\left[I_2G_1 - \frac{v}{R_S}I_1G_1 - \frac{v}{\omega_{2e}}\frac{\Gamma_e}{R_S}I_4G_1\right]$$

Simplifying this expression yields the longitudinal macrodispersivity as:

$$A_{11} = \frac{\sigma_f^2\lambda_1}{\gamma^2} - 2\frac{b_2}{R_S}\frac{\sigma_f^2\lambda_1}{\gamma} + \frac{\sigma_R^2}{R_S^2}\lambda_1 + 2\frac{\omega_{1e}v}{\omega_{2e}^2}\frac{\Gamma_e^2}{R_S^2} + \frac{v}{\omega_{2e}}\frac{\Gamma_e}{R_S}(I_4 - \frac{v}{R_S}I_5) \qquad (2.90)$$

The longitudinal macrodispersivity that results from this analysis consists of that obtained in Garabedian *et al.* [1988], plus additional terms that are brought by the intragrain diffusion/sorption process.

### Plume asymmetry

In addition to terms that contain first and second-order derivatives in space, there are also terms that contain mixed second-order space-time derivatives, second-order time derivatives and third-order spatial derivatives. The mixed derivative terms come from the temporal derivatives of the $\overline{R'S'}$ correlation term and the expression of the concentration difference $(\bar{S} - \bar{\Omega})$, equation (2.80). Second-order time derivatives are obtained when differentiating the $\overline{R'S'}$ correlation with respect to time. Third-order derivatives are found in the spatial derivative of the concentration difference $(\bar{S} - \bar{\Omega})$, equation (2.80). The mean equation can then be written as:

$$R_S \frac{\partial \bar{S}}{\partial t} = v A_{11} \frac{\partial^2 \bar{S}}{\partial \zeta_1^2} - \Phi_1 \frac{\partial^2 \bar{S}}{\partial t \partial \zeta_1} - \Phi_2 \frac{\partial \bar{S}}{\partial t^2} - \Psi_1 \frac{\partial^3 \bar{S}}{\partial \zeta_1^3} + \ldots \tag{2.91}$$

where,

$$\Phi_1 = -2I_1 + 2\frac{v}{R_S} I_3 + 2\frac{v\Gamma_e}{\omega_{2e} R_S} I_5 - \frac{\Gamma_e}{\omega_{2e}} I_4 \tag{2.92}$$

$$\Phi_2 = -I_3 - \frac{\Gamma_e}{\omega_{2e}} I_5 \tag{2.93}$$

$$\Psi_1 = 2(\frac{v\Gamma_e}{\omega_{2e} R_S})^2 I_4 - 2(\frac{\Gamma_e}{\omega_{2e}})^2 (\frac{v}{R_S})^3 I_5 \tag{2.94}$$

As in Gelhar *et al.* [1979], it can be shown that terms containing mixed second-order derivative terms in the moving coordinate system can be reduced to third-order spatial derivative terms. Following the analysis presented in Appendix D, the mean equation can be expressed in the original coordinate system.

$$R_S \frac{\partial \bar{S}}{\partial t} + v \frac{\partial \bar{S}}{\partial x_1} = v A_{11} \frac{\partial^2 \bar{S}}{\partial x_1^2} - \left( \Phi \frac{v}{R_S} A_{11} + \Psi \right) \frac{\partial^3 \bar{S}}{\partial x_1^3} + \ldots \tag{2.95}$$

with,

$$\Phi = -2I_1 + 2\frac{v}{R_S} I_3 \tag{2.96}$$

and,

$$\Psi = \left[ 2(\frac{v\Gamma_e}{\omega_{2e} R_S})^2 - \frac{v\Gamma_e}{\omega_{2e} R_S} A_{11} \right] I_4 + 2 \left[ \frac{\Gamma e}{\omega_{2e}} (\frac{v}{R_S})^2 A_{11} - (\frac{\Gamma_e}{\omega_{2e}})^2 (\frac{v}{R_S})^3 \right] I_5 \tag{2.97}$$

Notice that the transverse dispersion terms have been omitted here, since no analysis for the transverse macrodispersivities $A_{22}$ and $A_{33}$ has been developed as part of this work. The issue of modeling the transverse dispersion mechanism still remains to be resolved by stochastic transport theories, as explained in Section 4.3.

As it is explained in Chapter 3, the coefficient of the third-order derivatives in

space is associated with plume asymmetry *i.e., tailing.* Notice that the influences of the sorption processes in the mobile and immobile zones have been distinguished to explain their separate influence on the overall plume asymmetry.

## 2.3 Discussion of Results

An evaluation of the field scale coefficient expressions obtained from the stochastic analysis developed in this Chapter was performed using input parameters for two actual field situations. The two cases selected, because of data availability were sorption of Lithium to aquifer solids of the Otis Air Base in Cape Cod, Massachusetts [Garabedian *et al.*, 1988], and sorption of tetrachloroethene (PCE) onto Borden aquifer solids in Ontario, Canada [Roberts *et al.*, 1986, Ball and Roberts, 1991]. Table 2.1 presents the set of hydrologic and geochemical parameters used to describe these two field sites.

Table 2.1: Hydrologic and geochemical parameters in Cape Cod and Borden sites

| Parameter | Cape Cod | Borden |
|---|---|---|
| Sorbate | Lithium | PCE |
| $\sigma_f^2$ | 0.24[1] | 0.29 [2] |
| $\lambda_1$ | $2.6m$[1] | $2.8m$ [2] |
| $n$ | 0.39[1] | 0.33 [2] |
| $\tilde{n}$ | 0.1[3] | 0.013 [4] |
| $K_e$[5] | $110m/day$ [1] | $6m/day$ [1] |
| $v$ | $0.4m/day$[1] | $0.1m/day$ [2] |
| $\bar{\omega}$[6] | $108day^{-1}$ | $330day^{-1}$ |
| $R_S$ | $10^7$ | 6 [8] |

[1] [Garabedian *et al.*, 1991]
[2] [Sudicky, 1986]
[3] [Wood *et al.*, 1990]
[4] [Ball *et al.*, 1990]
[5] Effective hydraulic conductivity [Gelhar and Axness, 1983]
[6] Inverse of characteristic time scale from Tables 3.1 and C.1
[7] [Garabedian *et al.*, 1988]
[8] [Roberts *et al.*, 1986]

In these cases, the parameter $R_S$ describes the amount of total sorption that occurs in the aquifer, as obtained from field experiments. The value of this parameter does not distinguish between sorption onto solids in the mobile and immobile zones, and, as it was obtained from the analysis, it is the sum of these two processes, accounting for the intraparticle diffusion process. Table 2.2 shows the different values of the correlation slopes and residual variances for the transport parameters presented in Table 2.1.

Table 2.2: Correlation parameters for the mass transfer rate $\omega$ at the Cape Cod and Borden sites

CAPE COD

- mean mass transfer rate $\bar{\omega} = 108 day^{-1}$
- $b_3 = -200 day^{-1}$, $\sigma_{g3} = 98 day^{-1}$ ($CV_\omega = 50\%$, partial correlation)
- $b_4 = -780 day^{-1}$, $\sigma_{g4} = 382 day^{-1}$ ($CV_\omega = 50\%$, partial correlation)
- $b_3 = -256 day^{-1}$, $\sigma_{g3} = 0$ ($CV_\omega = 50\%$, perfect correlation)
- $b_4 = -999 day^{-1}$, $\sigma_{g4} = 0$ ($CV_\omega = 50\%$, perfect correlation)
- $b_3 = 0$, $\sigma_{g3} = 138 day^{-1}$ ($CV_\omega = 50\%$, uncorrelated)
- $b_4 = 0$, $\sigma_{g4} = 540 day^{-1}$ ($CV_\omega = 50\%$, uncorrelated)
- $b_3 = -273 day^{-1}$, $\sigma_{g3} = 147 day^{-1}$ ($CV_\omega = 75\%$)
- $b_4 = -1065 day^{-1}$, $\sigma_{g4} = 573 day^{-1}$ ($CV_\omega = 75\%$)
- $b_3 = -91 day^{-1}$, $\sigma_{g3} = 49 day^{-1}$ ($CV_\omega = 25\%$)
- $b_4 = -355 day^{-1}$, $\sigma_{g4} = 191 day^{-1}$ ($CV_\omega = 25\%$)

(continued next page)

- mean mass transfer rate $\bar{\omega} = 330 day^{-1}$
- $b_3 = -656 day^{-1}$, $\sigma_{g3} = 354 day^{-1}$ ($CV_\omega = 50\%$, partial correlation)
- $b_4 = -16666 day^{-1}$, $\sigma_{g3} = 8975 day^{-1}$ ($CV_\omega = 50\%$, partial correlation)
- $b_3 = -928 day^{-1}$, $\sigma_{g3} = 0$ ($CV_\omega = 50\%$, perfect correlation)
- $b_4 = -23569 day^{-1}$, $\sigma_{g4} = 0$ ($CV_\omega = 50\%$, perfect correlation)
- $b_3 = 0$, $\sigma_{g3} = 500 day^{-1}$ ($CV_\omega = 50\%$, uncorrelated)
- $b_4 = 0$, $\sigma_{g4} = 12692 day^{-1}$ ($CV_\omega = 50\%$, uncorrelated)
- $b_3 = -985 day^{-1}$, $\sigma_{g3} = 530 day^{-1}$ ($CV_\omega = 75\%$)
- $b_4 = -25004 day^{-1}$, $\sigma_{g3} = 13455 day^{-1}$ ($CV_\omega = 75\%$)
- $b_3 = -327 day^{-1}$, $\sigma_{g3} = 176 day^{-1}$ ($CV_\omega = 25\%$)
- $b_4 = -8301 day^{-1}$, $\sigma_{g3} = 4468 day^{-1}$ ($CV_\omega = 25\%$)

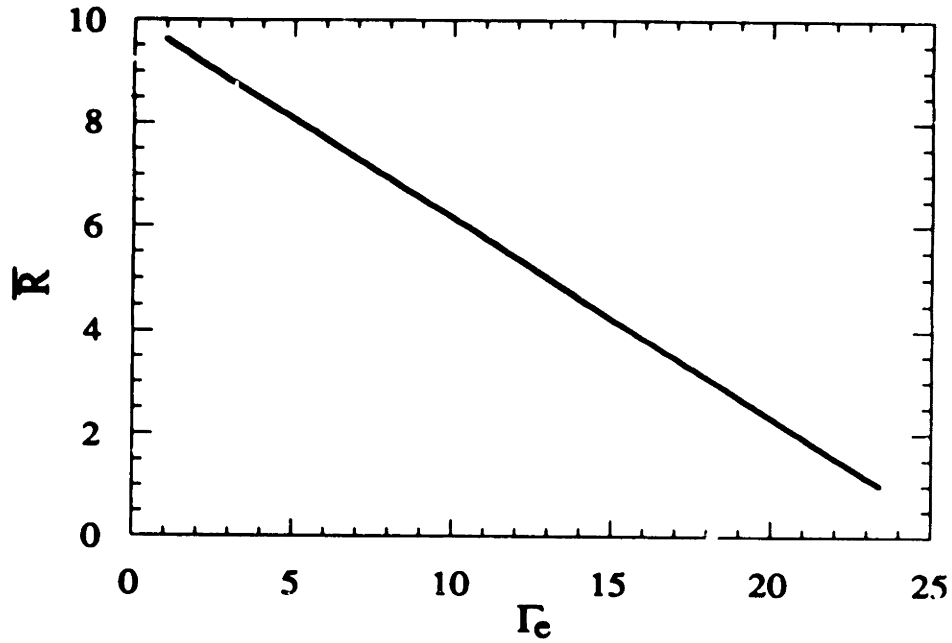


Figure 2-1: Effective retardation factor in the mobile zone as a function of the effective retardation factor in the immobile zone using parameters for the Cape Cod aquifer

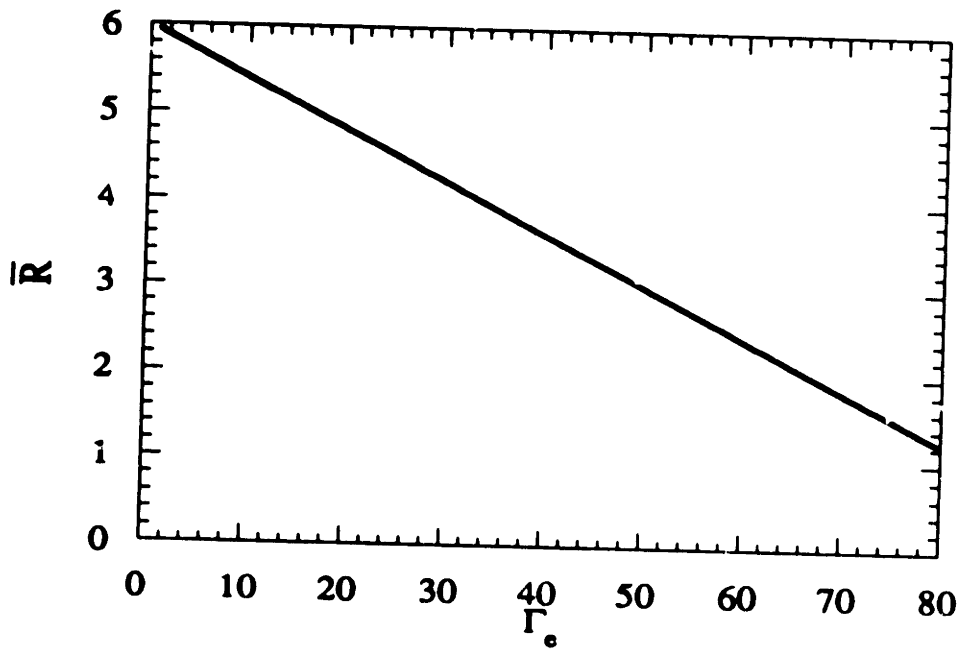


Figure 2-2: Effective retardation factor in the mobile zone as a function of the effective retardation factor in the immobile zone using parameters for the Borden aquifer

Given the total amount of bulk plume sorption, an infinite array of combinations is found for the parameters $\bar{R}$ and $\Gamma_e$ (equation 2.89). In the following plots, results for the different field scale coefficients are given with the parameter $\Gamma_e$ as an independent variable. Figures 2-1 and 2-2 present the relationship between the effective retardation factor in the mobile zone (also equal to the mean $\bar{R}$) and the effective retardation factor in the immobile zone $\Gamma_e$ for the Cape Cod and Borden aquifers. It is clear that, given the total amount of plume sorption, a value of $\Gamma_e$ uniquely defines a value for $\bar{R}$. In the following calculations, the correlation slopes for the random fields $R$ and $\omega$ with $f = lnK$ correspond to coefficients of variation of 25 %, 50 % and 75 % for these parameters. The slopes and residual variances corresponding to the cases presented here are listed in Table 2.2. Sensitivity to these slope values and coefficients of variation is explored in the results that follow.

Calculations using equation (2.90) for the contributions of aquifer heterogeneities (first three terms on the RHS of the equation) and intragrain diffusion/sorption (last two terms on the RHS of the equation) to the longitudinal macrodispersivity $A_{11}$ are presented in Figures 2-3 and 2-4. For all values of the immobile zone retardation factor, it is apparent that the influence of the intragrain processes is negligible compared to the influence of natural heterogeneities for the set of parameters considered. For a given different situation, the theory, and in particular equation (2.90) provides a framework to quantify the influences of intragrain processes and natural heterogeneities on field scale dispersion.

Figures 2-5 and 2-6 present results obtained for the longitudinal macrodispersivity $A_{11}$ for different values of the mean transfer factor $\bar{\omega}$ that span three orders of magnitude. For the given fixed coefficient of variation of 50% in the $\omega$ random field, the macrodispersivity is relatively insensitive to the mean value $\bar{\omega}$ at the Borden site. For the Cape Cod results, some variation of the results is obtained at higher values of the immobile zone retardation factor. The influence of the intragrain processes on the longitudinal macrodispersivity appears to be greater at the Cape Cod site for lower values of the mean transfer factor $\bar{\omega}$, this is, at higher values of the characteristic time of the intragrain diffusion process. The transfer factor is dependent on the tortuosity

of the transport path of the solute through the grain material [Wu and Gschwend, 1986, Ball and Roberts, 1991]. The values of $\bar{\omega}$ presented in Table 2.1 assume a value of tortousity of 2. However, recent experimental findings on batch sorption studies have reported values of tortuosity two orders of magnitude higher [Harmon *et al.*, 1992]. If tortuosity values are indeed in this range, it is expected that the effects of intragrain processes on the field scale transport coefficients will be significantly increased. This is indicative of a need to focus experimental investigations on determining the magnitude of the tortuosity parameter. The stochastic theory presented here serves the purpose of determining the threshold values for this parameter that produce an effect on the overall transport process.

The sensitivity of the longitudinal macrodispersivity to the variability in the transfer factor $\omega$ is presented in Figures 2-7 through 2-10. In general, the value of $A_{11}$ appears to be higher for a larger coefficient of variation $CV_\omega$ and for a stronger correlation with $lnK$. Sensitivity to variability in retardation is shown in Figures 2-11 through 2-14. In this case, considerable differences are found in the longitudinal macrodispersivity, which is consistent with the findings of Garabedian *et al.* [1988], where the value of $A_{11}$ depends strongly on the slope of the $R - lnK$ correlation.

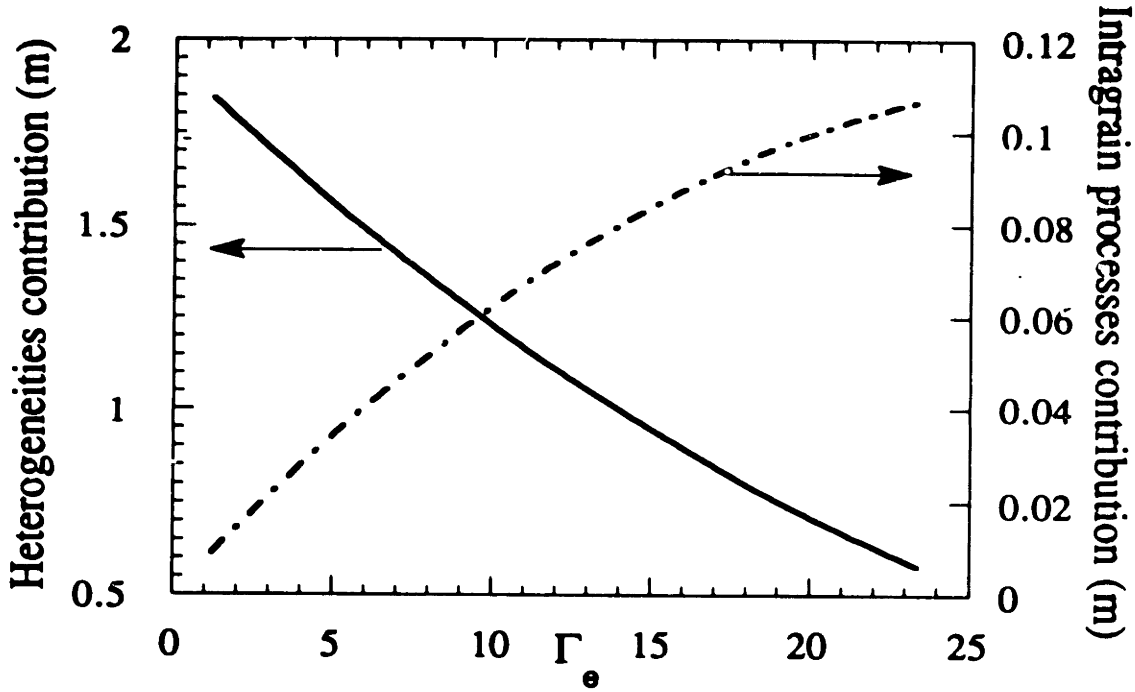


Figure 2-3: Relative contributions of aquifer heterogeneities and intragrain processes to the longitudinal macrodispersivity $A_{11}$ using parameters for the Cape Cod aquifer.

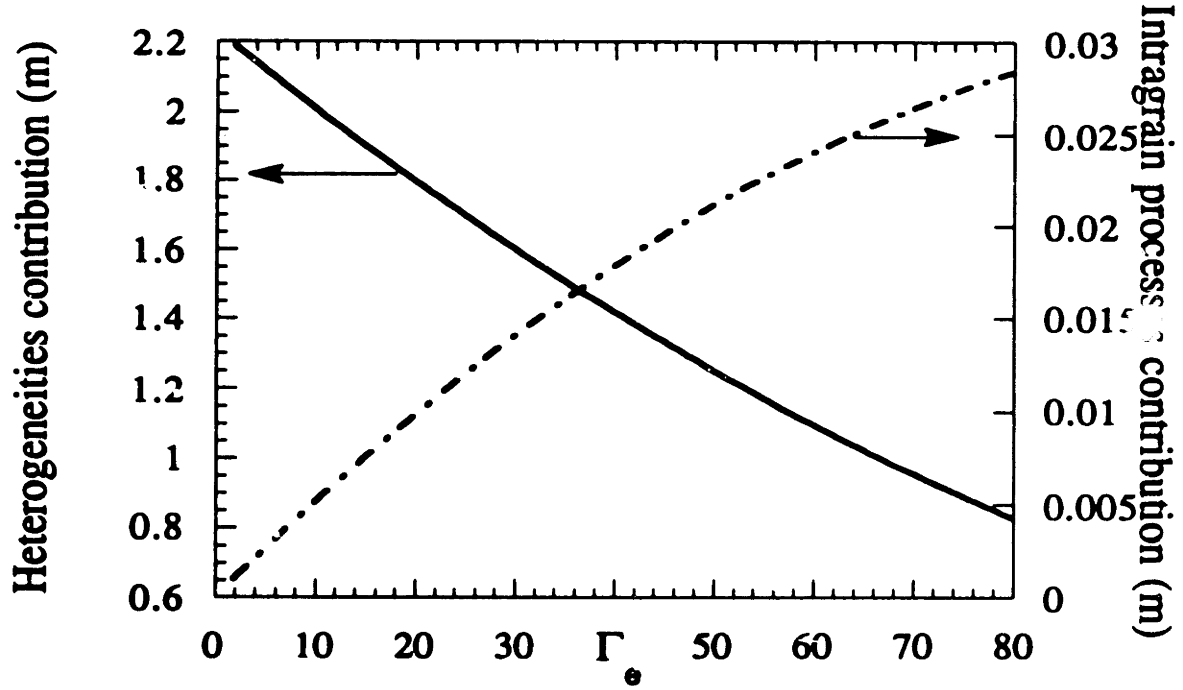


Figure 2-4: Relative contributions of aquifer heterogeneities and intragrain processes to the longitudinal macrodispersivity $A_{11}$ using parameters for the Borden aquifer.

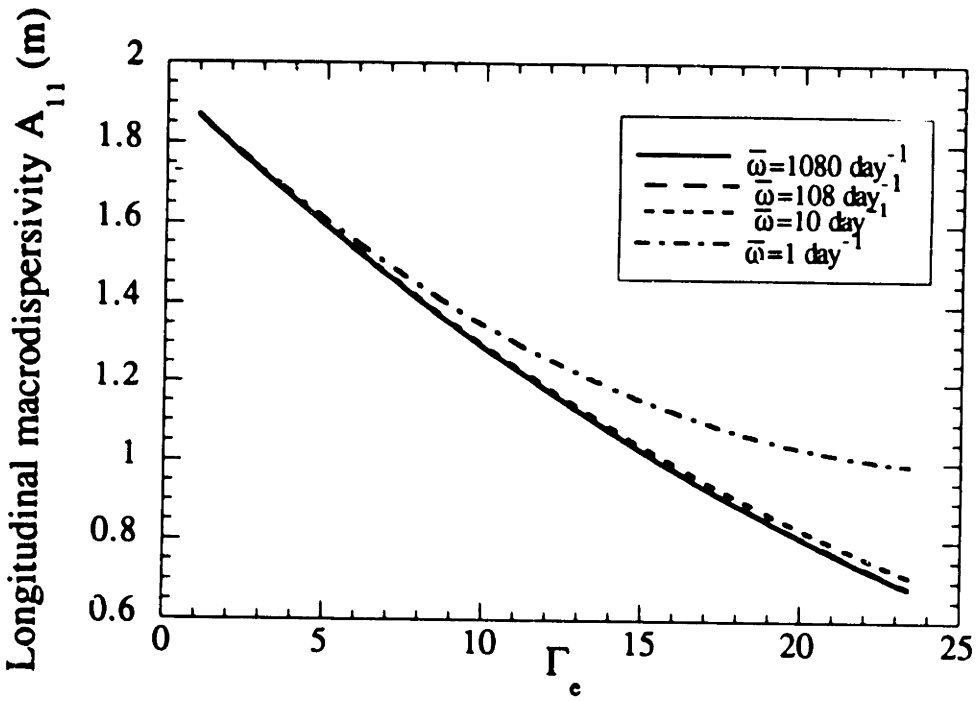


Figure 2-5: Longitudinal macrodispersivity as a function of the effective retardation factor in the immobile zone using parameters for the Cape Cod aquifer.

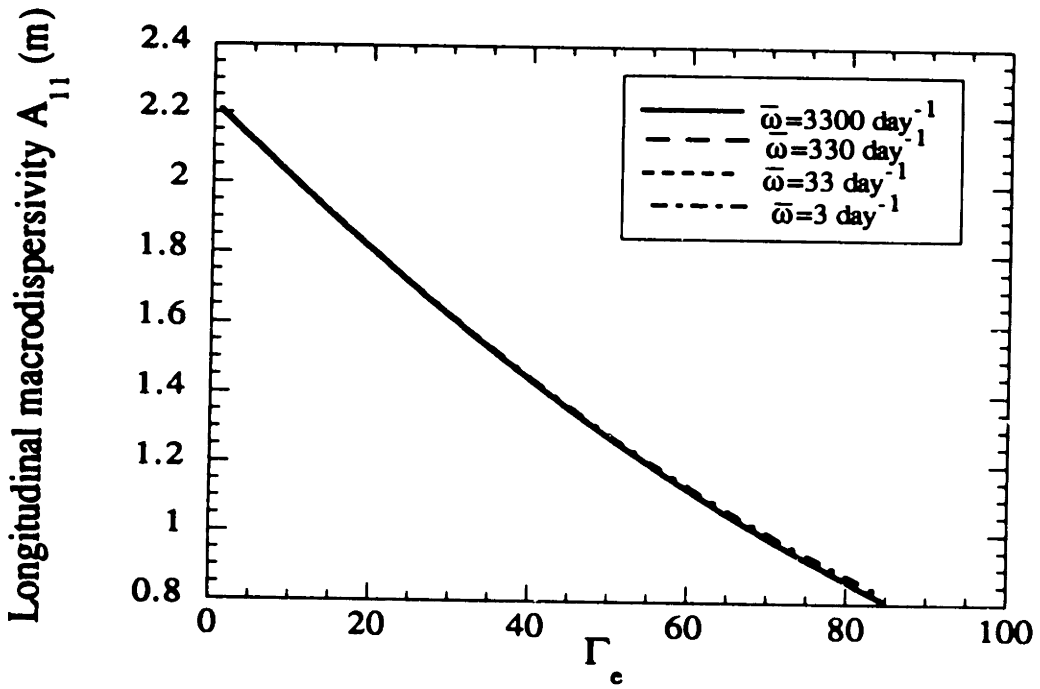


Figure 2-6: Longitudinal macrodispersivity as a function of the effective retardation factor in the immobile zone using parameters for the Borden aquifer.

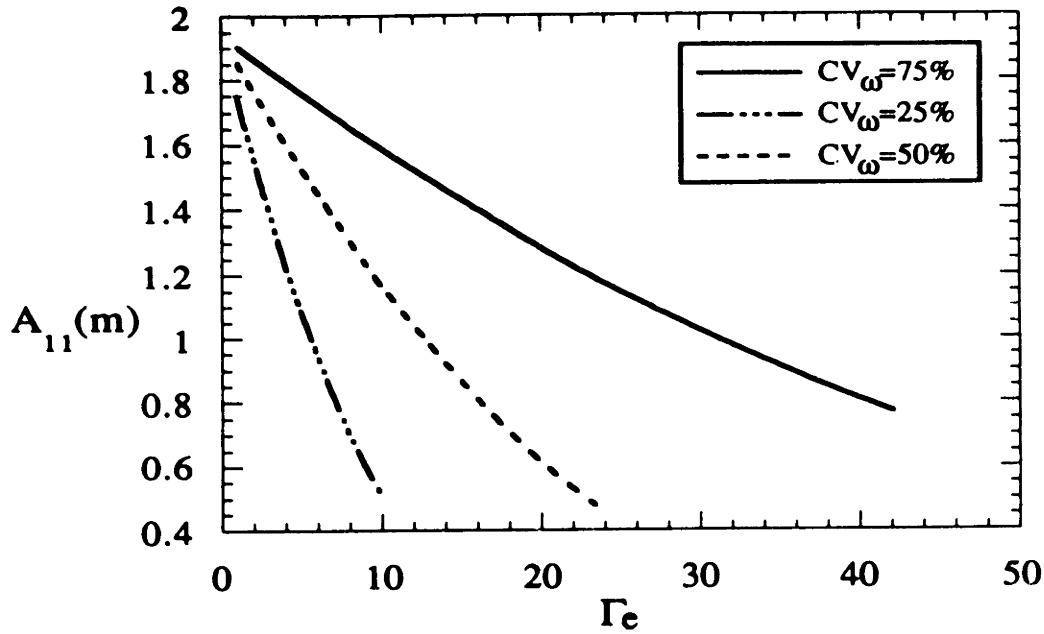


Figure 2-7: Sensitivity of the longitudinal macrodispersivity to variability in the solute transfer factor for the Cape Cod aquifer parameters.

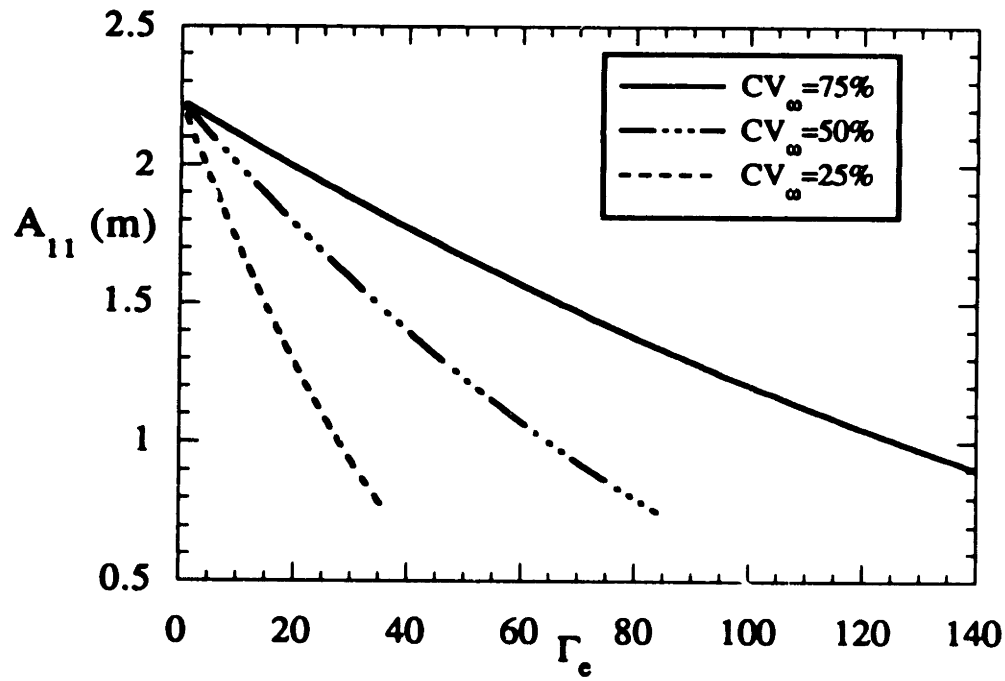


**Figure 2-8: Sensitivity of the longitudinal macrodispersivity to variability in the solute transfer factor for the Borden aquifer parameters.**

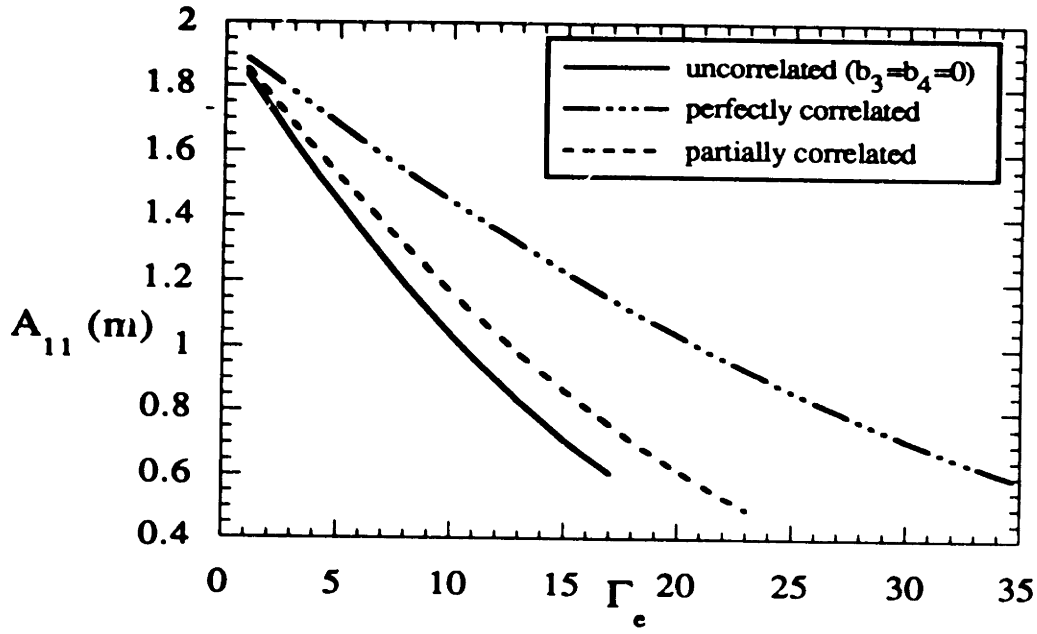


Figure 2-9: Sensitivity of the longitudinal macrodispersivity to the correlation of solute transfer and log-hydraulic conductivity for the Cape Cod aquifer parameters.

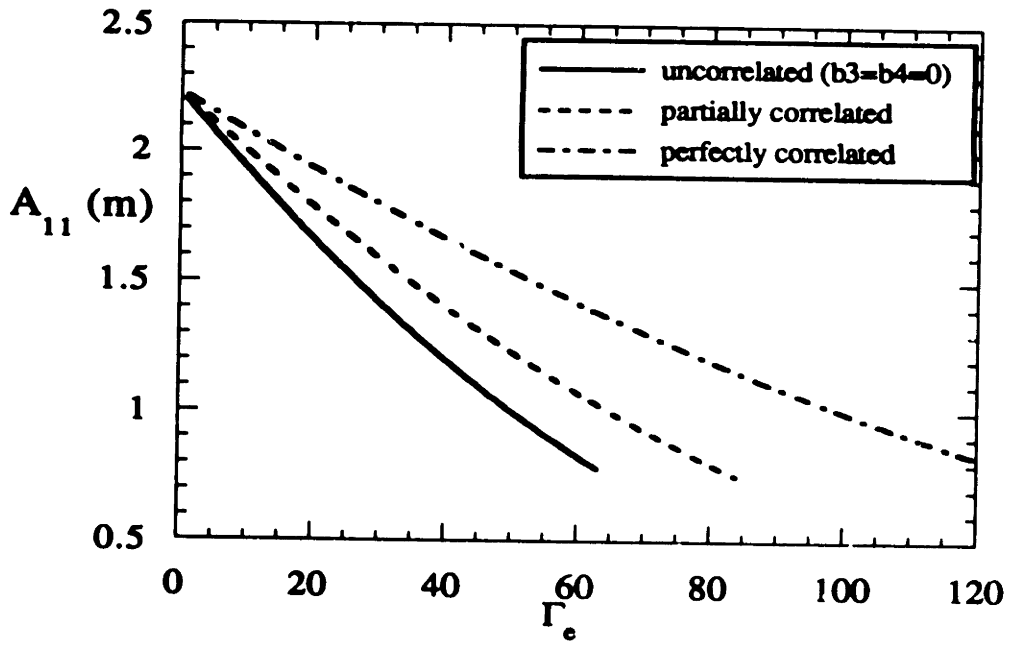


Figure 2-10: Sensitivity of the longitudinal macrodispersivity to the correlation of solute transfer and log-hydraulic conductivity for the Borden aquifer parameters.

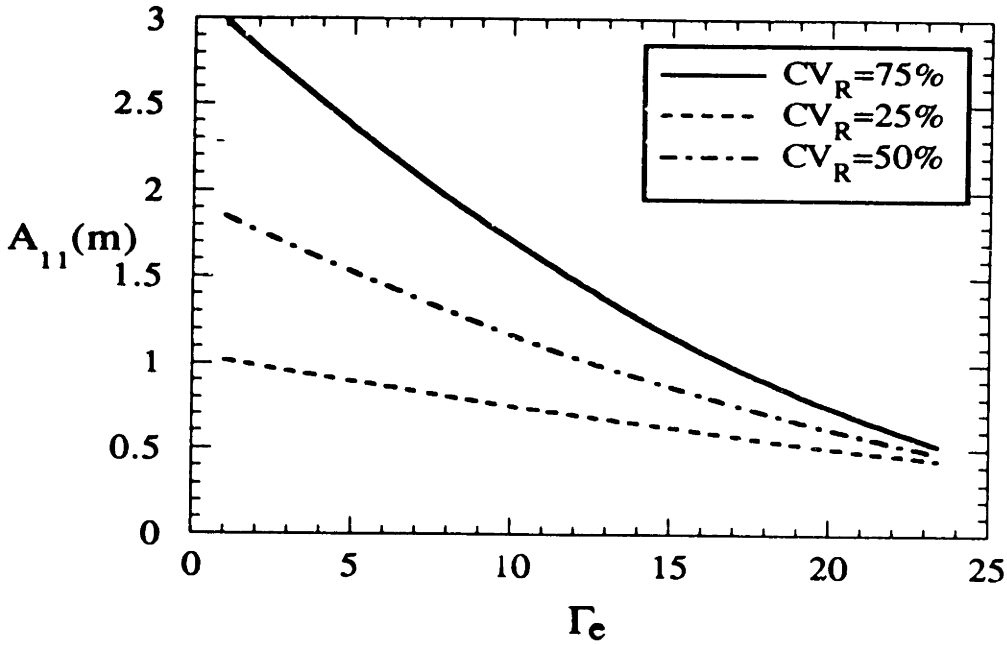


Figure 2-11: Sensitivity of the longitudinal macrodispersivity to variability in the retardation factor for the Cape Cod aquifer parameters.

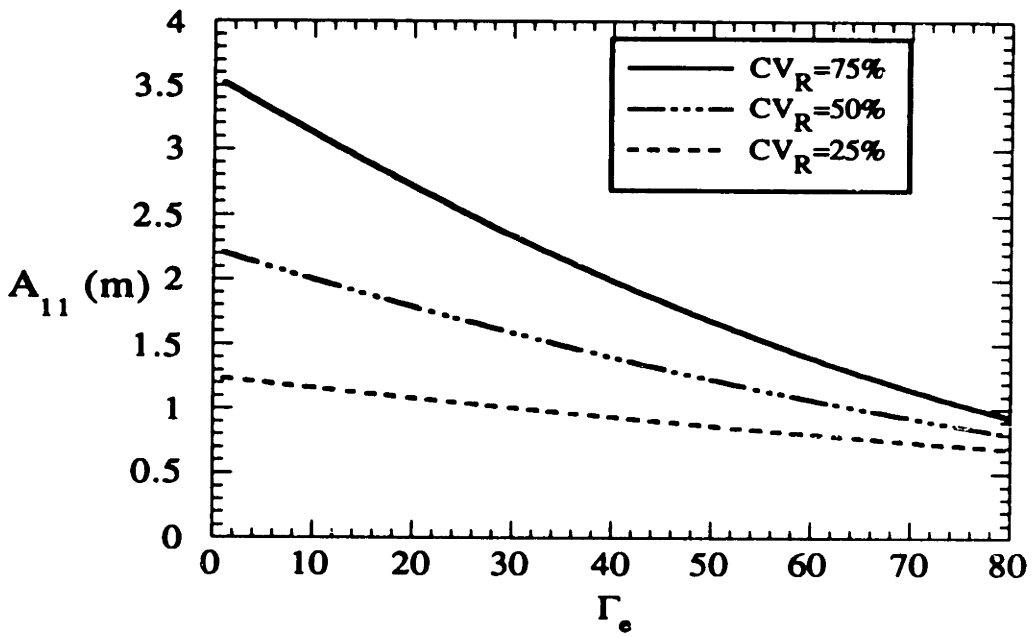


Figure 2-12: Sensitivity of the longitudinal macrodispersivity to variability in the retardation factor for the Borden aquifer parameters.

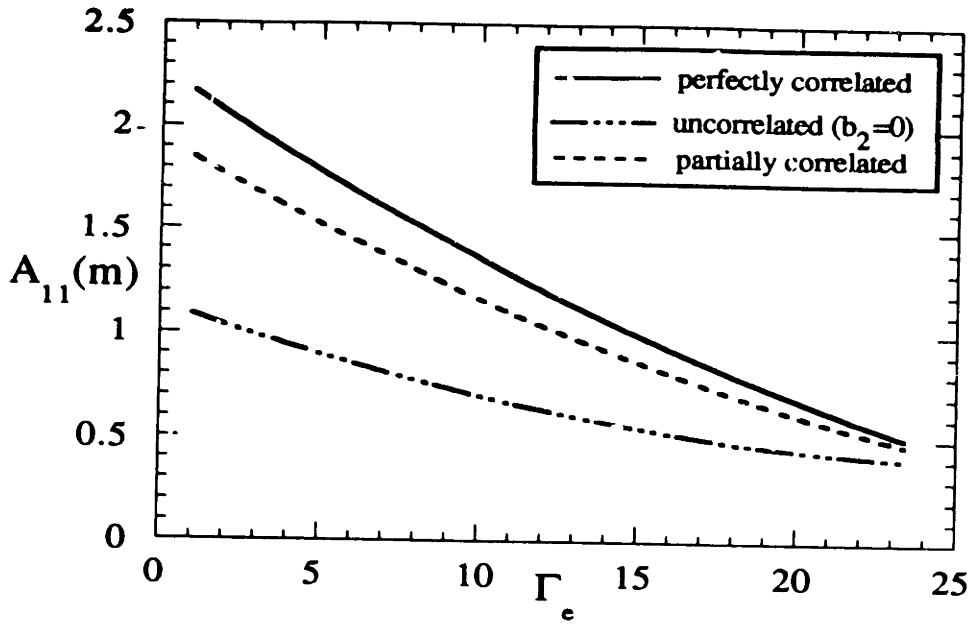


Figure 2-13: Sensitivity of the longitudinal macrodispersivity to the correlation of retardation and log-hydraulic conductivity for the Cape Cod aquifer parameters.

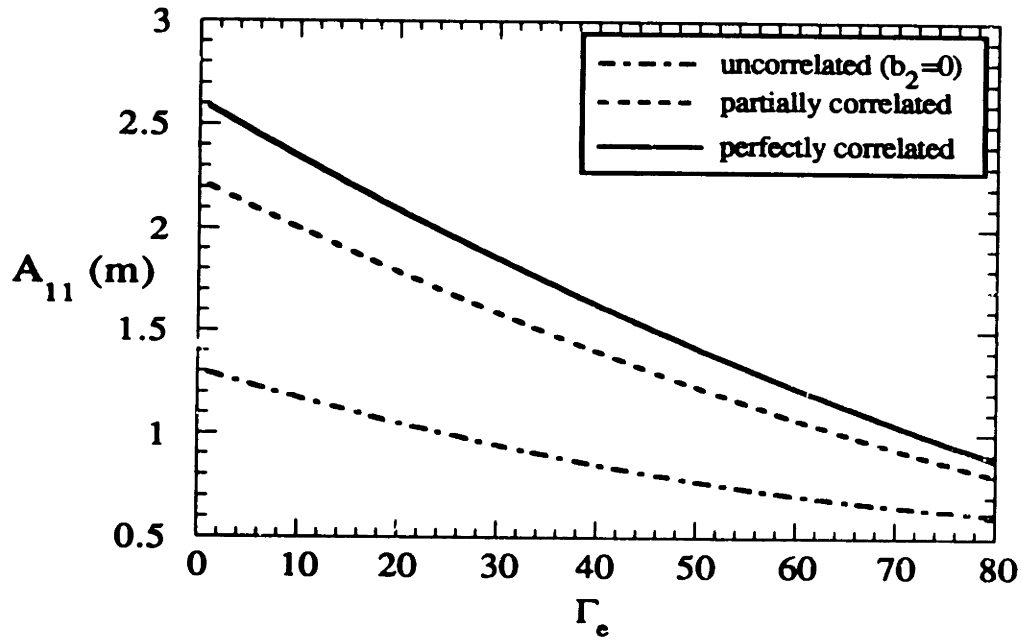


Figure 2-14: Sensitivity of the longitudinal macrodispersivity to the correlation of retardation and log-hydraulic conductivity for the Borden aquifer parameters.

Figures 2-15 and 2-16 present the values of the coefficients of the third order spatial derivative terms in the effective transport equation 2.95. These coefficients can be used to represent the plume asymmetric features, as it is explained in detail in Chapter 3. These results are presented here by separating the asymmetry effects produced by heterogeneities in aquifer parameters and by intragrain diffusion/sorption. The contributions of heterogeneities and intragrain processes to plume asymmetry are comparable at high values of $\Gamma_e$. However, in the lower immobile retardation factor regime, natural variability in aquifer properties can be used to explain plume asymmetry. These results consistently indicate that the influence of intragrain processes on plume asymmetry can be important at higher values of the immobile zone retardation factor, and that there is a need to carefully consider and understand the magnitude of the intragrain diffusion and sorption parameters. The theory presented here provides a theoretical guiding tool to compare and quantify the relative influences of intragrain processes and aquifer heterogeneities and to identify the critical threshold values of the parameters that produce significant influences in the observed plume tailing process.

As it was the case for macrodispersivity, sensitivity to the variability in retardation also proved to be more significant than sensitivity to transfer factor variability for these results, as presented in Figures 2-17 through 2-24.

In general, this series of results indicate that the dependence of the field scale coefficients of dispersion and asymmetry on the intragrain diffusion and sorption processes at times much larger than the characteristic time scale for these processes is controlled by the magnitude of the intragrain rate processes (transfer factor). The preliminary calculations performed for the Cape Cod and Borden sites suggest a relatively minor influence for the assumed value of the tortuosity parameter. This issue is further explored in determining the time scales that occur in the field by developing an analysis of the transient sorption processes, which is the focus of Chapter 3.

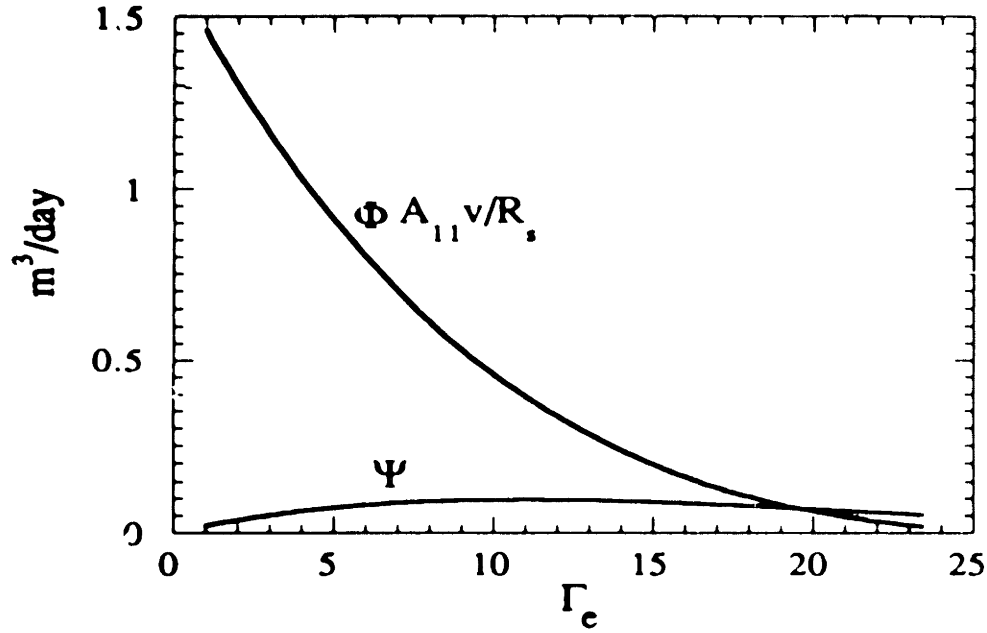


Figure 2-15: Coefficient of third-order spatial derivative as a function of the effective retardation factor in the immobile zone using parameters for the Cape Cod aquifer.

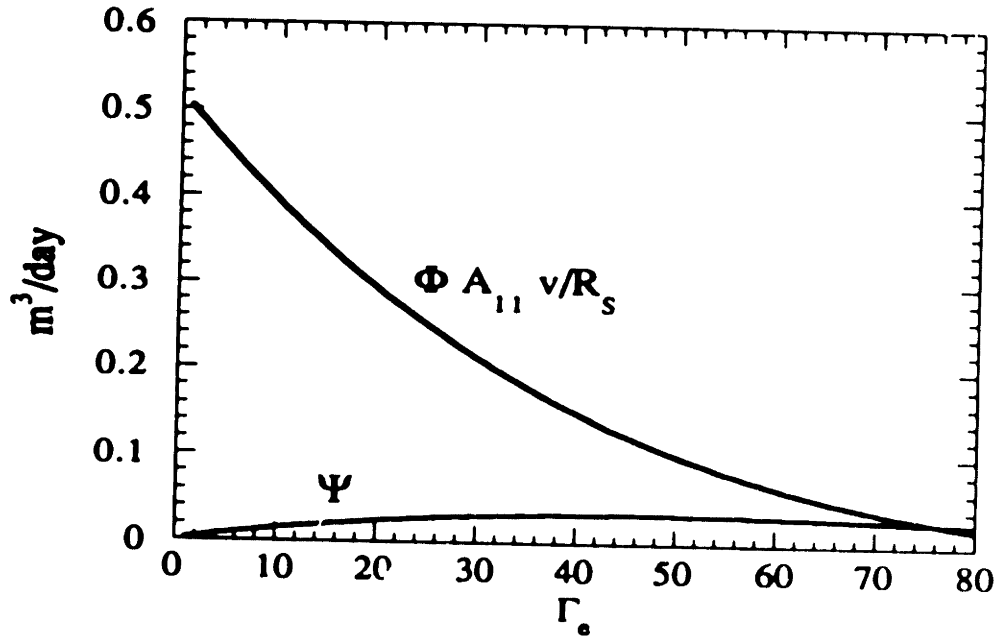


Figure 2-16: Coefficient of third-order spatial derivative as a function of the effective retardation factor in the immobile zone using parameters for the Borden aquifer.

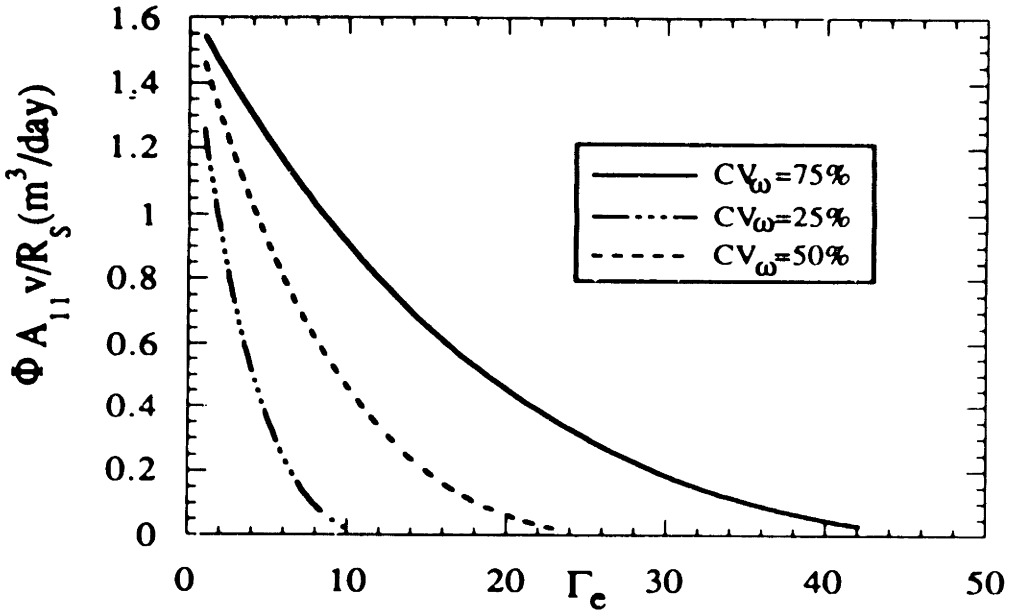


Figure 2-17: Sensitivity of the third-order spatial derivative coefficient to variability in the solute transfer factor for the Cape Cod aquifer parameters.

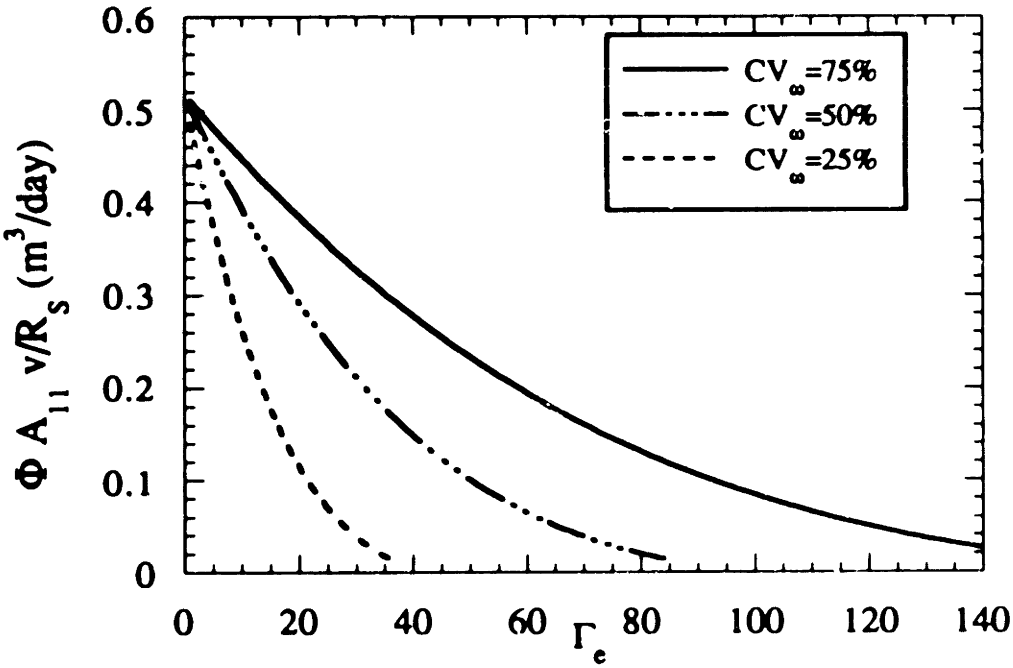


Figure 2-18: Sensitivity of the third-order spatial derivative coefficient to variability in the solute transfer factor for the Borden aquifer parameters.

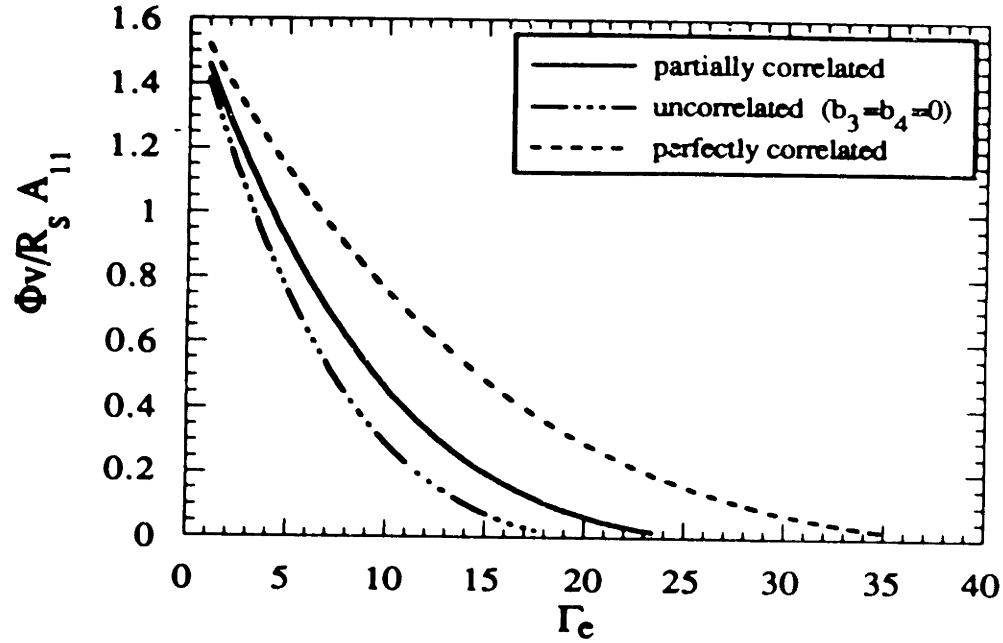


Figure 2-19: Sensitivity of the third-order spatial derivative coefficient to the correlation of solute transfer and log-hydraulic conductivity for the Cape Cod aquifer parameters.

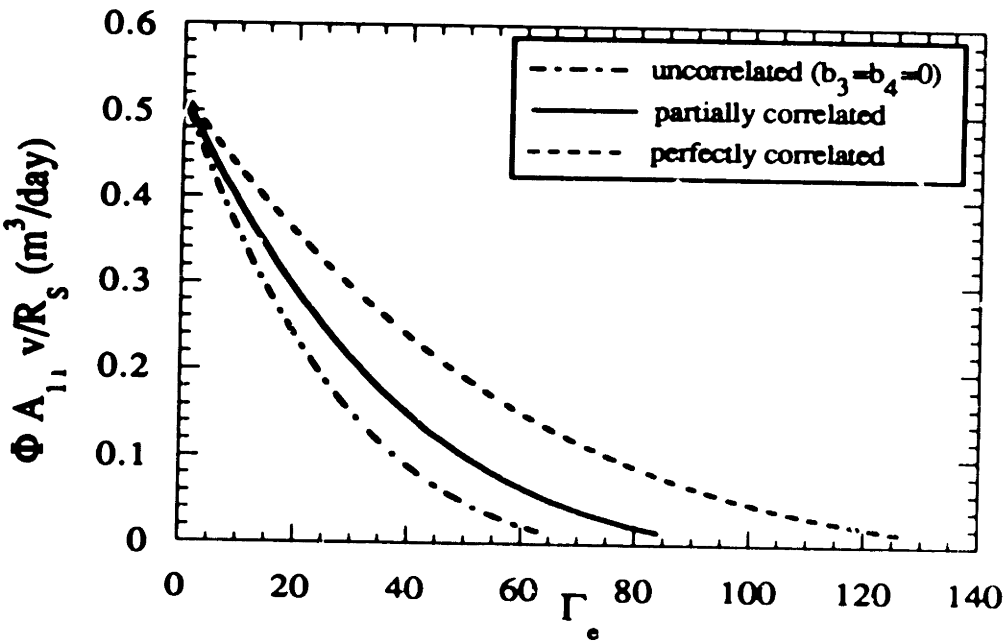


Figure 2-20: Sensitivity of the third-order spatial derivative coefficient to the correlation of solute transfer and log-hydraulic conductivity for the Borden aquifer parameters.

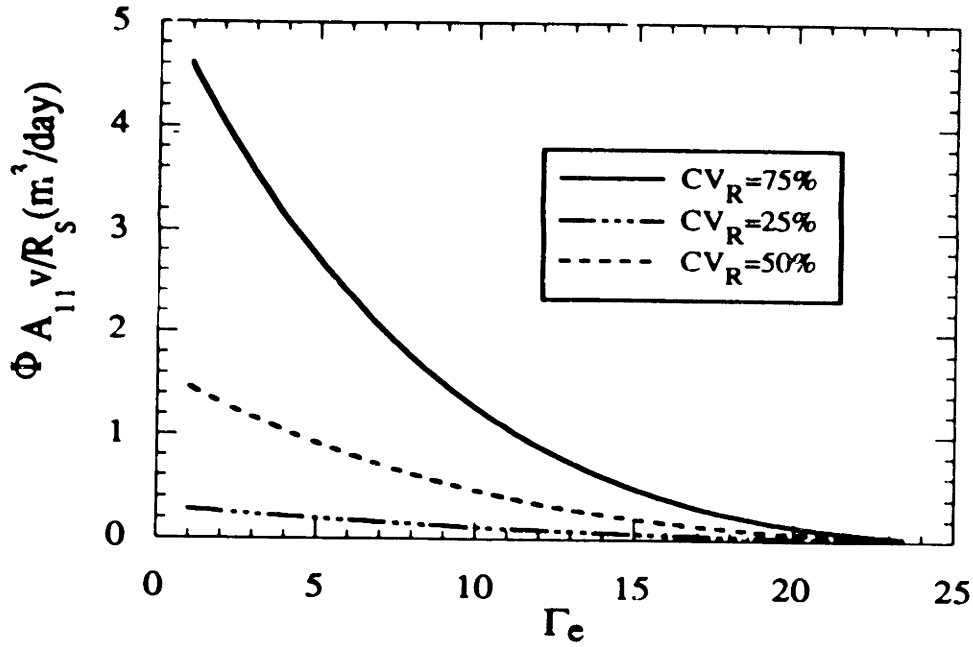


Figure 2-21: Sensitivity of the third-order spatial derivative coefficient to variability in the retardation factor for the Cape Cod aquifer parameters.

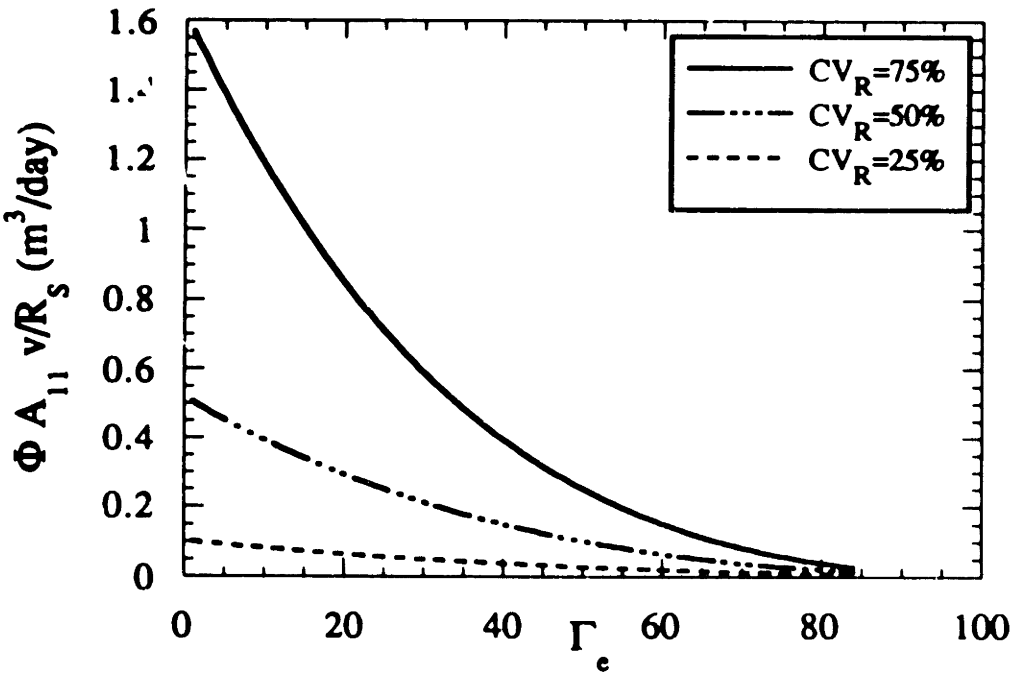


Figure 2-22: Sensitivity of the third-order spatial derivative coefficient to variability in the retardation factor for the Borden aquifer parameters.

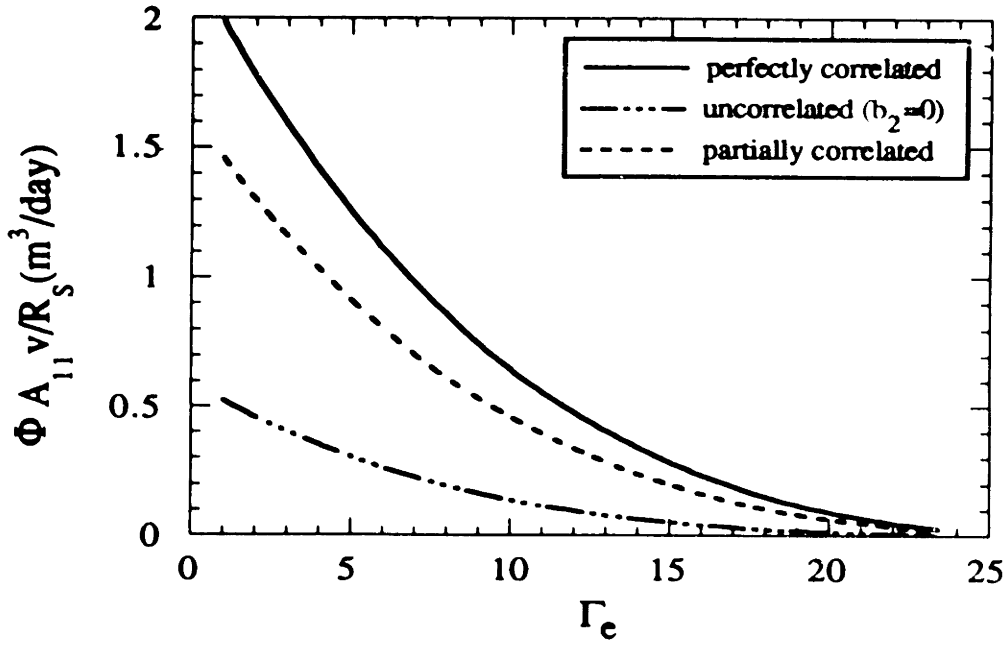


Figure 2-23: Sensitivity of the third-order spatial derivative coefficient to the correlation of retardation and log-hydraulic conductivity for the Cape Cod aquifer parameters.

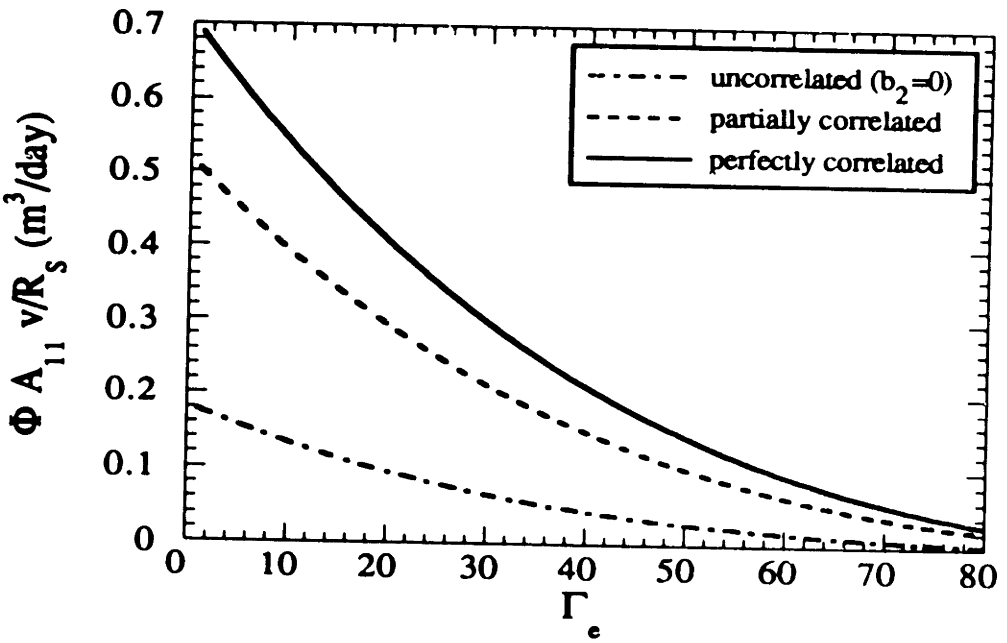


Figure 2-24: Sensitivity of the third-order spatial derivative coefficient to the correlation of retardation and log-hydraulic conductivity for the Borden aquifer parameters.

## 2.4 Conclusions

The analysis developed in this Chapter is focused on determining the influence of the processes of diffusion and sorption of a reactive solute in zones of water immobilization within a porous material. The effects of intragrain diffusion/sorption on the bulk plume characteristics were studied regarding retardation, dispersion and plume asymmetry. The following quantitative assessments are based on calculations using parameters for sorption of lithium onto sediments in a site in Cape Cod, Massachusetts, and for sorption of tetrachloroethene (PCE) onto sediments from the Borden site in Ontario, Canada. However, the stochastic theory developed in this Chapter provides a general framework to analyze the effects of intragrain processes and natural heterogeneities on the field scale transport of reactive solutes in groundwater.

The overall coefficient of retardation, herein referred as effective retardation factor, is found to be the sum of the amounts of sorption that occur in the zones of mobile and immobile water within the aquifer material. Bulk retardation factors observed in the field will thus have contributions from sorption onto sites in both zones. However, in field studies, it is unlikely that it is possible to distinguish between the two processes. The results obtained for the longitudinal macrodispersivity and for the coefficient of third-order derivatives in the mean transport equation show that the influence of intragrain processes on field scale transport characteristics of solute plumes is dependent upon the magnitude of the controlling parameters of these processes, *i.e.*, transfer factor and effective immobile zone retardation factor. The difficulty in distinguishing between immobile and mobile zones in the field suggests that the sorption process can be assumed to be a single, time-dependent process.

The calculations presented for the Cape Cod and Borden sites show that increased dispersion effects observed for reactive plumes can be explained by the heterogeneous mobile zone sorption process, and that the contribution of intraparticle diffusion/sorption to macrodispersivity is not significant for these field cases. In a more general context, the theoretical developments presented here suggest that the contribution of intragranular diffusion to the field scale dispersivity is comparable to

that of the instantaneous linear sorption to the grain surfaces only for lower values of the transfer factor $\omega$ (higher tortuosity), and for higher values of the intragrain retardation factor. This is indicative of a need to further investigate the magnitude of these controlling factors at particular field sites in order to quantitatively assess the influence of intragrain processes on the overall transport of contaminating solutes.

Calculations of sensitivity to these parameters verify field observations [Garabedian *et al.*, 1988] in that macrodispersivity is significantly influenced by the correlation between retardation and log-hydraulic conductivity, and that the effective transport coefficients are sensitive to variability in the intraparticle diffusion/sorption and mobile retardation processes. This, once again, points in the direction of a need to experimentally quantify the magnitude and variability of the sorption process. The stochastic theory presented in this Chapter serves both as a guide in determining the controlling parameters and as a framework to link laboratory and field scale features of reactive solute transport.

# Chapter 3

# An analysis of the transient sorption process

## 3.1 Introduction

The issue of using an equilibrium assumption for the process of mass exchange between the solid and aqueous phases in an aquifer, as opposed to considering sorption to be a kinetically controlled process has received an increased attention recently [Curtis *et al.*, 1986, Roberts *et al.*, 1986, Ball and Roberts, 1991b, Selroos and Cvetkovic, 1992]. Also, the importance of incorporating the intrinsic heterogeneity of natural aquifer environments has been recognized in the literature [Garabedian *et al.*, 1988, Kabala and Sposito, 1990, Robin *et al.*, 1991]. Only the latter articles which have been developed using equilibrium assumptions for the sorption process deal explicitly with natural heterogeneity in the aquifer material and physico-chemical parameters. It is apparent from these research efforts that investigating the effects of equilibrium *vs.* kinetics on the sorption process could help to understand the transient characteristics of laboratory and field-observed retardation factors. This information, of course, may be used in the design of environmental remediation schemes where sorption onto the solid phases in the aquifer is an important component of the overall contamination scenario.

In one of a series of articles, Roberts *et al.* [1986] find a tendency for the retar-

dation factor of a number of halogenated organic compounds in the Borden site to increase with time over a two year observation period. Kabala and Sposito [1990], have also studied the problem of linear instantaneous sorption of reactive solutes in heterogeneous aquifers. They derive a mean transport equation in which the effective bulk retardation factor is time dependent, but they do not present any specific calculations to show the time-varying characteristics of this field scale parameter. More recently, Ball and Roberts [1991a,b] have studied the equilibrium distribution coefficients for PCE on batch sorption experiments using Borden aquifer sediments, finding equilibration times in the order of days. These results are in agreement with those obtained by Curtis *et al.* [1986]. Spatial variability of sorptive properties in the Borden aquifer has been recognized by Mackay *et al* [1986].

The issue of time-dependence of the retardation factors and the time scales at which this dependence occurs has not been yet satisfactorily resolved. It could be a result of nonlinear equilibrium sorption which leads to higher values of the distribution coefficients when solution concentrations diminish over time as a result of dispersion. It could be a result of aquifer natural heterogeneity. But it could also be explained by recognizing that the sorptive mass transfer rates can be slow with respect to advection in the pore fluids. Numerical simulations performed by Sudicky [1990] involving conservative solute migration through a random, synthesized permeability field similar to Borden indicate a fairly minor effect of intragrain porosity on bulk plume migration rates. However, Wood *et al.* [1990] suggest that the effect of intragrain porosity will be more pronounced for reactive solutes than for non-reacting ones.

The time dependence of the effective dispersivity or macrodispersivity of solute plumes also represents a concern among researchers [Gelhar, 1987, Dagan, 1988, Naff, 1990]. For reactive solutes, the time-varying retardation factor can be expected to produce an influence on the time evolution of the field-scale dispersion coefficient. And by the same token, higher moments like plume asymmetry are also expected to be time dependent. The time evolution of the plume characteristics of retardation, dispersion and skewness constitutes the main focus of this Chapter.

Effective retardation factors, macrodispersivities and plume skewness coefficients

can be obtained from field measurements by calculating moments of the concentration distribution. These moments, which can be derived theoretically from the corresponding governing equations, have been found to be directly related to the effective transport coefficients of solute plumes [Gelhar *et al.*, 1979, Garabedian *et al.*, 1988, Naff, 1990, Chrysikopoulos *et al.*, 1992]. This methodology is used in this Chapter to analyze the time evolution of the plumes zeroth, first, second and third moments, which in turn define field-scale features of retardation, dispersion and asymmetry. Burr [1992] presents a detailed numerical investigation of reactive solute transport incorporating aquifer three dimensional heterogeneity and diffusion rate limited sorption. The results presented show no appreciable effect of the diffusion rate limitation on the time evolution of the computed spatial moments and effective retardation and dispersion coefficients of reactive plumes. This finding supports the results presented in Chapter 2. An evaluation of these computed moments could not be assessed analytically because of a lack of theoretically derived expressions for reactive solutes. These expressions are developed in this Chapter.

The following sections present and discuss a stochastic analysis of the transient sorption process, incorporating the effects of natural heterogeneity, intragrain diffusion rate limitations, linear and nonlinear equilibrium isotherms. Following this, the method of moments is used to derive expressions for the time evolution of the plume aqueous mass, center of mass displacement, longitudinal second moment and skewness coefficient. This model is aimed at gaining a better understanding of the factors that control the field scale retardation factors, macrodispersivities and skewness coefficients, and to what extent each of the aforementioned mechanisms is important in these overall features of sorbing contaminant plumes.

## 3.2 Laboratory experiments: intragrain diffusion time scale

In a laboratory batch sorption experiment scale, the two-zone intragrain diffusion/sorption model presented in Chapter 2 is used by assuming two different components, namely,

concentrations of the solute in the external and intragrain zones denoted by $S$ and $\Omega$. No water velocity or concentration gradients are now assumed for both species to represent batch experimental conditions. The system of governing equations that results from this conceptual model is presented and solved in Appendix C.

This model can be used to describe quantitatively the sorption process time scales that occur in a laboratory batch experiment. The parameter $\omega^{-1}$ is essentially a time scale given by an effective diffusivity and the squared radius of the pores,

$$\omega = \frac{D_e}{a^2} \tag{3.1}$$

with $D_e$ obtained from a physical model of diffusion through tortuous media. Introducing a correcting factor to account for the tortuosity of the diffusive transport paths through the porous material, we have:

$$D_e = \frac{D_m}{\chi} \tag{3.2}$$

where $D_m$ is the molecular diffusivity of the compound in water, and $\chi > 1$ is defined as the tortuosity parameter of the porous medium.

A bulk estimate of the radius $a$ of the pores can be obtained from the mean hydraulic conductivity using Hazen's empirical relation [Freeze and Cherry, pp. 350, 1979]

$$\bar{K} = 4a^2 \tag{3.3}$$

with $\bar{K}$ given in $\frac{cm}{s}$ and $a$ in $mm$.

The following are two specific calculations performed for actual field scale situations reported in Garabedian *et al.* [1988] using lithium as the solute, and Curtis *et al.* [1986], Ball and Roberts [1991] using tetrachloroethene (PCE) as the solute. In both cases, solute sorption was studied both in laboratory and field scales. If no degradation process is occuring, conservation of total mass requires:

$$R_{obs} = R + \frac{\tilde{n}}{n}\Gamma \tag{3.4}$$

This equation can be rewritten as:

$$n\ R_{obs} = n + \rho K_d + \tilde{n} + \tilde{n}\Gamma \tag{3.5}$$

The terms on the right hand side of this equation represent the fractions of the total amount of solute mass present in the aqueous external, solid external, aqueous intragrain and solid intragrain media, respectively. These just add up to the total solute mass in the aquifer in the left hand side. This means that once the observed retardation factor is obtained, the retardation factors in the external and intragrain zones are related through equation (3.4). These retardation factors are used to calculate the time scale governing the mass exchange between the zones from equation (C.10) in Appendix C:

$$\tau_{id} = \left(\frac{\omega_1}{R} + \frac{\omega_2}{\Gamma}\right)^{-1} = \frac{1}{\omega}\left(\frac{1}{nR} + \frac{1}{\tilde{n}\Gamma}\right)^{-1} \tag{3.6}$$

The following is an example calculation using parameters for PCE at the Borden site in Ontario, Canada [Curtis *et al.*, 1986, Ball and Roberts, 1991a,b]. For this case, the retardation factor observed was $R_{obs} = 6$. The intragrain porosity was reported by Ball *et al.* [1990] as $\tilde{n} = 0.013$. Table 3.1 shows the array of retardation factors in the external and internal zones that would combine to give the observed value $R_{obs}$, and the corresponding time scale $\tau$ obtained from equation (3.6).

Table 3.1: Batch scale parameters for PCE at the Borden site.

| R | $\Gamma$ | $\tau_{id}$ (day) |
|---|---|---|
| 1 | 125 | 1 |
| 2 | 100 | 1.2 |
| 3 | 75 | 1 |
| 4 | 50 | 0.6 |
| 5 | 25 | 0.2 |
| 5.9 | 1 | $<< 1$ |

The results for the characteristic time scale $\tau_{id}$ show an agreement with experimental findings in Borden aquifer sediments [Curtis *et al.*, 1986, Ball and Roberts, 1991b]. Essentially, the characteristic times observed on a laboratory scale are reproduced by the intragrain diffusion/sorption model, as given in the preceeding analysis and by the time scale results developed in Chapter 2. However, time scales that are increased by two orders of magnitude with respect to those observed in batch experiments have been observed for the same chemical under field conditions [Roberts *et al.*, 1986]. Although the asymptotic value of the retardation factors observed in both cases are essentially the same, the time elapsed to reach these values has been found to be in the order of hundreds of days for a number of halogenated organic compounds that include PCE. This suggests that in the field, an effect that is not achieved under laboratory conditions is causing this gap in the time scales referred to above. Similar results have been obtained using parameters for Lithium sorption onto sediments of an aquifer in Cape Cod, Massachusetts. These results are displayed in Appendix C.

The inclusion of natural aquifer heterogeneity has been found to explain large scale effects not predicted by smaller scale analyses [Gelhar and Axness, 1983, Dagan, 1984]. In the following sections, the development of a transient analysis of the sorption process is presented to gain an understanding of the effects of heterogeneities on the field scale time evolution of the retardation factor.

## 3.3 Solution methodology: natural heterogeneities time scale

In view of the developments presented in Section 3.2, the time evolution of retardation factors at a field scale suggests that other mechanism rather than diffusion and subsequent sorption onto intragrain zones is producing the transient characteristics of the sorption process in field situations. The following analysis focuses on the influence of heterogeneities of the aquifer material in this time evolution. In this analysis, sorption is considered as a single-component process, this is, without considering the presence of two distinct zones, as it was developed earlier in this Chapter and in Chapter 2. Since interest is now placed on time scales much larger than those obtained from the intragrain diffusion/sorption model, the assumption of a single sorbed component is reasonable.

As a starting point for the analysis of the transient single-component sorption process, the time evolution of the second-order correlations in the mean transport equation for the reactive solute must be analyzed. It has been shown that these second-order correlations produce field scale effects on the coefficients of retardation [Kabala and Sposito, 1990] and dispersion [Kabala and Sposito, 1990, Naff, 1990]. In this conceptual framework, the mean equation (2.37) takes the form presented in Equation (100) of Garabedian *et al.* [1988]:

$$\bar{R}\left(\frac{\partial \bar{S}}{\partial t} - \frac{v}{R_S}\frac{\partial S}{\partial \zeta_1}\right) + \frac{\partial}{\partial t}\overline{R'S'} - \frac{v_i}{R_S}\frac{\partial}{\partial \zeta_i}\overline{R'S'} + v\frac{\partial \bar{S}}{\partial \zeta_1} + \frac{\partial}{\partial \zeta_i}\overline{v_i'S'} = \frac{\partial}{\partial \zeta_i}D_{ij}\frac{\partial S}{\partial \zeta_j} \qquad (3.7)$$

Here, $R_S$ is the effective retardation factor to be determined in the subsequent analysis by imposing the condition of zero advective effective terms in the moving coordinate system, as developed in Chapter 2.

By analyzing this equation term by term, it is apparent that transient effects in the effective transport coefficients must be produced by time varying cross correlations between retardation and solute concentration $\overline{R'S'}$ and velocity and solute

concentration $\overline{v_i' S'}$. In order to analyze these terms, the governing ordinary differential equation for the spectral amplitude $dZ_S$, equation (2.50), must be solved. Rewriting this equation,

$$\frac{\partial dZ_S}{\partial t} + \frac{ivk_1 + D_{ij}k_ik_j}{\bar{R}} = \frac{G_j}{\bar{R}} dZ_{v_j} - \left(\frac{\partial \bar{S}}{\partial t} + \frac{v}{R_S} G_1\right) \frac{dZ_R}{\bar{R}} \tag{3.8}$$

The solution to this differential equation is:

$$dZ_S(\mathbf{k}, t) = \int_0^t exp[-\beta(t-\tau)] \left[G_j(\tau) \frac{dZ_{v_j}}{\bar{R}} - \left(\frac{\partial \bar{S}}{\partial \tau} + \frac{v}{R_S} G_1(\tau)\right) \frac{dZ_R}{\bar{R}}\right] d\tau \tag{3.9}$$

with

$$\beta(\mathbf{k}) = \frac{ivk_1 + D_{ij}k_ik_j}{\bar{R}} \tag{3.10}$$

Two approximations are now introduced into the analysis. First, in the frame of reference moving with the solute plume, changes of the mean concentration in time are assumed to be negligible. Second, since the integral to be calculated is composed of exponentially-weighted contributions from earlier times $\tau < t$, the major contribution to the result comes from the value $\tau = t$. This means that the concentration gradient $G_j(\tau)$ can be replaced in the integral by $G_j(t)$, so that the integral can be readily evaluated. This approximation is consistent with the fact that the concentration gradient varies slowly in time in the moving coordinate system, as explained in Gelhar [1987].

By using the Spectral Representation Theorem, the second order cross correlation between retardation and solute concentration and velocity and solute concentration are given by:

$$\overline{R'S'} = I_3(t) \frac{v}{R_S} \frac{\partial \bar{S}}{\partial \zeta_1} - I_1(t) \frac{\partial \bar{S}}{\partial \zeta_j} \tag{3.11}$$

$$\overline{v_i' S'} = I_1(t) \frac{v}{R_S} \frac{\partial \bar{S}}{\partial \zeta_1} - I_2(t) \frac{\partial \bar{S}}{\partial \zeta_j} \tag{3.12}$$

where,

$$I_1(t) = \int_{-\infty}^{\infty} \frac{S_{Rv_j} d\mathbf{k}}{iv_i k_1 + D_{ij} k_i k_j} \int_0^t exp[-\beta(t-\tau)] d\tau = \frac{1}{R} \int_{-\infty}^{\infty} \frac{1 - e^{-\beta t}}{\beta} S_{Rv_j} d\mathbf{k} \quad (3.13)$$

$$I_2(t) = \int_{-\infty}^{\infty} \frac{S_{v_i v_j} d\mathbf{k}}{ivk_1 + D_{ij} k_i k_j} \int_0^t exp[-\beta(t-\tau)] d\tau = \frac{1}{R} \int_{-\infty}^{\infty} \frac{1 - e^{-\beta t}}{\beta} S_{v_i v_j} d\mathbf{k} \quad (3.14)$$

$$I_3(t) = \int_{-\infty}^{\infty} \frac{S_{RR} d\mathbf{k}}{ivk_1 + D_{ij} k_i k_j} \int_0^t exp[-\beta(t-\tau)] d\tau = \frac{1}{R} \int_{-\infty}^{\infty} \frac{1 - e^{-\beta t}}{\beta} S_{RR} d\mathbf{k} \quad (3.15)$$

From these equations it follows that

$$\frac{\partial}{\partial t} \overline{R' S'} = \frac{v}{R_S} \frac{\partial \tilde{S}}{\partial \zeta_1} \frac{\partial I_3}{\partial t} - \frac{\partial \tilde{S}}{\partial \zeta_j} \frac{\partial I_1}{\partial t} + \frac{v}{R_S} I_3 \frac{\partial^2 \tilde{S}}{\partial t \partial \zeta_1} - I_1 \frac{\partial^2 \tilde{S}}{\partial t \partial \zeta_j} \quad (3.16)$$

The last two terms on this expression, which contain mixed time-space derivatives have been shown to produce plume skewness effects [Appendix D and Gelhar *et al.*, 1979]. The first two terms contain first-order spatial derivatives which will contribute to the advective component of the field scale transport equation, and thus to the effective retardation factor $R_S$. The time derivatives of the integrals $I_1$ and $I_3$ are found to be:

$$\frac{\partial I_1}{\partial t} = \frac{1}{R} \int_{-\infty}^{\infty} S_{Rv_j} e^{-\beta(\mathbf{k})t} d\mathbf{k} \quad (3.17)$$

$$\frac{\partial I_3}{\partial t} = \frac{1}{R} \int_{-\infty}^{\infty} S_{RR} e^{-\beta(\mathbf{k})t} d\mathbf{k} \quad (3.18)$$

An analytical evaluation of the integrals $I_1$, $I_2$ and $I_3$, as well as the time derivatives of $I_1$ and $I_3$ is detailed in Appendix E. Notice that at large times, the time derivative terms of the integrals vanish, and the result is identical to that obtained by Garabedian *et al.* [1988] using a large-time analysis. In their work, at large times,

transient effects in the effective retardation factor produced by these vanishing terms are not observed, and the effective retardation factor is equal to the mean.

This finding actually represents a more general result: the effects of transients in the storage term of the transport equation for a given solute vanish at large times. For instance, this result is applicable to a conservative solute with random porosity. In this case the results at large times are those presented in Gelhar [1987]. At initial times, however, some effect is expected given the presence of additional advective terms like those in equation (3.11).

The expressions for the field scale coefficients of retardation follows. Since the advective terms must be zero in the moving coordinate system,

$$-v\frac{\bar{R}}{R_S}+\frac{v}{R_S}\frac{\sigma_R^2}{\bar{R}}exp(-\frac{vt}{\lambda_1\bar{R}}-\frac{b_2\sigma_f^2 v}{\gamma\bar{R}}exp(-\frac{vt}{\lambda_1\bar{R}})+v=0 \tag{3.19}$$

from which,

$$R_S=\frac{1-(1)\frac{\sigma_R^2}{\bar{R}}exp(-\frac{vt}{\lambda_1\bar{R}})}{1-\frac{b_2\sigma_f^2}{\gamma\bar{R}}exp(-\frac{vt}{\lambda_1\bar{R}})}\bar{R} \tag{3.20}$$

where $CV_R$ is the coefficient of variation of the retardation factor random field $R$.

Notice that for large time, the effective retardation factor is equal to the mean, which was shown by Garabedian *et al.* [1988]. Notice, that the effective transient retardation factor is affected by the cross-correlation of retardation and flow velocity and by the autocorrelation of the local retardation factor field. This result is analogous to that presented by Kabala and Sposito [1990], although they present their result in spectral form, without introducing any particular spectral function for the cross-correlation spectra.

The dispersion terms in the mean equation are obtained from the spatial derivatives of the $\overline{v_i'S'}$ and $\overline{R'S'}$ cross correlations. The second derivative terms of concentrations can be grouped together to define a longitudinal macrodispersivity following the procedure described in Chapter 2 and Garabedian *et al.* [1988],

$$\alpha_L v - 2\frac{v}{R_S} I_1 + I_2 + \frac{v}{R_S} I_3 = v A_{11} \tag{3.21}$$

The integrals in this expression are developed in Appendix E neglecting local dispersion and using a stratified aquifer approximation $\delta = (\frac{\lambda_2}{\lambda_1})^2 << 1$ [Gelhar and Axness, 1983 ]. The expression for the transient longitudinal macrodispersivity is then found to be:

$$A_{11} = \left[\frac{\sigma_f^2 \lambda_1}{\gamma^2} - 2\frac{b_2}{\bar{R}}\frac{\sigma_f^2 \lambda_1}{\gamma} + \frac{\sigma_R^2}{\bar{R}^2}\lambda_1\right][1 - exp(-\frac{vt}{\lambda_1 \bar{R}})] \tag{3.22}$$

A characteristic time scale due to heterogeneity in the aquifer material appears in the expressions for the effective retardation factor and longitudinal macrodispersivity, equations (3.20) and (3.22). This time scale,

$$\tau_h = \frac{vt}{\lambda_1 \bar{R}} \tag{3.23}$$

can be calculated and compared with the time scale that results from the intragrain processes.

$$\tau_h \ ? \ \tau_{id}$$

This comparison provides a quantitative criterion to determine the relative importance of intragrain processes and aquifer heterogeneities on the transient characteristics of reactive plume development. A calculation can be made using parameters for the Borden aquifer [Sudicky, 1986] $\sigma_f^2 = 0.29$, $\lambda_1 = 2.8\ m$ $v = 0.1\ m/day$, and a mean retardation factor of $\bar{R} = 6$ for the contaminant solute PCE, as in Section 3.2. This results in a time scale of approximately 168 days, which is consistent with the time scale of variation reported in Roberts *et al.* [1986]. For the case under study, these results indicate that the time scale $\tau_h$ is significantly larger than the intragrain time scale $\tau_{id}$, which suggests that the transient characteristics of the bulk retardation factor for PCE at Borden are controlled by the natural heterogeneities of the Borden aquifer. From this result, it appears that heterogeneity of hydraulic and chemical

properties of an aquifer material is able to explain the transient characteristics of the field scale transport parameters of retardation and dispersion. This implies that although the intragrain diffusion process is the controlling process under a laboratory scale, under field conditions the effects of heterogeneities control the time evolution of the plume retardation and dispersion for this particular chemical at this particular site. In a more general situation, a comparison between the two time scales for different sorbate compounds at different field sites provides a quantitative criterion for assessing the relative importance of heterogeneities and intragrain processes.

With respect to the longitudinal macrodispersivity, equation (3.22), an equivalent result had been obtained by Naff [1990] for a conservative tracer. For the effective retardation factor, the result presented in equation (3.20) provides a simple analytical expression to calculate the magnitude of the field scale coefficient of retardation as the plume develops in time. This is perhaps the central and most important finding of the preceeding analysis.

In order to provide a comparison of the theoretical results of this section with actual field experimental estimates of plume characteristics, the following section presents the development of analytical spatial moment expressions for plume retardation, dispersion and asymmetry.

## 3.4 Moment analysis

Spatial moments of solute distributions can be utilized to describe bulk plume characteristics of total mass in solution, plume retardation, macrodispersion and asymmetry. These moments provide an aggregate way to test and compare the analytical results obtained using the spectral stochastic methodology developed in the previous sections.

Spatial moments are obtained by integrating the governing effective transport equation in space. For this case, the partial differential equation of transport for the mean concentration after dropping transverse dispersion terms:

$$R_S\frac{\partial \bar{S}}{\partial t} + v\frac{\partial \bar{S}}{\partial x} = vA_{11}\frac{\partial^2 \bar{S}}{\partial x^2} - \Phi\frac{v}{R_S}A_{11}\frac{\partial^3 \bar{S}}{\partial x^3} \tag{3.24}$$

The equations describing total mass in solution, center of mass displacement, longitudinal second moment and skewness coefficient are presented here and derived in Appendix F.

1. Zeroth moment (total mass in solution), equation (F.6):

$$M_0(t) = \frac{M_T}{R_S(t)} \tag{3.25}$$

2. First moment (center of mass displacement $\bar{x}$), equation (F.12):

$$\bar{x}(t) = \frac{vt}{\bar{R}} + \lambda_1\left(1 - \frac{b_2\sigma_f^2}{\gamma\bar{R}CV_R^2}\right)ln\left[\frac{1 - CV_R^2 exp(-\frac{vt}{\lambda_1\bar{R}})}{1 - CV_R^2}\right] \tag{3.26}$$

3. Second moment (longitudinal plume variance $\sigma_X^2$), equations (F.22) through (F.25):

$$\sigma_X^2(z) = 2\lambda_1^2\left[\frac{\sigma_f^2}{\gamma^2}T_1(z) - 2AT_2(z) + 2B^2T_3(z)\right] \tag{3.27}$$

$$T_1(z) = z + \frac{A}{B}(e^{-z} - 1) - (1 - \frac{A-1}{B} + \frac{A}{B^2})ln\left[\frac{1 - Be^{-z}}{1 - B}\right] \tag{3.28}$$

$$T_2(z) = z + (\frac{2A+1}{B} - 1 - \frac{2A+1}{B^2} + \frac{A^2}{B^3})\left[\frac{1}{1 - Be^{-z}} - \frac{1}{1 - B}\right] + \frac{A^2}{B^2}(e^{-z} - 1)$$
$$+ (1 - \frac{2A+1}{B^2} + \frac{A^2}{B^3})ln\left[\frac{1 - Be^{-z}}{1 - B}\right] \tag{3.29}$$

$$T_3(z) = z + \frac{A^3}{B^3}(e^{-z} - 1) + \frac{(A-B)^3(B-1)}{2B^4}\left(\frac{1}{(1 - Be^{-z})^2} - \frac{1}{(1 - B)^2}\right)$$

$$-\frac{(A-B)^2(B^2+2AB-3A)}{B^4}\left[\frac{1}{1-Be^{-z}}-\frac{1}{1-B}\right]+\frac{3A^3-3A^2B-A^3B+B^4}{B^4}ln\left[\frac{1-Be^{-z}}{1-B}\right] \tag{3.30}$$

with,

$$z=\frac{vt}{\lambda_1 \bar{R}}$$

and,

$$A=\frac{b_2\sigma_f^2}{\gamma\bar{R}}; \qquad B=CV_R^2$$

4. Third moment (plume skewness $S_X$), equation (F.32):

$$S_X(\bar{x})=S_X(0)+\frac{3}{\sigma_X^3(\bar{x})}\frac{\Phi}{R_S}[\sigma_X^2(\bar{x})-\sigma_X^2(0)] \tag{3.31}$$

Theoretical evaluations of the zeroth, first, second and third moments for a solute plume can be performed using parameters for a given field situation. A comparison between the theoretically calculated moments and those estimated on the previously discussed field experiments on Borden and Cape Cod will help in gaining an understanding on the validity and limitations of the stochastic results developed in this work. This is the basis for the discussion of results that follows.

## 3.5 Results and discussion

The analytical expressions derived using the stochastic analysis presented in the previous sections were utilized to calculate the transient effects in the field scale coefficients of retardation and dispersion, and the time evolution of the spatial moments of reactive solute plumes. Two different field cases were considered: the Borden organic tracer test [Roberts *et al.*, 1986] and the Cape Cod tracer test [Garabedian *et al.*, 1988, Garabedian *et al.*, 1991, Hess *et al.*, 1992]. The parameters used in these calculations are listed in Table 3.2.

Table 3.2: Batch scale parameters for Lithium at the Cape Cod site.

| Parameter | Borden | Cape Cod |
|---|---|---|
| $\sigma_f^2$ | 0.29 | 0.24 |
| $\lambda_1(m)$ | 2.8 | 2.6 |
| $v(m/day)$ | 0.1 | 0.4 |
| $\bar{R}$ | 6 | 10 |

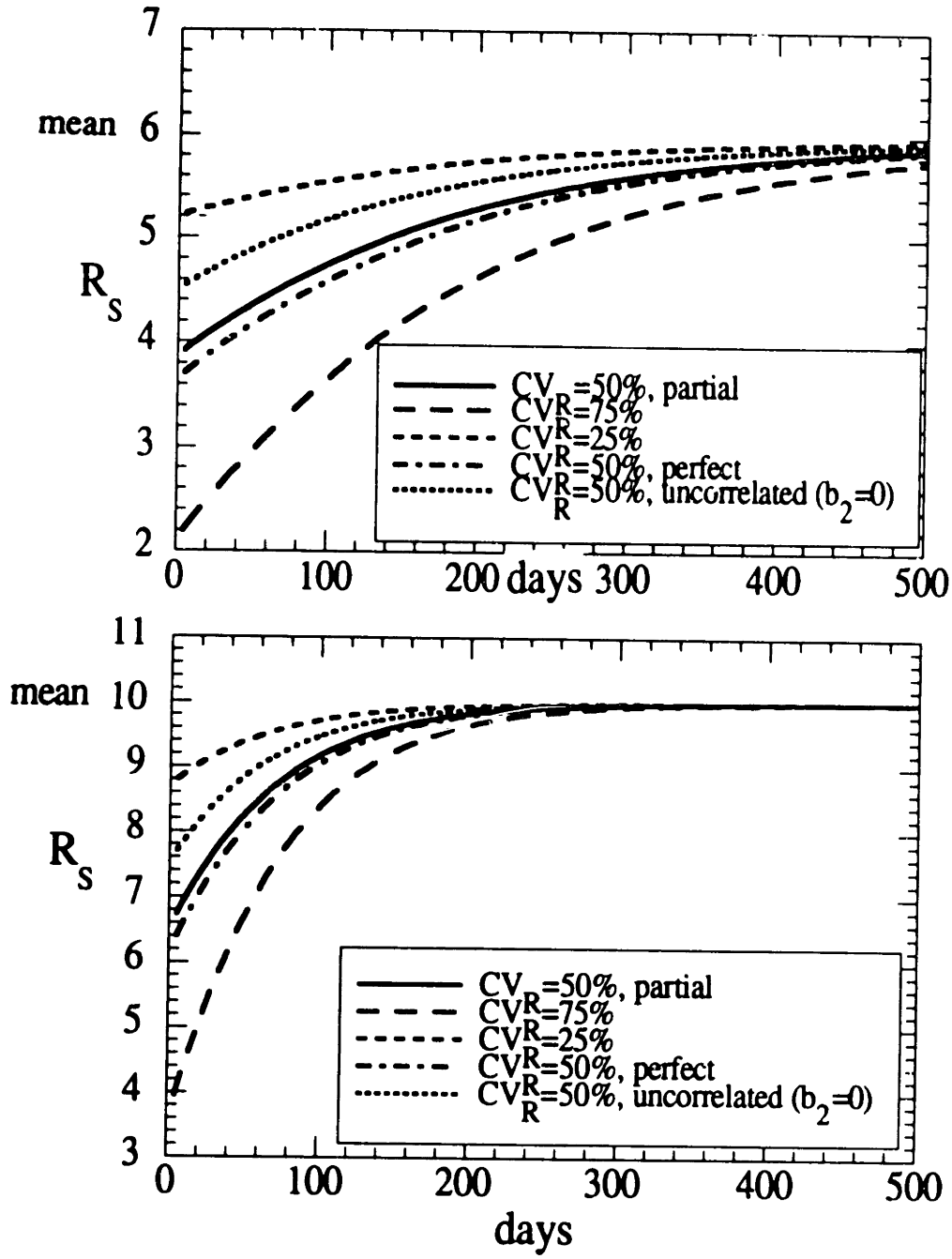


**Figure 3-1: Effective retardation factor $R_S$ obtained using parameters for the Borden (above) and Cape Cod (below) sites**

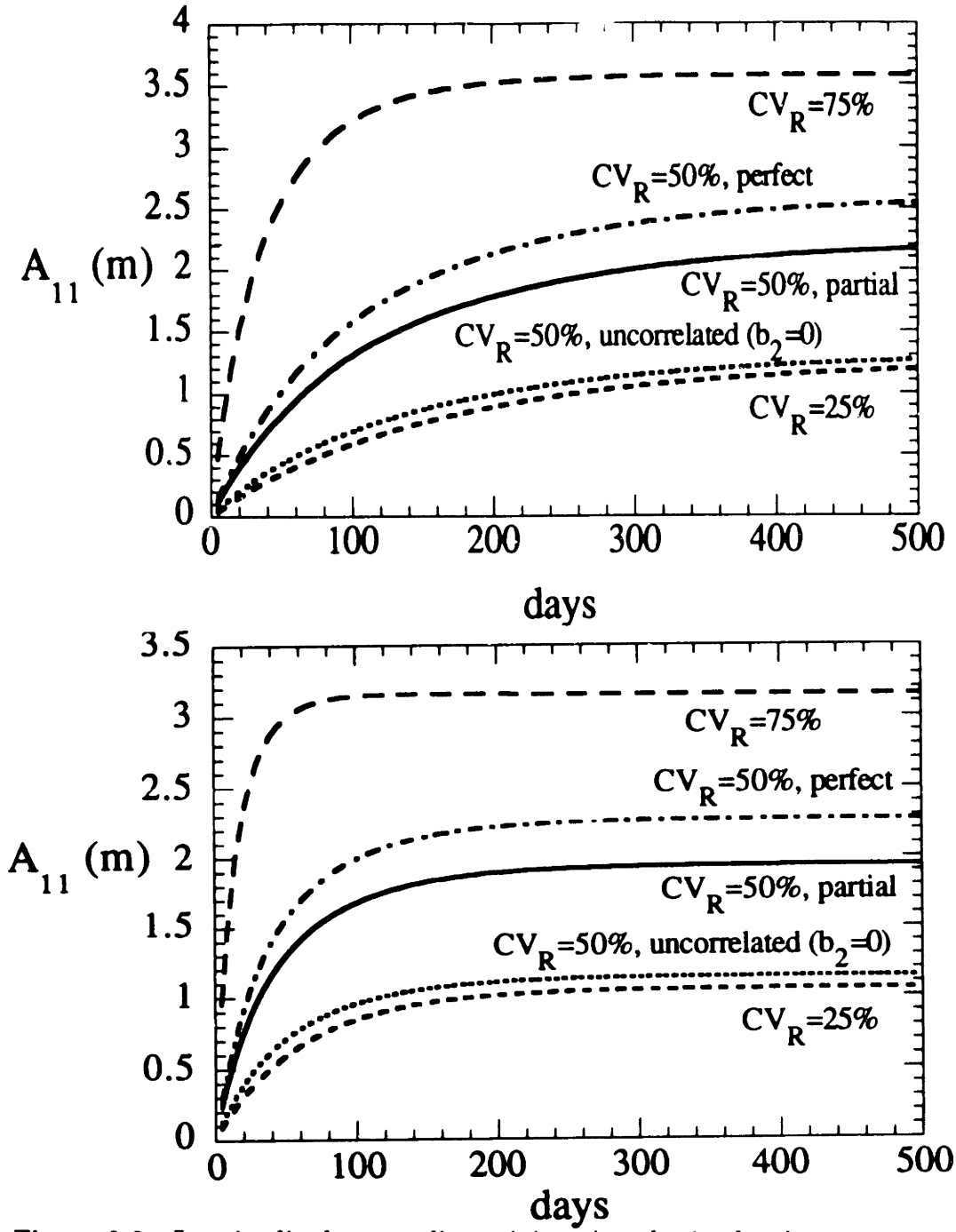


**Figure 3-2:** Longitudinal macrodispersivity $A_{11}$ obtained using parameters for the Borden (above) and Cape Cod (below) sites

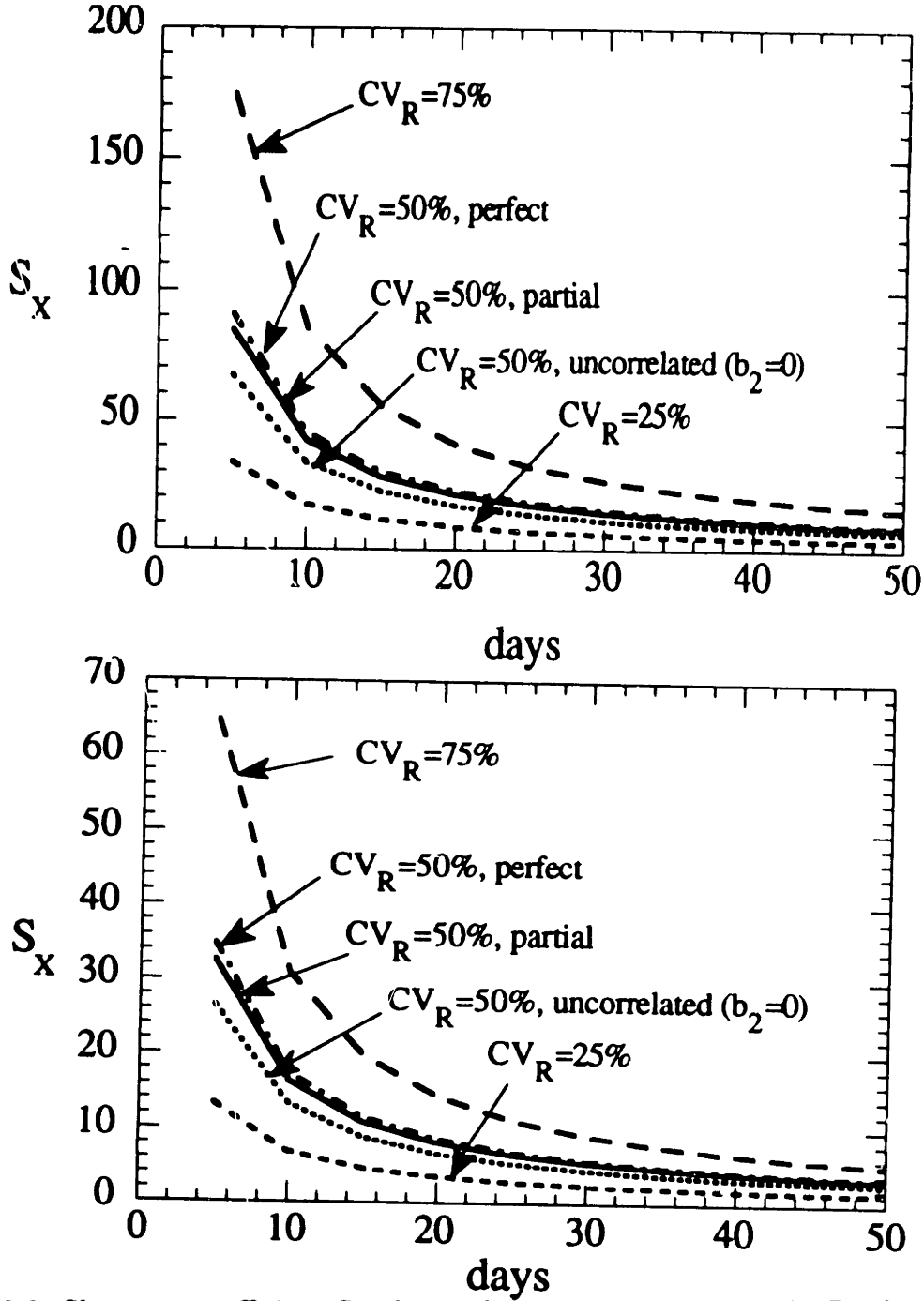





**Figure 3-3:** Skewness coefficient $S_X$ obtained using parameters for the Borden (above) and Cape Cod (below) sites

Figures 3-1 through 3-3 show plots of the time dependent effective retardation factors, longitudinal macrodispersivities and skewness coefficients for the field cases under consideration. The time scale of variation of the effective parameters can be observed to be in the order of hundreds of days for the retardation factor and macrodispersivity, which is consistent with the results presented in Roberts *et al.* [1986] for a number of organic chemicals at Borden. These results also show the same order of magnitude for the time scale using parameters for the Cape Cod site. This time scale, predicted from the heterogeneous nature of the aquifer material in equations (3.20) and (3.22) is able to represent what is observed in the field. The asymptotic limits for the effective retardation factor and longitudinal macrodispersivity are reached after a mean displacement $\frac{vt}{R}$ of about 10 correlation lengths $\lambda_1$.

The time evolution of the skewness coefficient shows a sharp decay after a short period of time. No estimates of third moments for any of these reactive plumes is found in the literature surveyed that could aid in the comparison with the stochastic theory results. The numerical results of Dasinger [1989] for a conservative solute also show a rapid decay of the plume skewness with mean travel distance.

### 3.5.1 Analysis of the Borden organic tracer test

Although there have been estimates of spatial moments for conservative tracers [Freyberg, 1986, Rajaram and Gelhar, 1991], no estimates of second or third moments for reactive plumes has been reported for the Borden organic tracers. Because of this gap in field moment estimates for the Borden site, the data set for these organic compounds, *i.e.*, Carbon Tetrachloride $CCl_4$, Bromoform $CHBr_3$, Tetrachloroethene $PCE$, Dichlorobenzene $DCB$ and Hexachloroethane $HCE$, was analyzed using the procedure outlined in Rajaram and Gelhar [1991] for the zeroth through third spatial moments to estimate total mass in solution, center of mass displacement, longitudinal second moments and skewness coefficients.

Table 3.3: Classification of organic chemicals data at Borden

| Date | Days | CTET | BROM | PCE | DCB | HCE |
|---|---|---|---|---|---|---|
| 08/24/82 | 1 | R[1] | L[2] | NR[4] | NR | NR |
| 09/01/82 | 9 | L | L | NR | R | N[3] |
| 09/08/82 | 16 | N | N | NR | N | N |
| 09/21/82 | 29 | R | R | N | L | L |
| 10/05/82 | 43 | N | N | N | N | N |
| 10/25/82 | 65 | N | N | N | N | N |
| 11/17/82 | 85 | L | R | R | N | N |
| 09/08/83 | 380 | R | R | L | N | BDL[5] |
| 10/04/83 | 407 | L | L | L | L | BDL |
| 05/18/84 | 633 | L | N | L | N | BDL |
| 08/01/84 | 709 | N | N | N | N | BDL |

This data set was divided into eleven snapshots of each of the organic plumes that take place over a period of two years, from August 1982 to August 1984. The data was then visualized in three dimensions in order to provide a judgement about the extent to which the plumes had been sampled spatially. Rajaram and Gelhar [1991] report some plume truncation occuring for the conservative tracer plume data set. Each of the snapshots was then classified according to their reliability in terms of whether or not they capture most of the spatial extent of the organic plumes. This classification is presented in Table 3.3. Some examples to illustrate the classification criterion are presented in Figures 3-4 through 3-6.

[1] R: Data set is reliable
[2] L: Data set is less reliable
[3] N: Data set is not reliable
[4] NR: Concentration field not reported at this sampling session
[5] NR: Concentration field below detection limit

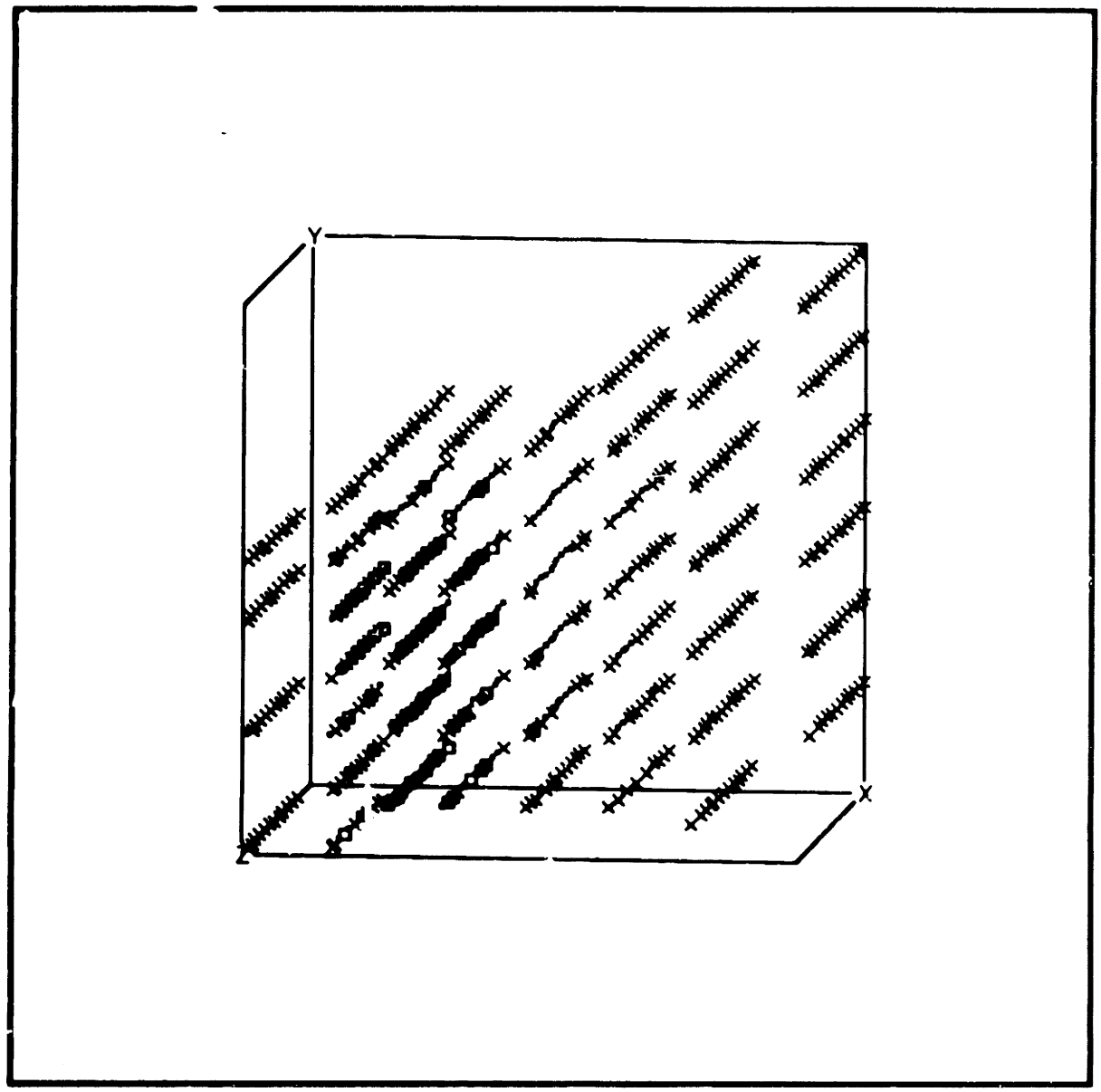


Figure 3-4: Examples of reliable data sets on the Borden site organic tracer test

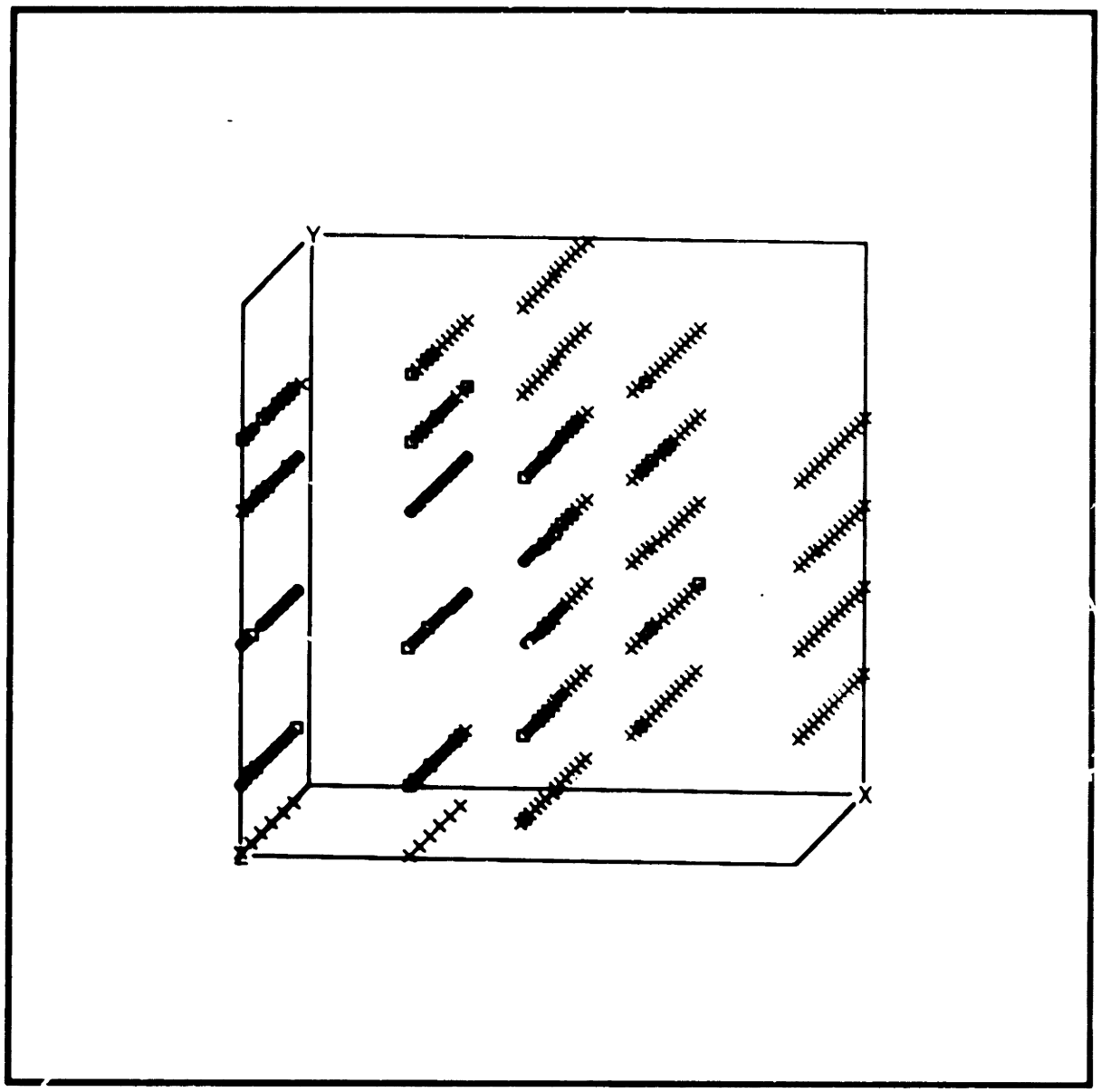


Figure 3-6: Examples of not reliable data sets on the Borden site organic tracer test

Unfortunately, in most cases the plumes have been truncated, so the reliability of the moments that are estimated using this data is highly questionable, and a statement of validity of the stochastic theory predictions cannot be made to this point. The results of this data analysis is presented here in terms of spatial moment estimates, and the associated theoretical results are compared to the experimental estimates for $CCl_4$ and $PCE$. The moment estimates curves are presented as a function of the variability of the retardation factor and its correlation with log-hydraulic conductivity. Case 1 corresponds to a coefficient of variation $CV_R = 75\%$ and a partial correlation with log-hydraulic conductivity, this is, the variance is divided equally between a correlation with $f = lnK$ given by a slope $b_2$, and an uncorrelated residual $g_2$, as in Chapter 2. Cases 2,3 and 4 show results using a $CV_R = 50\%$ with the random field $R$ perfectly correlated, partially correlated and uncorrelated ($b_2 = 0$)with $f = lnK$. Case 5 presents the results for $CV_R = 25\%$, partially correlated. It is apparent that the spatial moments, specially the longitudinal second moment, are quite sensitive to variability of the retardation factor, and that quantifying this variability is important in obtaining better estimates of these moments.

The compounds Bromoform, Dichlorobenzene and Hexachloroethane have been reported to undergo a decay process [Roberts *et al.*, 1986], and the calculations performed as part of this work also suggest that some mass of these compounds is disappearing, which makes their comparison with the theoretical results a useless task, since the analysis presented in the previous sections does not account for solute decay. The estimates for $HCE$ have been omitted since the data for this compound was either unreliable or non-existent. The estimates for the rest of the compounds are presented in Figures 3-7 through 3-10.

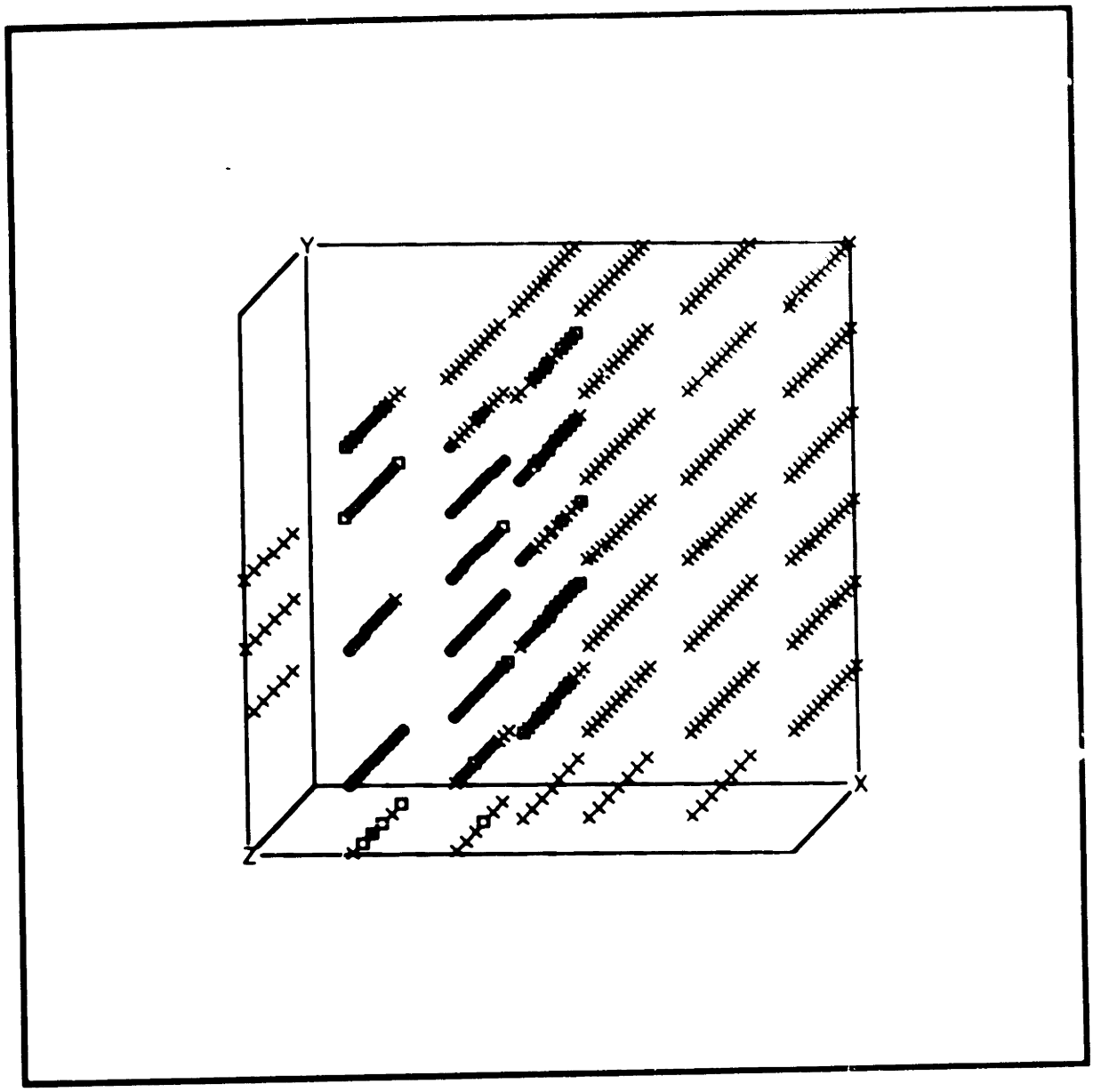


Figure 3-5: Examples of less reliable data sets on the Borden site organic tracer test

DCB 09/21/82

x (0-1 ppb)
□ (1-10 ppb)
● (10-100 ppb)

Unfortunately, in most cases the plumes have been truncated, so the reliability of the moments that are estimated using this data is highly questionable, and a statement of validity of the stochastic theory predictions cannot be made to this point. The results of this data analysis is presented here in terms of spatial moment estimates, and the associated theoretical results are compared to the experimental estimates for $CCl_4$ and $PCE$. The moment estimates curves are presented as a function of the variability of the retardation factor and its correlation with log-hydraulic conductivity. Case 1 corresponds to a coefficient of variation $CV_R = 75\%$ and a partial correlation with log-hydraulic conductivity, this is, the variance is divided equally between a correlation with $f = lnK$ given by a slope $b_2$, and an uncorrelated residual $g_2$, as in Chapter 2. Cases 2,3 and 4 show results using a $CV_R = 50\%$ with the random field $R$ perfectly correlated, partially correlated and uncorrelated ($b_2 = 0$)with $f = lnK$. Case 5 presents the results for $CV_R = 25\%$, partially correlated. It is apparent that the spatial moments, specially the longitudinal second moment, are quite sensitive to variability of the retardation factor, and that quantifying this variability is important in obtaining better estimates of these moments.

The compounds Bromoform, Dichlorobenzene and Hexachloroethane have been reported to undergo a decay process [Roberts *et al.*, 1986], and the calculations performed as part of this work also suggest that some mass of these compounds is disappearing, which makes their comparison with the theoretical results a useless task, since the analysis presented in the previous sections does not account for solute decay. The estimates for $HCE$ have been omitted since the data for this compound was either unreliable or non-existent. The estimates for the rest of the compounds are presented in Figures 3-7 through 3-10.

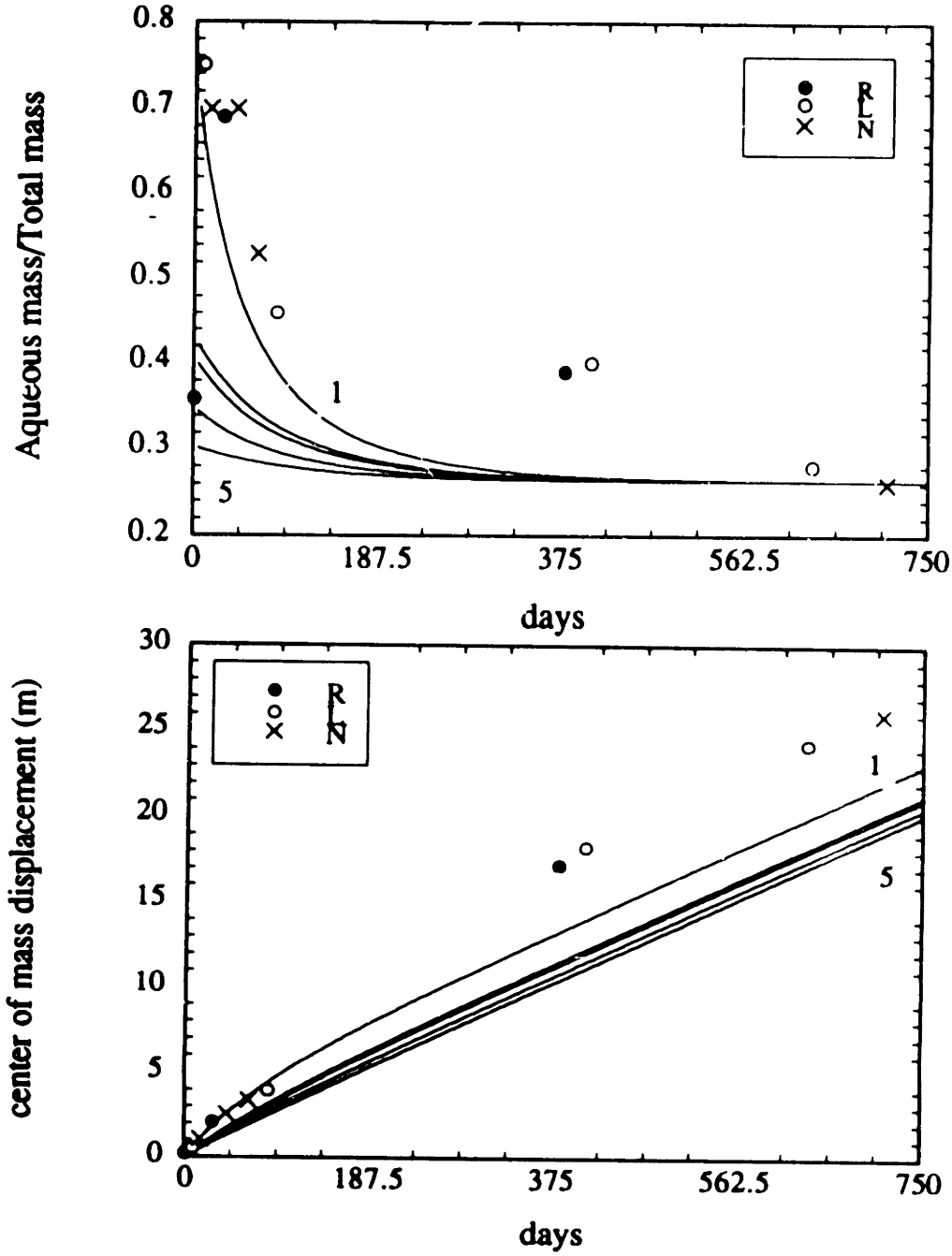





Figure 3-7: Estimates of spatial moments and stochastic theory applications for $CCl_4$ at the Borden site (this and next page)

Figure 3-7 (cont.)

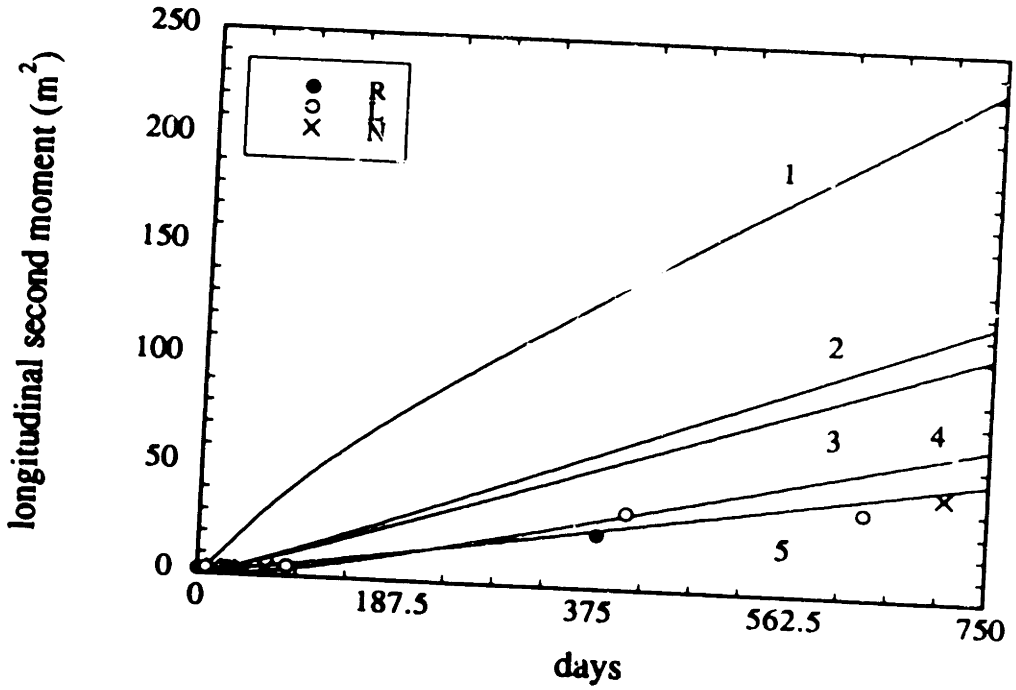


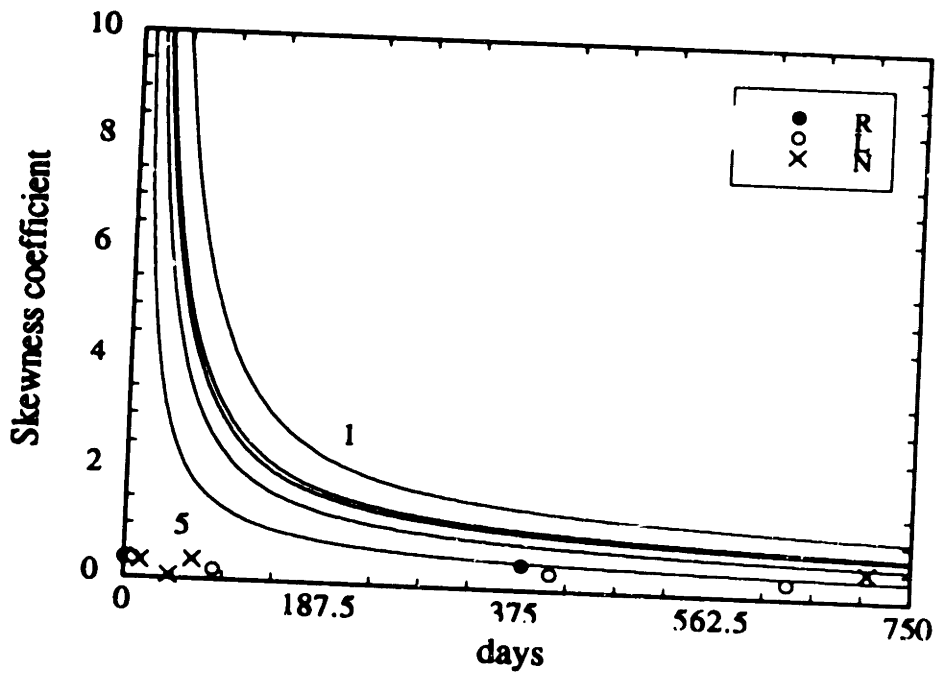

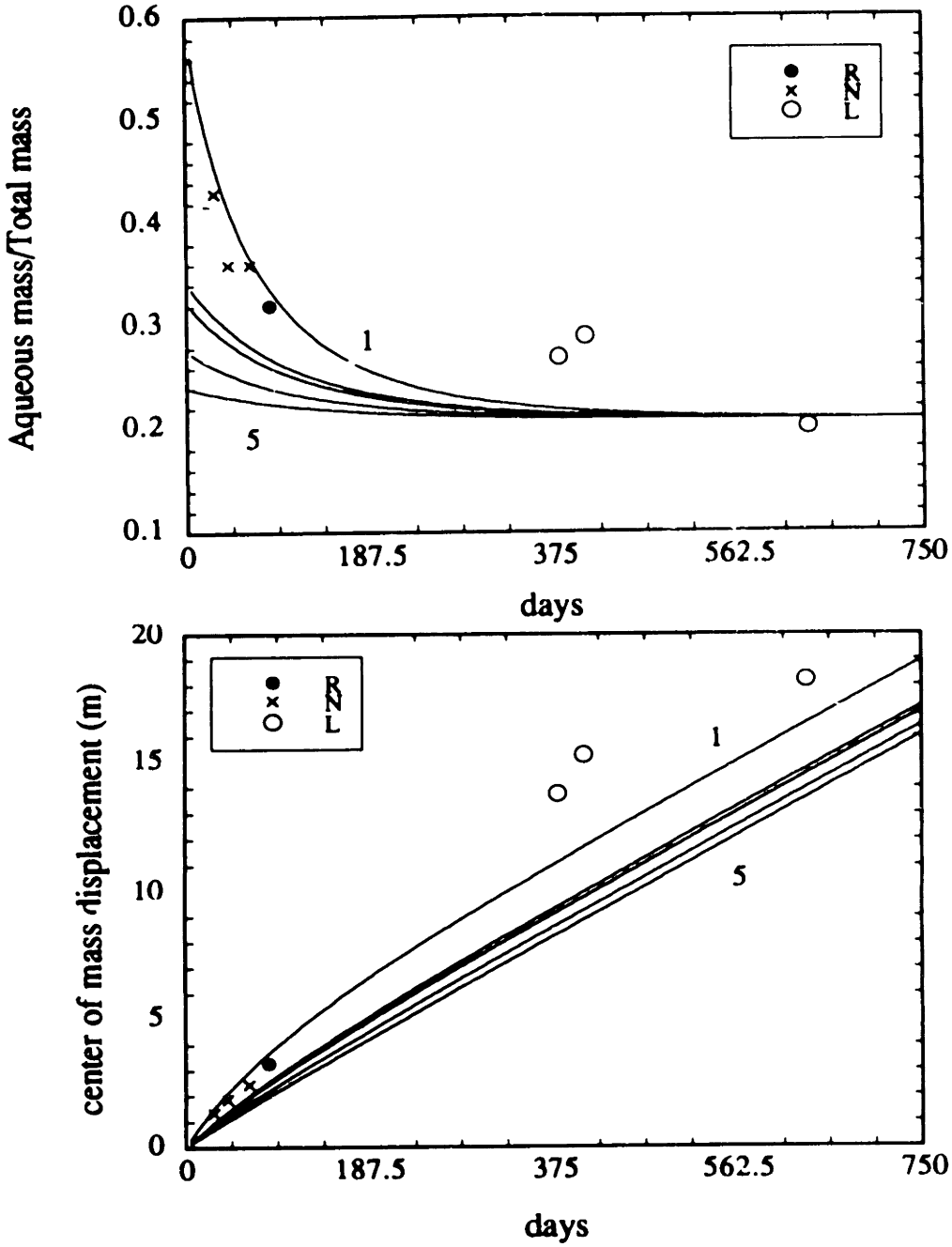


Figure 3-8: Estimates of spatial moments and stochastic theory applications for $PCE$ at the Borden site (this and next page).

Figure 3-8 (cont.)

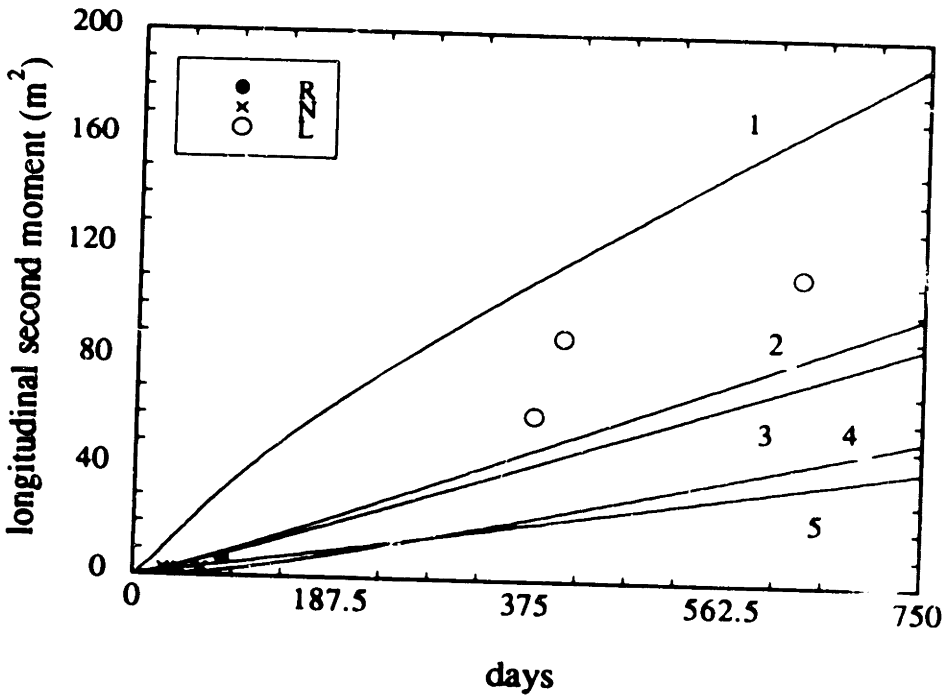


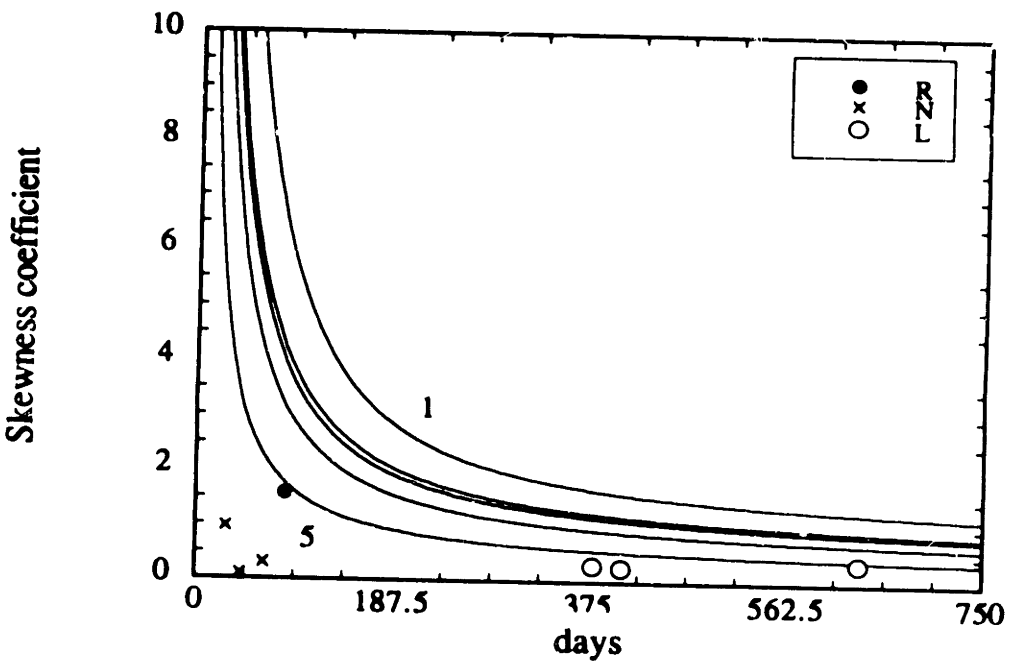

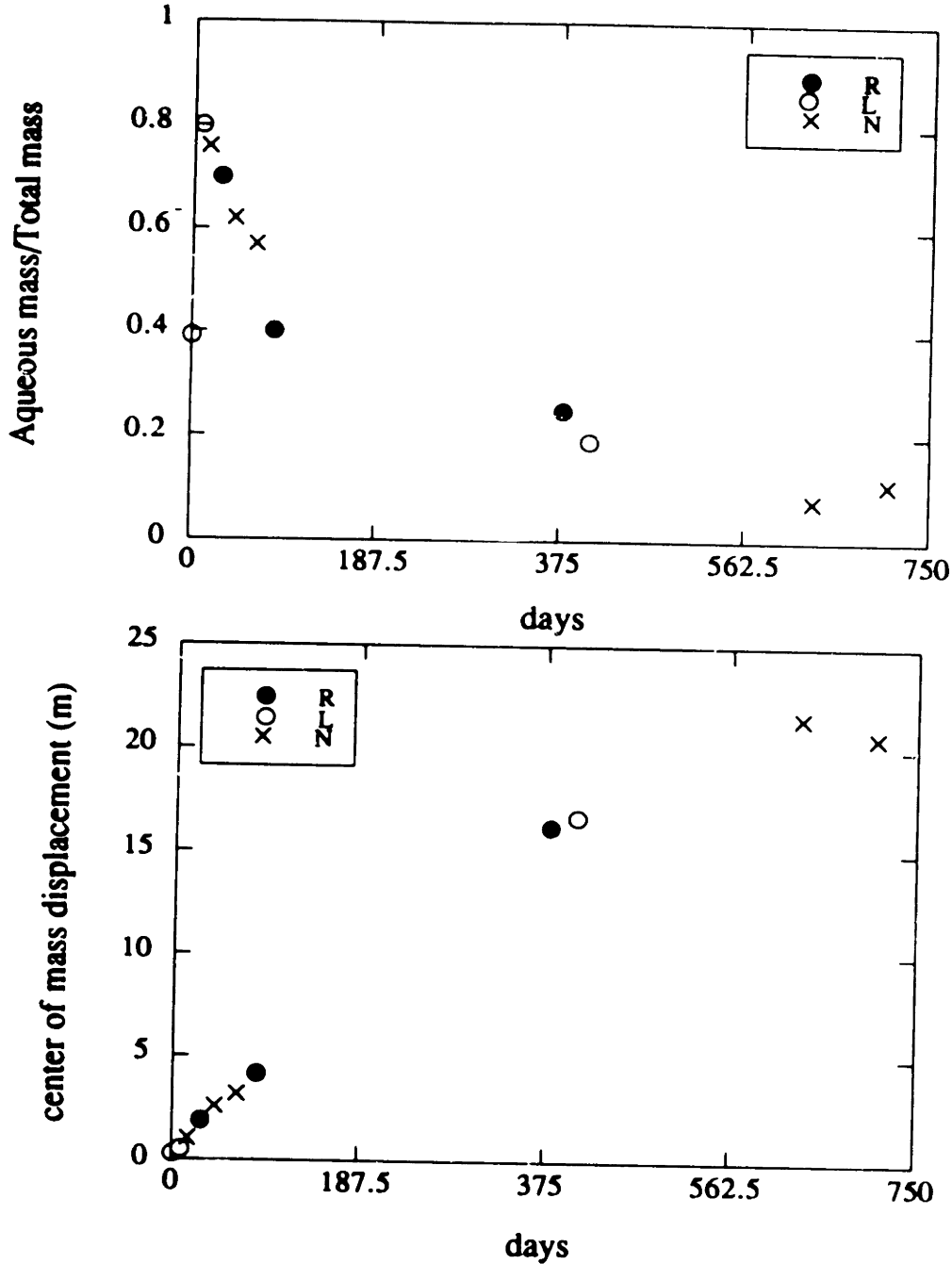


Figure 3-9: Estimates of spatial moments for $CHBr_3$ at the Borden site (this and next page).

Figure 3-9 (cont.)

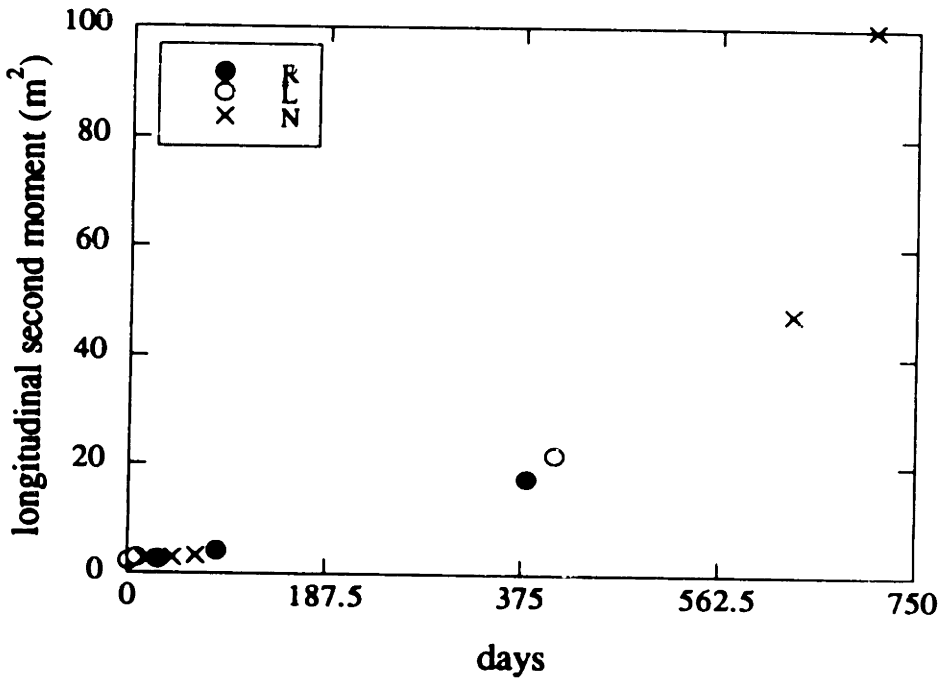

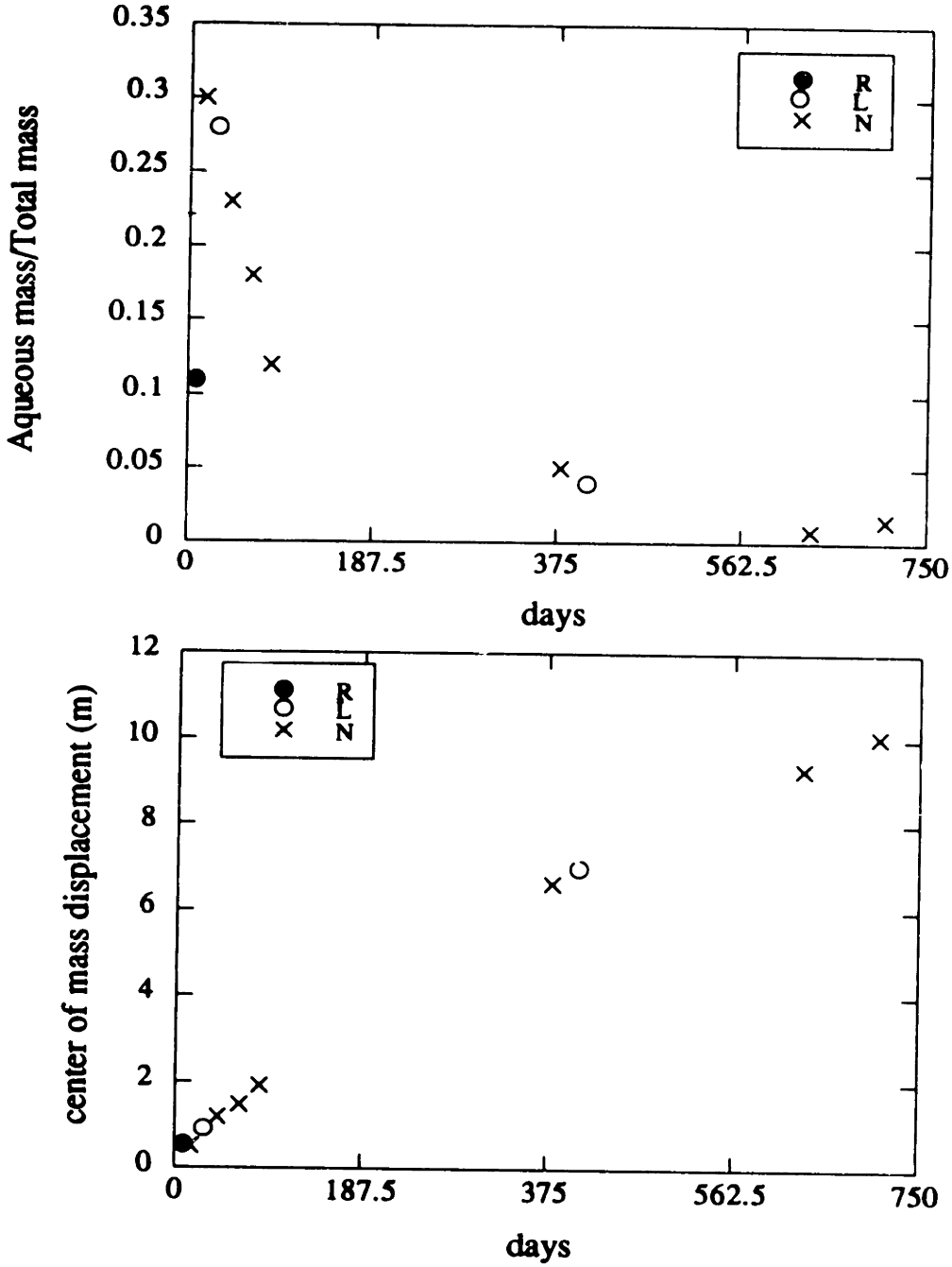


Figure 3-10: Estimates of spatial moments for $DCB$ at the Borden site (this and next page).

Figure 3-10 (cont.)

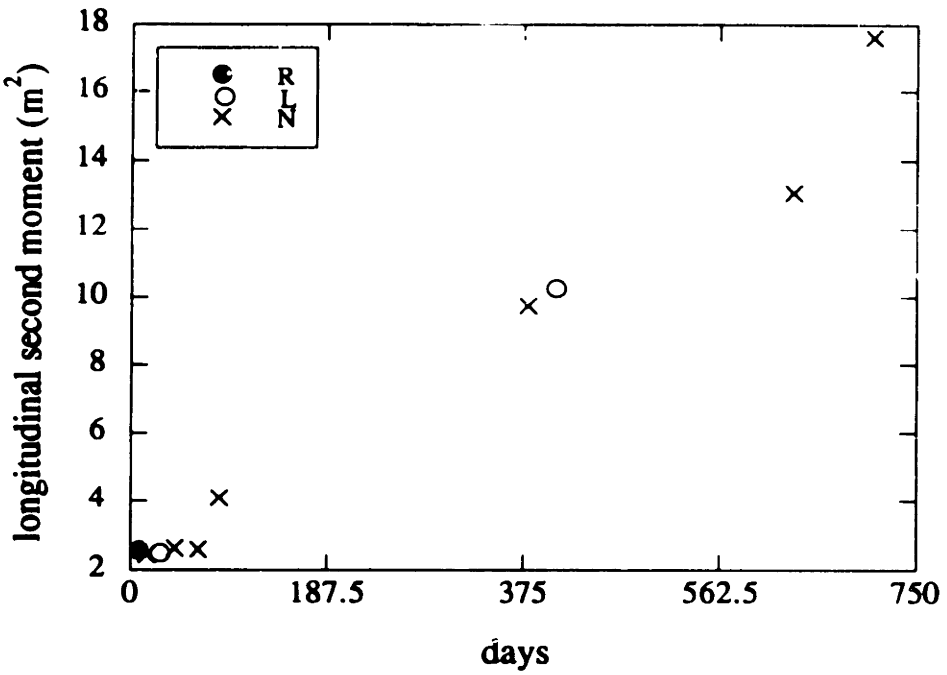

### 3.5.2 Comparison with numerical simulations

The numerical simulations of Burr [1992] for reactive solute transport were compared to the stochastic results derived for the spatial moments. The parameters used in these simulations are:

- $\sigma_f^2 = 0.18$
- $\lambda_1 = \lambda_2 = 5.1m$; $\lambda_3 = 0.2m$
- $\alpha_T = 0.005m$
- $\bar{R} = 4.8$; $CV_R = 0.38$ (perfectly correlated with $f = lnK$)
- $v = 0.082\frac{m}{day}$

A comparison of the results for the first and second moments is given in Figure 3-11. In order to account for source and domain size effects in the simulations, the analytical results are corrected by the ratio of the numerical to analytical nonreactive longitudinal macrodispersivity. The numerically computed conservative solute macrodispersivity is $0.43m$, and the analytical result is $\frac{\sigma_f^2 \lambda_1}{\bar{R}^2} = 0.77m$. The ratio is then 0.56 for this case. Even with these effects accounted for, there is a difference between the analytical and numerical results for the longitudinal second moment. This difference can be explained by the fact that local dispersion effects in the vertical direction ($i = 3$) become important in these calculations. The parameter describing transverse dispersion influence in the vertical direction is [Gelhar and Axness, 1983]:

$$r = \frac{\alpha_T \lambda_1}{\lambda_3^2} = 0.6 \approx O(1)$$

So, given these parameters, it is apparent that transverse dispersion effects in the vertical direction cannot be neglected. These effects produce a lesser longitudinal macrodispersivity [Gelhar and Axness, 1983]. Naff [1990] presents a numerical evaluation of an exact analytical expression for the effect of the

transverse dispersion. For this value of the nondimensional parameter $r$, a reduction in the longitudinal dispersivity on the order of 25% can be expected for this case. This correction would decrease the gap between the longitudinal second moment curves in Figure 3-11.

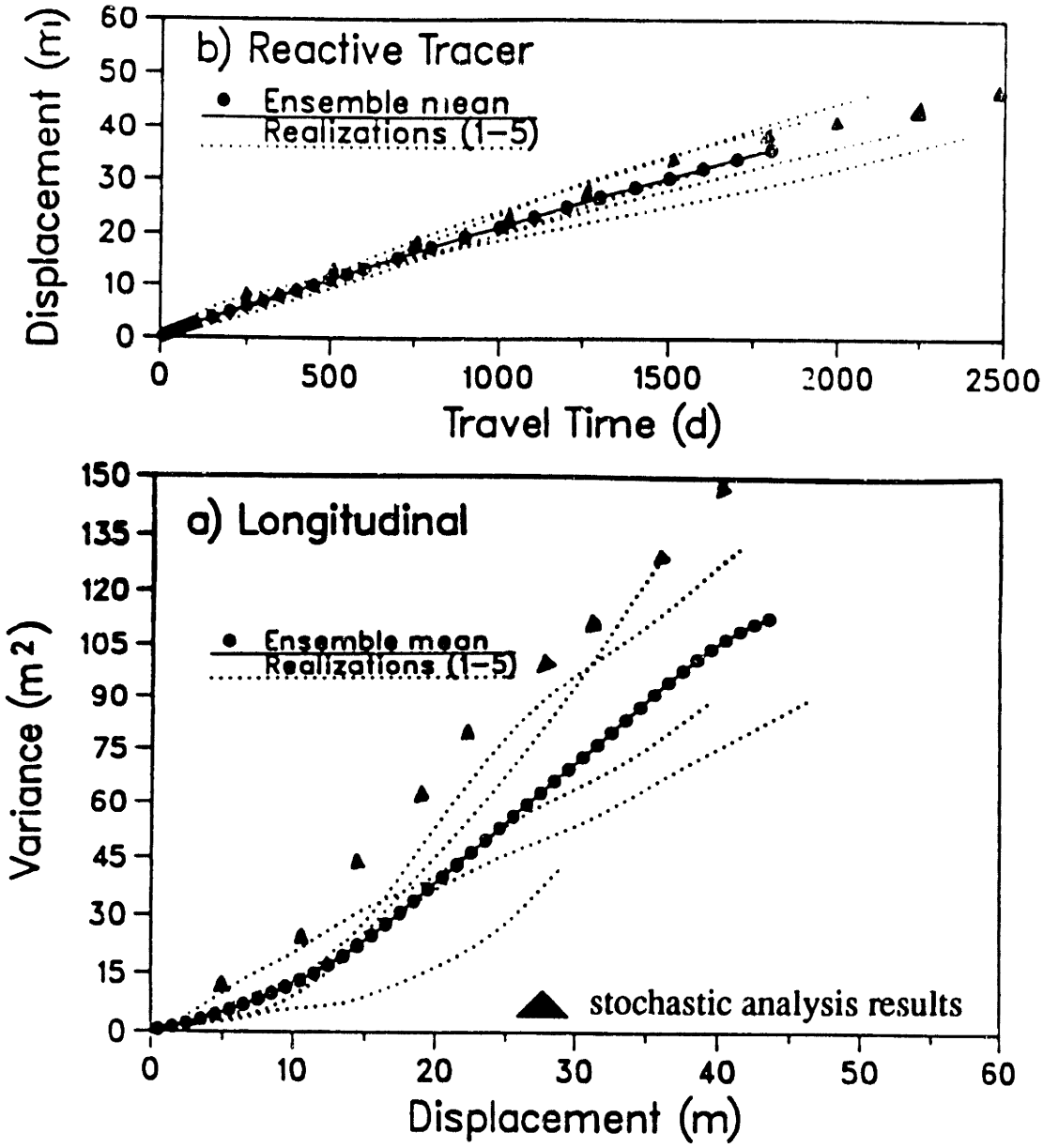


Figure 3-11: Comparison of analytical results with the numerical simulations of Burr [1992] for the first and second longitudinal spatial moments. The triangular marks correspond to analytical evaluations of the spatial moments using the effective coefficients derived through the stochastic theory.

### 3.5.3 Application to the Cape Cod reactive tracer test

The estimates of zeroth, first and second moments presented in Garabedian *et al.* [1988] are compared here with results obtained using the prediction equations for these moments, equations (3.25) through (3.31). This comparison does not yield satisfactory results in terms of the applicability of the stochastic theory, as it is shown in Figures 3-12 through 3-14. However, for this case, where the sorbate chemical is Lithium, the sorption isotherms that have been reported in Garabedian *et al.* [1988] are nonlinear (see Figure 3-15), so the analysis developed here under the assumption of a linear isotherm cannot be expected to reproduce these results. An approximate analysis using *Freundlich* type isotherms that yields somewhat improved results is presented in Appendix G.

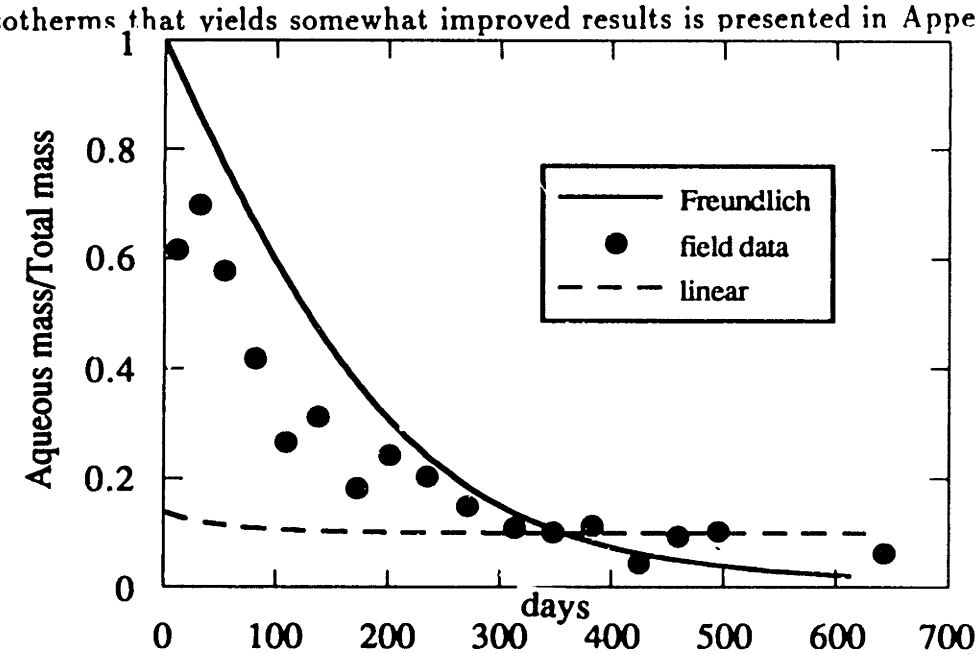


Figure 3-12: Estimates of zeroth moments for Lithium at the Cape Cod site.

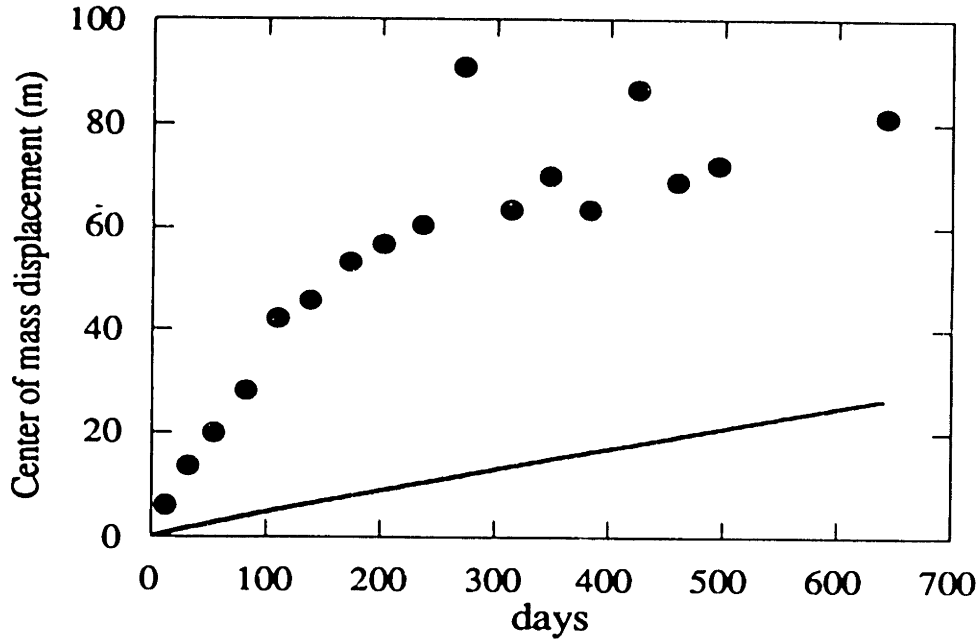


Figure 3-13: Estimates of first moments for Lithium at the Cape Cod site.

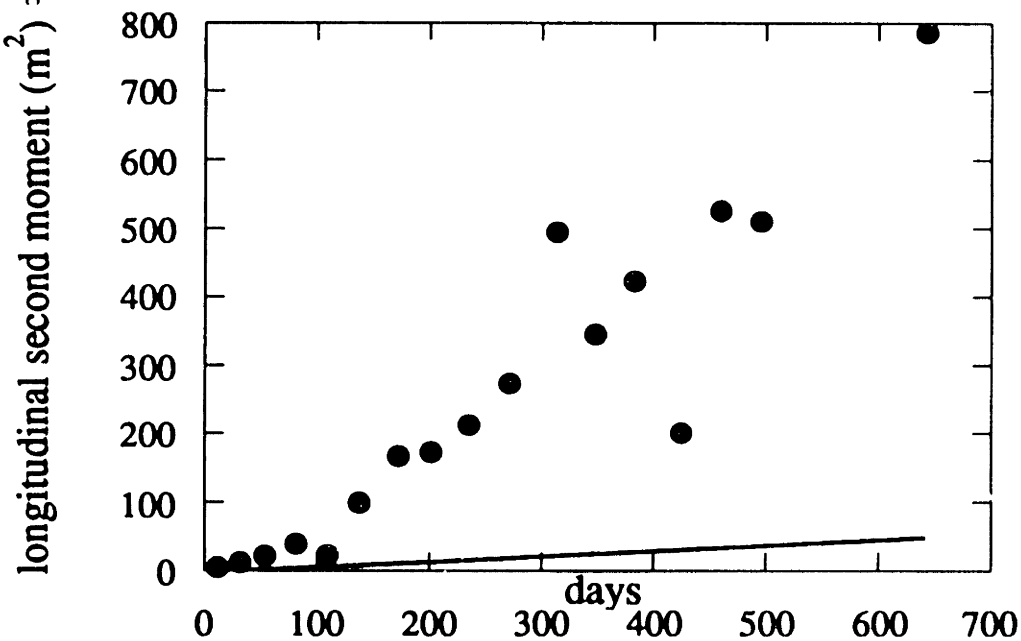


Figure 3-14: Estimates of second moments for Lithium at the Cape Cod site.

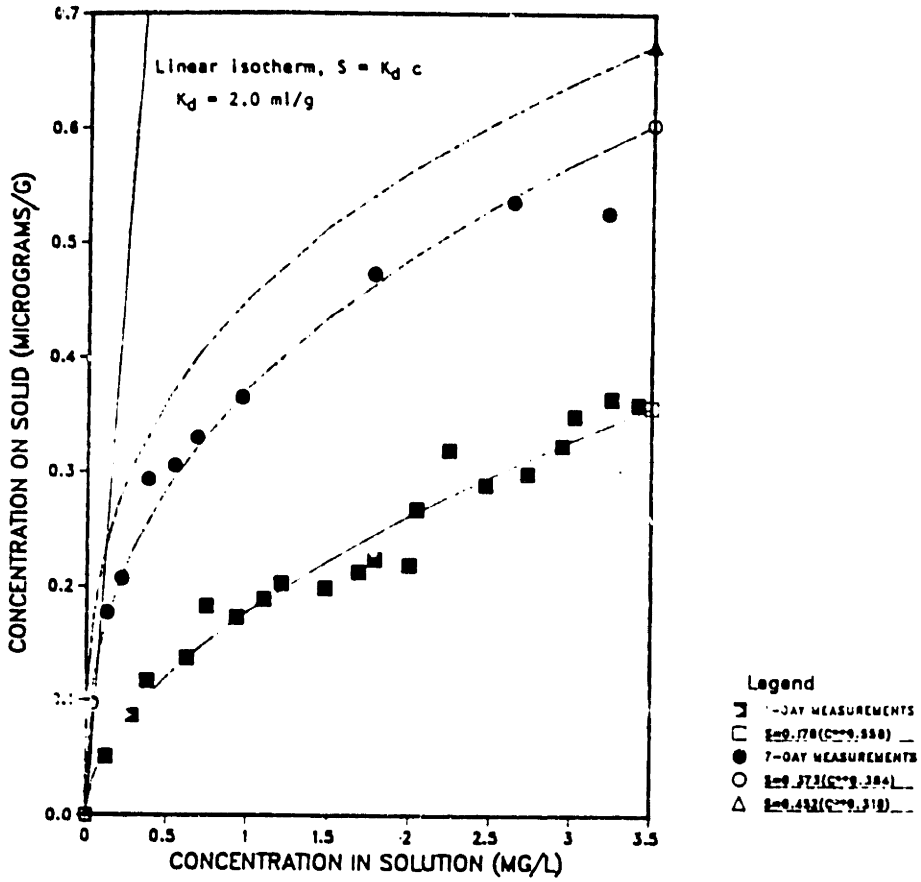


Figure 3-15: Nonlinear sorption isotherms for Lithium at the Cape Cod site, from Garabedian *et al.*, [1988].

The following are plots showing the effective retardation factor and longitudinal macrodispersivity as a function of the mean concentration $\bar{S}$. Notice that as time passes and the mean concentration is decreased as a result of dissolution, in Figure 3-16 the effective retardation factor is increased, so the slope of the first moment in time is decreased. This explains the downward concave shape of the curve on Figure 3-13. In Figure 3-17, by the same token, as concentrations decrease in time, the macrodispersivity increases, and so the slope of the longitudinal second moment in time as presented in Figure 3-14. In view of this, it is apparent that nonlinearities in the sorption isotherm must be considered to adequately represent retardation of chemicals wich are sorbed according to this class of isotherms.

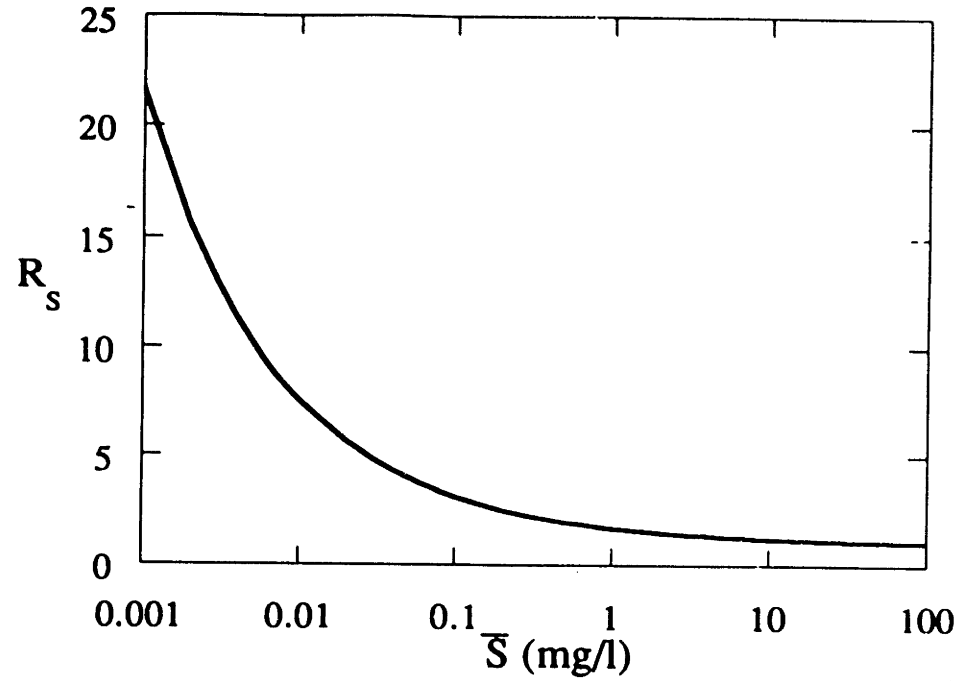


Figure 3-16: Effective nonlinear retardation factor using parameters for Lithium sorption at the Cape Cod site.

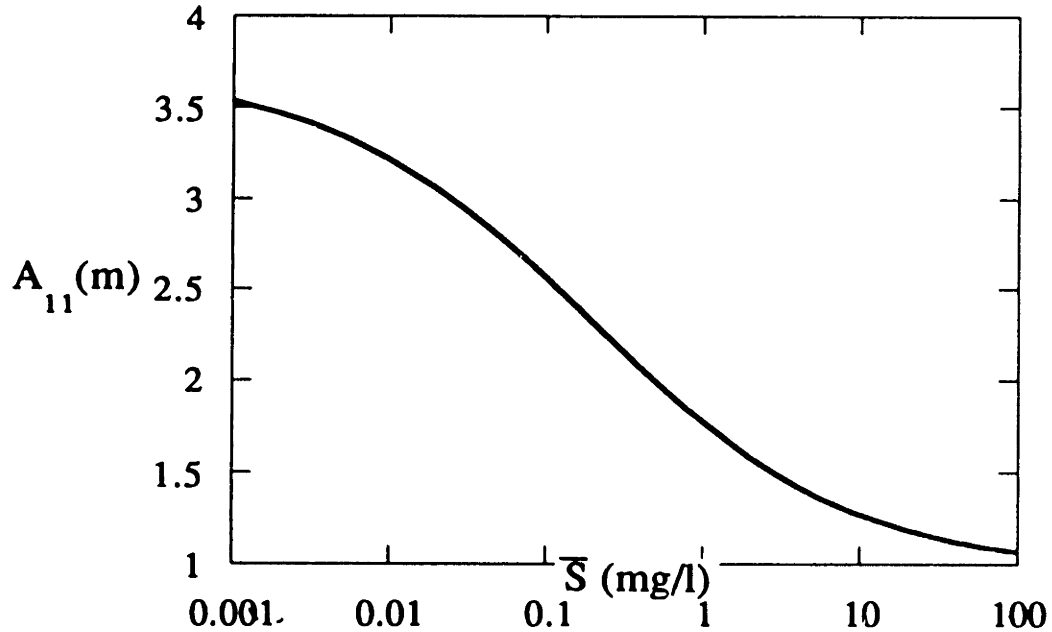


Figure 3-17: Nonlinear longitudinal macrodispersivity using parameters for Lithium sorption at the Cape Cod site.

## 3.6 Concluding remarks

### 3.6.1 Spatial moments evolution

The transient analysis of the effective retardation factor and macrodispersivity for the linear isotherm case allows for an analytical evaluation of the zeroth, first, second and third moments for a reactive solute plume in time. These moments represent respectively the mass in solution, center of mass displacement, plume variance and skewness coefficient. These expressions were used to assess the applicability of the developed stochastic approach to experimental investigations [Roberts *et al.*, 1986].

Zeroth moment calculations for the Borden site were in reasonable agreement with the estimates obtained from the tracer test data, although these estimates are questionable given the significant truncation on some of the data snapshots. For the Cape Cod site, the theory developed using a linear form for the sorption isotherm does not seem to be reproduce field moment estimates. This may be explained by the fact that a local nonlinear isotherm has been observed. An approximate calculation of the zeroth moment evolution assuming a Gaussian concentration profile yields results that compare favorably to these field observations of mass in solution. This indicates that nonlinearities in the isotherm play an important role in the field scale characteristics of reactive plumes, and that linear isotherms should not be used in modeling transport of solutes that are subject to an ion exchange process, such as lithium at Cape Cod.

Calculations for the first moment also indicate a significant agreement with field experiments for the linear isotherm case at Borden. The better spatial moment predictions occured with the zeroth and first moments estimates for all the organic tracers. The effects of data truncation are more pronounced in the longitudinal second moment prediction for the Borden case, although the right order of magnitude can be estimated for its time evolution using the stochastic analysis results. For the third moment, the theory was not validated

using the Borden data. It is apparent that truncation influences on the skewness coefficient is strong, since no trend was observed in estimates of this parameter, and the sharp decrease in time predicted by the stochastic theory is not present in the results.

For the nonlinear sorption case at the Cape Cod site, the concentration dependence of the retardation factor can be used to explain qualitatively the concave time evolution curve for the center of mass displacement. Also, the concentration dependence of the longitudinal macrodispersivity is able to explain the increasing slope observed in the time evolution curve for the second moment in the nonlinear case. An analytical evaluation of the nonlinear sorption process was not possible for the first and higher moments.

The asymmetry observed in field plumes, where the concentration contours exhibit so called tails of low concentrations towards the point of injection can be explained in terms of natural heterogeneities. This analysis predicts a positive value for the skewness coefficient, so that the concentration profiles are expected to be skewed to the back of the plume, which indeed has been shown to occur in the field. Results presented in Chapter 2 using parameters for the Cape Cod and Borden sites, suggest that the influence of the intragrain diffusion mechanism is not significant relative to the asymmetry produced by the aquifer variability for values of the tortousity parameter of $2 - 3$. In this range of tortuosities, this points in the direction of recommending modeling of the sorption process in the field as a one-stage process, where the time evolution of plume skewness is controlled by natural aquifer heterogeneities.

### 3.6.2 General

The following is a list of the main findings resulting from a stochastic analysis of time-dependent sorption in heterogeneous aquifers.

(a) The time-dependence of the field scale retardation factor observed in the Borden site plume [Roberts *et al.*, 1986] can be explained by an analysis of the time evolution of the cross-correlation between retardation and concentration perturbations. An exact formulation valid for all times is obtained, with the effective retardation factor asymptotically approaching the mean value after large travel distance/time (see next conclusion). Developing times calculations performed using parameters corresponding to the Borden plume are in agreement with the time scales observed in the field. Calculations of the time scales associated with intragranular diffusion/sorption at this site indicate that this process can explain local, short-time characteristics of the Borden plume, but that these do not prevail at the field scale travel times. At other field sites, the time scale of the effective retardation factor is a result of the competing intragrain processes and aquifer heterogeneities. The analysis developed in this Chapter provides a theoretical framework to evaluate the controlling mechanism at a field scale.

(b) The transient analysis for the longitudinal macrodispersivity indicates that it is initially proportional to the mean travel distance and that the asymptotic limit presented by Garabedian *et al.* [1988] is reached after a travel distance in the order of 4 times this value. This developing distance also applies for the effective retardation factor.

(c) Calculations of sensitivity to these parameters verifies that the macrodispersivity is significantly influenced by the correlation between retardation and log-hydraulic conductivity, and that the effective transport coefficients are relatively insensitive to the intragrain diffusion/sorption process when the characteristic time of this process is much smaller than that corresponding to natural heterogeneities. This is the case for the calculations performed using parameters for PCE sorption at Borden. This yields two important recommendations. First, detailed paired measurements of distribution coefficients and hydraulic conductivity measurements are necessary

in order to quantify the correlation between these variables, a dominant parameter in the results obtained. Second, a realistic modeling of sorption at a field scale can be achieved by considering it a single stage equilibrium process if the time scales involved for intragrain processes are found to be much smaller than those calculated from natural aquifer variability. Expressions for both of these time scales have been derived and presented here.

# Part II

# Stochastic analysis of oxygen-limited biodegradation in groundwater

# Chapter 4

# Modeling biodegradation in heterogeneous aquifers with a steady microbial population

## 4.1 Introduction

Biodegradation of organic contaminants in groundwater is a problem that brings together three different research areas. The first, groundwater flow physics, has been a traditional problem studied among hydrologists and engineers. The second, the partitioning process of the contaminant mass between the solid and aqueous phases in an aquifer has been investigated by chemists for some time now. The third is the way by which the indigenous microbial populations interact with the physics and chemistry of the medium to degrade the undesired contaminant. Considering the important influence biodegradation may have in the fate of environmentally hazardous chemicals, it is apparent that we should begin to incorporate microbial processes into our conceptual and quantitative models of subsurface contaminant transport. This is a sizable challenge because microbial systems are quite complex and probably less understood than the

hydrological and chemical components of these models. In order to assemble a model capable of estimating dispersion, sorption and biodegradation rates over scales larger than those in laboratory experiments, the spatial variability of the hydrological, chemical and microbiological processes involved must be considered in a systematic way. This inherent variability can be treated using a stochastic description that conceives these processes as being random.

The idea of a stochastic approach to analyze the dispersion of solutes transported in aquifers is not a new one. There exist a number of research efforts which have used stochastic methods to predict field-scale coefficients of dispersion. Gelhar and Axness [1983]; Gelhar *et al.* [1979] and the papers by Dagan [1984],[1988] can be viewed as the most representative of these efforts. In all of these cases, the theory predicts coefficients of dispersion, referred to as macrodispersivities, that are much larger than those obtained in laboratory column experiments. This theory is able to explain the results of field tracer tests, where dispersion is also found to be larger than that measured at a laboratory scale [Sudicky and Cherry, 1979]. The underlying cause of this increase in dispersion is the heterogeneity of the hydraulic conductivity in the aquifer. This heterogeneity can cause significant variations in fluid velocity that result in an increase spreading by separating the solute plume into packets that move at different rates.

Sorption of organic chemicals in the subsurface can be often described by using local equilibrium considerations. Perhaps the simplest description is the assumption of a linear reversible equilibrium relationship between the amount of contaminant in the sorbed and solution phases. Garabedian *et al.* [1988] use this linear approximation and find that the distribution and mixing of a reactive solute is strongly affected by heterogeneous adsorption to aquifer sediments. Their results show an order of magnitude increase in the longitudinal macrodispersion with the underlying source of heterogeneity being the variability of hydraulic conductivity.

At a field scale, microbiological processes are perhaps the least understood of the three components of this problem. The growth dynamics of microorganisms has been described using Monod-type kinetics [Billen *et al.*, 1988, Chiang *et al*, 1989, Taylor and Jaffe, 1990, Chen *et al*, 1992], which assume that growth is controlled by limiting factors such as oxygen, substrate or other nutrients. No relationship between growth rates and aquifer heterogeneities is found in the literature, though it has been recognized that spatial variability of the growth parameters exists [Baker, 1986, Schafer and Kinzelbach, 1991].

The analytical developments that follow are aimed at predicting the field coefficients of retardation, dispersion and decay of a soluble hydrocarbon undergoing advection, sorption and biodegradation in subsurface environments, and demonstrating the application of the results on one or more actual contaminated field sites. The analysis uses the transport equations for the contaminant and dissolved oxygen as the starting point, and builds on the spectral perturbation approach of Gelhar and Axness [1983] and Garabedian *et al.* [1988]. The basic motivation underlying this research is a search for improved methods for predicting the fate of groundwater contaminants under realistic field conditions.

## 4.2 Methodology of Solution

This Section introduces the formulation of the problem and the methodology of solution. The formulation of the problem is presented here in terms of the local transport equations for the contaminant, the dissolved oxygen and the microbial biomass, with the latter assumed to be at steady state. Appropriate source/sink terms are included in these equations to account for contaminant mass exchange between the aqueous and solid phases in the aquifer (sorption process), and for oxygen-limited biodegradation of the contaminant. Following this, the solution methodology, similar to the one employed in Gelhar and Axness [1983] and Garabedian *et al.* [1988], is described highlighting the differences that arise due

to nonlinearities in the source/sink terms and to the multiple species present in the problem.

### 4.2.1 Governing Equations

The local transport equations can be described by a system of coupled nonlinear partial differential equations. The contaminant sorption process is modeled using a linear isotherm to represent the proportionality between the amount of contaminant in the aqueous and solid phases in the aquifer. As it was suggested above, the Monod-type model has been adopted to represent the contaminant degradation in the presence of an adapted microbial population and an electron acceptor (oxygen). This yields the transport equation for an organic substrate undergoing advection, dispersion, equilibrium linear sorption to the soil particle surfaces and biodegradation:

$$R\frac{\partial S}{\partial t} + \frac{\partial (v_i S)}{\partial x_i} = \frac{\partial}{\partial x_i} D_{ij} \frac{\partial S}{\partial x_j} - r(S, C, M) \tag{4.1}$$

Here, $S$ is the aqueous concentration of the contaminant, $C$ is the dissolved oxygen concentration, $M$ is the active microbial biomass concentration, $v_i$ is the local velocity field, $D_{ij}$ is the local dispersion coefficient and $R$ is the local retardation factor based on a bulk density of the aquifer $\rho$, a linear distribution coefficent $K_d$, and an aquifer saturated porosity $n$ in the form [Freeze and Cherry, 1979]:

$$R = 1 + \frac{\rho K_d}{n} \tag{4.2}$$

The local flow field is found using Darcy's equation along with conservation of mass. For steady flow in a locally isotropic medium this is expressed as:

$$\frac{\partial}{\partial x_i}\left(K\frac{\partial h}{\partial x_i}\right) = 0$$

$$q_i = -K\frac{\partial h}{\partial x_i}$$

$$v_i = \frac{q_i}{n} \tag{4.3}$$

Here, $K$ is the hydraulic conductivity which is assumed to be locally isotropic, $h$ is the hydraulic head and $q_i$ is the specific discharge vector. The biodegradation source term is given by the dual Monod expression:

$$r(S, C, M) = \kappa M \left(\frac{S}{S_0 + S}\right)\left(\frac{C}{C_0 + C}\right) \tag{4.4}$$

where $\kappa$ represents the decay rate of the conmtaminant, and $S_0$ and $C_0$ are the half saturation constants for the contaminant and the dissolved oxygen. Notice that this expression implies that oxygen is a limiting factor for microbial growth. A similar equation of transport applies for the dissolved oxygen, without any terms to account for sorption (oxygen is not sorbed), and including a stoichiometric factor $W$ as a ratio of oxygen to contaminant consumed.

$$\frac{\partial C}{\partial t} + \frac{\partial (v_i C)}{\partial x_i} = \frac{\partial}{\partial x_i} D_{ij} \frac{\partial C}{\partial x_j} - W r(S, C, M) \tag{4.5}$$

Finally, a steady-state active microbial population is assumed, so the microbial mass which is actually biodegrading the contaminant is considered to be time-invariant, *i.e.* growth is balanced with death in time [Rifai and Bedient, 1990, Hornberger *et al*, 1992]. In this situation, the microbial population is only spatially varying, and:

$$\frac{\partial M}{\partial t} = 0 \tag{4.6}$$

This completes the set of governing equations that is used to develop expressions for the field-scale transport coefficients by employing the subsequent stochastic analysis.

### 4.2.2 Random Fields

#### Hydrologic Processes

As presented in Chapter 2, the aquifer log-hydraulic conductivity is modeled as a stochastic process, represented by the equations:

$$f(\mathbf{x}) = lnK(\mathbf{x}) \tag{4.7}$$

Once again, $f(\mathbf{x})$ can be expressed as the sum of its ensemble mean $f$ and a perturbation $f'$.

$$f = \bar{f} + f' \tag{4.8}$$

The variations represented by $f'$ are described by a three-dimensional statistically anisotropic exponential autocovariance spectrum:

$$S_{ff} = \frac{\sigma_f^2 \lambda_1 \lambda_2 \lambda_3}{\pi^2[1 + (k_1\lambda_1)^2 + (k_2\lambda_2)^2 + (k_3\lambda_3)^2]^2} \tag{4.9}$$

#### Geochemical Processes

The geochemical reaction treated in this analysis is the instantaneous, reversible and linear adsorption of the contaminant to the solid surfaces in the aquifer,

$$\tilde{S} = K_d S \tag{4.10}$$

where $\tilde{S}$ is the concentration in the solid phase ($mg/g$). A stochastic analysis of the heterogeneity of the ratio of the distribution coefficient $K_d$ and the porosity $n$ that appears in the expression for the local retardation factor, equation (2.2) can be written in terms of a stationary mean and a perturbation as well:

$$y = \frac{\rho K_d}{n} = \bar{y} + y' \tag{4.11}$$

Following the approach in Garabedian *et al.* [1988], the distribution coefficient is related to the log-hydraulic conductivity field by a linear relation:

$$y = a_2 + b_2 f + \eta \tag{4.12}$$

where $\eta$ is a zero-mean uncorrelated residual so that its cross-spectrum with $f'$ is

$$S_{f\eta} = 0 \tag{4.13}$$

The mean is,

$$\bar{y} = a_2 + b_2 \bar{f} \tag{4.14}$$

and the perturbation is

$$y' = b_2 f' + \eta \tag{4.15}$$

Using this formulation, the random form of the retardation factor is found to be:

$$R = 1 + y \tag{4.16}$$

with a mean and perturbation given by:

$$\bar{R} = 1 + \bar{y} \tag{4.17}$$

$$R' = y' \tag{4.18}$$

### Microbiological Processes

By introducing the assumption of a time-invariant microbial population, the parameter $\kappa M$ which appears in the dual Monod expression can be lumped into a single random field of the form:

$$w = \kappa M = \bar{w} + w' \tag{4.19}$$

Once again, a linear relation between this growth rate-biomass concentration parameter and log-hydraulic conductivity is assumed:

$$w = a_1 + b_1 f + \delta \tag{4.20}$$

with a mean given by

$$\bar{w} = a_1 + b_1 \bar{f} \tag{4.21}$$

and a perturbation:

$$w' = b_1 f' + \delta \tag{4.22}$$

As it was the case for the distribution coefficient, no correlation is assumed to exist between the $f'$ and $\delta$ perturbations so that their cross-spectrum is

$$S_{f\delta} = 0 \tag{4.23}$$

**Transport Variables**

The flow field $v_i$, and the concentrations $S$ and $C$ can also be represented by their respective means and perturbations:

$$v_i = \bar{v}_i + v_i' \tag{4.24}$$

$$S = \bar{S} + S' \tag{4.25}$$

$$C = \bar{C} + C' \tag{4.26}$$

### 4.2.3 Development of Spectral Equations

As in Chapter 2, with the assumption of uni-directional mean flow, the coordinate system $x_i$ is aligned such that the $x_1$ direction is along the direction of the mean flow:

$$\bar{v}_1 = v; \quad \bar{v}_2 = \bar{v}_3 = 0$$

The local dispersion tensor is approximated as in equation (2.29 with $\alpha_L$ being the local longitudinal dispersivity and $\alpha_T$ the local transverse dispersivity. A second-order Taylor series expansion for the dual Monod expression centered on the mean concentrations proves itself convenient in the subsequent analyses:

$$r(S,C,M) = r + r_S S' + r_C C' + r_{SS} S'^2 + r_{CC} C'^2 + r_{SC} S'C'$$

$$r = r(\bar{S},\bar{C},M)$$

$$r_S = (\frac{\partial r}{\partial S})_{\bar{S},\bar{C}}$$

$$r_C = (\frac{\partial r}{\partial C})_{\bar{S},\bar{C}}$$

$$r_{SS} = (\frac{\partial^2 r}{\partial S^2})_{\bar{S},\bar{C}}$$

$$r_{CC} = (\frac{\partial^2 r}{\partial C^2})_{\bar{S},\bar{C}}$$

$$r_{SC} = (\frac{\partial^2 r}{\partial S \partial C})_{\bar{S},\bar{C}} \tag{4.27}$$

The perturbed quantities for $R, v_i, S, C, y$ and $w$ are substituted in the transport equations for the contaminant and dissolved oxygen, (4.1) and (4.5). Once all terms are expanded in terms of means and perturbations, the expectation of these equations produces:

$$\bar{R}\frac{\partial \bar{S}}{\partial t} + \frac{\partial}{\partial t}\overline{R'S'} + \bar{v}_i\frac{\partial \bar{S}}{\partial x_i} + \frac{\partial}{\partial x_i}\overline{v_i'S'} = \frac{\partial}{\partial x_i}D_{ij}\frac{\partial \bar{S}}{\partial x_j} - \psi(\bar{S},\bar{C}) \tag{4.28}$$

$$\frac{\partial \bar{C}}{\partial t} + \bar{v}_i\frac{\partial \bar{C}}{\partial x_i} + \frac{\partial}{\partial x_i}\overline{v_i'C'} = \frac{\partial}{\partial x_i}D_{ij}\frac{\partial \bar{C}}{\partial x_j} - W\psi(\bar{S},\bar{C}) \tag{4.29}$$

$$\psi(\bar{S},\bar{C}) = \bar{r} + \overline{r_S'S'} + \overline{r_C'C'} + \overline{r_{SS}}\overline{S'^2} + \overline{r_{CC}}\overline{C'^2} + \overline{r_{SC}}\overline{S'C'} \tag{4.30}$$

Subtracting these mean equations from the original transport equations and dropping higher-order terms, produces first-order approximations describing the

concentration perturbations:

$$R'\frac{\partial \bar{S}}{\partial t} + \bar{R}\frac{\partial S'}{\partial t} + \bar{v}_i\frac{\partial S'}{\partial x_i} + v_i'\frac{\partial \bar{S}}{\partial x_i} = \frac{\partial}{\partial x_i}D_{ij}\frac{\partial S'}{\partial x_j} - (r' + \overline{r_S}S' + \overline{r_C}C') \quad (4.31)$$

$$\frac{\partial C'}{\partial t} + \bar{v}_i\frac{\partial C'}{\partial x_i} + v_i'\frac{\partial \bar{C}}{\partial x_i} = \frac{\partial}{\partial x_i}D_{ij}\frac{\partial C'}{\partial x_j} - W(r' + \overline{r_S}S' + \overline{r_C}C') \quad (4.32)$$

In order to properly describe the changes in the means and perturbations of the concentrations as the contaminant and dissolved oxygen plumes move with the advective flow, a set of moving coordinate systems that follow the mean flow of each of the plumes in space is introduced. For the contaminant

$$\zeta_1 = x_1 - \frac{vt}{R_S}; \zeta_2 = x_2; \zeta_3 = x_3 \quad (4.33)$$

and for the dissolved oxygen

$$\xi_1 = x_1 - \frac{vt}{R_C}; \xi_2 = x_2; \xi_3 = x_3 \quad (4.34)$$

Here, $R_S$ and $R_C$ are the effective retardation factors for the contaminant and the dissolved oxygen respectively. These coefficients have to be determined in the subsequent analyses. The space and time derivatives are transformed according to:

$$\left(\frac{\partial}{\partial t}\right)_x = \left(\frac{\partial}{\partial t}\right)_\zeta - \frac{v}{R_S}\frac{\partial}{\partial \zeta_1} \quad (4.35)$$

$$\left(\frac{\partial}{\partial x_i}\right)_t = \left(\frac{\partial}{\partial \zeta_i}\right)_t \quad (4.36)$$

Similar expressions apply for the oxygen moving coordinate system.

By substituting these coordinate changes, the mean equations can now be written as:

$$\bar{R}\left(\frac{\partial \bar{S}}{\partial t} - \frac{v}{R_S}\frac{\partial \bar{S}}{\partial \zeta_1}\right) + \frac{\partial}{\partial t}\overline{R'S'} - \frac{v_i}{R_S}\frac{\partial}{\partial \zeta_i}\overline{R'S'} + v\frac{\partial \bar{S}}{\partial \zeta_1} + \frac{\partial}{\partial \zeta_i}\overline{v_i'S'} =$$

$$\frac{\partial}{\partial \zeta_i} D_{ij} \frac{\partial \bar{S}}{\partial \zeta_j} - \psi(\bar{S}, \bar{C}) \tag{4.37}$$

$$\frac{\partial \bar{C}}{\partial t} - \frac{v}{R_C} \frac{\partial \bar{C}}{\partial \xi_1} + v \frac{\partial \bar{C}}{\partial \xi_1} + \frac{\partial}{\partial \xi_i} \overline{v_i' C'} = \frac{\partial}{\partial \xi_i} D_{ij} \frac{\partial \bar{C}}{\partial \xi_j} - W \psi(\bar{S}, \bar{C}) \tag{4.38}$$

and the perturbation equations result in:

$$R'(\frac{\partial \bar{S}}{\partial t} - \frac{v}{R_S} \frac{\partial \bar{S}}{\partial \zeta_1}) + \bar{R}(\frac{\partial S'}{\partial t} - \frac{v}{R_S} \frac{\partial S'}{\partial \zeta_1}) + v \frac{\partial S'}{\partial \zeta_1} + v_i' \frac{\partial \bar{S}}{\partial \zeta_i} =$$

$$\frac{\partial}{\partial \zeta_i} D_{ij} \frac{\partial S'}{\partial \zeta_j} - (\bar{r_S} S' + \bar{r_C} C' + r') \tag{4.39}$$

$$\frac{\partial C'}{\partial t} - \frac{v}{R_C} \frac{\partial C'}{\partial \xi_1} + v \frac{\partial C'}{\partial \zeta_1} + v_i' \frac{\partial \bar{C}}{\partial \xi_i} = \frac{\partial}{\partial \xi_i} D_{ij} \frac{\partial C'}{\partial \xi_j} - W(\bar{r_S} S' + \bar{r_C} C' + r') \tag{4.40}$$

The second order terms which involve correlations between perturbations in flow and concentrations, sorption and concentrations, and decay and concentrations, as well as variances and covariances of the concentration fields are used to predict field-scale effects in retardation dispersion and decay. The calculation of these terms involves solving the partial differential equations of the perturbation equations using the spectral approach presented in Gelhar and Axness [1983] and Miralles-Wilhelm *et al* [1992]. The perturbed quantities are assumed to be statistically homogeneous and represented by [Lumley and Panofsky, 1964]:

$$S' = \int_{-\infty}^{\infty} e^{i\mathbf{k}.\mathbf{x}} dZ_S(\mathbf{k}) \tag{4.41}$$

$$C' = \int_{-\infty}^{\infty} e^{i\mathbf{k}.\mathbf{x}} dZ_C(\mathbf{k}) \tag{4.42}$$

$$v_i' = \int_{-\infty}^{\infty} e^{i\mathbf{k}.\mathbf{x}} dZ_{v_i}(\mathbf{k}) \tag{4.43}$$

$$y' = \int_{-\infty}^{\infty} e^{i\mathbf{k}.\mathbf{x}} dZ_y(\mathbf{k}) \tag{4.44}$$

$$w' = \int_{-\infty}^{\infty} e^{i\mathbf{k}.\mathbf{x}} dZ_f(\mathbf{k}) \tag{4.45}$$

Using these representations along with,

$$G_i = -\frac{\partial \bar{S}}{\partial \zeta_i}; \quad F_i = -\frac{\partial \bar{C}}{\partial \xi_i} \tag{4.46}$$

the perturbation equations in spectral space result in:

$$dZ_R\left(\frac{\partial \bar{S}}{\partial t} - \frac{v}{R_S}\frac{\partial \bar{S}}{\partial \zeta_1}\right) + \bar{R}\frac{\partial dZ_S}{\partial t} + ivk_1 dZ_S - \frac{\partial \bar{S}}{\partial \zeta_i} dZ_{v_i} = -D_{ij}k_i k_j dZ_S$$

$$- (\bar{r_S} dZ_S + \bar{r_C} dZ_C + dZ_r) \tag{4.47}$$

$$\frac{\partial dZ_C}{\partial t} + ivk_1 dZ_C - \frac{\partial \bar{C}}{\partial \xi_i} dZ_{v_i} = -D_{ij}k_i k_j dZ_C - W(\bar{r_S} dZ_S + \bar{r_C} dZ_C + dZ_r) \tag{4.48}$$

A simplification to the analysis can be made by recognizing that since the contaminant and dissolved oxygen plumes are undergoing a transformation process, it is also necessary to follow the plumes in time. This is achieved by scaling the concentration spectral amplitudes $dZ_S$ and $dZ_C$ according to the following (see Appendix B):

$$dZ_S = dZ_S exp\left(-\int_0^t \frac{r_{se}}{\bar{R}} dt'\right) - \int_0^t \frac{r_{ce}}{\bar{R}} dZ_C exp\left(-\int_{t'}^t \frac{r_{se}}{\bar{R}} dt''\right) dt' \tag{4.49}$$

$$dZ_C = dZ_C exp\left(-\int_0^t W.r_{ce} dt'\right) - \int_0^t W r_{se} dZ_S exp\left(-\int_{t'}^t W r_{ce} dt''\right) dt' \tag{4.50}$$

The result of this scaling introduces the spectral amplitudes for the non-decaying quantities $dZ_S$ and $dZ_C$ and the effective decay functions $r_{se}$ and $r_{ce}$, similar to the procedure presented in Chapter 2. These effective decay functions in turn define effective decay coefficients for the contaminant and dissolved oxygen, as explained in the next Section. Once this scaling is done, the perturbation equations are transformed to:

$$\bar{R}\frac{\partial dZ_S}{\partial t}exp\left(-\int_0^t \frac{r_{se}}{\bar{R}}dt'\right) + (ivk_1 + D_{ij}k_ik_j + \bar{r_S} - r_{se})dZ_S + dZ_R(\frac{\partial \bar{S}}{\partial t} + \frac{v}{R_S}G_1)$$

$$- G_j dZ_{v_j} + (\bar{r_C} - r_{ce})dZ_C + dZ_r = 0 \tag{4.51}$$

$$\frac{\partial dZ_C}{\partial t}exp\left(-\int_0^t W.r_{ce}dt'\right) + (ivk_1 + D_{ij}k_ik_j + W.\bar{r_C} - W.r_{ce})dZ_C$$

$$- F_j dZ_{v_j} + W(\bar{r_S} - r_{se})dZ_S + WdZ_r = 0 \tag{4.52}$$

Next, at large times, changes of these scaled concentration spectral amplitudes can be considered negligible [Gelhar *et al.*, 1979; Garabedian *et al.*, 1988; Welty,1989] and dropped to produce a set of linear algebraic equations for the original spectral amplitudes $dZ_S$ and $dZ_C$.

$$(ivk_1+D_{ij}k_ik_j+\bar{r_S}-r_{se})dZ_S+dZ_R(\frac{\partial \bar{S}}{\partial t}+\frac{v}{R_S}G_1)-G_jdZ_{v_j}+(\bar{r_C}-r_{ce})dZ_C+dZ_r = 0 \tag{4.53}$$

$$(ivk_1 + D_{ij}k_ik_j + W.\bar{r_C} - W.r_{ce})dZ_C - F_jdZ_{v_j} + W(\bar{r_S} - r_{se})dZ_S + dZ_r = 0 \tag{4.54}$$

The expressions for $dZ_S$ and $dZ_C$ are then found to be:

$$dZ_S = \frac{1}{\Delta}[\frac{\partial \bar{S}}{\partial t}(W\bar{r_C}-ivk_1)dZ_R+(W.\bar{r_C}-ivk_1)(\frac{v}{R_S}dZ_R-dZ_{v_i})G_i-\bar{r_C}dZ_{v_i}F_i-ivk_1dZ_r] \tag{4.55}$$

$$dZ_C = \frac{1}{\Delta}[W.\bar{r_S}\frac{\partial \bar{S}}{\partial t}dZ_R + W.\bar{r_S}(\frac{v}{R_S}dZ_R - dZ_{v_i})G_i - (\bar{r_S} - ivk_1)F_i - W.ivk_1dZ_r] \tag{4.56}$$

$$\Delta = (ivk_1+D_{ij}k_ik_j+\bar{r_S}-r_{se})(ivk_1+D_{ij}k_ik_j+W.\bar{r_C}-W.r_{ce})-W(r_S-r_{se})(r_C-r_{ce}) \tag{4.57}$$

In order to find the second-order cross correlation terms that appear in the mean transport equations, the SRT [Lumley and Panofsky, 1964] must be invoked. Hence,

$$\overline{R'S'} = \int_{-\infty}^{\infty} S_{RS}d\mathbf{k} = \int_{-\infty}^{\infty} E[dZ_R dZ_S^*] \tag{4.58}$$

$$\overline{v_i' S'} = \int_{-\infty}^{\infty} S_{v_i S} d\mathbf{k} = \int_{-\infty}^{\infty} E[dZ_{v_i} dZ_S^*] \tag{4.59}$$

$$\overline{v_i' C'} = \int_{-\infty}^{\infty} S_{v_i C} d\mathbf{k} = \int_{-\infty}^{\infty} E[dZ_{v_i} dZ_C^*] \tag{4.60}$$

$$\overline{w' S'} = \int_{-\infty}^{\infty} S_{w S} d\mathbf{k} = \int_{-\infty}^{\infty} E[dZ_f dZ_S^*] \tag{4.61}$$

$$\overline{w' C'} = \int_{-\infty}^{\infty} S_{w C} d\mathbf{k} = \int_{-\infty}^{\infty} E[dZ_f dZ_C^*] \tag{4.62}$$

In these expressions the (*) stands for the complex conjugate of the given quantity. In a similar fashion as that explained in Chapter 2, the spectral amplitudes involved in these expressions are related to the spectral amplitude of the log-conductivity perturbations $dZ_f$. The flow field perturbations $dZ_{v_i}$ follow equation (2.61):

$$dZ_{v_i} = \frac{K_l}{n}(J_i - J_j \frac{k_i k_j}{k^2}) dZ_f \tag{4.63}$$

Also, the spectral amplitudes for retardation and decay are related to $dZ_f$ from the relations between $R'$ and $w'$ with $f'$ (4.15) and (4.22):

$$dZ_R = b_2 dZ_f + dZ_\eta \tag{4.64}$$

$$dZ_w = b_1 dZ_f + dZ_\delta \tag{4.65}$$

Finally, the autocovariance function of the residuals $\delta$ and $\eta$ can be expected to appear in some of these second-order correlation terms. Both residuals are assumed to have a negative exponential autocovariance function with spectra:

$$S_{\eta\eta} = \frac{\sigma_\eta^2 \lambda_1 \lambda_2 \lambda_3}{\pi^2 (1 + \lambda_1^2 k_1^2 + \lambda_2^2 k_2^2 + \lambda_3^2 k_3^2)^2} \tag{4.66}$$

A similar expression applies for the residual $\delta$.

The integrals that appear in the expressions for the second order correlation terms can be classified into six groups, according to the following forms:

$$I_1 = \int_{-\infty}^{\infty} \frac{S_{v_i v_j} d\mathbf{k}}{\Delta} \tag{4.67}$$

$$I_2 = \int_{-\infty}^{\infty} \frac{S_{wv_j} d\mathbf{k}}{\Delta}; (or S_{Rv_j}) \tag{4.68}$$

$$I_3 = \int_{-\infty}^{\infty} \frac{S_{ww} d\mathbf{k}}{\Delta}; (or S_{RR}, SwR, etc.) \tag{4.69}$$

$$I_4 = \int_{-\infty}^{\infty} \frac{ivk_1 S_{v_i v_j} d\mathbf{k}}{\Delta} \tag{4.70}$$

$$I_5 = \int_{-\infty}^{\infty} \frac{ivk_1 S_{wv_j} d\mathbf{k}}{\Delta}; (or S_{Rv_j}) \tag{4.71}$$

$$I_6 = \int_{-\infty}^{\infty} \frac{ivk_1 S_{ww} d\mathbf{k}}{\Delta}; (or S_{RR}, SwR, etc.) \tag{4.72}$$

These integrals are evaluated in H for a three-dimensional statistically anisotropic spectrum $S_{ff}$.

Using the results of these integrals, the second-order correlation terms can be calculated. In the correlations that involve decay and concentrations, it must be noted that because Monod kinetics are being used to represent the source/sink terms for both transported species,

$$r_S = w \frac{S_0}{(\bar{S} + S_0)^2} \frac{\bar{C}}{\bar{C} + C_0} \tag{4.73}$$

$$r_C = w \frac{C_0}{(\bar{C} + C_0)^2} \frac{\bar{S}}{\bar{S} + S_0} \tag{4.74}$$

$$r' = w' \frac{\bar{S}}{\bar{S} + S_0} \frac{\bar{C}}{\bar{C} + C_0} \tag{4.75}$$

$$r'_S = w' \frac{S_0}{(\bar{S} + S_0)^2} \frac{\bar{C}}{\bar{C} + C_0} \tag{4.76}$$

$$r'_C = w' \frac{C_0}{(\bar{C} + C_0)^2} \frac{\bar{S}}{\bar{S} + S_0} \tag{4.77}$$

Therefore,

$$dZ_r = dZ_w \frac{S_0}{\bar{S} + S_0} \frac{\bar{C}}{\bar{C} + C_0} \tag{4.78}$$

In this way, the following are the resulting expressions for the second-order correlations in equations (4.58) through (4.62). All integrals are listed in Apprndix H:

$$\overline{R'S'} = -\bar{r_C} G_i I_7 + n\bar{r_C} W I_{16} - (\frac{\partial S}{\partial t} + \frac{v}{R_S} G_1)(I_{12} + W n \bar{r_C} I_{14}) + G_i(I_8 + W \bar{r_C} I_7) - (I_{13} + W \bar{r_C} I_{16}) \tag{4.79}$$

$$\overline{v_i' S'} = -\frac{1}{n}(\frac{\partial S}{\partial t} + \frac{v}{R_S} G_1)(I_8 + W n \bar{r_C} I_7) + \frac{1}{n} G_j (I_{11} + W n \bar{r_C} I_{10}) - I_9 - W n \bar{r_C} I_{15} \tag{4.80}$$

$$\overline{v_i' C'} = W \bar{r_S}[(\frac{\partial S}{\partial t} + \frac{v}{R_C} G_1) I_1 - G_j I_{10} + I_{15}] - \frac{1}{n} F_j (I_{11} + n \bar{r_S} I_{10}) - W(I_9 + n \bar{r_S} I_{15}) \tag{4.81}$$

$$\overline{r_S' S'} = -n \bar{r_C} W_i I_{20} - (\frac{\partial S}{\partial t} + \frac{v}{R_S} G_1)(I_{22} + W n \bar{r_C} I_{23}) + G_i (I_{24} + W n \bar{r_C} I_{20}) - n I_{25} \tag{4.82}$$

$$\overline{r_C' C'} = W n \bar{r_S}[(\frac{\partial S}{\partial t} + \frac{v}{R_S} G_1) I_{26} - G_i I_{17} + n I_{18}] + F_i (I_{19} + n \bar{r_S} I_{17}) - W n (I_{21} + n \bar{r_S} I_{18}) \tag{4.83}$$

### 4.2.4 Field-Scale Coefficients

Field-scale transport and transformation coefficients can be derived from the second-order correlation terms that appear in the mean transport equations. Based on the resulting expressions for the spectral amplitudes $dZ_S$ and $dZ_C$,

(4.55) and (4.56), and those that result from the SRT [(equations (4.79) through (4.83)], these terms, in general, can be written as sums of:

(a) Decay terms, (zeroth-order derivatives of concentrations) which are grouped together to define the field-scale or effective decay coefficients. The effective decay coefficients for the contaminant and dissolved oxygen are found from the effective decay functions $r_{se}$ and $r_{ce}$. In this case, since Monod kinetics are considered to represent the source/sink functions for both species,

$$r_{se} = \kappa_e \bar{M} \frac{S_0}{(\bar{S}+S_0)^2} \frac{\bar{C}}{\bar{C}+C_0} \tag{4.84}$$

$$r_{ce} = \kappa_e \bar{M} \frac{C_0}{(\bar{C}+C_0)^2} \frac{\bar{S}}{\bar{S}+S_0} \tag{4.85}$$

So, in the mean equation for the contaminant species all decay terms are lumped in just one term, described by its effective decay coefficient, which is found to be:

$$\kappa_e = \bar{\kappa} - \frac{\phi \lambda_1}{\bar{M}} \frac{b_1^2 \sigma_f^2 + \sigma_\delta^2}{v(1+\chi)} \tag{4.86}$$

Here,

$$\phi = \frac{S_0}{(\bar{S}+S_0)^2} \frac{\bar{C}}{\bar{C}+C_0} + W \frac{C_0}{(\bar{C}+C_0)^2} \frac{\bar{S}}{\bar{S}+S_0} \tag{4.87}$$

and,

$$\chi = \frac{[1 + 4\frac{\lambda_1^2}{v^2}\phi^2(b_1^2\sigma_f^2 + \sigma_\delta^2)]^{1/2} - 1}{2} \tag{4.88}$$

$$\chi = \chi s + \chi c \tag{4.89}$$

where,

$$\chi_S = \frac{\lambda_1(\bar{r_S} - r_{ss})}{v} \tag{4.90}$$

$$\chi_C = \frac{\lambda_1 W(\bar{r_C} - r_{cs})}{v} \tag{4.91}$$

(b) Advection terms, (first-order derivatives of concentrations) which lead to the calculation of the field-scale retardation coefficients, referred to as effective retardation factors. In the mean transport equations, the advective terms must cancel in the moving coordinate system for each of the equations. Therefore,

$$R_S = \bar{R} - \frac{b_1 b_2}{(\kappa - \kappa_e)\bar{M}} \chi_S \sigma_f^2 \left[ \frac{1 + \chi_C}{1 + \chi} - \frac{\chi_C}{\chi} \right] \tag{4.92}$$

$$R_C = \frac{1}{1 + \frac{W_n}{v} \bar{r_C} I_{20}} \tag{4.93}$$

(c) Dispersion terms, (second-order derivatives of concentrations) which produce the field-scale dispersion coefficient or macrodispersivities [Gelhar *et al.*, 1979; Gelhar and Axness, 1983; Dagan, 1984, 1988]. All dispersion terms are grouped together and the macrodispersivities are defined by the relation [Garabedian *et al.*, 1988]:

$$- v A_{ij} \frac{\partial^2 \bar{S}}{\partial \zeta^2} \tag{4.94}$$

$$- v B_{ij} \frac{\partial^2 \bar{C}}{\partial \xi^2} \tag{4.95}$$

In this work, emphasis is placed on the longitudinal components of macrodispersion. Field experiments [Garabedian *et al.*, 1988] have shown that longitudinal mixing is the dominant dispersion process. The longitudinal dispersion coefficients $A_{11}$ for the contaminant and $B_{11}$ for the dissolved

oxygen ($i = j = 1$) can then be calculated to be (see I):

$$A_{11} = A'_{11}\frac{1}{\chi s + 1} \tag{4.96}$$

$$B_{11} = B'_{11}\frac{1}{\chi c + 1} \tag{4.97}$$

where

$$A'_{11} = (1 - \frac{\gamma b_2}{R_S})^2\frac{\sigma_f^2\lambda_1}{\gamma^2} + \frac{\sigma_\eta^2\lambda_1}{R_S^2} \tag{4.98}$$

$$B'_{11} = \frac{\sigma_f^2\lambda_1}{\gamma^2} \tag{4.99}$$

and the flow factor $\gamma$ is given by:

$$\gamma = \frac{vn}{K_l J_1} \tag{4.100}$$

An interesting feature of this two-component transport analysis is that cross-dispersion terms appear in the mean transport equations for both the contaminant and the dissolved oxygen. These consist of second order derivatives of the mean contaminant concentration $\bar{S}$ in the mean transport equation for $\bar{C}$ and vice versa. Cross-macrodispersivities can then be determined by grouping these terms together. Results from these calculations are referred to in the next Section.

(d) Other terms, which are not of the form of any of the above, usually involve cross space-time derivatives and other non-classical terms. These terms usually lead to plume skewness effects, as it was shown in Chapter 2 for a single component system. Treatment of these terms, which are expected to be small for large displacement [Gelhar *et al.*, 1979] is beyond the scope of the two-component analysis developed in this Chapter.

Following this analysis, a field scale transport equation for the contaminant can be written as,

$$R_S \frac{\partial \bar{S}}{\partial t} = \frac{\partial}{\partial \zeta_1} v A_{11} \frac{\partial \bar{S}}{\partial \zeta_1} - \kappa_e \bar{M} \frac{\bar{S}}{\bar{S} + S_0} \frac{\bar{C}}{\bar{C} + C_0} \tag{4.101}$$

A similar equation applies for the dissolved oxygen, with its own transport and transformation coefficients.

$$R_C \frac{\partial \bar{C}}{\partial t} = \frac{\partial}{\partial \xi_1} v B_{11} \frac{\partial C}{\partial \xi_1} - W \kappa_e \bar{M} \frac{\bar{S}}{\bar{S} + S_0} \frac{\bar{C}}{\bar{C} + C_0} \tag{4.102}$$

The differences and characteristics of these coefficients will form the basis for the presentation and discussion of results that follow.

Following this analysis, a field-scale transport equation for the contaminant can be written as,

$$R_S \frac{\partial \bar{S}}{\partial t} = \frac{\partial}{\partial \zeta_1} v A_{11} \frac{\partial \bar{S}}{\partial \zeta_1} - \kappa_e \bar{M} \frac{\bar{S}}{\bar{S} + S_0} \frac{\bar{C}}{\bar{C} + C_0} \tag{4.101}$$

A similar equation applies for the dissolved oxygen, with its own transport and transformation coefficients.

$$R_C \frac{\partial \bar{C}}{\partial t} = \frac{\partial}{\partial \xi_1} v B_{11} \frac{\partial C}{\partial \xi_1} - W \kappa_e \bar{M} \frac{\bar{S}}{\bar{S} + S_0} \frac{\bar{C}}{\bar{C} + C_0} \tag{4.102}$$

The differences and characteristics of these coefficients will form the basis for the presentation and discussion of results that follow.

## 4.3 Discussion of Results

### 4.3.1 General Results: The Borden Site

The results obtained from the analytical calculations outlined above are presented in this Section. Table 4.1 lists hypothetical parameters based in part on the field scale tracer test at the Borden Site in Ontario, Canada. These parameters were used in the evaluations of the expressions that were developed in the analysis for the effective retardation factors, macrodispersivities and effective decay coefficients.

The set of hydrologic parameters $\sigma_f^2, \lambda_1$ and $v$ were taken from Sudicky [1986] for the Borden site. The parameters $\bar{R}, \bar{\kappa}, \bar{M}, S_0, C_0$ and $W$ were taken from Macquarrie [1988]. The mean retardation factor $\bar{R}$ resulted from an average value obtained from sorption experiments using Borden aquifer sand. The mean active microbial biomass concentration $\bar{M}$ was calculated by using the results of viable plate counts and a bacterial weight of $10^{-12}$ grams per cell. The utilization ratio for oxygen $W$ (on a mass basis) was taken from the stoichiometric reaction of benzene to carbon dioxide and water. The value of the dissolved oxygen half-saturation constant $C_0$ was obtained from Longmuir [1954]. The other two parameters were obtained by fitting a two-dimensional model to experimental breakthrough data [Macquarrie, 1988].

The different values of the correlations and residual variances presented were determined by fixing a coefficient of variation for the sorption and decay processes *i.e.* $y$ and $w$. Once this is done, the variances can be specified and the coefficients $b_1, \sigma_\delta, b_2$ and $\sigma_\eta$ can be found by:

$$\sigma_w^2 = b_1^2 \sigma_f^2 + \sigma_\delta^2 \tag{4.103}$$

$$\sigma_y^2 = b_2^2 \sigma_f^2 + \sigma_\eta^2 \tag{4.104}$$

In this case, half of the variance was attributed to the correlation with $lnK$ and

the other half to the corresponding residuals, and the coefficients of variation for sorption and decay were held at 25%, 50% and 75%. Negative correlations ($b_1, b_2 < 0$) were presumed because less permeable finer grained materials are expected to exhibit greater sorptive capacity and microbial activity by virtue of their relatively larger surface area.

Table 4.1: Hypothetical parameters for the Borden site

HYDROLOGY

- porosity $n = 0.33$
- variance of lnK $\sigma_f^2 = 0.29$
- horizontal correlation length of f: $2.8m$
- vertical correlation length of f: $0.12m$
- groundwater velocity $v = 0.1\frac{m}{day}$

SORPTION

- mean retardation factor for the contaminant=1.4
- $b_2 = -1.$, $\sigma_\eta = 0.45$ (50 % coefficient of variation)
- $b_2 = -1.5$, $\sigma_\eta = 0.66$ (75 % coefficient of variation)
- $b_2 = -0.51$, $\sigma_\eta = 0.21$ (25 % coefficient of variation)

BIODEGRADATION

- DO half-saturation constant $0.1\frac{mg}{l}$
- contaminant half-saturation constant $0.5\frac{mg}{l}$
- mean active microbial biomass concentration= $0.23\frac{mg}{l}$
- mean decay rate $\bar{\kappa}$=$0.493/day$

- stoichiometric factor $W = 3.13$
- $b_1 = -0.05\frac{mg/l}{day}$, $\sigma_\delta = 0.05$ (50% coefficient of variation)
- $b_1 = -0.075\frac{mg/l}{day}$, $\sigma_\delta = 0.075\frac{mg/l}{day}$ (75% coefficient of variation)
- $b_1 = -0.025\frac{mg/l}{day}$, $\sigma_\delta = 0.025\frac{mg/l}{day}$ (25% coefficient of variation)

Figure 4-1 presents the results obtained for the effective decay rate. This parameter must be calculated first in order to be able to evaluate the other field scale coefficients (effective retardation factors and macrodispersions). As an overall result, the effective decay rate is moderately decreased from the mean decay rate value of $0.493/day$. If one notices the expression for the decay rate (4.86), this decrease is brought by heterogeneities in the decay rate, both correlated and uncorrelated with the $lnK$ field. This means that if the decay rate is constant, it can be used to correctly predict mass losses under biodegradation. In this case the variability of $lnK$ and $K_d$ do not affect the effective decay rate. For the more realistic cases found in groundwater, using the mean decay rate will result in over-predictions of the rate of biotransformation of the contaminant. Although the curves presented vary differently for high and low dissolved oxygen regimes, deviations of the effective decay rate from the mean for a coefficient of variation of 50% are moderate (a factor of 2 at the most). The decrease of the decay rate from its mean value is a general result of the stochastic analysis developed here.

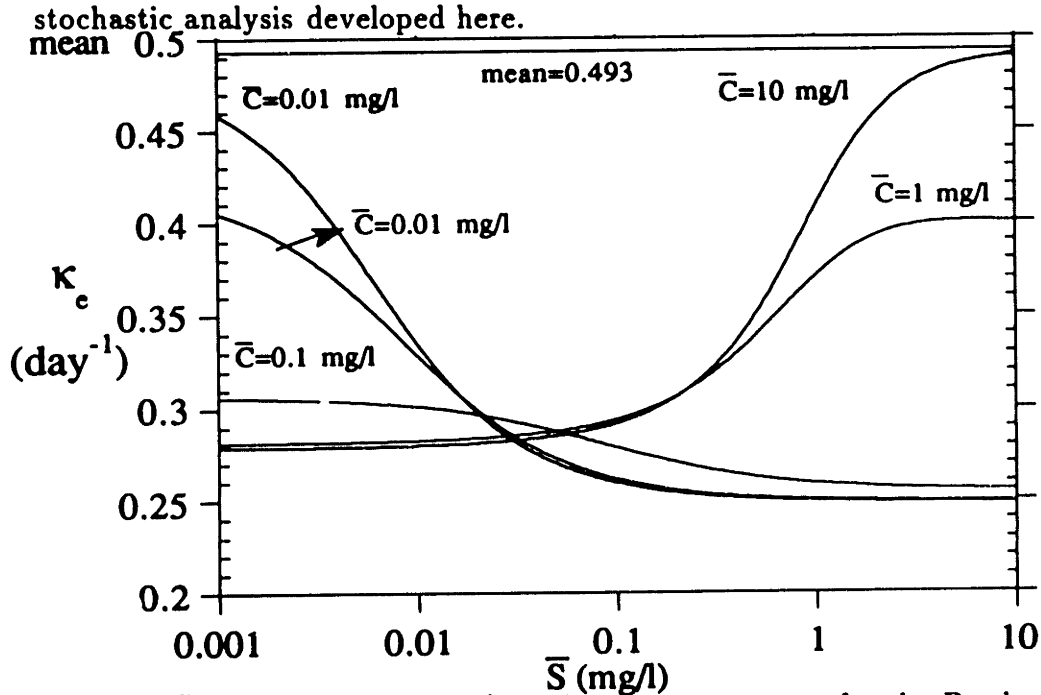


Figure 4-1: Effective decay rate evaluated using parameters for the Borden site .

Departures of the effective retardation factor from the mean are illustrated in Figure 4-2. For a situation where biodegradation is not occurring, Garabedian *et al.* [1988] find that the effective retardation factor is equal to the mean. In the cases presented, the effective retardation for the contaminant decreases slightly (15% at most) from the mean value. This decrease is caused by the correlation terms between the retardation factor and the decay rate in the mean equation for the contaminant, as can be observed from the expression for the effective retardation factor, (4.92).

Since both the decay rate and the retardation factor are negatively correlated with $lnK$, it is the same to say that they are positively correlated with each other, and thus the decreasing effects on the decay rate found above explain the decrease of the effective retardation from its mean value.This decrease is more pronounced in the concentration regimes where the biodegradation activity is high, *i.e.*, where there is plenty of oxygen to transform the contaminant. In the case of the dissolved oxygen, there are no significant variations (less than 1%) of the effective retardation coefficient from the non-retarded value of 1.0. In all cases, the variations of the effective retardation factor are weaker than those observed for the effective decay rate.

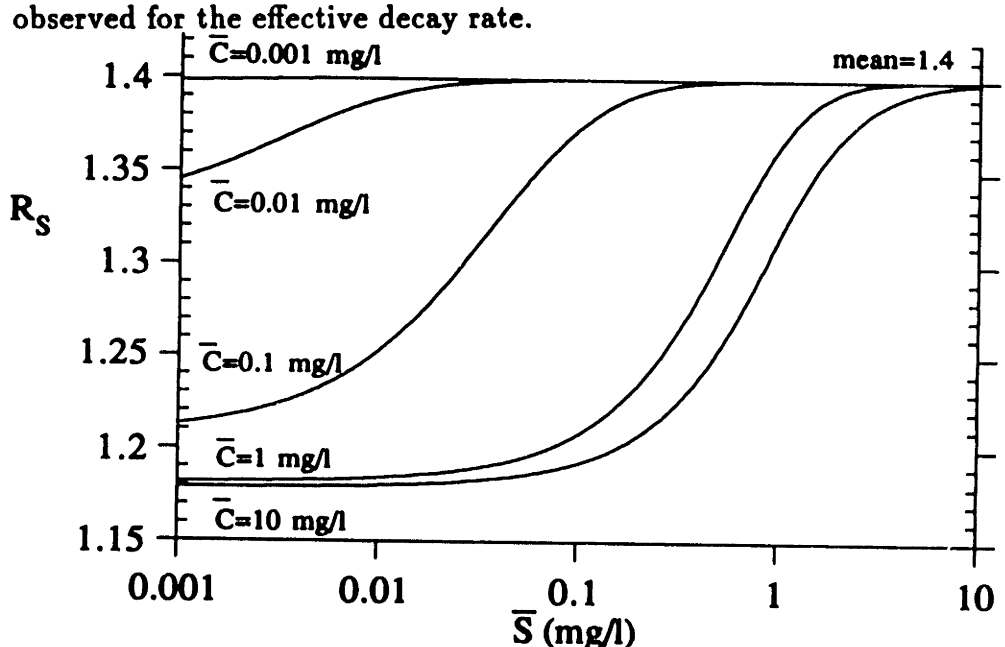


Figure 4-2: Effective retardation factor $R_S$ evaluated using parameters for the Borden site .

The sequence from Figures 4-3 to 4-7 show plots of the longitudinal macrodispersivities for the contaminant and the dissolved oxygen. These are perhaps the field coefficients that show the more interesting features of the interaction between the hydrologic, sorption and biodegradation processes in groundwater. First, the macrodispersions for the contaminant and dissolved oxygen differ by a factor of 3 to 4 in most cases. This difference is caused by two mechanisms: one the one hand, sorption of the contaminant has been found to cause dramatic increases in macrodispersivity [Garabedian *et al.*,1988], and this is why the contaminant has higher macrodispersion than the dissolved oxygen, which is not sorbed. On the other hand, the effects of the biodegradation process is to decrease the macrodispersivities. This effect influences both the contaminant and the dissolved oxygen. The mass losses of the contaminant and dissolved oxygen due to the biotransformation causes a decrease in the amount of mass that is able to disperse, and this causes both macrodispersivities to decrease from their values in a non-biodegradation situation [Gelhar and Axness, 1983; Garabedian *et al.*, 1988].

The other important feature is that macrodispersivities can vary significantly with concentrations (over 300% in some cases). This is in contrast to the behavior of the effective retardation and decay coefficients which showed only modest changes. In the case of the contaminant, its macrodispersivity tends to increase with increasing mean contaminant concentration, and to decrease with increasing mean dissolved oxygen concentration. The higher the contaminant concentration, the more mass of it that is able to disperse for a given dissolved oxygen concentration. This is seen clearly in the sequence of figures presented. When $\bar{C} = 10mg/l$, there is plenty of oxygen available for biodegradation, so the macrodispersivity starts low, because most of the contaminant mass is being biodegraded. As the contaminant concentration is increased, the biodegradation process starts becoming 'saturated' (that is, there is more contaminant in solution than the amount which the reaction with the oxygen is capable of degrading) and more mass starts to get dispersed. When the contaminant con-

centration is high enough - around 10 times the threshold value $S_0$ - the dissolved oxygen is only capable of reacting with a small fraction of the contaminant, and most of the mass is dispersed. It is here that the macrodispersivity reaches its maximum value.

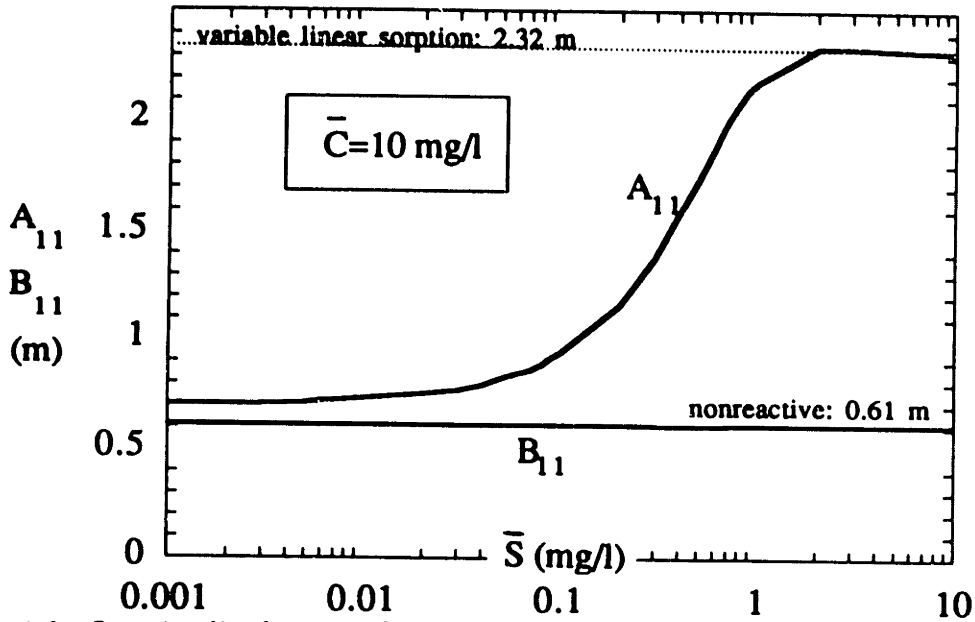


Figure 4-3: Longitudinal macrodispersivities $A_{11}$ and $B_{11}$ for $C = 10\frac{mg}{l}$ based on parameters for the Borden site .

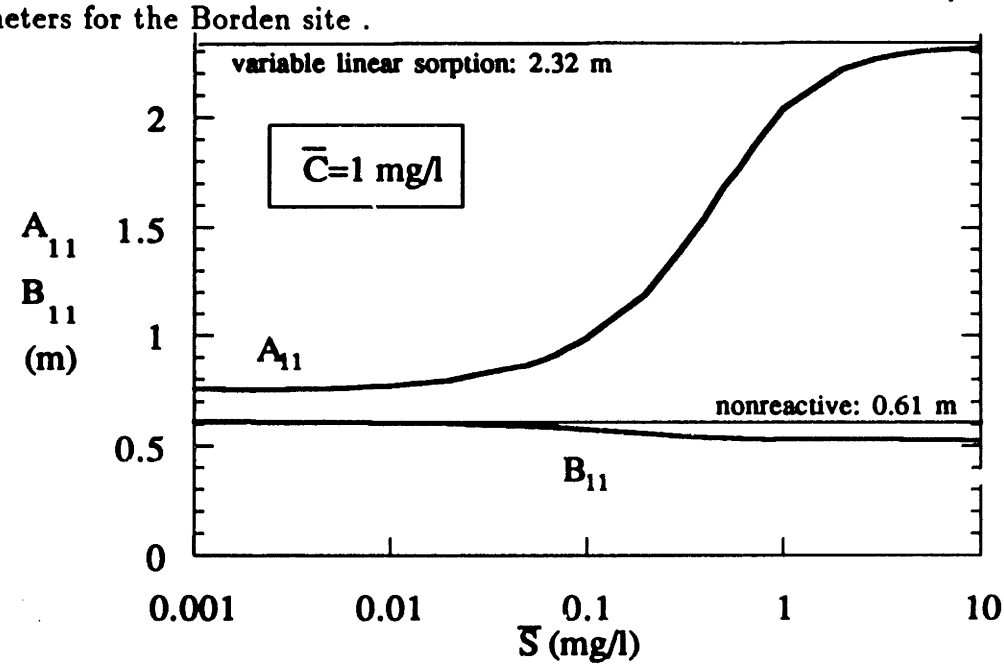


Figure 4-4: Longitudinal macrodispersivities $A_{11}$ and $B_{11}$ for $\bar{C} = 1\frac{mg}{l}$ based on parameters for the Borden site .

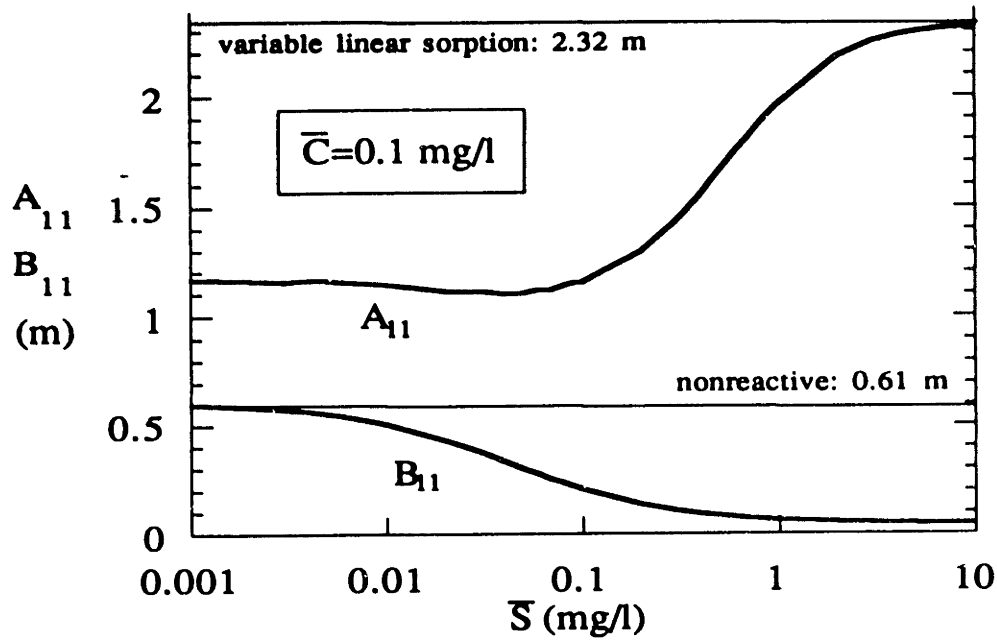


Figure 4-5: Longitudinal macrodispersivities $A_{11}$ and $B_{11}$ for $\bar{C} = 0.1\frac{mg}{l}$ based on parameters for the Borden site .

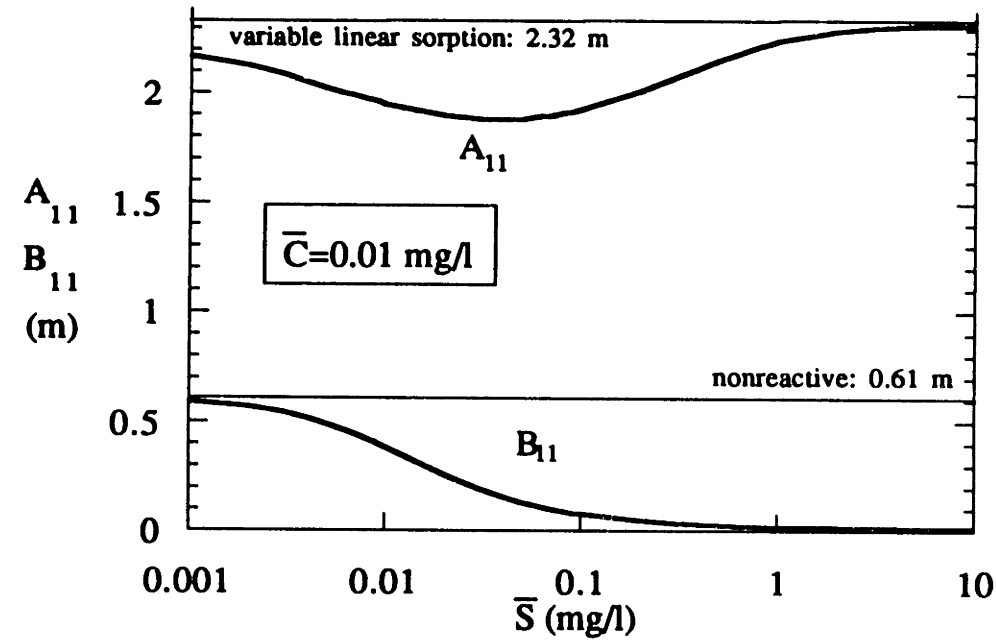


Figure 4-6: Longitudinal macrodispersivities $A_{11}$ and $B_{11}$ for $\bar{C} = 0.01\frac{mg}{l}$ based on parameters for the Borden site .

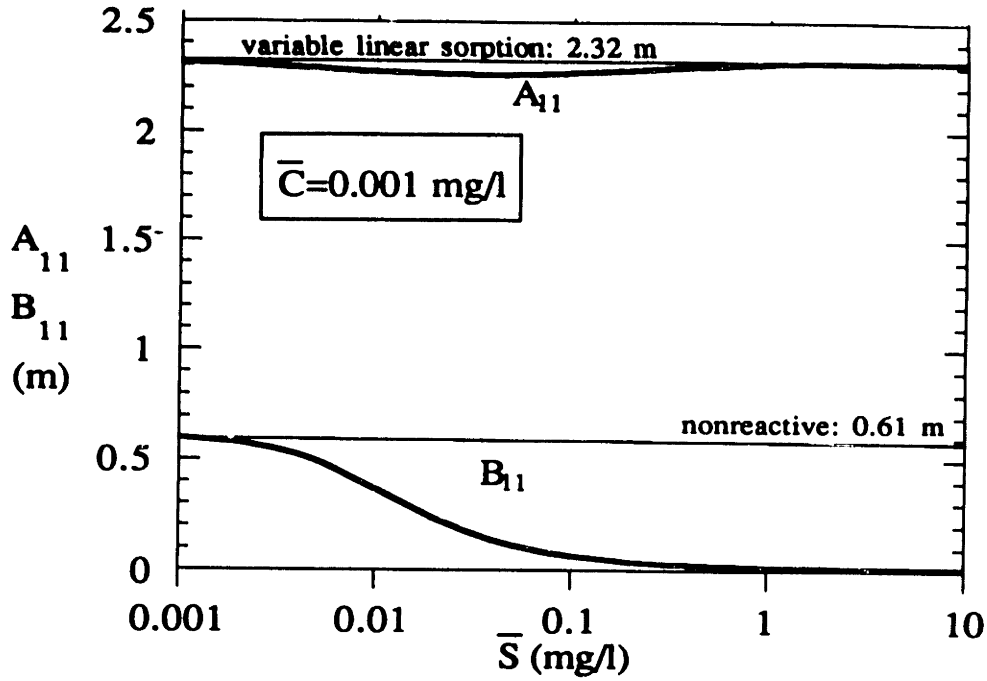


Figure 4-7: Longitudinal macrodispersivities $A_{11}$ and $B_{11}$ for $\bar{C} = 0.001 \frac{mg}{l}$ based on parameters for the Borden site .

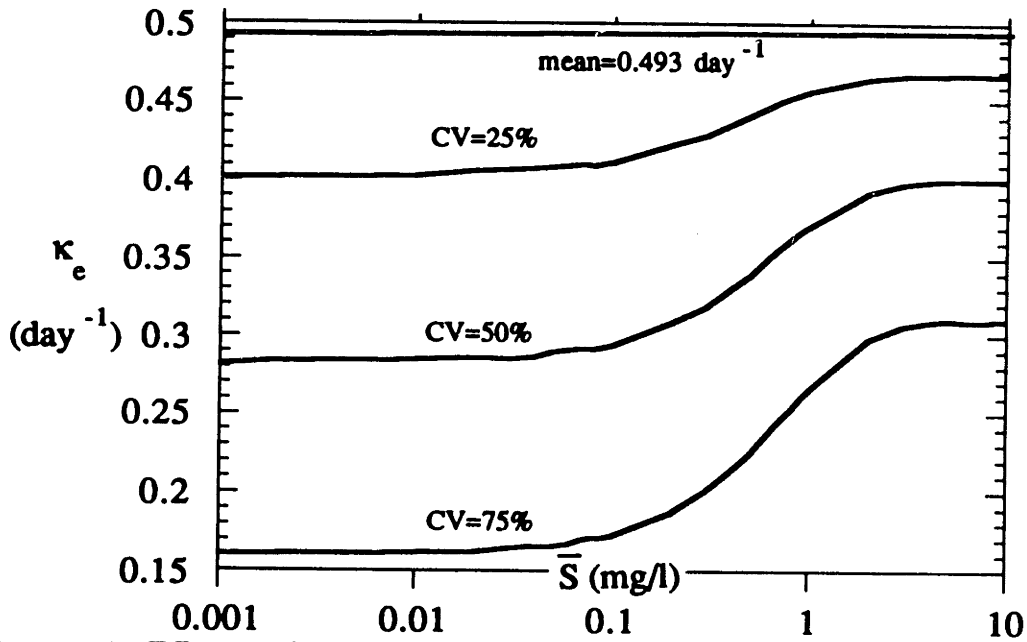


Figure 4-8: Effective decay rate as influenced by variability of decay rate, based on parameters for the Borden site ; $\bar{C} = 1 \frac{mg}{l}$.

In the other extreme, when dissolved oxygen is scarce, the biodegradation reaction is not able to occur at a large scale, because of the oxygen deficiency, and most of the contaminant just disperses. The same reasoning applies for the dissolved oxygen macrodispersivity: it increases for increasing mean dissolved oxygen concentration, and it decreases for higher mean contaminant concentrations. In all of these cases, there is an interaction between the decay and dispersion processes for both species, and there is the additional component of sorption for the contaminant which tends to produce the large difference observed between their macrodispersivities.

In calculating the transverse components of the macrodispersivities, the stochastic theory presented here predicts values of the order of the local transverse dispersivity $\alpha_T$ (mm). The first order approximation for the transport equation (order of $\sigma_f^2$) is not able to capture higher order effects that may play an important role in the transverse macrodispersivities $A_{22}$ and $A_{33}$ [Dagan, 1988]. In this case, terms of the order of $\sigma_f^4$ are potentially much larger than those mentioned above, and thus it may be crucial to incorporate these terms in order to obtain an appropriate representation of the field-scale transverse dispersion process. Theoretical developments [Rehfeldt, 1988; Naff, 1989] also indicate that unsteady flow effects play an important role in transverse dispersion, and these effects seem to be important at the Borden [Sudicky, 1986] and Cape Cod [Garabedian *et al.*, 1991] sites. The question of transverse dispersion mechanisms is an issue that remains to be resolved even for nonreactive solutes; we do not address the issue here.

Calculations performed for the cross dispersion terms show that the cross-macrodispersivities are much smaller (at least two orders of magnitude less) than the leading macrodispersivities in each of the mean transport equations. Since these cross-macrodispersion coefficients are multiplying second order derivatives of concentrations, an assessment of the relative importance of the cross-dispersion terms requires knowledge of the contaminant and dissolved oxygen plume concentration profiles, either from field measurements or by mean flow numerical simulations. Thus, these unanticipated terms deserve further attention.

The sensitivity of the field scale coefficients to variability in the decay rate is

shown in Figures 4-8, 4-9 and 4-10. In Figure 4-8, a higher variability produces a higher deviation of the effective decay rate from the mean value. It can be seen that for moderate variabilities such as 25%, the effective decay rate is equal to the mean for all practical purposes. Even for a variability as high as 75%, the effective decay comes down only to a half of the mean at the least. This confirms the assertion that the variations in the decay rate from its mean to the field scale value are modest.

Figures 4-9and 4-10 show the influence of decay variability on macrodispersion. If there is no variability in decay, the effective decay rate is equal to the mean, and hence the effective decay functions $r_{se}$ and $r_{ce}$ are equal to their mean counterparts $\bar{r}_S$ and $\bar{r}_C$. This means that macrodispersivities will not be affected by the biodegradation term in this case. However, when variability in decay is present, macrodispersivities can vary, and the higher this variability is, the greater is the variation of both macrodispersivities with concentration. The effective retardation factor does not vary significantly (less than 5%) with decay variability.

Figure 4-11 shows the sensitivity of the effective retardation to variability in the sorption process (variability in the retardation factor). The effects on the effective retardation are the weakest that are encountered, and this is true for the wide range of coefficients of variation treated here. Even for a variability as high as 75% in the retardation factor, the effective retardation coefficient varies less than 15% from the mean at the most. Because of this, it is fair to say that for this case, sorption effects can be practically predicted by using the mean retardation factor. However, this theory provides a quantitative way of predicting the field scale retardation process in cases where small variations may occur.

Finally, Figure 4-12 shows the influence of retardation variability on the contaminant longitudinal macrodispersivity $A_{11}$. The effects shown are similar to those described by Garabedian *et al.* [1988], where macrodispersivities were increased significantly when $K_d$ is negatively correlated with $lnK$. The higher coefficient of variation of retardation is associated with a higher magnitude negative correlation $K_d - lnK$, which produces higher macrodispersivities. Here, there is the additional mechanism of biodegradation, which produces the concentration dependence in $A_{11}$. Neither the

dissolved oxygen macrodispersivity, nor the effective decay rate are affected by this variability in retardation.

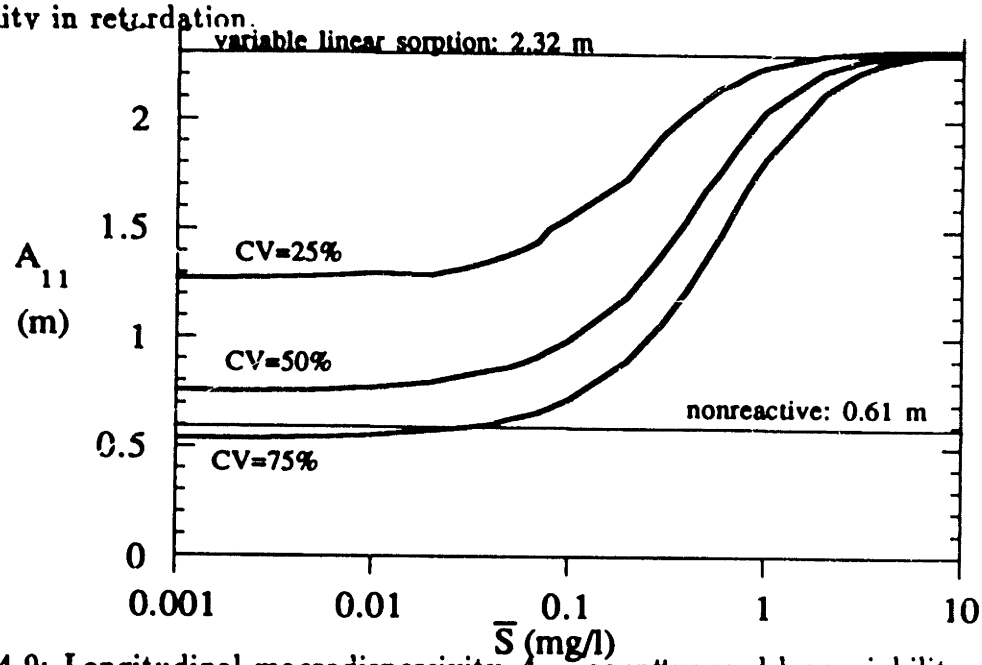


Figure 4-9: Longitudinal macrodispersivity $A_{11}$ as influenced by variability of decay rate, based on parameters for the Borden site ; $\bar{C} = 1\frac{mg}{l}$.

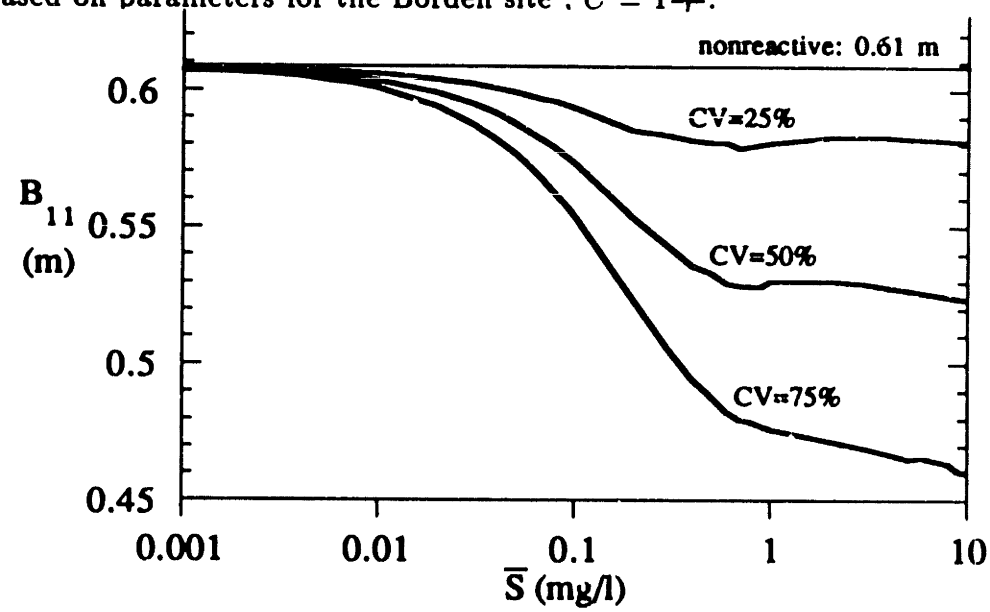


Figure 4-10: Longitudinal macrodispersivity $B_{11}$ as influenced by variability of decay rate, based on parameters for the Borden site ; $\bar{C} = 1\frac{mg}{l}$.

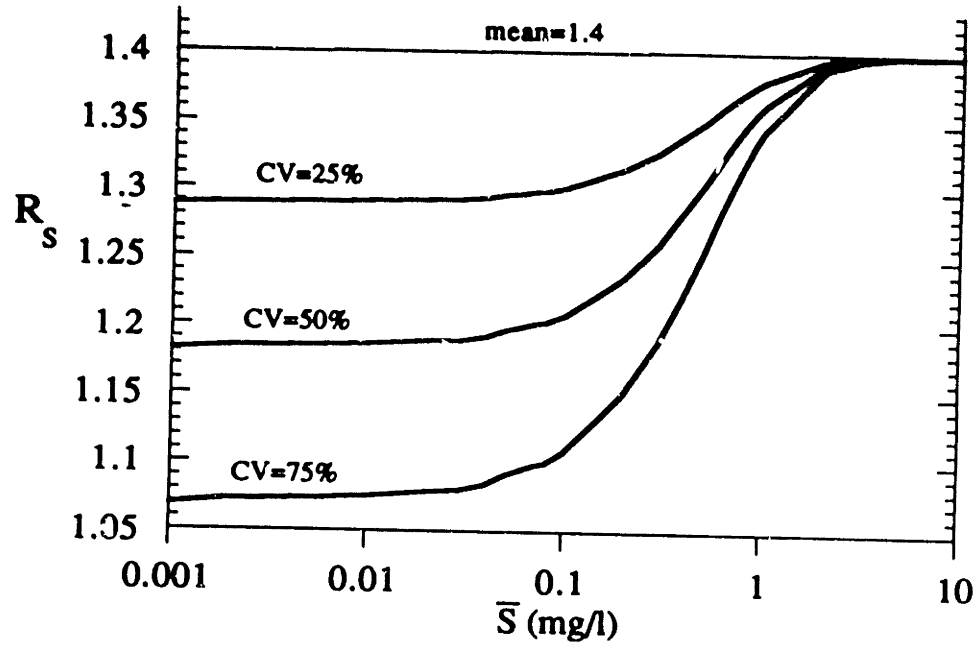


Figure 4-11: Effective retardation factor $R_S$ as influenced by variability of retardation, based on parameters for the Borden site ; $\bar{C} = 1\frac{mg}{l}$.

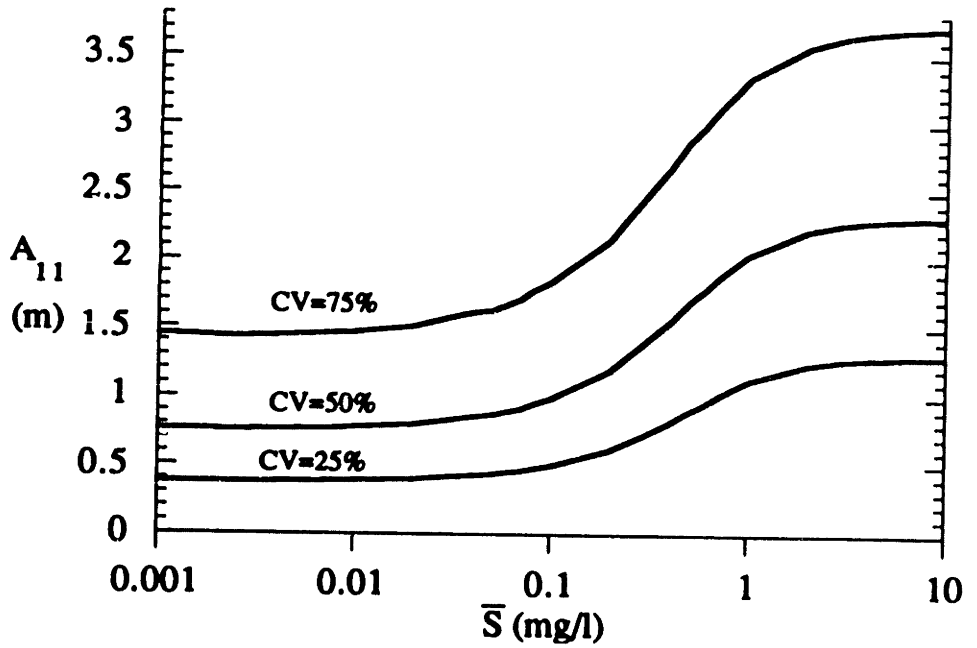


Figure 4-12: Longitudinal macrodispersivity $A_{11}$ as influenced by variability of retardation, based on parameters for the Borden site ; $\bar{C} = 1\frac{mg}{l}$.

### 4.3.2 Application of the analysis to the Traverse City site

The Traverse City site in Michigan has been contaminated since 1969, when a spill of aviation gasoline from an underground storage tank at the U.S. Coast Guard Air Station at Traverse City contaminated a shallow, sandy, water table aquifer. Groundwater moving through the spill produced a large plume that eventually moved off the base and affected a number of domestic water wells in a residential area. The spill contained at least 25,000 gallons of aviation gasoline, which drained to the water table 6 feet below the land surface [Wilson *et al.*, 1990]. The contaminant present in the site at highest aqueous concentrations is toluene [Twenter *et al.*, 1985]. A brief description of some of the plume characteristics and the group of hydrologic, chemical and microbiological parameters used in modeling the fate of the contaminant plume is shown in Table 4.2.

For the Traverse City case, data relating the microbiological, chemical and hydrologic parameters is less abundant than that for the Borden site. For instance, no variability data is available in the literature, so an arbitrary value of $\sigma_f^2 = 1$ was used in order to present results with a higher degree of aquifer variability. The horizontal correlation length $\lambda_1$ was chosen to be approximately 5% of the plume length. The porosity $n$, groundwater velocity $v$ and the mean retardation factor for toluene in the site were taken from Twenter *et al.* [1985].

Recent data for biodegradation indicate that toluene is more slowly degraded than benzene at the site [Wilson *et al.*, 1990]. Because of this, a smaller mean decay rate was chosen to represent the biodegradation process. The values of the other biodegradation parameters were chosen as those for the Borden site, except the stoichiometric factor $W$, which was taken from Wilson *et al.* [1990]. In this case, the coefficients of variation for sorption and decay were held at 50%, and the values of the correlations and residual variances were varied accordingly in order to study the sensitivity of the results to each of these parameters separately.

Table 4.2: Parameters for Traverse City site

## HYDROLOGY

The hydraulic gradient is $J = 0.004$ (measured from map and reported) and the effective hydraulic conductivity is $K_{eff} = 36.6\frac{m}{day}$. The contaminant plume longitudinal scale is 1.3 $km$ approximately. Other parameters are:

- porosity $n = 0.3$
- variance of lnK $\sigma_f^2 = 1.0$
- horizontal correlation length of f: $50m$
- vertical correlation length of f: $1m$
- groundwater velocity $v = 0.5\frac{m}{day}$

These parameters satisfy Darcy's equation.

## SORPTION

- mean retardation factor for the contaminant=1.8 (from references).
- $b_2 = -0.9$, $\sigma_\eta = 0$ (50 % coefficient of variation)
- $b_2 = -0.85$, $\sigma_\eta = 0.3$ (50 % coefficient of variation)
- $b_2 = -0.67$, $\sigma_\eta = 0.6$ (50 % coefficient of variation)
- $b_2 = 0$, $\sigma_\eta = 0.9$ (50 % coefficient of variation)

## BIODEGRADATION

- DO half-saturation constant $0.1\frac{mg}{l}$
- contaminant half-saturation constant $0.5\frac{mg}{l}$

- mean microbial biomass concentration= $0.2\frac{mg}{l}$
- mean maximum growth rate=$0.1/day$
- stoichiometric factor $W = 1.25$
- $b_1 = -0.018\frac{mg/l}{day}$, $\sigma_\delta = 0$ (50% coefficient of variation)
- $b_1 = -0.017\frac{mg/l}{day}$, $\sigma_\delta = 0.0035\frac{mg/l}{day}$ (50% coefficient of variation)
- $b_1 = -0.013\frac{mg/l}{day}$, $\sigma_\delta = 0.007\frac{mg/l}{day}$ (50% coefficient of variation)
- $b_1 = 0$, $\sigma_\delta = 0.01\frac{mg/l}{day}$ (50% coefficient of variation)

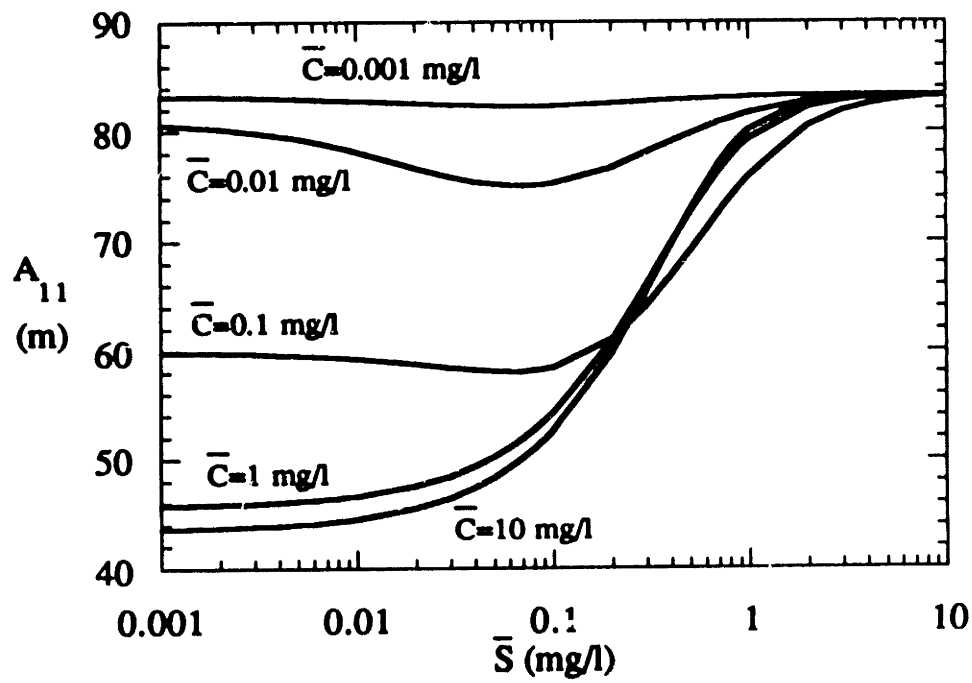


Figure 4-13: Longitudinal macrodispersivity $A_{11}$ based on parameters for the Traverse City site .

Figures 4-13 and 4-14 show plots of the longitudinal macrodispersivities $A_{11}$ and $B_{11}$. In this case, the magnitudes of the macrodispersivities are significantly higher due to the larger scale. The general features observed are the same as those explained above. The macrodispersion for a given species - contaminant and dissolved oxygen - increases with its own concentration, and decreases as the concentration of the other species is increased. The value of $B_{11}$ can vary within an order of magnitude depending on the concentration conditions, from approximately $1.5m$ to over $18m$. Once again, it is demonstrated that the contaminant and dissolved oxygen macrodispersivities are widely different in magnitude as a consequence of the contaminant sorption process. The values of the macrodispersivities in the absence of biodegradation ($w = 0$) are $A'_{11} = 83.3m$, and $B'_{11} = 18.2m$. The influence of the variability in the biodegradation process is one of decreasing macrodispersivities from their values when the decay rate is constant.

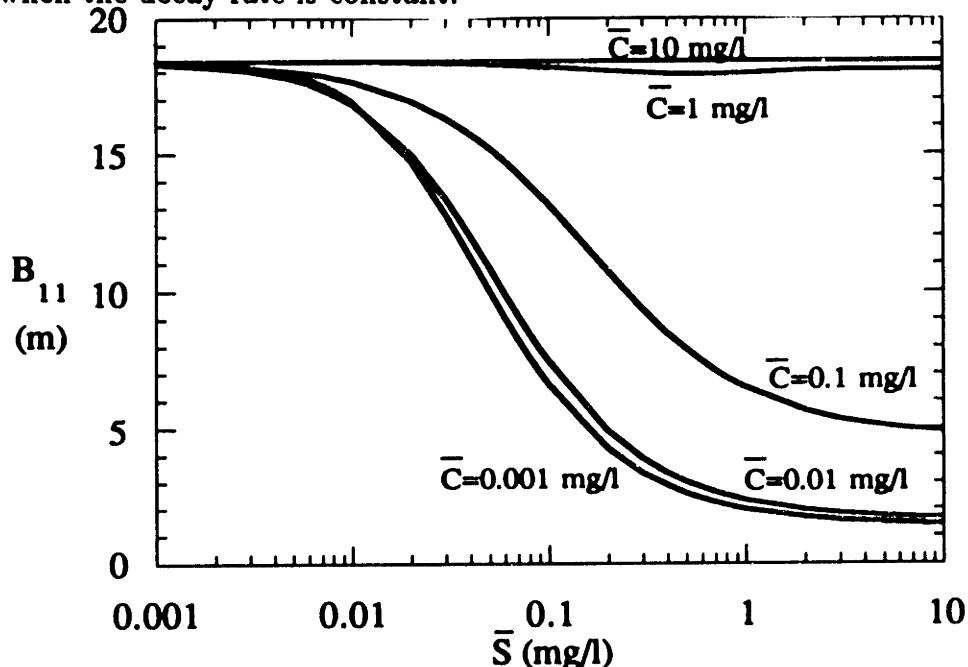


Figure 4-14: Longitudinal macrodispersivity $B_{11}$ based on parameters for the Traverse City site .

With regard to the effective retardation and decay coefficients, some of the features present in the results for the Borden site are also observed here. In Figure 4-15, results for the effective retardation factor show a more significant decrease than that for the Borden site from the mean retardation value of 1.8, approximately a 25 % decrease at the lowest retardation value. The same trend of a higher decrease when more microbial activity is taking place is observed, since the minimum value of $R_S$ is reached at the lowest concentrations of the contaminant and the highest concentration of dissolved oxygen. Figure 4-16 shows plots for the effective decay rate, where in this case a variation of around 70 % as oppose to 50 % for the Borden site parameters is obtained. In general, these findings indicate that at higher values of aquifer variability and length scales ($\sigma_f^2\lambda_1$) the effects of the biodegradation process are effectively accentuated.

A sensitivity analysis for this set of parameters was performed, but in this case, the coefficients of variation of the decay rate and retardation factor were held constant at 50 %, and the slopes and residuals of their correlations with $lnK$ (coefficients $b_1, \delta, b_2$ and $\eta$, respectively) were varied accordingly.

In Figure 4-17, the results obtained show that the effective decay rate is sensitive to the correlation with $lnK$, in particular that more deviation from the mean is observed for less correlation with $lnK$, reaching a maximum decrease for uncorrelated decay rate $w$, *i.e.* $b_1 = 0$ . This is a relevant feature that highlights the importance of making paired measurements of $\kappa$ and $lnK$ on sets of samples in order to evaluate the degree of correlation. In Figure 4-18, however, this correlation does not seem to be an influential factor to the calculation of the macrodispersivities, since all curves are practically the same for all values of $b_1$ considered. The influence of the $K_d - lnK$ correlation is presented in Figures 4-19 and 4-20 The parameter $b_2$ has a dramatic influence in the macrodispersivity $A_{11}$. This confirms the results obtained by Garabedian *et al.* [1988]. The influence on the effective retardation, although not as dramatic, proves to be significant. These results confirm the fact that the $K_d - lnK$ correlation is an important factor controlling the dispersion and sorption processes under biodegradation as well.

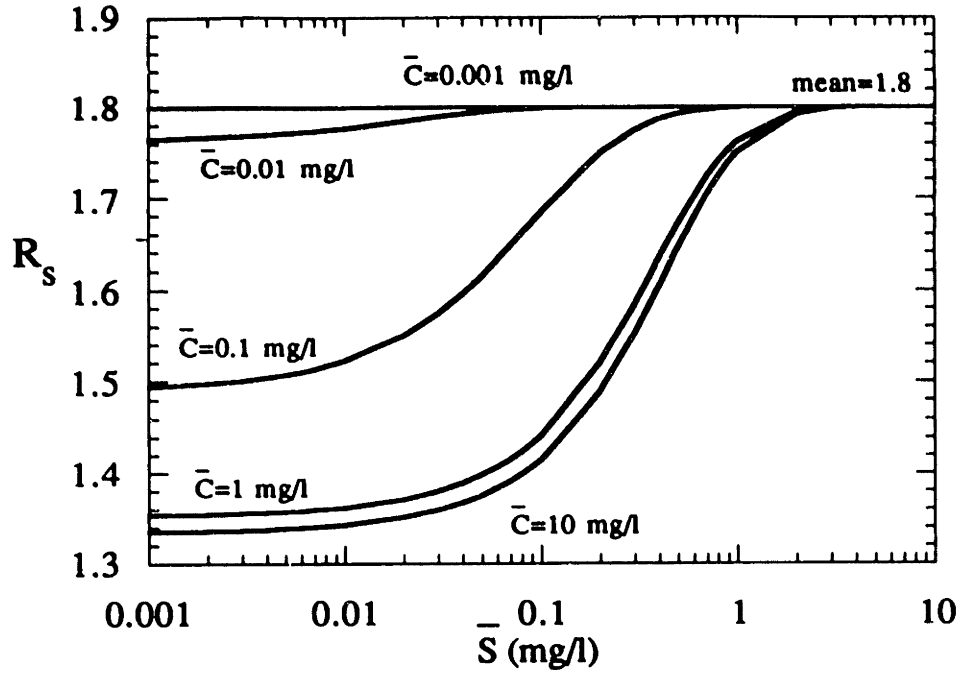


Figure 4-15: Effective retardation factor $R_S$ evaluated using parameters for the Traverse City site .

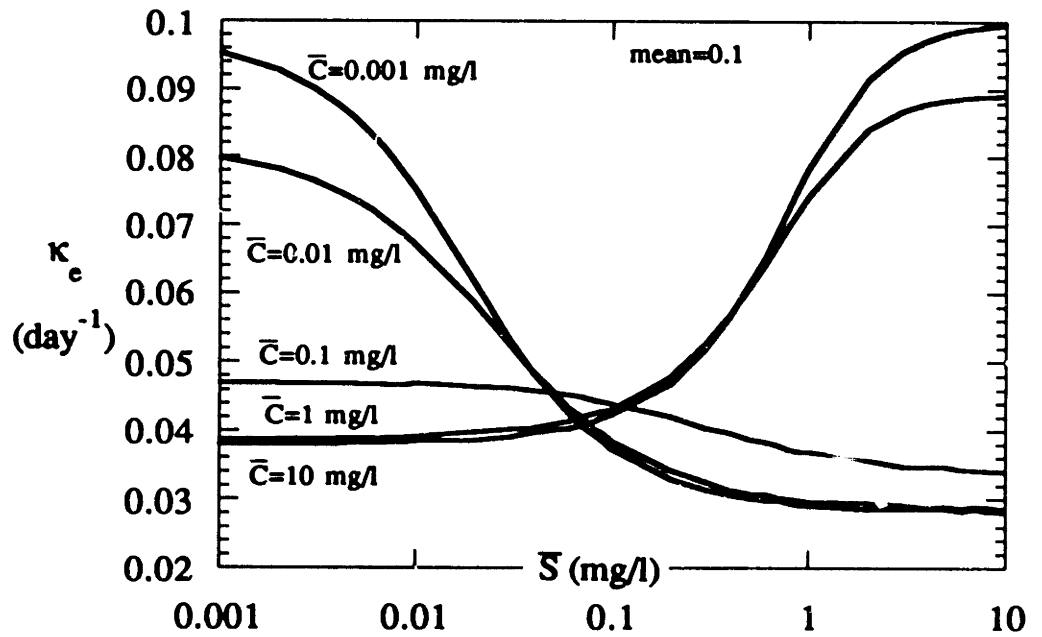


Figure 4-16: Effective decay rate evaluated using parameters for the Traverse City site .

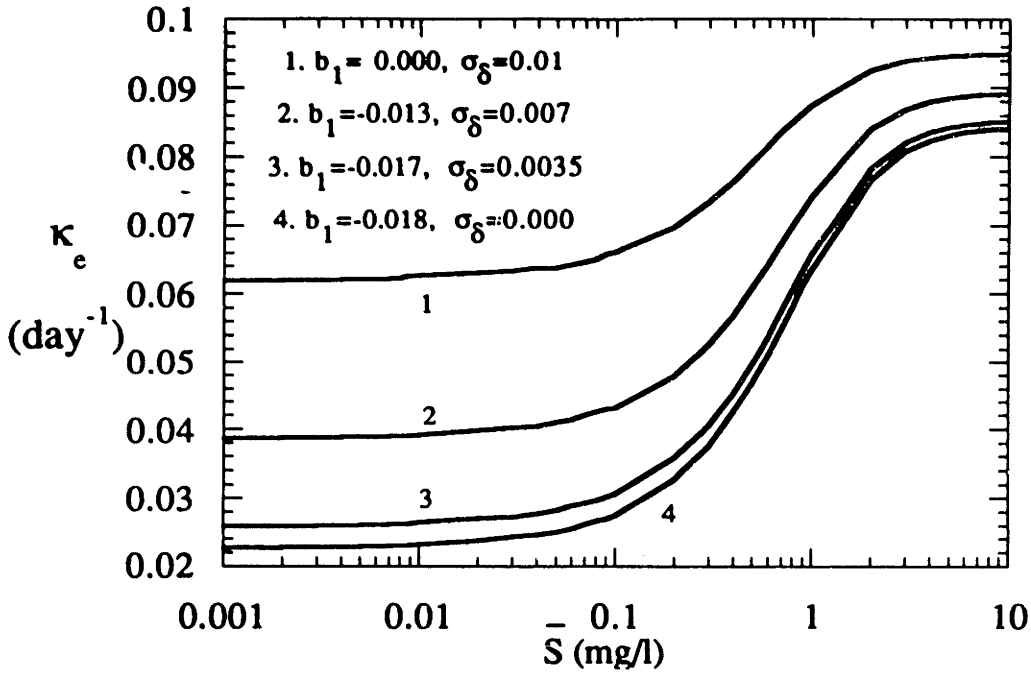


Figure 4-17: Effective decay rate as influenced by the parameters $b_1$ and $\sigma_\delta$, based on parameters for the Traverse City site ; $\bar{C} = 1\frac{mg}{l}$.

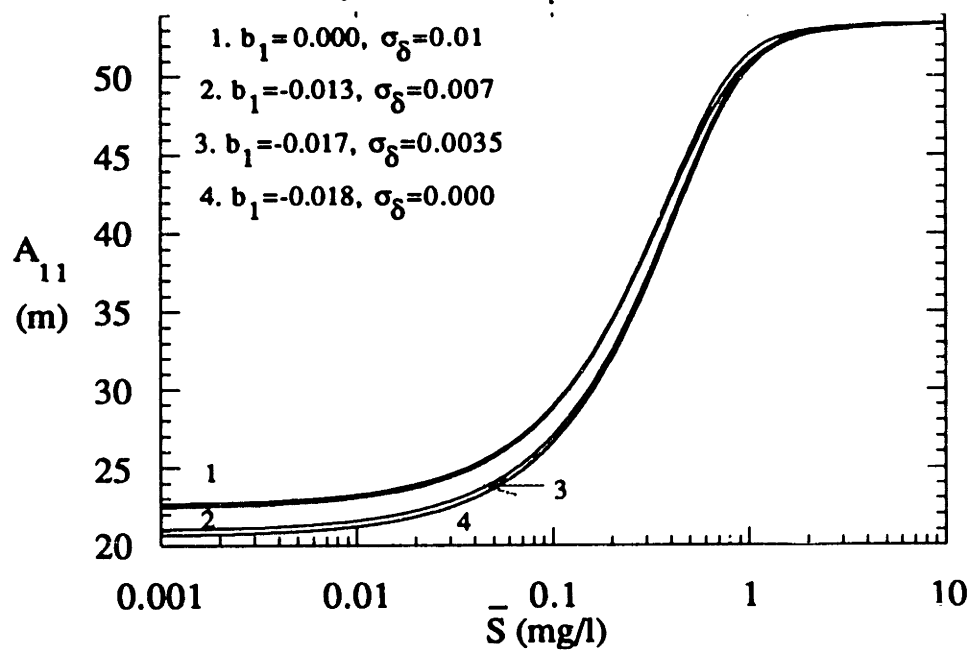


Figure 4-18: Longitudinal macrodispersivity as influenced by the parameters $b_1$ and $\sigma_\delta$, based on parameters for the Traverse City site ; $\bar{C} = 1\frac{mg}{l}$.

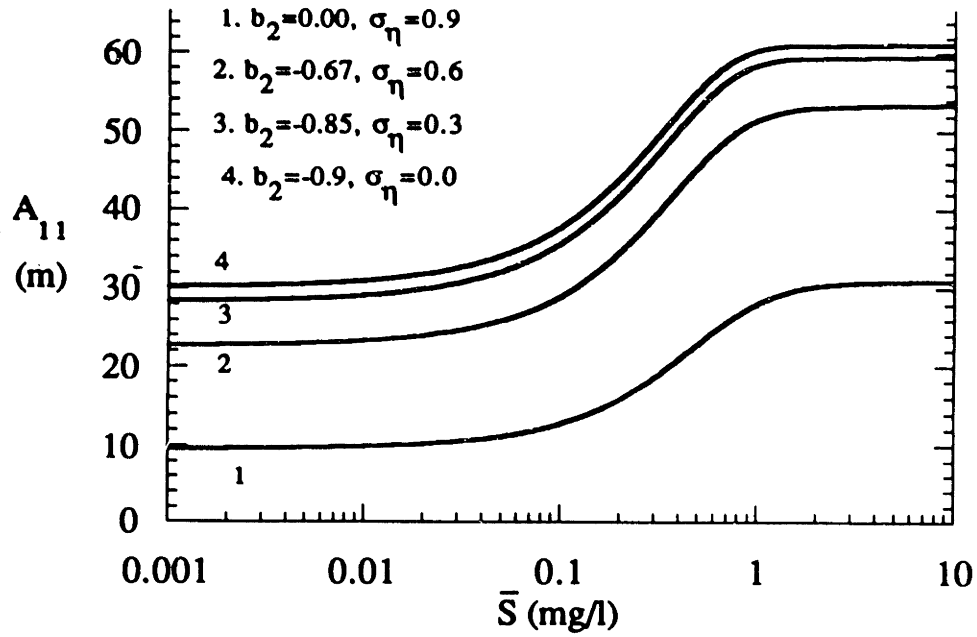


Figure 4-19: Longitudinal macrodispersivity $A_{11}$ as influenced by the parameters $b_2$ and $\sigma_\eta$, based on parameters for the Traverse City site ; $\bar{C} = 1\frac{mg}{l}$.

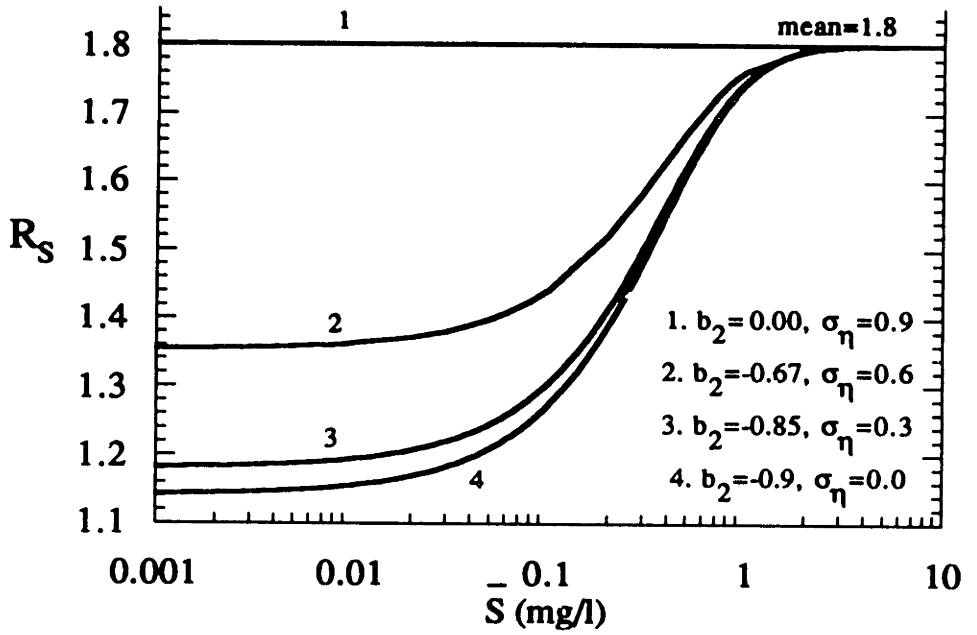


Figure 4-20: Effective retardation factor $R_S$ as influenced by the parameters $b_2$ and $\sigma_\eta$, based on parameters for the Traverse City site ; $\bar{C} = 1\frac{mg}{l}$.

## 4.4 Summary and Conclusions

The stochastic theory developed in this investigation provides a framework for analyzing two-component reactive transport in three-dimensionally heterogeneous, statistically anisotropic aquifers. The stochastic approach, which is based on a locally stationary, small-perturbation approximation, provides a systematic way of aggregating the effects of complex heterogeneities into relatively simple equations describing field-scale transport and transformation. The methodology presented here is able to handle a general functional form of the source/sink term, in which Monod kinetics represent a particular case.

In particular, on oxygen-limited biodegradation, the presence of heterogeneities have strong effects on the longitudinal macrodispersivities for the contaminant and the dissolved oxygen, which are found to be considerably different in magnitude under most concentration regimes. The field scale decay rate is always less than the mean. Consequently, calculations based on the mean decay rate will significantly over-predict the overall rate of biodegradation of the contaminant. Based on the calculations performed for the Borden and Traverse City sites, the effective decay rate may be reduced by a factor of 2 or 3 relative to the mean. The effective retardation factor is less than the mean under a negative sorption-log conductivity correlation. The opposite effect is created with a positive correlation. In any case, the effects of heterogeneities on retardation are weaker than those for macrodispersivities and effective decay rate. The influence of the sorption and biodegradation correlations with the log-conductivity field appear to be a dominant feature controlling the field scale dispersion process. The effective decay rate and the longitudinal macrodispersivities are significantly influenced by the decay-log conductivity correlation. In a similar way, the sorption-log conductivity correlation has an important effect on the longitudinal macrodispersivity for the contaminant.

In this work, the emphasis has been placed on longitudinal macrodispersion. Prior experimental and numerical investigations indicate that this is the dominant mechanism of plume dispersion process. The problem of transverse dispersion at a field scale

has not been resolved by the stochastic theory to this point, and we do not address the issue in this investigation. Also, the results are applicable only where the mean concentrations vary slowly in space so that the concentration gradients can be approximated as only time-dependent. This condition is realistic far from input sources, where the plumes have dispersed such that the gradients appear approximately constant on the scale of the concentration variability. This is why contaminant spills, as opposed to continuous sources, are the kind of field problems for which this kind of analysis is useful. This assumption, plus that of ergodocity, limits the applicability of the analysis to large time, large displacement problems.

These results have important practical implications. Computer models currently used [*e.g.* Rifai, 1988] to simulate the biodegradation process under field conditions, presume that the same dispersion coefficient applies for the contaminant and the dissolved oxygen. The results of this investigation show that this is not the case, and provide a quantification of the difference between these field-scale dispersivities. Also, the results demonstrate the importance of making paired measurements of sorption and decay with hydraulic conductivity on field samples, in order to determine the controlling correlations of the biodegradation process mentioned above. In this way, the stochastic theory serves as a guide to set priorities for data collection purposes, in the sense that it indicates which data should be collected in the field and how the data should be interpreted to determine field-scale transport coefficients.

In order to determine the applicability of the analytical results to real field cases, it is recommended at this point that mean flow simulations using the predicted field scale transport and transformation coefficients are performed and compared with measurements of plume evolution in actual contaminated sites. Also, detailed numerical simulations like the ones presented in Miralles-Wilhelm *et al* [1992] can serve as a tool to evaluate the stochastic model. A comparison of the stochastic theory with these detailed simulations is presented in Chapter 5.

The inclusion of non-linear sorption isotherms, which was shown to affect reactive plume behavior considerably in Chapter 3, the transient development of the microbial population dynamics, and an improved formulation for the transverse components

of the macrodispersivity tensor pose potential further developments of this line of investigation. Treatment of the growth dynamics of the microorganisms, and its effect on the characteristics of biodegradable plumes is the subject of Chapter 5.

# Chapter 5

# Biodegradation in heterogeneous aquifers with transient microbial dynamics

## 5.1 Introduction

In Chapter 4, an analysis of the transport equations for a contaminant solute and dissolved oxygen undergoing biodegradation was pursued assuming a microbial population in steady state. This assumption was made with the understanding that established populations of microorganisms existed within the aquifer at large times since the introduction of the contaminant into the system. However, transients in the microbial population dynamics could be expected since both the contaminant and dissolved oxygen plumes are moving in space, sweeping through areas where these indigenous microbial populations are established and where a sudden increase in the amount of a substrate may cause growth and/or death of microorganisms.

At a field scale, growth and death dynamics of microorganisms are perhaps the component of the biodegradation problem which has been least studied to this point. The strongest assumptions that are imbedded in any model of biodegradation really emerge from the biological source terms in the transport equations. The issue of conceptualization of the physical presence of the microorganisms in the subsurface is a

major point of difference between modeling approaches of biodegradation in groundwater. Biofilms are widely recognized as an acceptable description [Taylor and Jaffe, 1991], though the idea of isolated colonies of microorganisms has not been discarded. In both cases, the growth dynamics of the microorganisms have been described using Monod-type kinetics. This description, which is similar to the Michaelis-Menten expression for enzyme activity, introduces a number of parameters that have to be determined before any model can be utilized. These parameters are the maximum growth rate $\kappa$, the microbial biomass $M$ and the half saturation constants for the limiting nutrients considered. These parameters must be experimentally determined, or drawn from prior investigations, and this is where the difficulty arises. There are a number of reasons for this, but it basically amounts to unavailability of data.

First, measurements of growth and death rates in the field are rare in the literature, and their estimation carries high levels of uncertainty [Harvey and George, 1987]. The very limited data available on growth and death rates has been obtained in laboratory conditions, it is very sparse, and has high levels of uncertainty [Baker, 1986, Billen *et al.*, 1988]. Secondly, the values for the half saturation constants are usually obtained in bioreactor experiments, which require knowledge of the particular microorganism (or group of microorganisms) and the particular organic compound under study. Information regarding specific microorganisms capable of degrading specific organic compounds is often abundant but very specific to the particular environmental conditions involved. For example, benzene and toluene, two of the most common gasoline derivatives have been matched with *Pseudomonas putida* and *Bacillus sp* [Kobayashi and Rittman, 1989], while halogenated aromatics such as 1,4 dichlorobenzene have been found to be biodegraded by a consortium in groundwater [Boyle, 1989]. Interaction between biodegradable substrates has also been reported [Alvarez *et al.*, 1991]. If a broader statement must be made, then bacteria and fungi are primarily responsible for the degradation of hydrocarbons in the environment [Leahy and Colwell, 1990]. Microbial biomass data is relatively more abundant, though it is still obtained in the laboratory and it is environment-specific. A recent review of aquatic bacteriological methods [Fry, 1988] presents a large number of estimates of mean cell volumes for

different aquatic environments. These mean cell volumes (biovolumes) can be converted into biomass by using a conversion factor that is based on reference values of bacterial density, dry weight/wet weight ratio and carbon/dry weight ratio. However, no variability of the values presented is reported. Again, detailed measurements of biovolumes under specific field conditions are still necessary. Because of these considerations, a generalization approach that can be used for modeling purposes is a major task in itself.

This Chapter focuses on studying the effects of incorporating transient microbial dynamics in the system of transport equations for a contaminant and dissolved oxygen. This essentially is equivalent to increasing the number of components to three, since a partial differential equation for the microbial mass in the system is introduced to describe biomass conservation under growth and death dynamics caused by the interation with the flow field and with the two other components in the system. By comparing the results obtained with this analysis with those obtained in Chapter 4, a better understanding of the influence of the potential growth/death of microorganisms on a contaminated environment is expected.

## 5.2 Governing equations and development of spectral equations

In this section, transient effects in the microbial population growth dynamics are incorporated into an analysis similar to that presented in Chapter 4. For this purpose, an active biomass balance equation that accounts for substrate or oxygen limited growth, and death may be written as:

$$\frac{\partial M}{\partial t} + \frac{1}{R_m}\frac{\partial (v_i M)}{\partial x_i} = \frac{1}{R_m}\frac{\partial}{\partial x_i} D_{ij}\frac{\partial M}{\partial x_j} + Yr(S, C, M) - \beta M \qquad (5.1)$$

In this equation, $Y$ is the microbial yield (biomass produced per unit mass of substrate degraded), $\beta$ is a first-order death rate of microorganisms, and a linear proportion between free-living and attached microbes is assumed. For most natural

conditions in groundwater, microorganisms are mostly attached to the solids and therefore $R_m >> 1$ [Chiang *et al.*, 1991]. In view of this, the following analysis is developed using a simplified version of this equation,

$$\frac{\partial M}{\partial t} = Yr(S, C, M) - \beta M \tag{5.2}$$

This governing equation represents a mass conservation statement for the third component of the problem, which is the active microbial biomass. In this context, this component is also described as a sum of a ensemble mean and a perturbation, as it was done in Chapter 4 for the contaminant and dissolved oxygen concentrations.

$$M = \bar{M} + M' \tag{5.3}$$

Since the biomass is now a dependent variable, the contaminant decay rate parameter $\kappa$ is then considered to be a random field, with a mean and a perturbation related to those of the log-hydraulic conductivity field. The same applies for the retardation factor $R$. Recalling these expressions from Chapter 4:

$$\kappa = \bar{\kappa} + \kappa' \tag{5.4}$$

$$\bar{\kappa} = a_1 + b_1 \bar{f} \tag{5.5}$$

$$\kappa' = b_1 f' + \delta \tag{5.6}$$

$$R = \bar{R} + R' \tag{5.7}$$

$$\bar{R} = a_2 + b_2 \bar{f} \tag{5.8}$$

$$R' = b_2 f' + \eta \tag{5.9}$$

Also, for generality, it is assumed that the microbial death rate $\beta$ can also be decomposed into a mean and a random fluctuation, related to the mean and perturbations of the log-hydraulic conductivity field $f = lnK$:

$$\beta = \bar{\beta} + \beta' \tag{5.10}$$

$$\bar{\beta} = a_3 + b_3 \bar{f} \tag{5.11}$$

$$\beta' = b_3 f' + v \tag{5.12}$$

Following the procedure presented in Chapter 4, the source term describing microbial growth is expanded in a Taylor series around the mean concentrations according to:

$$r(S, C, M) = r + r_S S' + r_C C' + r_M M' + ...$$

$$r = r(\bar{S}, \bar{C}, M)$$

$$r_S = (\frac{\partial r}{\partial S})_{\bar{S},\bar{C},\bar{M}}$$

$$r_C = (\frac{\partial r}{\partial C})_{\bar{S},\bar{C},\bar{M}}$$

$$r_M = (\frac{\partial r}{\partial M})_{\bar{S},\bar{C},\bar{M}} \tag{5.13}$$

These expressions can be replaced into the governing equation (5.2) to produce mean and perturbation equations given by:

$$\frac{\partial \bar{M}}{\partial t} = Y \left[\bar{r} + \overline{r'_S S'} + \overline{r'_C C'} + \overline{r'_M M'}\right] - \bar{\beta}\bar{M} - \overline{\beta' M'} \tag{5.14}$$

$$\frac{\partial M'}{\partial t} = Y \left[r' + \bar{r_S} S' + \bar{r_C} C' + \bar{r_M} M'\right] - \bar{\beta} M' - \beta' \bar{M} \tag{5.15}$$

Introducing Fourier-Stieltjes Representations for the perturbed quantities, the per-

turbation equation is written in spectral space as:

$$\frac{\partial dZ_M}{\partial t} - Y\bar{r_S}dZ_S - Y\bar{r_C}dZ_C + (\bar{\beta} - Y\bar{r_M})dZ_M + YdZ_r + \bar{M}dZ_\beta = 0 \qquad (5.16)$$

In order to obtain a simplified large time solution to this equation where the time derivative term is neglected, this equation must be scaled according to (see Appendix B):

$$dZ_M = dZ_{\hat{M}} exp\left[-\int_0^t (\beta_e - Yr_{me})dt'\right] + \int_0^t Y(r_{se}dZ_S + r_{ce}dZ_C) exp\left[-\int_{t'}^t (\beta_e - Yr_{me})dt''\right] dt' \qquad (5.17)$$

Here, $dZ_{\hat{M}}$ is the scaled perturbation quantity whose time derivative can be dropped at large times, and introduces the expressions for the effective death rate, and effective source functions $r_{se}, r_{ce}$ and $r_{me}$. These will be determined in the analysis that follows. This scaling reduces the perturbation equation to:

$$\frac{\partial dZ_{\hat{M}}}{\partial t} exp\left[-\int_0^t (\beta_e - Yr_{me})dt'\right] - Y(\bar{r_S} - r_{se})dZ_S - Y(\bar{r_C} - r_{ce})dZ_C$$

$$+ (\bar{\beta} - \beta_e - Y\bar{r_M} + Yr_{me})dZ_M + YdZ_r + \bar{M}dZ_\beta = 0 \qquad (5.18)$$

At large times, the equation is reduced to an algebraic equation in the concentration spectral amplitudes $dZ_S, dZ_C, dZ_M$:

$$-Y(\bar{r_S} - r_{se})dZ_S - Y(\bar{r_C} - r_{ce})dZ_C + (\bar{\beta} - \beta_e - Y\bar{r_M} + Yr_{me})dZ_M + YdZ_r + \bar{M}dZ_\beta = 0 \qquad (5.19)$$

This equation must be solved simultaneously with the spectral equations obtained for $dZ_S$ and $dZ_C$, equations (4.53) and (4.54), modified to include the perturbation in the microbial biomass to obtain solutions for the large time spectral amplitudes of the concentration perturbations:

$$(ivk_1 + D_{ij}k_ik_j + \bar{r_S} - r_{se})dZ_S + dZ_R(\frac{\partial \bar{S}}{\partial t} + \frac{v}{R_S}G_1)$$

$$- G_j dZ_{v_j} + (\bar{r_C} - r_{ce})dZ_C + (\bar{r_M} - r_{me})dZ_M + dZ_r = 0 \qquad (5.20)$$

$$(ivk_1 + D_{ij}k_ik_j + W.\bar{r_C} - W.r_{ce})dZ_C - F_j dZ_{v_j}$$

$$+ W(\bar{r_S} - r_{se})dZ_S + W(\bar{r_M} - r_{me})dZ_M + WdZ_r = 0 \qquad (5.21)$$

The solution to this set of algebraic equations is:

$$dZ_S\Delta = \left[ivk_1(\bar{\beta} - \beta_e - Y\bar{r_M} + Yr_{me}) + W(\bar{\beta} - \beta_e)(\bar{r_C} - r_{ce})\right]$$

$$\left[G_i dZ_{v_i} - dZ_R(\frac{\partial \bar{S}}{\partial t} + \frac{v}{R_S}G_1) - dZ_r\right]$$

$$- (\bar{\beta} - \beta_e)(\bar{r_C} - r_{ce})(F_i dZ_{v_i} - WdZ_r) - ivk_1(\bar{r_M} - r_{me})(YdZ_r + \bar{M}dZ_\beta) \qquad (5.22)$$

$$dZ_C\Delta = -W(\bar{r_S} - r_{se})(\bar{\beta} - \beta_e)\left[G_i dZ_{v_i} - dZ_R(\frac{\partial \bar{S}}{\partial t} + \frac{v}{R_S}G_1) - dZ_r\right]$$

$$+ \left[ivk_1(\bar{\beta} - \beta_e - Y\bar{r_M} + Yr_{me}) + (\bar{\beta} - \beta_e)(\bar{r_S} - r_{se})\right](F_i dZ_{v_i}$$

$$- WdZ_r) - ivk_1W(\bar{r_M} - r_{me})(YdZ_r + \bar{M}dZ_\beta) \qquad (5.23)$$

$$dZ_M\Delta = ivk_1Y(\bar{r_S} - r_{se})\left[G_i dZ_{v_i} - dZ_R(\frac{\partial \bar{S}}{\partial t} + \frac{v}{R_S}G_1) - dZ_r\right]$$

$$- \left[-v^2k_1^2 + ivk_1(\bar{r_S} - r_{se} + W\bar{r_C} - Wr_{ce})\right](YdZ_r + \bar{M}dZ_\beta)$$

$$+ ivk_1Y(\bar{r_C} - r_{ce})(F_i dZ_{v_i} - WdZ_r) \qquad (5.24)$$

with,

$$\Delta = -(\bar{\beta} - \beta_e - Y\bar{r_M} + Yr_{me})v^2k_1^2 + ivk_1(\bar{\beta} - \beta_e)(\bar{r}_S - r_{se} + W\bar{r}_C - Wr_{ce}) \quad (5.25)$$

## 5.3 Solution methodology

In this section, the methodology of solution followed to obtain effective transport and transformation coefficients for the contaminant, dissolved oxygen and biomass is described for two different microbial growth dynamics scenarios. First, a treatment of the transient dynamics for the growth and death of biomass is considered using the preceeding analysis. Secondly, the particular situation where the mean growth and death of microorganisms are balanced in time is treated to study the conditions under which an equilibrium in the mean biomass is reached. This second case can be used to compare with the results of Chapter 4, where an equilibrium in the total microbial biomass is assumed. In both case, microbial growth is assumed to followed the Monod expression:

$$r(S, C, M) = \kappa M \frac{S}{S_0 + S} \frac{C}{C_0 + C} \quad (5.26)$$

with corresponding functions,

$$\bar{r} = \bar{\kappa}\bar{M} \frac{\bar{S}}{S_0 + S} \frac{\bar{C}}{C_0 + C} \quad (5.27)$$

$$\bar{r}_S = \bar{\kappa}\bar{M} \frac{S_0}{(S_0 + \bar{S})^2} \frac{C}{C_0 + C} \quad (5.28)$$

$$\bar{r}_C = \bar{\kappa}\bar{M} \frac{S}{S_0 + S} \frac{C_0}{(C_0 + \bar{C})^2} \quad (5.29)$$

$$\bar{r}_M = \bar{\kappa} \frac{\bar{S}}{S_0 + S} \frac{\bar{C}}{C_0 + C} \quad (5.30)$$

Using the theoretical results of the preceeding section, the second order correlation

terms that appear in the mean equation for the biomass (5.14) can be derived using the Spectral Representation Theorem. These terms are,

$$\overline{r'_S S'} = \int_{-\infty}^{\infty} E[dZ^*_{r_S} dZ_S] = \bar{M}\frac{S_0}{(S_0+\bar{S})^2}\frac{C}{C_0+C}\int_{-\infty}^{\infty} E[dZ^*_\kappa dZ_S] \tag{5.31}$$

$$\overline{r'_C C'} = \int_{-\infty}^{\infty} E[dZ^*_{r_C} dZ_C] = \bar{M}\frac{S}{S_0+S}\frac{C_0}{(C_0+\bar{C})^2}\int_{-\infty}^{\infty} E[dZ^*_\kappa dZ_C] \tag{5.32}$$

$$\overline{r'_M M'} = \int_{-\infty}^{\infty} E[dZ^*_{r_M} dZ_M] = \frac{\bar{S}}{S_0+S}\frac{\bar{C}}{C_0+C}\int_{-\infty}^{\infty} E[dZ^*_\kappa dZ_M] \tag{5.33}$$

$$\overline{\beta' M'} = \int_{-\infty}^{\infty} E[dZ^*_\beta dZ_M] \tag{5.34}$$

These second order correlations involve a number of integral expressions, similar to those presented in Chapter 4 and Appendix H. These integrals are developed and listed in Appendix J. The mean equation (5.14) is then arranged to develop the expressions for the effective growth and death rates of the microorganisms.

$$\begin{aligned}
\frac{\partial \bar{M}}{\partial t} &= Y[\bar{r} - v(\bar{\beta} - \beta_e - Y\bar{r}_M + Yr_{me})\Pi_4 - W(\bar{\beta}-\beta_e)(\bar{r}_C - r_{ce})\Pi_5 \\
&+W(\bar{\beta}-\beta_e)(\bar{r}_C - r_{ce})\Pi_5 - vY(\bar{r}_M - r_{me})\Pi_4 - v\bar{M}(\bar{r}_M - r_{me})\Pi_6 \\
&+W(\bar{r}_S - r_{se})(\bar{\beta}-\beta_e)\Pi_7 - vW(\bar{\beta}-\beta_e - Y\bar{r}_M + Yr_{me})\Pi_8 \\
&-W(\bar{\beta}-\beta_e)(\bar{r}_S - r_{se})\Pi_7 - vWY(\bar{r}_M - r_{me})\Pi_8 - vW\bar{M}(\bar{r}_M - r_{me})\Pi_9 \\
&-vY(\bar{r}_S - r_{se})\Pi_{10} + v^2Y\Pi_{11} + v^2\bar{M}\Pi_{12} + vY(\bar{r}_S - r_{se} + W\bar{r}_C - Wr_{ce})\Pi_{10} \\
&+v\bar{M}(\bar{r}_S - r_{se} + W\bar{r}_C - Wr_{ce})\Pi_{13} - vWY(\bar{r}_C - r_{ce})\Pi_{10}] \\
&-\bar{\beta}\bar{M} - [-vY(\bar{r}_S - r_{se})\Pi_{14} - v^2Y\Pi_{15} + vY(\bar{r}_S - r_{se} + W\bar{r}_C - Wr_{ce})\Pi_{14} \\
&+ v\bar{M}(\bar{r}_S - r_{se} + W\bar{r}_C - Wr_{ce})\Pi_{16} - vWY(\bar{r}_C - r_{ce})\Pi_{14}]
\end{aligned} \tag{5.35}$$

## 5.4 Effective transport and transformation coefficients

### 5.4.1 Effective microbial growth and death rates

The field scale coefficients of microbial growth and death are defined so that equation (5.35) is rewritten as:

$$\frac{\partial \bar{M}}{\partial t} = [Y\kappa_e \frac{\bar{S}}{S_0+\bar{S}} \frac{\bar{C}}{C_0+\bar{C}} - \beta_e]\bar{M} \tag{5.36}$$

After simplifying the mean equation for the microbial biomass, equation (5.35), the effective growth rate can be found by rearanging the remaining terms inside the bracket multiplying the microbial yield $Y$. The effective rate of microbial growth is found by the same analysis that produced the effective decay coefficient in Chapter 4, essentially an effective *Monod* growth rate. When microbial growth is allowed, the effective rate of this growth is also the effective decay rate for the contaminant and dissolved oxygen, given that the source terms in each governing equation is identical (with the corresponding stoichiometric factors). Also, the effective death rate is found by rearranging the terms inside the second bracket. The results for the integral expressions from Appendix J are introduced to obtain implicit expressions for the effective growth and death rates as:

$$\bar{\kappa} - \kappa_e = \frac{v^2 Y}{\phi_1}\left[\frac{\bar{S}}{S_0+\bar{S}}\frac{\bar{C}}{C_0+\bar{C}}\right]\frac{b_1^2\sigma_f^2+\sigma_\delta^2}{\chi(1+\chi)} + v^2\frac{b_1 b_3}{\phi_1}\frac{\sigma_f^2}{\chi(1+\chi)} \tag{5.37}$$

$$\bar{\beta} - \beta_e = v\bar{M}(\bar{\kappa}-\kappa_e)\left[\frac{S_0}{(S_0+\bar{S})^2}\frac{\bar{C}}{C_0+\bar{C}} + W\frac{C_0}{(C_0+\bar{C})^2}\frac{\bar{S}}{S_0+\bar{S}}\right]\frac{b_3^2\sigma_f^2+\sigma_\upsilon^2}{\phi_2}\frac{\chi}{1+\chi}$$

$$+ v^2 Y\frac{b_1 b_3}{\phi_1}\frac{\bar{S}}{S_0+\bar{S}}\frac{\bar{C}}{C_0+\bar{C}}\frac{\sigma_f^2}{\chi(1+\chi)} \tag{5.38}$$

with,

$$\phi_1 = v^2(\bar{\beta} - \beta_e - Y\bar{r}_M + Yr_{me}) \tag{5.39}$$

$$\phi_2 = v(\bar{\beta} - \beta_e)(\bar{r}_S - r_{se} + W\bar{r}_C - Wr_{ce}) \tag{5.40}$$

$$\chi = \frac{\phi_2 \lambda_1}{\phi_1} \tag{5.41}$$

Here, $\lambda_1$ is the correlation length in the flow direction of the $lnK$ perturbation spectrum, equation (4.9):

$$S_{ff} = \frac{\sigma_f^2 \lambda_1 \lambda_2 \lambda_3}{\pi^2[1 + (k_1\lambda_1)^2 + (k_2\lambda_2)^2 + (k_3\lambda_3)^2]^2} \tag{5.42}$$

Equations (5.37) and (5.38) are a set of nonlinear coupled algebraic equations that must be solve numerically in order to obtain the values of the effective parameters $\kappa_e$ and $\beta_e$. These coefficients will also be used to determine the field scale coefficients of retardation and dispersion in the following sections.

### 5.4.2 Effective retardation factors and macrodispersivities

In order to evaluate the effective retardation factors and the longitudinal macrodispersivities for the contaminant and dissolved oxygen, the second order correlations in the mean equations for these components must be analyzed. Recall equations (4.37) and (4.38) using the source term expansion (5.13):

$$\bar{R}\left(\frac{\partial \bar{S}}{\partial t} - \frac{v}{R_S}\frac{\partial \bar{S}}{\partial \zeta_1}\right) + \frac{\partial}{\partial t}\overline{R'S'} - \frac{v_i}{R_S}\frac{\partial}{\partial \zeta_i}\overline{R'S'} + v\frac{\partial \bar{S}}{\partial \zeta_1} + \frac{\partial}{\partial \zeta_i}\overline{v_i'S'} =$$

$$\frac{\partial}{\partial \zeta_i}D_{ij}\frac{\partial \bar{S}}{\partial \zeta_j} - [\bar{r} + \overline{r_S'S'} + \overline{r_C'C'} + \overline{r_M'M'}] \tag{5.43}$$

$$\frac{\partial \bar{C}}{\partial t} - \frac{v}{R_C}\frac{\partial \bar{C}}{\partial \xi_1} + v\frac{\partial \bar{C}}{\partial \xi_1} + \frac{\partial}{\partial \xi_i}\overline{v_i'C'} = \frac{\partial}{\partial \xi_i}D_{ij}\frac{\partial \bar{C}}{\partial \xi_j} - W[\bar{r} + \overline{r_S'S'} + \overline{r_C'C'} + \overline{r_M'M'}] \tag{5.44}$$

The second order correlations that appear in these equations are $\overline{R'S'}, \overline{v_i'S'}, \overline{v_i'C'}$, and those coming from the source terms $\overline{r_S'S'}, \overline{r_C'C'}, \overline{r_M'M'}$. These correlations can be found again by using the Spectral Representation Theorem, as in equations (4.58) through (4.60), and equations (5.31) through (5.33). Focus is placed in the longitudinal components *i.e.*, $i = j = 1$. These correlations are:

$$\overline{R'S'} = v(\bar{\beta} - \beta_e - Yr_M + Yr_{me})G_1\Pi_{17} + W(\bar{\beta} - \beta_e)(\bar{r}_C - r_{ce})G_1\Pi_{18}$$

$$-v\left(\frac{\partial \bar{S}}{\partial t} + \frac{v}{R_S}G_1\right)(\bar{\beta} - \beta_e - Yr_M + Yr_{me})\Pi_{19} - \left(\frac{\partial \bar{S}}{\partial t} + \frac{v}{R_S}G_1\right)(\bar{\beta} - \beta_e)(\bar{r}_C - r_{ce})\Pi_{20}$$

$$-(\bar{\beta} - \beta_e - Yr_M + Yr_{me})\Pi_{21} - W(\bar{\beta} - \beta_e)(\bar{r}_C - r_{ce})\Pi_{22} - (\bar{\beta} - \beta_e)(\bar{r}_C - r_{ce})F_1\Pi_{18}$$

$$+ W(\bar{\beta} - \beta_e)(\bar{r}_C - r_{ce})\Pi_{22} - Y(\bar{r}_M - r_{me})\Pi_{21} - \bar{M}(\bar{r}_M - r_{me})\Pi_{23} \qquad (5.45)$$

$$\overline{v_i'S'} = v(\bar{\beta} - \beta_e - Yr_M + Yr_{me})G_1\Pi_{24} + W(\bar{\beta} - \beta_e)(\bar{r}_C - r_{ce})G_1\Pi_{25}$$

$$-v\left(\frac{\partial \bar{S}}{\partial t} + \frac{v}{R_S}G_1\right)(\bar{\beta} - \beta_e - Yr_M + Yr_{me})\Pi_{17} - W\left(\frac{\partial \bar{S}}{\partial t} + \frac{v}{R_S}G_1\right)(\bar{\beta} - \beta_e)(\bar{r}_C - r_{ce})\Pi_{18}$$

$$- (\bar{\beta} - \beta_e)\Pi_{26} - (\bar{\beta} - \beta_e)(\bar{r}_C - r_{ce})F_1\Pi_{25} - \bar{M}(\bar{r}_M - r_{me})\Pi_{27} \qquad (5.46)$$

$$\overline{v_i'C'} = -W(\bar{\beta} - \beta_e)(\bar{r}_S - r_{se})G_1\Pi_{25} + W\left(\frac{\partial \bar{S}}{\partial t} + \frac{v}{R_S}G_1\right)(\bar{\beta} - \beta_e)(\bar{r}_S - r_{se})\Pi_{18}$$

$$+W(\bar{\beta} - \beta_e)(\bar{r}_S - r_{se})\Pi_{28} + v(\bar{\beta} - \beta_e - Yr_M + Yr_{me})F_1\Pi_{24} + (\bar{\beta} - \beta_e)(\bar{r}_S - r_{se})F_1\Pi_{25}$$

$$-W(\bar{\beta} - \beta_e - Yr_M + Yr_{me})\Pi_{26} - W(\bar{\beta} - \beta_e)(\bar{r}_S - r_{se})\Pi_{28}$$

$$- WY(\bar{r}_M - r_{me})\Pi_{26} - W\bar{M}v(\bar{r}_M - r_{me})\Pi_{27} \qquad (5.47)$$

$$\overline{r_S'S'} = v(\bar{\beta} - \beta_e - Yr_M + Yr_{me})G_1\Pi_{28} + W(\bar{\beta} - \beta_e)(\bar{r}_C - r_{ce})G_1\Pi_{30}$$

$$-v\left(\frac{\partial \bar{S}}{\partial t} + \frac{v}{R_S}G_1\right)(\bar{\beta} - \beta_e - Yr_M + Yr_{me})\Pi_{29} - \left(\frac{\partial \bar{S}}{\partial t} + \frac{v}{R_S}G_1\right)(\bar{\beta} - \beta_e)(\bar{r}_C - r_{ce})\Pi_{31}$$

$$-(\bar{\beta} - \beta_e - Yr_M + Yr_{me})\Pi_4 - W(\bar{\beta} - \beta_e)(\bar{r}_C - r_{ce})\Pi_5 - (\bar{\beta} - \beta_e)(\bar{r}_C - r_{ce})F_1\Pi_{30}$$

$$+ W(\bar{\beta} - \beta_e)(\bar{r}_C - r_{ce})\Pi_5 - Y(\bar{r}_M - r_{me})\Pi_4 - \bar{M}(\bar{r}_M - r_{me})\Pi_6 \qquad (5.48)$$

$$\overline{r'_C C'} = -W(\bar{\beta} - \beta_e)(\bar{r}_S - r_{se})G_1\Pi_{32} + W\left(\frac{\partial \bar{S}}{\partial t} + \frac{v}{R_S}G_1\right)(\bar{\beta} - \beta_e)(\bar{r}_S - r_{se})\Pi_{33}$$

$$+W(\bar{\beta} - \beta_e)(\bar{r}_S - r_{se})\Pi_7 + v(\bar{\beta} - \beta_e - Yr_M + Yr_{me})F_1\Pi_{36} + (\bar{\beta} - \beta_e)(\bar{r}_S - r_{se})F_1\Pi_{32}$$

$$-W(\bar{\beta} - \beta_e - Yr_M + Yr_{me})\Pi_8 - W(\bar{\beta} - \beta_e)(\bar{r}_S - r_{se})\Pi_7$$

$$- WY(\bar{r}_M - r_{me})\Pi_8 - W\bar{M}v(\bar{r}_M - r_{me})\Pi_9 \qquad (5.49)$$

$$\overline{r'_M M'} = vY(\bar{r}_S - r_{se})G_1\Pi_{34} - vY(\bar{r}_S - r_{se})\left(\frac{\partial \bar{S}}{\partial t} + \frac{v}{R_S}G_1\right)\Pi_{35}$$

$$-vY(\bar{r}_S - r_{se})\Pi_{10} + v^2Y\Pi_{11} - vY(\bar{r}_S - r_{se} + W\bar{r}_C - Wr_{ce})\Pi_{10} + v^2\bar{M}\Pi_{12}$$

$$- v\bar{M}(\bar{r}_S - r_{se} + W\bar{r}_C - Wr_{ce})\Pi_{13} + vY(\bar{r}_C - r_{ce})F_1\Pi_{34} - vWY(\bar{r}_C - r_{ce})\Pi_{10} \quad (5.50)$$

**Advective terms**

The advective terms that appear in the mean transport equations (5.43) and (5.44) must add to zero, since these equations are expressed in corresponding moving coordinate systems. This produces two equations to determine the effective retardation factors for the contaminant and dissolved oxygen.

In the mean equation for the contaminant, the advective terms that appear are grouped together,

$$v[\frac{\bar{R}}{R_S} - 1] + v(\bar{\beta} - \beta_e - Yr_M + Yr_{me})(\Pi_{28} - \frac{v}{R_S}\Pi_{29}) + W(\bar{\beta} - \beta_e)(\bar{r}_C - r_{ce})(\Pi_{30} - \frac{v}{R_S}\Pi_{31})$$

$$- W(\bar{\beta} - \beta_e)(\bar{r}_S - r_{se})(\Pi_{32} - \frac{v}{R_S}\Pi_{33}) + vY(\bar{r}_S - r_{se})(\Pi_{34} - \frac{v}{R_S}\Pi_{35}) = 0 \quad (5.51)$$

Introducing the expressions for the integrals from Appendix J and after some manipulation, the effective retardation factor is found to be:

$$R_S = \bar{R} - \frac{b_1 b_2}{v} T_1 \frac{\sigma_f^2 \lambda_1}{1+\chi} + \frac{b_1 b_2}{v} T_1 \frac{\chi_C}{\chi(1+\chi)} \sigma_f^2 \lambda,$$

$$- \frac{b_1 b_2}{v} T_2 \frac{\chi_S}{\chi(1+\chi)} \sigma_f^2 \lambda_1 - \frac{Y b_1 b_2}{\bar{\beta} - \beta_e} T_0 \frac{\chi_C}{1+\chi} \sigma_f^2 \tag{5.52}$$

Here, the variables $\chi$ and $T_0, T_1, T_2$ are given by equations (J.6), (J.19), (J.20) and (J.21) in Appendix J, respectively. The variables $\chi_S$ and $\chi_C$ are defined as:

$$\chi_S = \frac{(\bar{\beta} - \beta_e)(\bar{r}_S - r_{se})}{(\bar{\beta} - \beta_e - Y r_M + Y r_{me})} \tag{5.53}$$

$$\chi_C = W \frac{(\bar{\beta} - \beta_e)(\bar{r}_C - r_{ce})}{(\bar{\beta} - \beta_e - Y r_M + Y r_{me})} \tag{5.54}$$

It can be easily verified that,

$$\chi_S + \chi_C = \chi \tag{5.55}$$

In the mean equation for the dissolved oxygen, the advection terms add to zero to produce:

$$v[\frac{1}{R_C} - 1] - (\bar{\beta} - \beta_e)(\bar{r}_C - r_{ce})\Pi_{30} + v(\bar{\beta} - \beta_e - Y r_M + Y r_{me})\Pi_{36}$$

$$+ (\bar{\beta} - \beta_e)(\bar{r}_S - r_{se})\Pi_{32} + vY(\bar{r}_C - r_{ce})\Pi_{34} = 0 \tag{5.56}$$

with the resulting expression for the retardation factor $R_C$,

$$\frac{1}{R_C} = 1 - \frac{b_1 T_1}{vW} \frac{\chi_C}{\chi(1+\chi)} \frac{\sigma_f^2 \lambda_1}{\gamma} - \frac{b_1 T_2}{v(1+\chi)} \frac{\sigma_f^2 \lambda_1}{\gamma}$$

$$+ \frac{b_1 T_2}{v} \frac{\chi_S}{\chi(1+\chi)} \frac{\sigma_f^2 \lambda_1}{\gamma} - \frac{Y b_1 T_0}{W(\bar{\beta} - \beta_e)} \frac{\chi_C}{1+\chi} \sigma_f^2 \tag{5.57}$$

The flow factor $\gamma$ is given by:

$$\gamma = \frac{nv}{exp[E(lnK)]J_1} \tag{5.58}$$

where $n$ is the soil porosity and $J_1$ is the mean hydraulic gradient in the flow direction.

**Dispersive terms**

As explained in Chapter 4, the dispersive terms in the mean equations (5.43) and (5.44) are grouped together to obtain the macrodispersivity tensors $A_{ij}$ and $B_{ij}$ for the contaminant and dissolved oxygen, respectively. Interest here is placed on the longitudinal components $i = j = 1$. We then have,

$$vA_{11} = v(\bar{\beta} - \beta_e - Yr_M + Yr_{me})\Pi_{24} + W(\bar{\beta} - \beta_e)(\bar{r}_C - r_{ce})\Pi_{25}$$

$$-\frac{v^2}{R_S}(\bar{\beta}-\beta_e-Yr_M+Yr_{me})\Pi_{17}-W\frac{v}{R_S}(\bar{\beta}-\beta_e)(\bar{r}_C-r_{ce})\Pi_{18}-W\frac{v}{R_S}(\bar{\beta}-\beta_e)(\bar{r}_C-r_{ce})\Pi_{18}$$

$$-\frac{v}{R_S}\left[v(\bar{\beta} - \beta_e - Yr_M + Yr_{me})(\Pi_{17} - \frac{v}{R_S}\Pi_{19}) + W(\bar{\beta} - \beta_e)(\bar{r}_C - r_{ce})(\Pi_{18} - \frac{v}{R_S}\Pi_{20})\right] \tag{5.59}$$

$$vB_{11} = v(\bar{\beta} - \beta_e - Yr_M + Yr_{me})\Pi_{24} + (\bar{\beta} - \beta_e)(\bar{r}_S - r_{se})\Pi_{25} \tag{5.60}$$

which yields expressions for the longitudinal macrodispersivities $A_{11}$ and $B_{11}$ analogous to those presented in Chapter 4:

$$A_{11} = A'_{11}\frac{1}{1 + \chi_S} \tag{5.61}$$

$$B_{11} = B'_{11}\frac{1}{1 + \chi_C} \tag{5.62}$$

with,

$$A'_{11} = \frac{\sigma_f^2\lambda_1}{\gamma^2}\left[1 - \frac{b_2\gamma}{R_S}\right]^2 + \frac{\sigma_\eta^2}{R_S^2}\lambda_1 \tag{5.63}$$

$$B'_{11} = \frac{\sigma_f^2 \lambda_1}{\gamma^2} \tag{5.64}$$

The following section presents and discusses results obtained by evaluating the expressions for the effective transport and transformation coefficients derived here. The discussions is centered on a comparison with the results developed in Chapter 4 in order to understand the influence of microbial growth dynamics on the field scale process of biodegradation.

## 5.5 Discussion of results

Evaluations of the expressions for the effective transport and transformation coefficients developed in the previous section are presented here. These results are presented in two stages. First, the field scale coefficients of growth, death, retardation and dispersion are calculated using parameters for a hypothetical case of benzene biodegradation at the Borden site in Ontario, Canada. The parameters used for these calculations are given in Table 4.1, with the addition of a mean death rate of microorganisms of $\bar{\beta} = 0.1 day^{-1}$, and a microbial yield of $Y = 0.4$.

### 5.5.1 DO concentration effects and sensitivity analysis

Figures 5-1 and 5-2 show the effective growth and death rates of the microorganisms degrading the contaminant compound in the presence of different dissolved oxygen (DO) levels. These results were obtained using a coefficient of variation of 50% for both the growth and death rate random fields with half of the variance due to a partial correlation with the log-hydraulic conductivity field ($b_1, b_3$ coefficients) and the other half due to uncorrelated residuals ($\sigma_\delta^2, \sigma_\upsilon^2$). In contrast to the results developed in Chapter 4, where the effective decay rate was at least 50% of the mean, the effect of heterogeneities on the effective microbial growth rate (*i.e.*, contaminant and DO effective decay rate) is strong; a decrease of an order of magnitude is observed at high mean contaminant and DO concentrations. The death rate is decreased by 25% at most over a wide range of both contaminant and DO mean concentrations. Also, the effects are more pronounced for high levels of DO, with almost no effects produced at the low dissolved oxygen concentration regimes. This is consistent with the fact that at high DO levels, microbial growth and thus biodegradation occur more readily, so the effects of microbial growth are expected to be enhanced. This was not the case depicted in Figure 4-1, where microbial growth was not allowed for, and the effects of different DO levels are not clearly distinct. This becomes a common characteristic of the problem in the results that follow.

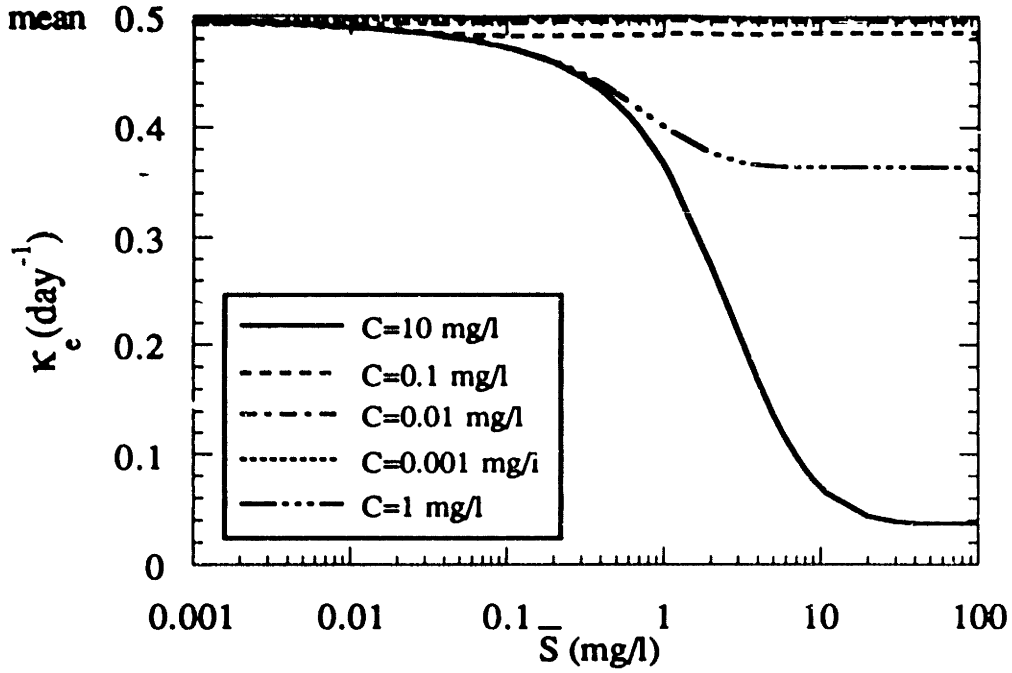


Figure 5-1: Effective microbial growth rate at different concentration regimes using parameters for the Borden site.

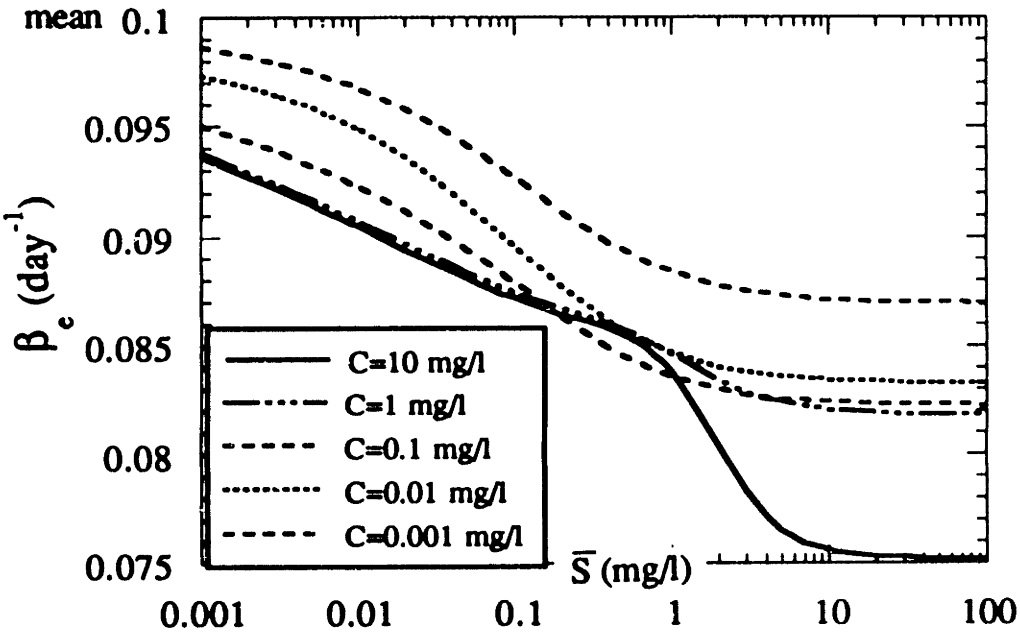


Figure 5-2: Effective microbial death rate at different concentration regimes using parameters for the Borden site.

The next set of plots show the effective retardation factor and longitudinal macrodispersivities for the contaminant and dissolved oxygen. In Figure 5-3, the plot for the effective retardation factor is very similar to that presented in Figure 4-2, which suggests that the effects of microbial growth dynamics on this parameter are weaker than those for the other field scale coefficients. The effective retardation factor for the dissolved oxygen was to be very close (5% maximum variation) to the mean value of unity.

The more interesting effects are observed for the longitudinal macrodispersivities $A_{11}$ and $B_{11}$ in Figures 5-4 and 5-5. These plots show significant differences with their Chapter 4 counterparts at high DO levels. At low DO levels, the biodegradation process is inhibited, and the results produced by this analysis are similar to the no net growth case presented in Chapter 4. The differences are found however, where DO levels are high, and the microorganisms are free to grow.

When dissolved oxygen concentrations are high, microorganisms grow with increasing contaminant concentrations following *Monod* kinetics, and contaminant macrodispersion decreases since most of the contaminant is being used for microbial growth. This decrease in macrodispersivity takes place to a point where microbial growth saturation occurs, and a further increase in $\bar{S}$ will no longer increase the rate of growth of microorganisms. This is when the contaminant plume spreading starts increasing to its asymptotic limit $A'_{11}$ (equation 5.61), where the source term in the governing equations reaches a zeroth-order limit and biodegradation effects are nonexistent. Dissolved oxygen macrodispersivity is only strongly affected at high DO levels, where it gets taken up by microbial growth, and its field scale dispersion decreases correspondingly.

On the other hand, in Chapter 4, the net rate of growth of the microoganisms is zero. This means that at high DO levels, the contaminant is not used for net microbial growth, and the higher the concentrations, the higher the field scale dispersion until it reaches its asymptotic limit $A'_{11}$. This process is similar to the increasing portion of Figure 5-4.

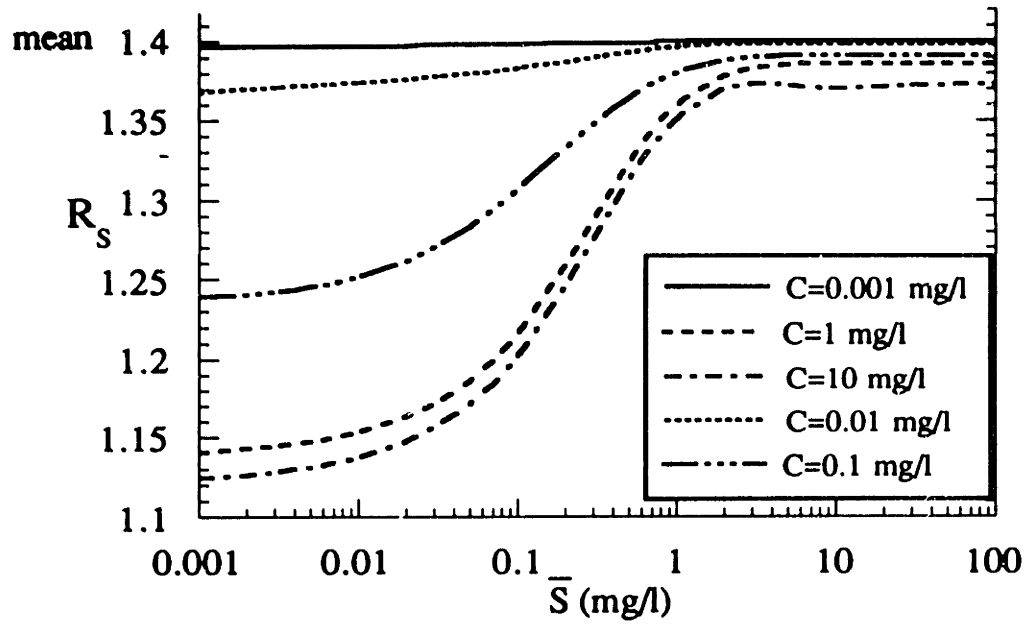


Figure 5-3: Effective contaminant retardation factor at different concentration regimes using parameters for the Borden site.

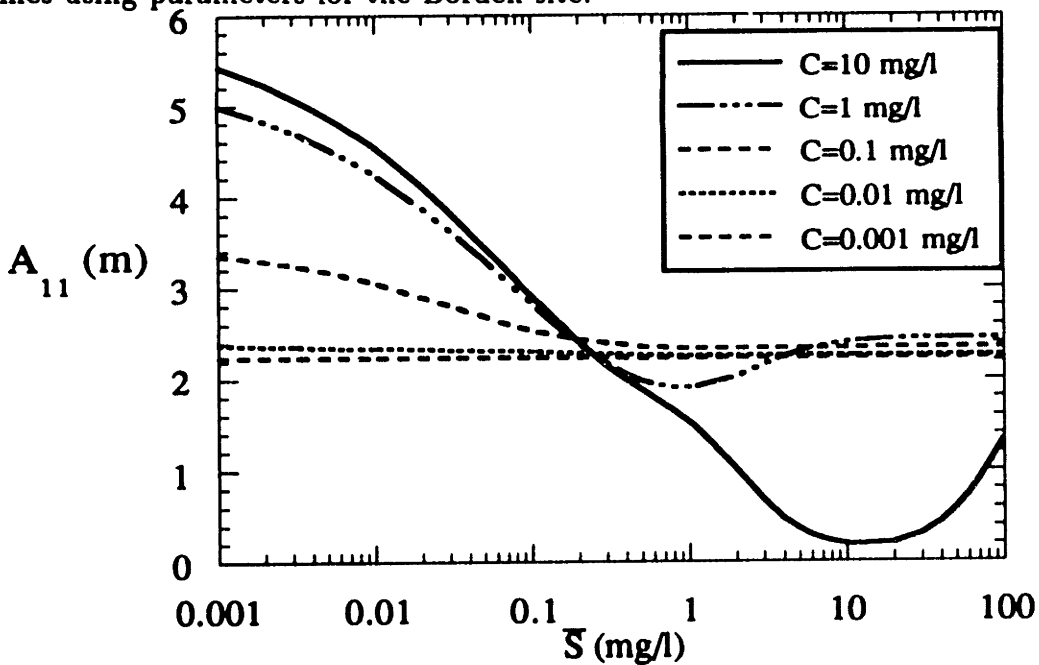


Figure 5-4: Longitudinal macrodispersivity for the contaminant $A_{11}$ at different concentration regimes using parameters for the Borden site.

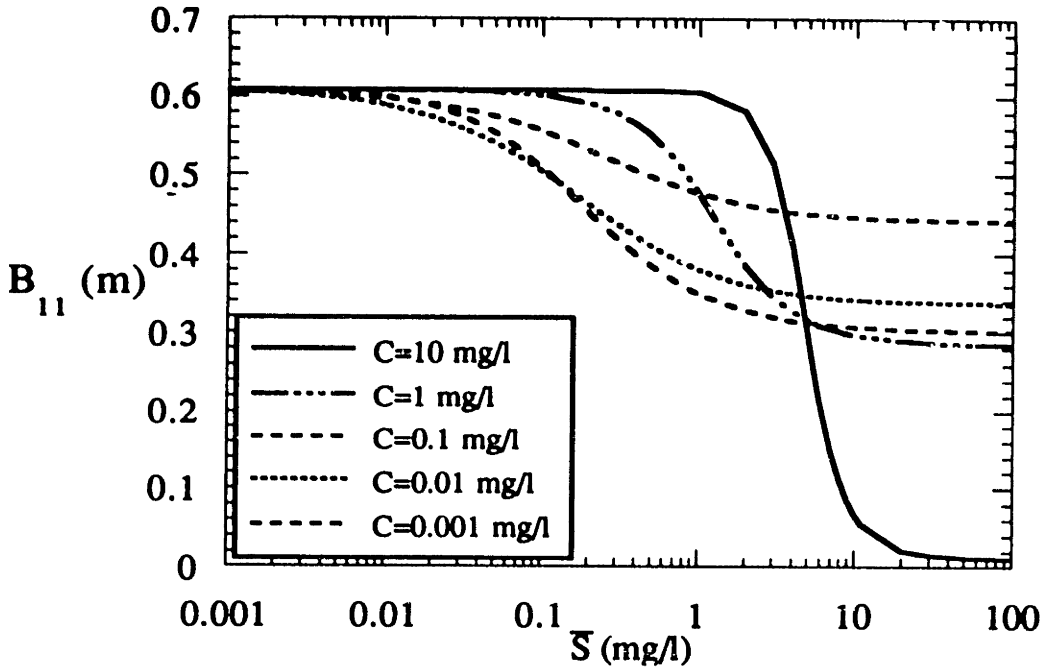


Figure 5-5: Longitudinal macrodispersivity for DO $B_{11}$ at different concentration regimes using parameters for the Borden site.

The sensitivity of the results to the parameters used, it is essentially found that the trends observed in the previous plots are accentuated for higher variabilities of the random fields. A weaker dependence on death rate variability is the exception to this rule. These results are consistent with those presented in Chapter 4. Sensitivity to the log-hydraulic conductivity field is viewed through the rest of the parameters, since it has been assumed that they are partially correlated with $f = lnK$. A summary of these results is provided in Table 5.1, and supporting plots are shown in Figures 5-6 through 5-10.

Table 5.1: Sensitivity of effective coefficients to parameter variability.

| Parameter | $\kappa_e$ | $\beta_e$ | $R_S$ | $A_{11}$ | $B_{11}$ |
|---|---|---|---|---|---|
| $\kappa$ | modest | modest | modest | strong | strong |
| $\beta$ | weak | weak | weak | modest | modest |
| $R$ | -[1] | - | modest | strong | - |

[1]No sensitivity of the DO macrodispersivity and effective growth and death rates to variability of the retardation factor.

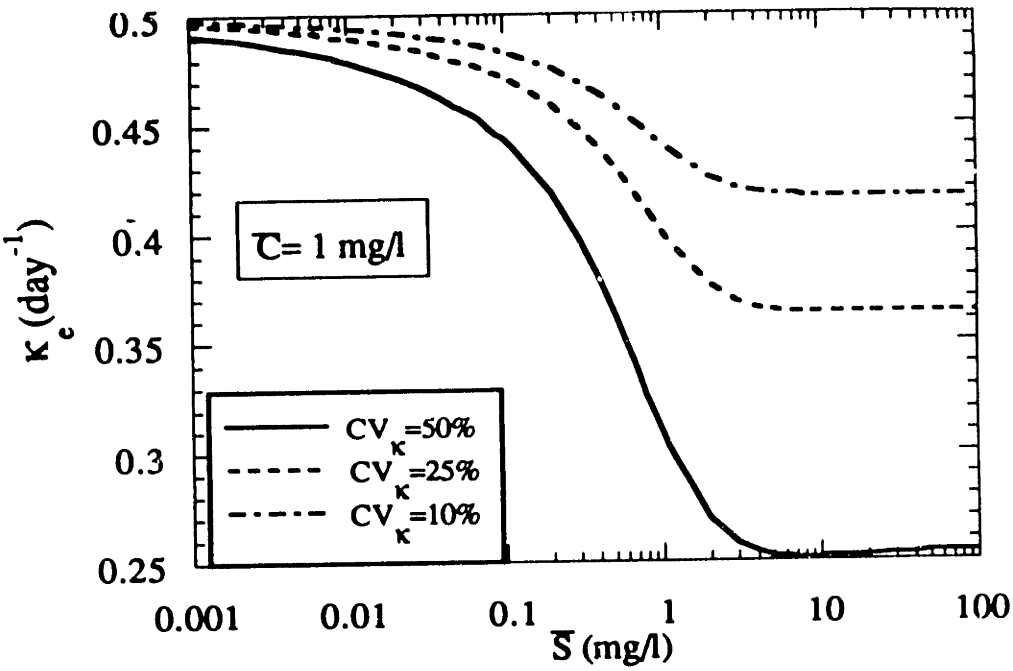


Figure 5-6: Sensitivity of effective growth rate to variability of the local growth rate parameter $\kappa$.

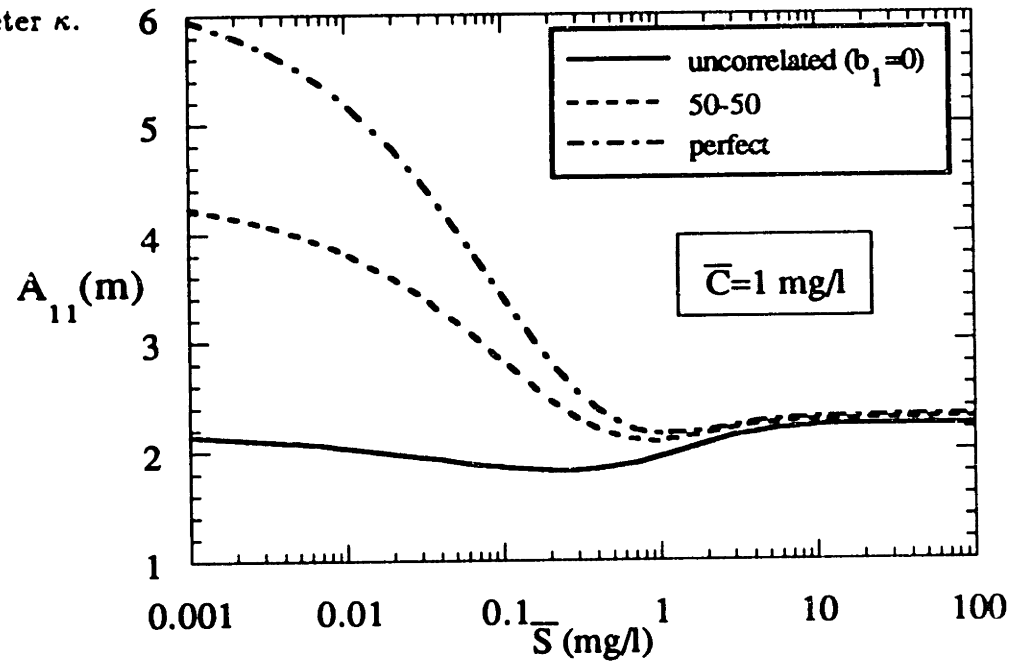


Figure 5-7: Sensitivity of contaminant longitudinal macrodispersivity to variability of the local growth rate parameter $\kappa$.

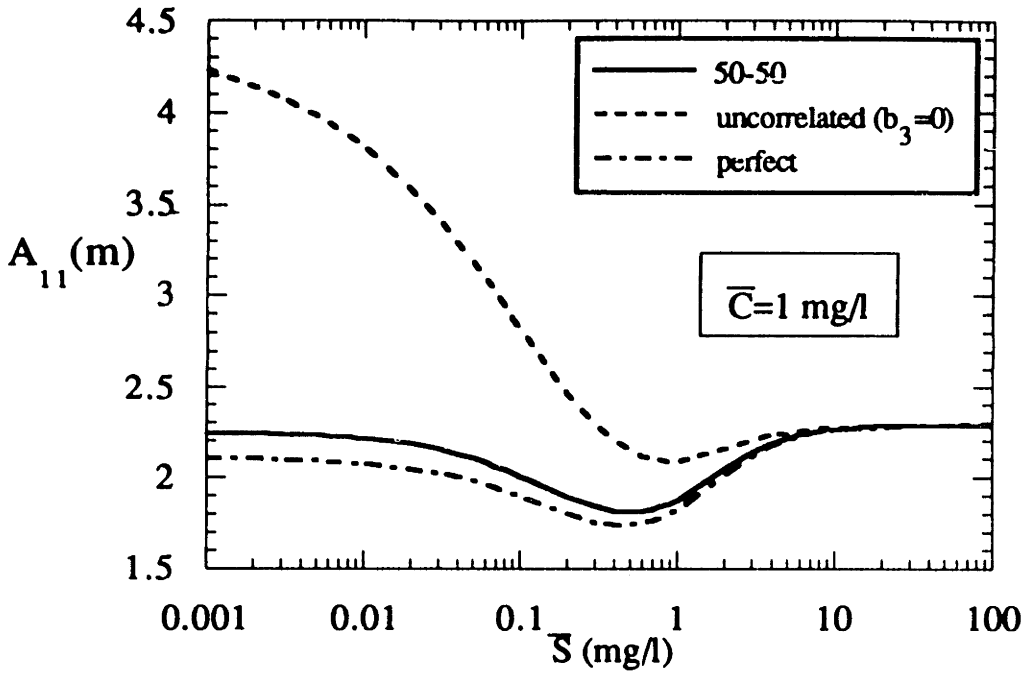


Figure 5-8: Sensitivity of the contaminant longitudinal macrodispersivity to variability of the local death rate parameter $\beta$.

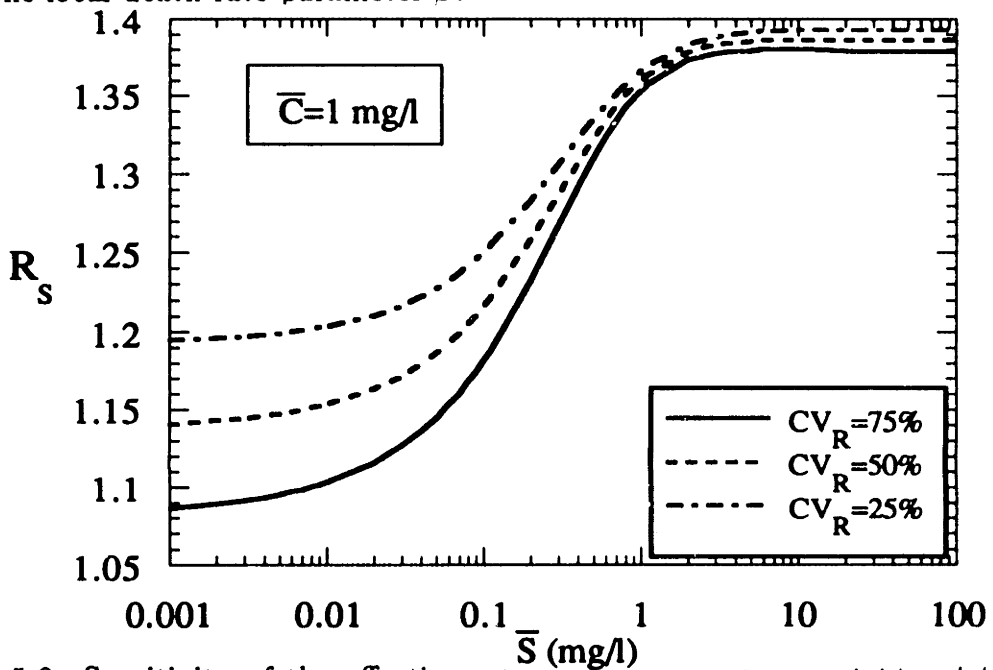


Figure 5-9: Sensitivity of the effective retardation factor to variability of the local retardation parameter $\bar{R}$.

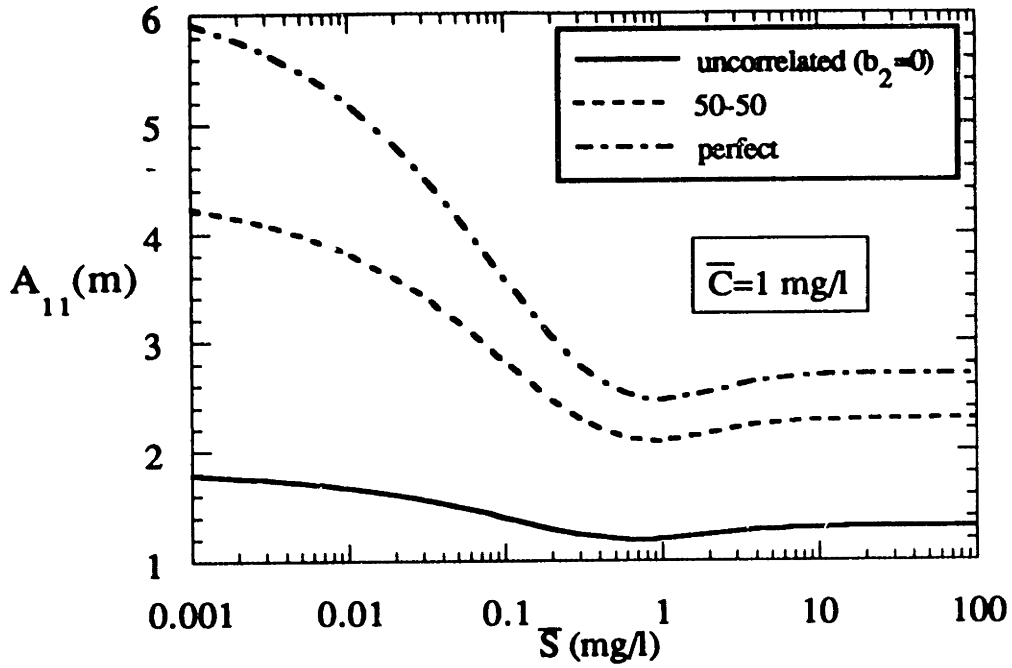


Figure 5-10: Sensitivity of the contaminant longitudinal macrodispersivity to variability of the local retardation parameter $R$.

### 5.5.2 Results for steady state in the mean biomass concentration

An interesting case to consider for the purpose of quantitatively justifying the assumptions of steady state *vs.* transient microbial growth dynamics, is the case where transient dynamics are considered, but the mean biomass concentration in the system is at steady state. This could serve as an approximation to the case when the spatial average of biomass concentrations is more or less constant in time, and time dependent deviations from this mean are assumed to be caused for example, by a set of contaminant/DO plumes sweeping through the aquifer and stimulating growth/death dynamics in doing so.

In this case, the left hand side of equation (5.36) is zero, and thus,

$$Y\kappa_e \frac{\bar{S}}{S_0 + \bar{S}} \frac{\bar{C}}{C_0 + \bar{C}} = \beta_e \tag{5.65}$$

This expression is essentially a nonlinear algebraic equation that can be used to determine the biomass concentration at 'equilibrium' for a given set of mean contaminant and DO concentrations. So in this case a mean biomass concentration is not assumed, but its value is dependent on the substrate and dissolved oxygen

present. Mathematically speaking, this is the solution to the differential equation for the biomass concentration, which is coupled with the transport equations for the mean contaminant and DO. The following set of plots show the equilibrium biomass concentrations and the longitudinal macrodispersivities associated with this set of contaminant/DO/biomass concentrations. Calculations for the other effective coefficients indicate modest effects of equilibrium on the retardation factor and effective growth/death rates compared to that on the longitudinal macrodispersivities.

Figure 5-11 presents the biomass concentrations at equilibrium for high and low mean DO levels as a function of mean contaminant concentrations. At high DO levels, oxygen is not limiting growth, and a small range of equilibrium concentrations is found. This indicates that transient dynamics are important at most concentration ranges when DO is not a limiting factor. On the other hand, when dissolved oxygen is scarce, microbial growth is inhibited to a point where a steady biomass concentration is reached at a larger concentration range. However, for all DO levels, the ranges of contaminant concentrations at which equilibrium occurs are relatively narrow, and therefore microbial growth dynamics are expected to take place over most contaminant and DO concentration ranges.

The longitudinal macrodispersivities for the contaminant and dissolved oxygen for these two cases are presented in Figures 5-12 and 5-13 to show the behavior of the field scale coefficients under these microbial dynamics. At high DO, both longitudinal macrodispersivities follow the same trend as for the transient case in Figures 5-4 and 5-5, with $A_{11}$ decreasing with increasing values of $\bar{S}$, and $B_{11}$ remaining practically a constant over this range. However, the values of $A_{11}$ are different, since a larger value of the mean biomass concentration $\bar{M}$ has been used for its calculation. At low dissolved oxygen levels, longitudinal macrodispersivities are essentially the same as those depicted in Figures 5-4 and 5-5, which in turn are also consistent with those found in Chapter 4 for these concentration ranges. This means that the theory developed here is consistent in predicting the same values of the effective parameters for the steady state and transient scenarios at low DO levels, where dissolved oxygen is a growth-limiting factor.

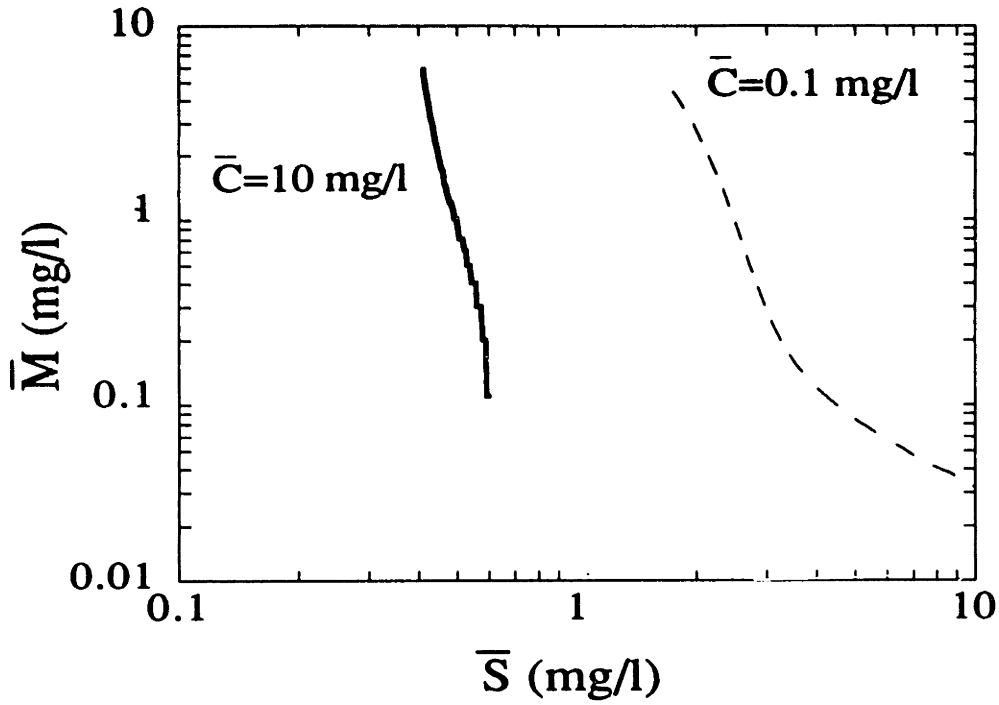


Figure 5-11: Equilibrium mean biomass concentration for high and low DO levels using parameters for the Borden site.

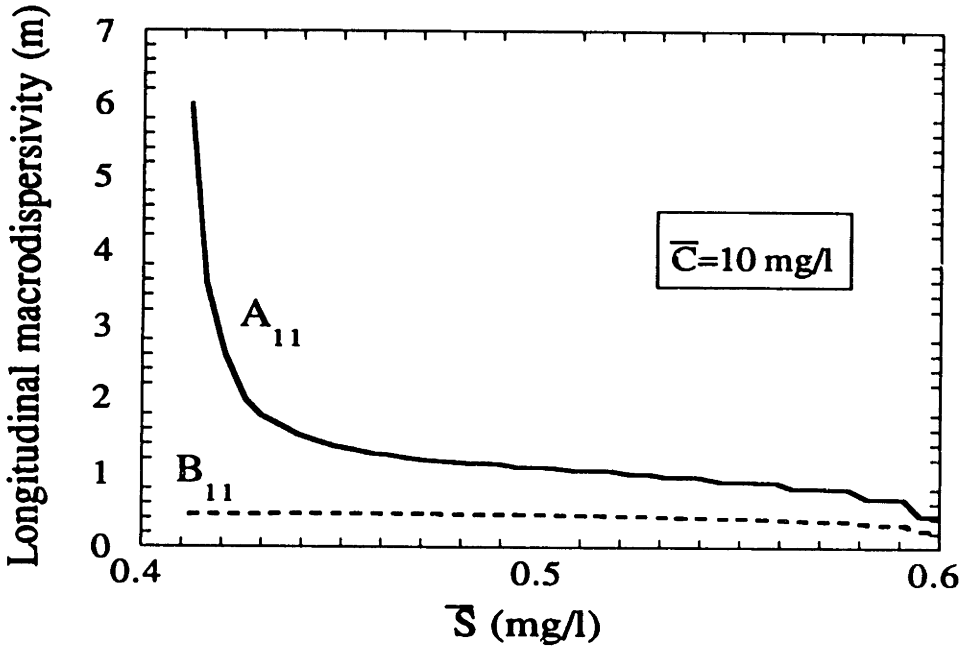


Figure 5-12: Equilibrium longitudinal macrodispersivities for high DO levels using parameters for the Borden site.

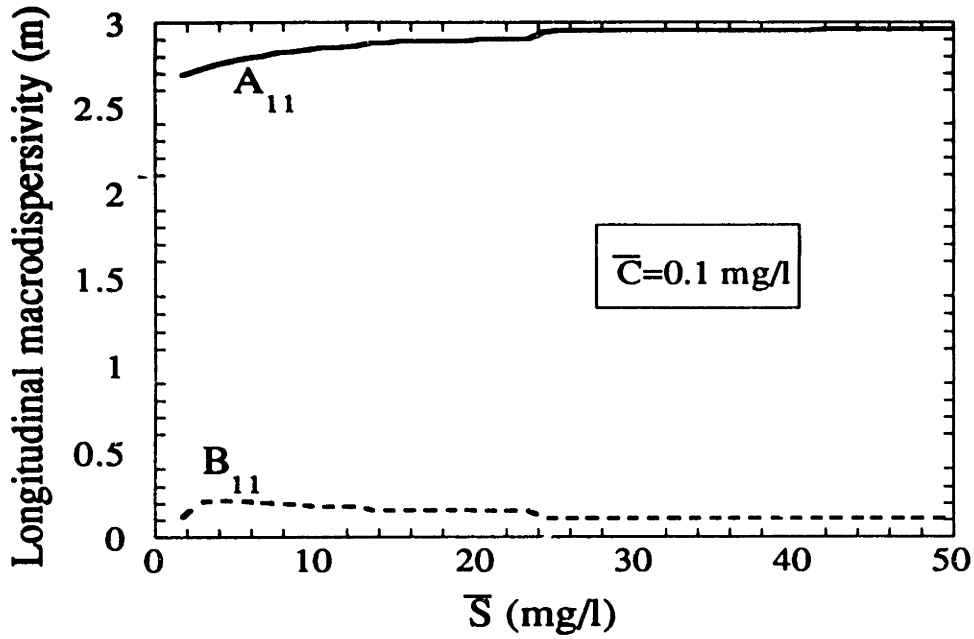


Figure 5-13: Equilibrium longitudinal macrodispersivities for low DO levels using parameters for the Borden site.

## 5.6 Lumped formulation moment simulations and results

The method of moments in Chapter 3 was used to obtain estimates of bulk plume characteristics at a field scale. Analytical expressions for total mass of a solute in an aquifer, position of the center of mass of the plume, and longitudinal second moment were derived by taking moments of the effective transport equation of a reactive species. In this section, this methodology is used to show how the theoretical results derived in this and the previous Chapter can be applied to actual field cases to predict these bulk plume characteristics for multicomponent transport involving sorption and biodegradation.

Spatial moments of the effective partial differential equations of transport are not analytically tractable because of the nonlinearities in the source term and in the calculation of the effective transport and transformation coefficients. An approximate way to compute the evolution in time of the spatial moments of a plume is to replace the dispersed plumes by rectangular distributions having uniform concentrations herein referred to as 'box-cars' [Miralles-Wilhelm *et al.*, 1992]. Inside the box-cars the concentration is taken equal to the spatial mean, and outside it is identically zero. Moments of these box-cars can be computed with the concentration dependence of the effective parameters appearing parametrically as a function of time. This allows for a computation of the spatial moments of contaminant, dissolved oxygen and biomass plumes. For the DO and the microorganisms, since there is expected to be some background concentrations in the aquifer, box-cars of oxygen deficiency and biomass excess instead of the regular concentrations $\bar{C}$ and $\bar{M}$ are used in order to have the condition of zero concentration outside the box-cars. Let $C_d$ be the symbol for oxygen deficiency, $M_{ex}$ the symbol for biomass excess and $C_{in}, M_{in}$ the background (initial) concentrations of DO and biomass in the aquifer. Then the coupled effective transport equations can be written as:

$$R_S \frac{\partial \bar{S}}{\partial t} + v \frac{\partial \bar{S}}{\partial x_1} = v A_{11} \frac{\partial^2 \bar{S}}{\partial x_1^2} + v A_{22} \frac{\partial^2 \bar{S}}{\partial x_2^2} + v A_{33} \frac{\partial^2 \bar{S}}{\partial x_3^2} =$$

$$- \kappa_e(M_{in} + \bar{M}_{ex})\frac{\bar{S}}{\bar{S} + S_0}\frac{C_{in} - \bar{C}_d}{C_{in} - \bar{C}_d + C_0} \tag{5.66}$$

$$\frac{\partial \bar{C}_d}{\partial t} + v\frac{\partial \bar{C}_d}{\partial x_1} = vB_{11}\frac{\partial^2 \bar{C}_d}{\partial x_1^2} + vB_{22}\frac{\partial^2 \bar{C}_d}{\partial x_2^2} + vB_{33}\frac{\partial^2 \bar{C}_d}{\partial x_3^2} =$$

$$- W\kappa_e(M_{in} + \bar{M}_{ex})\frac{\bar{S}}{\bar{S} + S_0}\frac{C_{in} - \bar{C}_d}{C_{in} - \bar{C}_d + C_0} \tag{5.67}$$

$$\frac{\partial \bar{M}_{ex}}{\partial t} = Y\kappa_e(M_{in} + \bar{M}_{ex})\frac{\bar{S}}{\bar{S} + S_0}\frac{C_{in} - \bar{C}_d}{C_{in} - \bar{C}_d + C_0} - \beta_e(M_{in} + \bar{M}_{ex}) \tag{5.68}$$

Spatial moments of the concentrations and source terms may be computed as:

$$M^S_{m,n,p} = \int_{-\infty}^{\infty} \bar{S}(\mathbf{x}) x_1^m x_2^n x_3^p d\mathbf{x}$$

$$M^{C_d}_{m,n,p} = \int_{-\infty}^{\infty} \bar{C}_d(\mathbf{x}) x_1^m x_2^n x_3^p d\mathbf{x}$$

$$M^{M_{ex}}_{m,n,p} = \int_{-\infty}^{\infty} \bar{M}_{ex}(\mathbf{x}) x_1^m x_2^n x_3^p d\mathbf{x}$$

$$M^r_{m,n,p} = \int_{-\infty}^{\infty} \left(\frac{\bar{S}}{\bar{S} + S_0}\right)\left(\frac{C_{in} - \bar{C}_d}{C_{in} - \bar{C}_d + C_0}\right) x_1^m x_2^n x_3^p d\mathbf{x} \tag{5.69}$$

Taking the spatial moments of equations (5.66) through (5.68) results in:

$$R_S(\bar{S}, \bar{C}_d, \bar{M}_{ex})\frac{dM^S_{0,0,0}}{dt} = -[\kappa_e(\bar{S}, \bar{C}_d, \bar{M}_{ex})]M^r_{0,0,0} \tag{5.70}$$

$$\frac{dM^{C_d}_{0,0,0}}{dt} = [W\kappa_e(\bar{S}, \bar{C}_d, \bar{M}_{ex})]M^r_{0,0,0} \tag{5.71}$$

$$\frac{dM^{M_{ee}}_{0,0,0}}{dt} = [Y\kappa_e(\bar{S},\bar{C}_d,\bar{M}_{ex})]M^r_{0,0,0} - \beta_e M^{M_{ee}}_{0,0,0} \tag{5.72}$$

$$R_S(\bar{S},\bar{C}_d,\bar{M}_{ex})\frac{dM^S_{1,0,0}}{dt} - vM^S_{0,0,0} = -[\kappa_e(\bar{S},\bar{C}_d,\bar{M}_{ex})]M^r_{1,0,0} \tag{5.73}$$

$$R_S(\bar{S},\bar{C}_d,\bar{M}_{ex})\frac{dM^S_{0,1,0}}{dt} = -[\kappa_e(\bar{S},\bar{C}_d,\bar{M}_{ex})]M^r_{0,1,0} \tag{5.74}$$

$$R_S(\bar{S},\bar{C}_d,\bar{M}_{ex})\frac{dM^S_{0,0,1}}{dt} = -[\kappa_e(\bar{S},\bar{C}_d,\bar{M}_{ex})]M^r_{0,0,1} \tag{5.75}$$

$$\frac{dM^{C_d}_{1,0,0}}{dt} - vM^{C_d}_{0,0,0} = [W\kappa_e(\bar{S},\bar{C}'_d\bar{M}_{ex})]M^r_{1,0,0} \tag{5.76}$$

$$\frac{dM^{C_d}_{0,1,0}}{dt} = [W\kappa_e(\bar{S},\bar{C}_d,\bar{M}_{ex})]M^r_{0,1,0} \tag{5.77}$$

$$\frac{dM^{C_d}_{0,0,1}}{dt} = [W\kappa_e(\bar{S},\bar{C}_d,\bar{M}_{ex})]M^r_{0,0,1} \tag{5.78}$$

$$\frac{dM^{M_{ee}}_{1,0,0}}{dt} = [Y\kappa_e(\bar{S},\bar{C}_d,\bar{M}_{ex})]M^r_{1,0,0} - \beta_e M^{M_{ee}}_{1,0,0} \tag{5.79}$$

$$\frac{dM^{M_{ee}}_{0,1,0}}{dt} = [Y\kappa_e(\bar{S},\bar{C}_d,\bar{M}_{ex})]M^r_{0,1,0} - \beta_e M^{M_{ee}}_{0,1,0} \tag{5.80}$$

$$\frac{dM^{M_{ee}}_{0,0,1}}{dt} = [Y\kappa_e(\bar{S},\bar{C}_d,\bar{M}_{ex})]M^r_{0,0,1} - \beta_e M^{M_{ee}}_{0,0,1} \tag{5.81}$$

$$R_S(\bar{S},\bar{C}_d,\bar{M}_{ex})\frac{dM^S_{2,0,0}}{dt} - 2vM^S_{1,0,0} = 2vA_{11}M^S_{0,0,0} - [\kappa_e(\bar{S},\bar{C}_d,\bar{M}_{ex})]M^r_{2,0,0} \tag{5.82}$$

$$R_S(\bar{S},\bar{C}_d,\bar{M}_{ex})\frac{dM^S_{0,2,0}}{dt} = 2vA_{22}M^S_{0,0,0} - [\kappa_e(\bar{S},\bar{C}_d,\bar{M}_{ex})]M^r_{0,2,0} \tag{5.83}$$

$$R_S(\bar{S},\bar{C}_d,\bar{M}_{ex})\frac{dM^S_{0,0,2}}{dt} = 2vA_{33}M^S_{0,0,0} - [\kappa_e(\bar{S},\bar{C}_d,\bar{M}_{ex})]M^r_{0,0,2} \tag{5.84}$$

$$\frac{dM^{C_d}_{2,0,0}}{dt} - 2vM^{C_d}_{1,0,0} = 2vB_{11}M^{C_d}_{0,0,0} + [W\kappa_e(\bar{S},\bar{C}_d,\bar{M}_{ex})]M^r_{2,0,0} \tag{5.85}$$

$$\frac{dM^{C_d}_{0,2,0}}{dt} = 2vB_{22}M^{C_d}_{0,0,0} + [W\kappa_e(\bar{S},\bar{C}_d,\bar{M}_{ex})]M^r_{0,2,0} \tag{5.86}$$

$$\frac{dM^{C_d}_{0,0,2}}{dt} = 2vB_{33}M^{C_d}_{0,0,0} + [W\kappa_e(\bar{S},\bar{C}_d,\bar{M}_{ex})]M^r_{0,0,2} \tag{5.87}$$

$$\frac{dM^{M_{ex}}_{2,0,0}}{dt} = [Y\kappa_e(\bar{S},\bar{C}_d,\bar{M}_{ex})]M^r_{2,0,0} - \beta_e M^{M_{ex}}_{2,0,0} \tag{5.88}$$

$$\frac{dM^{M_{ex}}_{0,2,0}}{dt} = [Y\kappa_e(\bar{S},\bar{C}_d,\bar{M}_{ex})]M^r_{0,2,0} - \beta_e M^{M_{ex}}_{0,2,0} \tag{5.89}$$

$$\frac{dM^{M_{ex}}_{0,0,2}}{dt} = [Y\kappa_e(\bar{S},\bar{C}_d,\bar{M}_{ex})]M^r_{0,0,2} - \beta_e M^{M_{ex}}_{0,0,2} \tag{5.90}$$

The box dimensions in Figure 5-15 are related to the spatial moments by:

$$\sigma_1 = 2\left[3\frac{M_{2,0,0}}{M_{0,0,0}} - 3\left(\frac{M_{1,0,0}}{M_{0,0,0}}\right)^2\right]^{\frac{1}{2}} \tag{5.91}$$

$$\sigma_2 = 2\left[3\frac{M_{0,2,0}}{M_{0,0,0}} - 3\left(\frac{M_{0,1,0}}{M_{0,0,0}}\right)^2\right]^{\frac{1}{2}} \tag{5.92}$$

$$\sigma_3 = 2\left[3\frac{M_{0,0,2}}{M_{0,0,0}} - 3\left(\frac{M_{0,0,1}}{M_{0,0,0}}\right)^2\right]^{\frac{1}{2}} \tag{5.93}$$

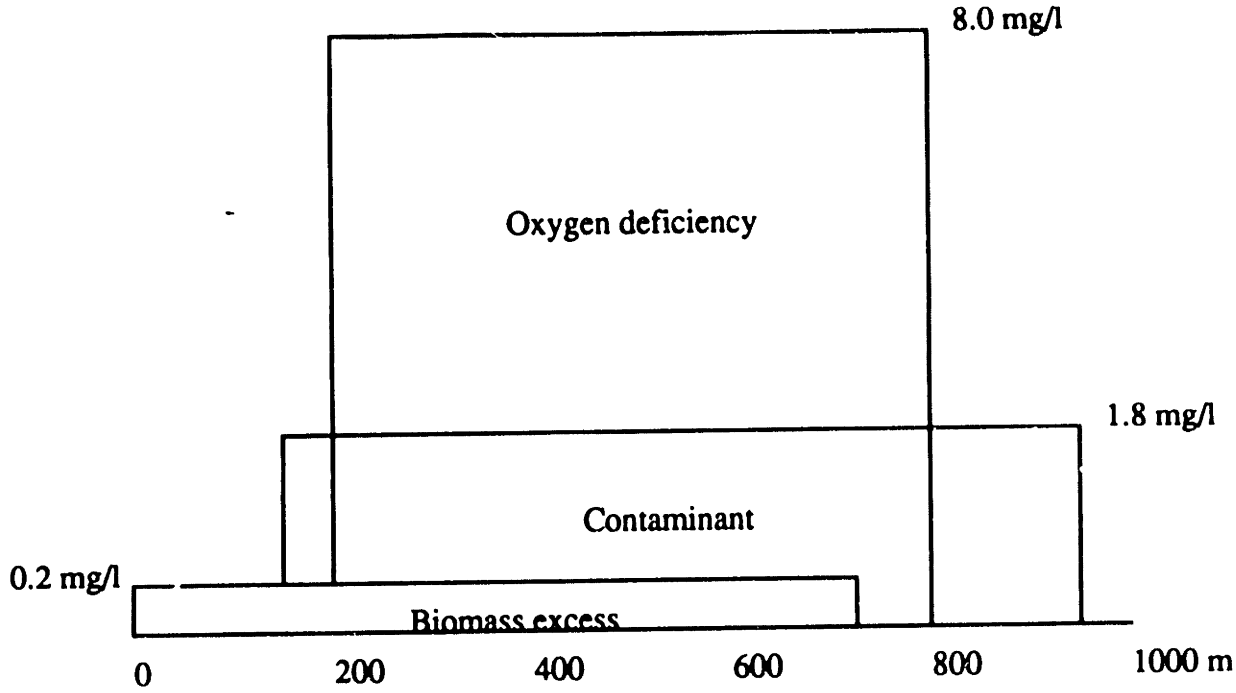


Figure 5-14: Box-car representation of plumes.

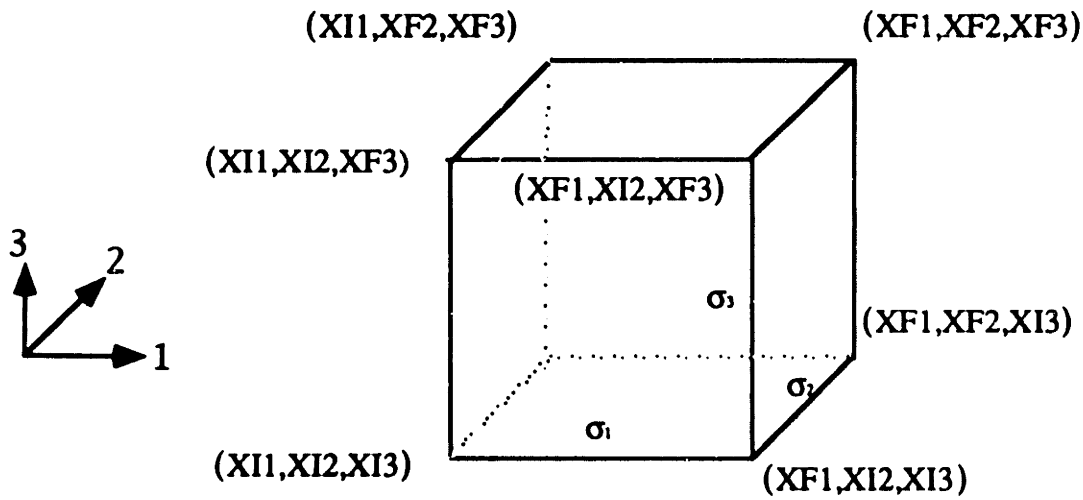


Figure 5-15: Box-car coordinates and dimensions.

Given the box dimensions of the contaminant, oxygen deficiency biomass excess, and the box concentrations at any time, the source term spatial moments are computed numerically, and the spatial moments of the three components are updated for a time discretization using a finite difference approximation. In this case, a simple Euler integration scheme has been employed to carry out the numerical integration in time. The spatial dimensions of the box-cars in Figure 5-15 (6 for each component, 18 total) are computed from equations (5.91) through (5.93), and the box concentrations (3 total) are computed using the zeroth moment (total mass in solution) of each component and dividing it by the total void volume within the box (porosity x box volume). These computed dimensions and concentrations are used to find the new spatial moments of the source term and thus updated spatial moments are found again for the next integration step. Therefore, the box-car moment simulation technique enables finding a set of twenty one coupled nonlinear ordinary differential equations which may be solved (with considerable less effort than the original partial differential equations) to get the time evolution of the contaminant, oxygen deficiency and biomass excess spatial moments.

Transverse dispersion coefficients were taken to be constant and equal to the local dispersivities, *i.e.*, $A_{22} = A_{33} = B_{22} = B_{33} = \alpha_T$. The transverse spreading observed in the numerical simulations for nonreactive solute transport in Miralles-Wilhelm *et al.* [1992] is of the same magnitude of what would result if local transverse dispersion was the only transverse spreading mechanism. However, field studies [*e.g.* Rajaram and Gelhar, 1991] reveal spreading in the transverse directions to be larger than what is associated with local dispersion. In any case, the two-component box-car predictions presented in Miralles-Wilhelm *et al.* [1992] show a relative insensitivity to transverse dispersion coefficients. A value of $\alpha_T = 0.005m$ was used for the cases included in this Section. The following simulations were performed to assess the applicability of the analytical results developed using the stochastic theory to field contamination scenarios.

### 5.6.1 Application to benzene contamination at the Borden site.

In this simulation, $30mg/l$ of benzene are introduced in a rectangular volume of $1.2m^3$. The background levels of DO and biomass are $4.0mg/l$ and $0.2mg/l$ respectively. Hydrologic, sorption and biodegradation parameters used in the simulation are the same as in the previous section and are listed in Table 4.1. Results from this simulation can also be compared with those presented in Miralles-Wilhelm *et al.* [1992], where a two-component box-car was implemented to simulate a steady state biomass situation.

Figure 5-14 shows the relative position of the contaminant, oxygen deficiency and biomass excess box-cars after $t = 500$ days from the introduction of the benzene mass. It appears that the entire oxygen deficiency plume lies within the benzene plume. This means that the core of the contaminant plume is being depleted of oxygen, so its degradation will be oxygen limited. A major portion of the biomass excess plume grows also within the contamination area, and some of it trails the other two plumes. This may be explained in the context of first order moments.

Figure 5-16 shows the time evolution of the zeroth moments for the three component system. The total dissolved mass of benzene appears to be dissapearing rapidly and the oxygen deficiency mass in the box increases due to biodegradation. The total biomass in the box grows rapidly initially where both the contaminant and DO are in relative abundance. However, when the benzene starts to reach lower levels and the oxygen deficiency builds up, microbial growth is offset by microbial decay, and the biomass is subsequently depleted. It is also important to observe the single point in time where microbial growth equilibrium is reached. This verifies the assertion that transient microbial dynamics take place during contaminant and dissolved oxygen plume evolution.

The displacement of the center of mass of each of the plumes is depicted in Figure 5-17. As it is expected, there is a relative retardation of the benzene plume with respect to the oxygen deficiency plume. An interesting feature represented here is the

apparent retardation observed for the biomass plume. Earlier in this Chapter, it was assumed that microorganisms were highly retarded (not advected). The simulation reproduces this feature of the theoretical model. Biomass is growing along the direction of benzene and DO plume movement, and the biomass plume then develops in the intersection zones of these two plumes, which results in the apparent retardation observed.

In growing with the benzene and DO plume development, the biomass plume also exhibits an apparent dispersion process, and its second moment grows in time as shown in Figure 5-18. If these results are interpreted in terms of macrodispersion, Figure 5-19 shows that the biomass plume has the fastest spreading with respect to bulk plume displacement initially.

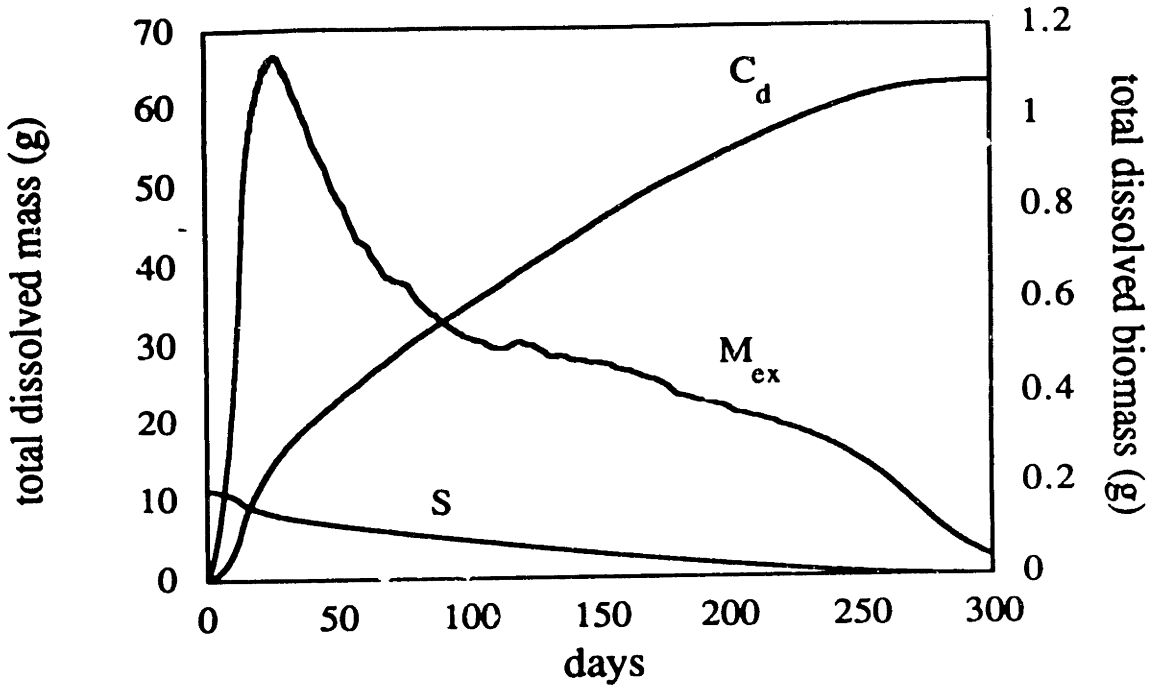


Figure 5-16: Zeroth moment evolution of benzene, DO and biomass plumes using a three-component box-car model.

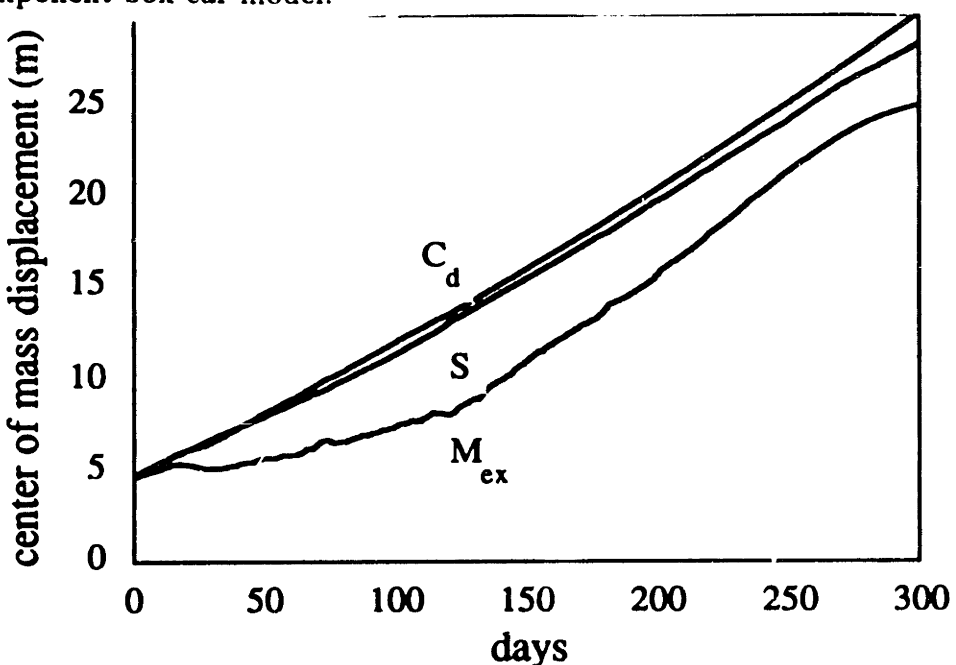


Figure 5-17: First moment evolution of benzene, DO and biomass plumes using a three-component box-car model.

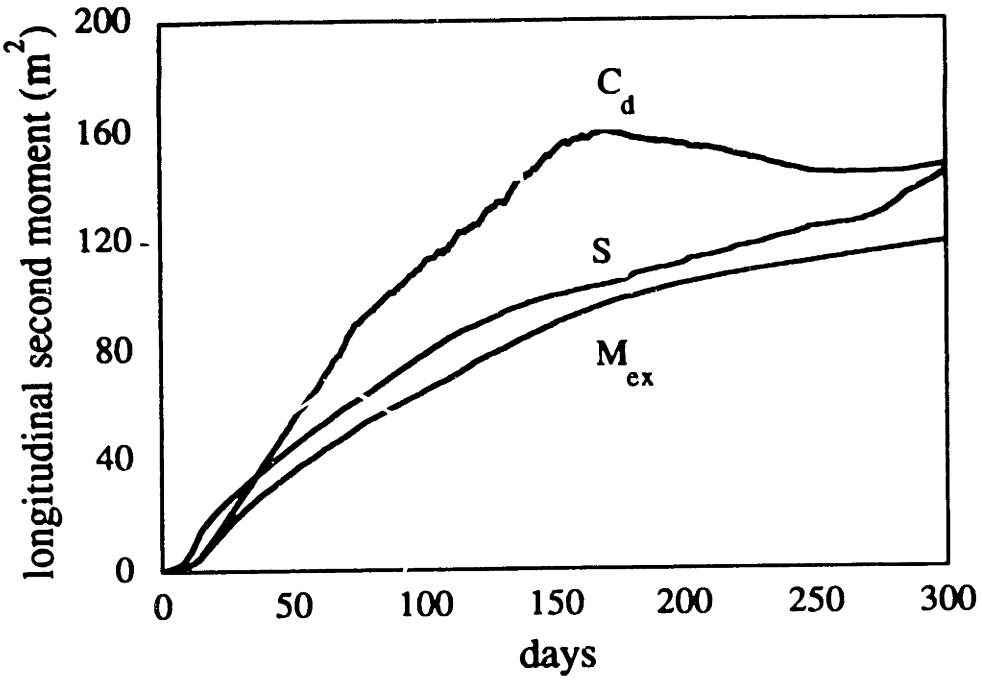


Figure 5-18: Longitudinal second moment evolution of benzene, DO and biomass plumes using a three-component box-car model.

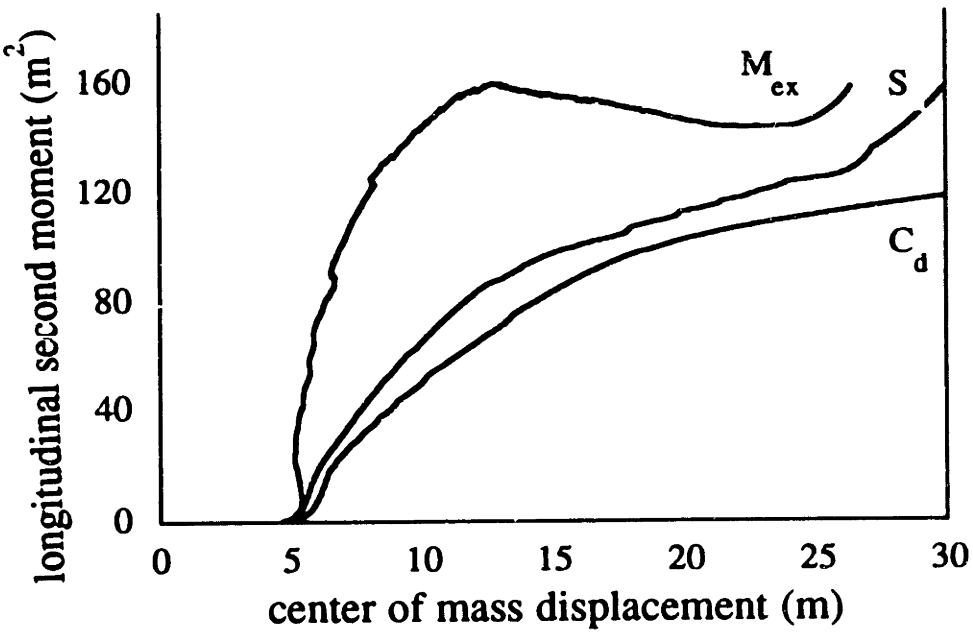


Figure 5-19: Longitudinal second moment evolution with respect to mean displacement using a three-component box-car model.

### 5.6.2 Comparison with numerical simulations

This Section discusses a comparison of the three-component box-car results for the benzene and DO plume evolution with the two-component box-car and detailed numerical simulations of Miralles-Wilhelm *et al.* [1992]. These simulations included a test case using parameters for a conservative solute at the Borden site, in order to compare the longitudinal macrodispersivity obtained numerically with the one predicted by the stochastic theory [Gelhar and Axness, 1983]. The ratio of the predicted ($0.61m$) to the computed ($0.17m$) was used to account for finite domain and contaminant source size effects which cause the results to differ from the infinite domain, point source derived stochastic theory. This was also the case in Chapter 3, where a scaling of the theoretical results was done to compare analytical moment calculations with the numerical simulations of Burr [1992].

In view of this, the longitudinal macrodispersivity predicted by the stochastic theory was scaled down by a factor of 3.5, and used both in a two-component box-car formulation [Miralles-Wilhelm *et al.*, 1992] and a the three-component box-car presented previously. In Figure 5-20, the box-car formulation (two and three-component) tends to underestimate the benzene mass loss due to biodegradation. This may be explained by the absence of a fringe of low benzene concentrations surrounded by high DO concentrations, which would cause a rapid consumption of benzene by microorganisms growing in the fringe. Consistently, Figure 5-21 shows an underestimation of DO consumption by the box-car model.

The box-car simulations show the retardation of the benzene plume with respect to the oxygen deficiency plume in Figure 5-22. These results compare favorably with the detailed numerical simulations of mean plume displacement. The limitation of the box-car approach becomes apparent in Figure 5-23 The numerical simulations predict a larger macrodispersivity (slope of the curves at large times) for DO than for benzene, whereas the box-car results show the opposite. It appears that the box-car is not able to capture the dispersion characteristics of the evolving plumes. This suggests that a distributed formulation for a mean transport model is necessary in order to describe second moment plume behavior.

In comparing two and three-component formulations, the zeroth and first spatial moments exhibit similar values and trends in time, so it appear that the effects of transient microbial dynamics on the bulk plume behavior of the other two components is not significant. For purposes of comparison, the maximum differences between the two and three component simulated curves are 20% for the benzene zeroth moment, 17% for the oxygen deficiency zeroth moment, 8% for the benzene first moment and 15% for the oxygen deficiency first moment. One of the reasons for this is that the change in biomass caused by growth is not considerably great (a factor of 5 at the most for the parameters used), and results are not very sensitive to the biomass present in the aquifer. This can also be explained by the fact that although transient microbial dynamics take place during the development of the plumes, the time scale at which microorganisms grow and die around the plumes is much smaller than the time scales of interest for field scale plumes (hours to days as compared to hundreds to thousands of days). This suggests that for field scale modeling purposes, the assumption of a steady state in the microorganisms concentration is adequate for estimating mass loss due to biotransformation and center of mass migration rates. However, it is recommended that this finding is assessed with a distributed model for bulk plume transport that is able to address the behavior of the spatial second moment.

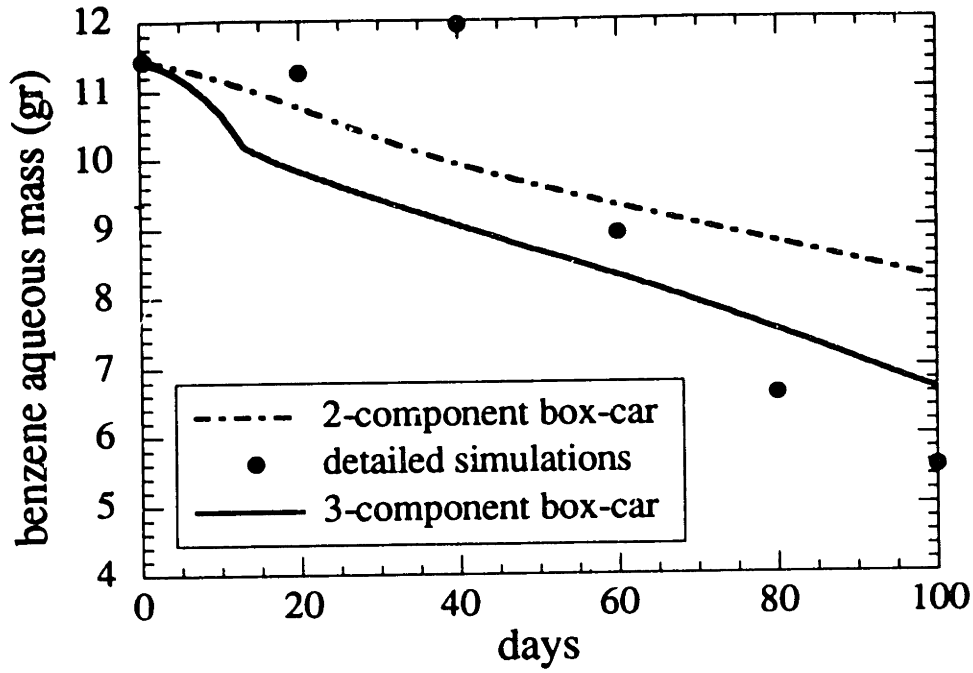


Figure 5-20: Comparison of zeroth moment evolution curves for benzene with detailed numerical simulations.

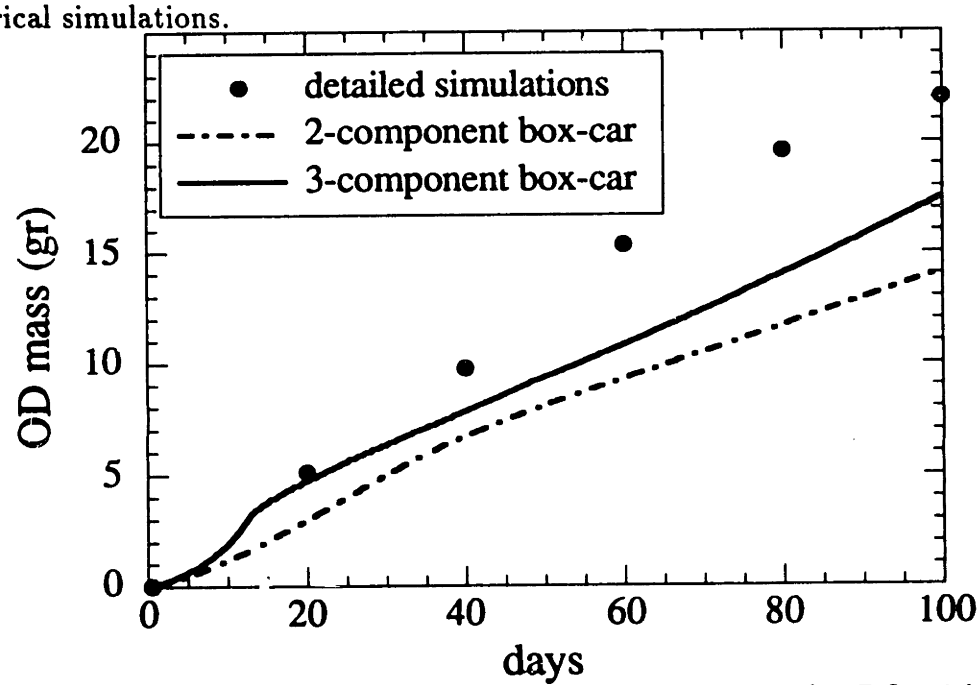


Figure 5-21: Comparison of zeroth moment evolution curves for DO with detailed numerical simulations.

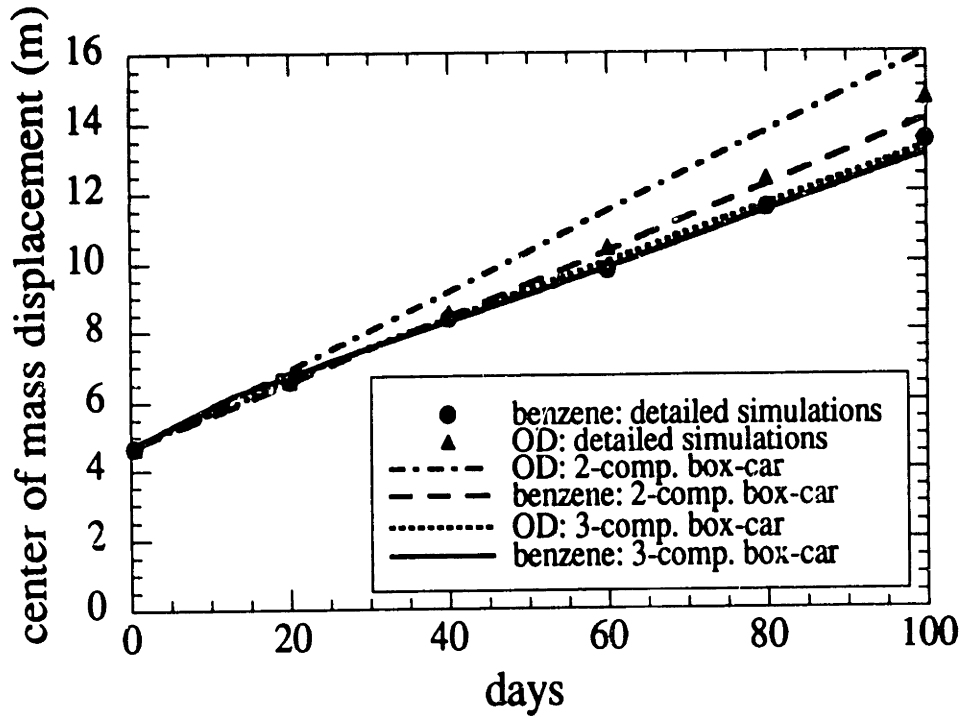


Figure 5-22: Comparison of first moment evolution curves for benzene and DO with detailed numerical simulations.

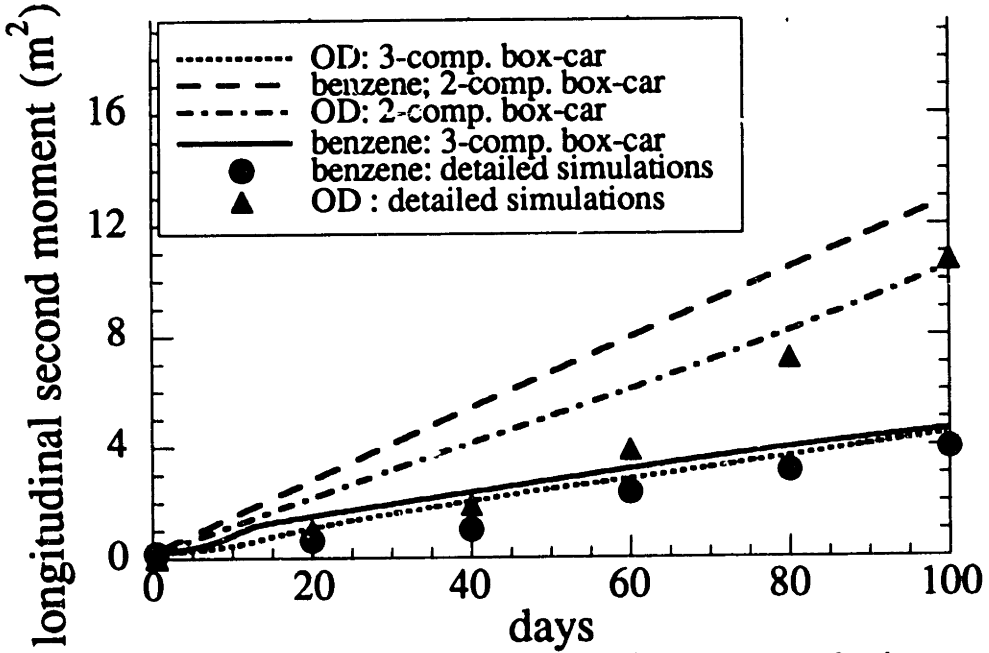


Figure 5-23: Comparison of second moment evolution curves for benzene and DO with detailed numerical simulations.

### 5.6.3 Application to Toluene contamination at Traverse City: enhanced biodegradation.

Two larger scale simulations using the box-car algorithm were performed for contamination by toluene at the Traverse City site in Traverse City, Michigan. A list of the parameters used for these simulations is presented in Table 4.2. A total contaminant mass of $150,000kg$ was spilled over a $50mx20mx10m$ area and let evolved in time in the first simulation to obtain estimates of bulk plume characteristics under naturally occuring biodegradation. A second simulation was performed, in which DO levels in the aquifer were kept high by injecting groundwater with background levels of DO whenever the oxygen deficiency reached a threshold ($1mg/l$ for this simulation). Transverse dispersion has been assumed as $\alpha_T = 0.005m$. This situation, depicted in Figure 5-24, represents, for example, a biodegradation enhancement process where fresh groundwater is injected into a well (or a number of wells) where DO levels are being monitored in time. A background dissolved oxygen concentration of $8mg/l$ was assumed, and the background biomass was taken to be $0.1mg/l$.

Figure 5-25 shows plots of the mass loss curve for toluene under natural and enhanced biodegradation scenarios. An interesting effect caused by the nonlinear concentration dependence of the contaminant effective decay coefficient is reflected in the earlier portion of the curves, where natural biodegradation occurs at a faster rate. At the early stages of the process where toluene concentrations are high, its decay is not oxygen-limited (DO is plentiful) and the effective growth rate of the microorganisms is controlling the decay process of toluene and DO. In Figure 5-1, it is shown that $\kappa_e$ is lower for increasing DO at high mean contaminant concentration levels. At the later stages of the process, however, the scarcity of oxygen becomes the controlling factor, and by adding DO to the system, faster rates of degradation are achieved. This effect is also reflected in Figure 5-26, where biomass concentrations are increased monotonically when continuously introducing DO into the aquifer, which is not the case for naturally occuring biodegradation.

The influence of enhancing biodegradation on the first and second moments of

the contaminant plume is presented in Figures 5-27 and 5-28. The effect on the displacement of the center of mass does not seem to be significant. However, a dramatic effect is produced on plume spreading, where enhancing biodegradation by keeping DO levels high reduces considerably the longitudinal second moment of the plume. Essentially, contaminant plume spreading is restricted by plume decay due to biodegradation.

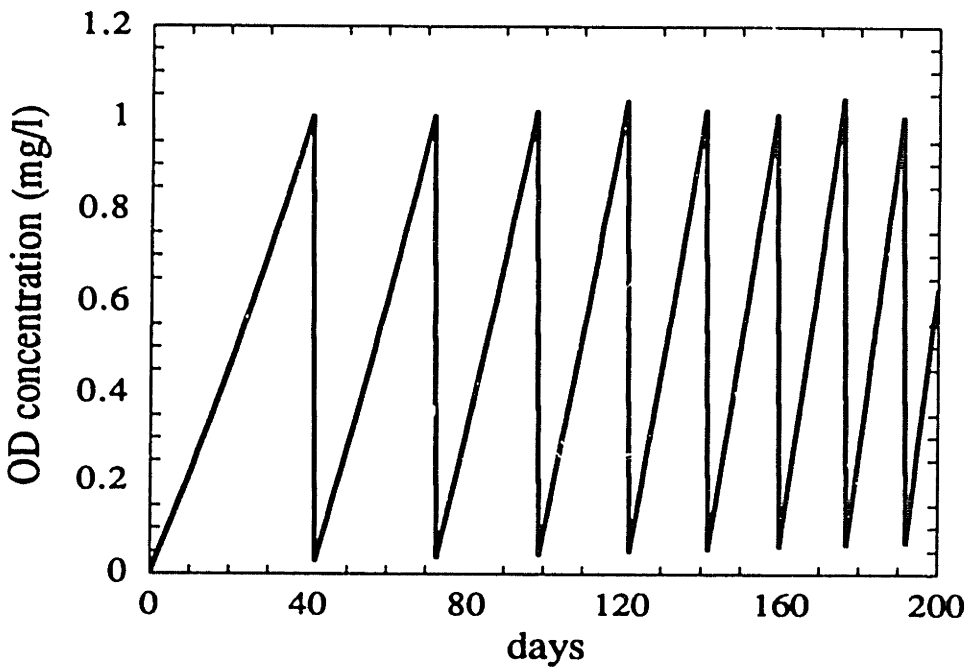


Figure 5-24: Dissolved oxygen injection to enhance biodegradation of Toluene at Traverse City.

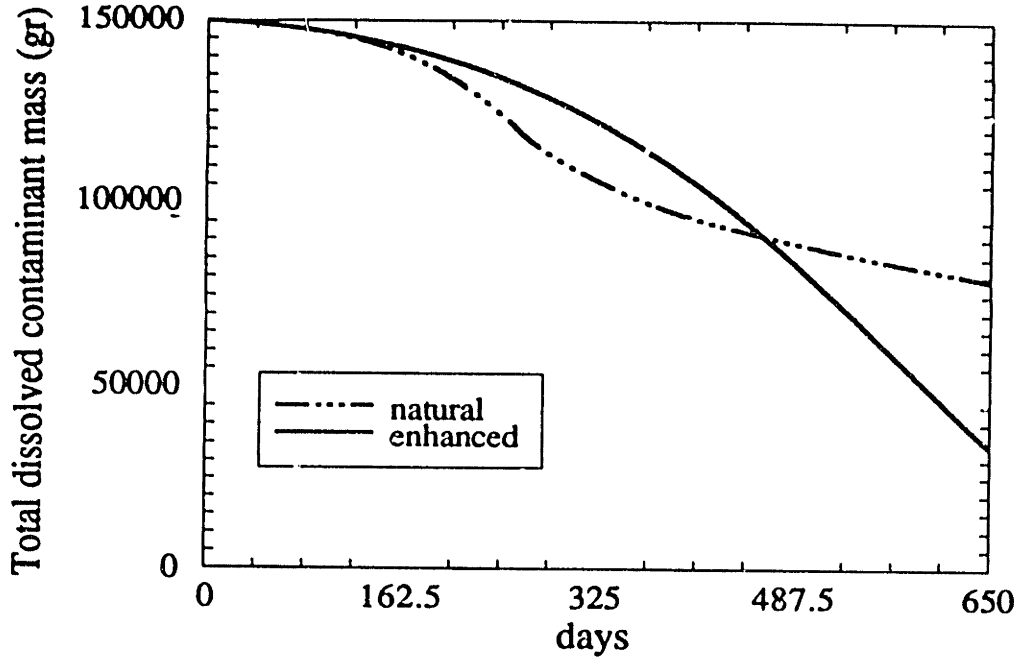


Figure 5-25: Toluene mass loss predictions for natural and enhanced biodegradation at Traverse City.

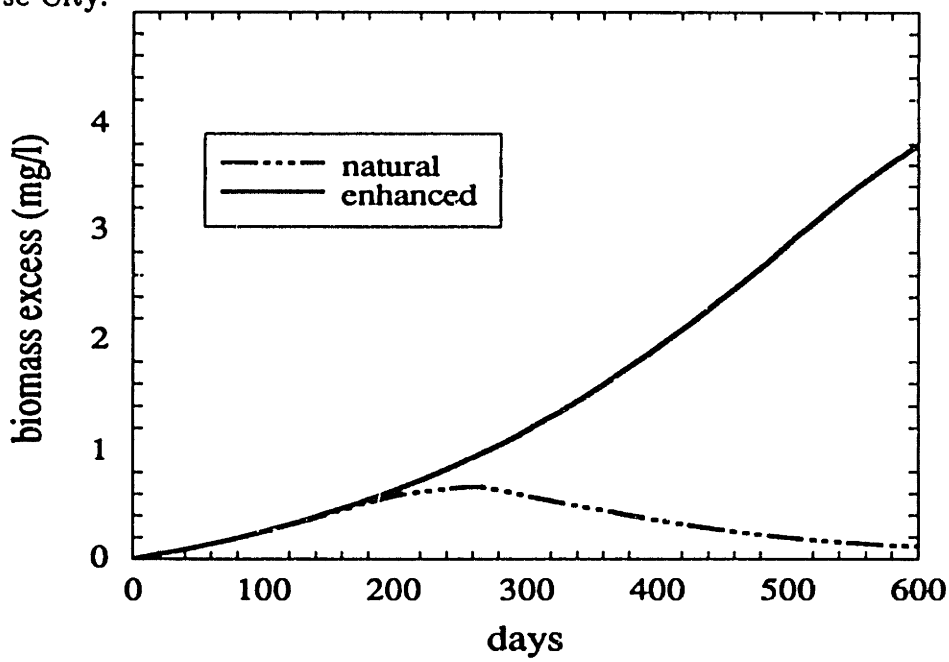


Figure 5-26: Biomass growth predictions for natural and enhanced biodegradation at Traverse City.

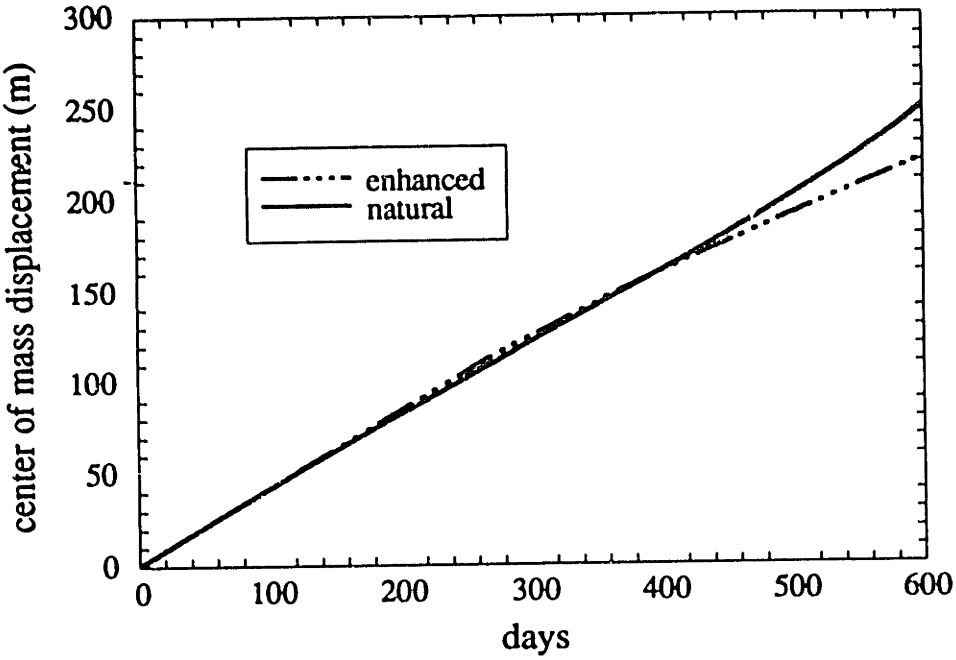


Figure 5-27: Effects of biodegradation enhancement on Toluene bulk plume movement at Traverse City.

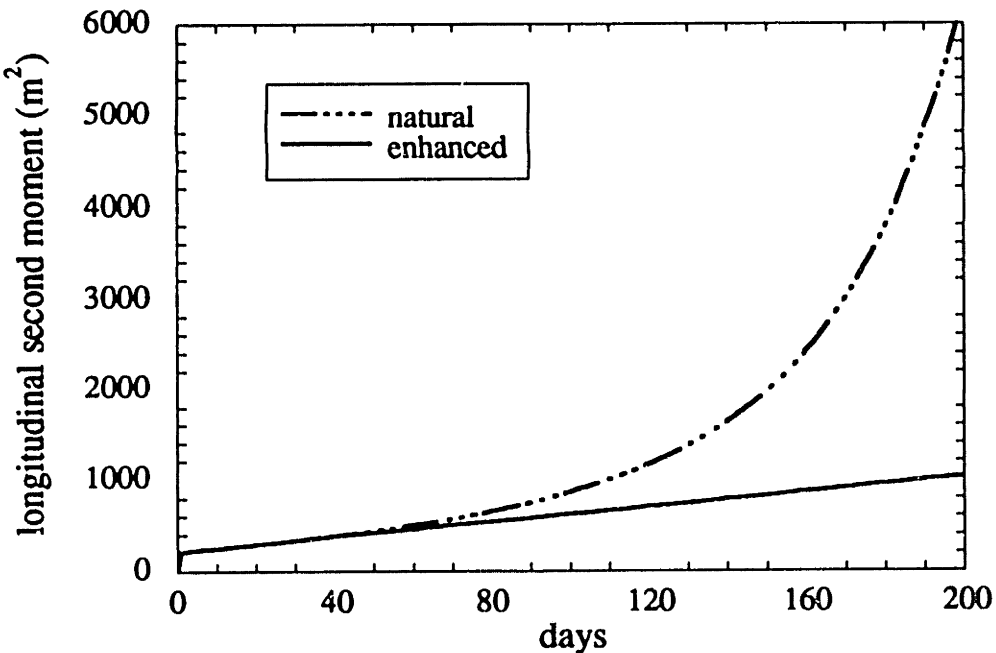


Figure 5-28: Effects of biodegradation enhancement on Toluene bulk plume longitudinal spreading at Traverse City.

## 5.7 Summary and conclusions

The analysis and results developed in this Chapter are aimed at gaining a better understanding of the effects of microbial growth dynamics on the problem of oxygen limited biodegradation treated in Chapter 4.

First of all, the field scale coefficients of transport and transformation under oxygen-limiting conditions are found to be consistent with the results presented in Chapter 4 for a steady state biomass. When oxygen is limiting biomass growth, the characteristics of the field scale coefficients are essentially the same as when no growth is considered. But when dissolved oxygen levels in the aquifer are higher, and biomass is allowed to grow in time, the concentration dependence of the effective coefficients is considerably changed, with microbial growth playing an important role in controlling the utilization of the contaminant and dissolved oxygen.

An analysis of time equilibrium conditions for the biomass concentration was performed in order to provide a scenario to which the analyses developed in Chapter 4 and this Chapter could be related. The results show that when microbial dynamics are considered, narrow ranges of equilibrium concentrations are reached, and thus that microbial growth will take place during most of the plume development and biodegradation process. This was also verified with numerical simulations using a lumped box-car formulation for the three-component system.

However, in studying bulk contaminant plume behavior at field scales, a preliminary assessment of the effects of microbial growth using this lumped box-car formulation, shows that these effects are not significant for estimating mass loss and bulk plume migration, judging by the comparison between two and three-component results for the zeroth and first spatial moments evolution in time. This overall finding may be explained in terms of the time scale of growth dynamics, which is much smaller than biodegradation time scales in the field, and by the fact that biomass concentrations are not greatly affected (not by orders of magnitude) by growth due to aquifer contamination. So it appears that for field scale modeling of contaminant and dissolved oxygen plume evolution, the assumption of an established microbial

population at steady state is adequate. It is recommended, however, that a more sophisticated lumped parameter formulation is sought to describe spatial second moment evolution in time.

A sensitivity analysis to parameter variability of the effective field scale coefficients shows a stronger effect on the longitudinal macrodispersivities for the contaminant and dissolved oxygen than for the other parameters. These results are also consistent with those developed in Chapter 4. Sensitivity to retardation and microbial growth rate are higher than that for microbial decay rate.

The lumped box-car model was used to assess the effects of enhancing biodegradation by injecting dissolved oxygen when levels fell below a certain limit. The results obtained show an effective enhancement in the biodegradation process, both by increasing the amount of biotransformed contaminant mass, and by reducing plume spreading. More sophisticated models that incorporate pump and treat and well recirculation can be used along with the analytical expressions derive here for the effective transport and transformation coefficients to assess more realistic and applied enhanced bioremediation scenarios.

Both the analytical results and the numerical simulations developed in this Chapter presume knowledge of the statistics and correlations of the different random fields involved: log-hydraulic conductivity, retardation, microbial growth and decay rates. This information, however, does not exist for actual contaminated field sites. Based on the findings presented here, it is recommended that measurements of sorption and microbial growth and decay (or biodegradation rates) paired with hydraulic conductivity are made in order to determine the statistics required to estimate the effective parameters. These parameters, in turn, can be used as input to models in field scale simulations that will aid in obtaining a more comprehensive picture of the biodegradation process.

# Chapter 6

# Conclusions, Limitations and Recommendations

## 6.1 Summary and Conclusions

The stochastic theory developed in this study demonstrates that natural chemical and microbiological heterogeneity combined with hydraulic heterogeneity can significantly alter the field scale processes of sorption and biodegradation. The main findings of this analytical investigation can be summarized in the following conclusions, which also convey recommendations for practical applications and further work in this field.

The first part of this thesis deals with a stochastic treatment of field scale transport of a reactive solute in groundwater. The theoretical developments of Chapters 2 and 3 are aimed at elucidating some of the questions raised in the recent literature regarding the influence of soil matrix diffusion and sorption on bulk plume behavior and the transient developments of field scale effective transport coefficients for reactive solutes.

In Chapter 2, an analysis of the influence of intragrain diffusion and sorption on the field scale characteristics of reactive solutes is presented. It is shown that the intragrain diffusion and sorption processes have a contribution to the effective retardation, longitudinal macrodispersivity, and plume asymmetry. The total amount of plume retardation is found to be the addition of the amounts sorbed onto the grain and intragrain surfaces. In the field, however, it would be quite difficult to

distinguish between these two quantities. The effects of intragrain processes on plume dispersion and asymmetry were calculated using parameters for sorption of PCE at the Borden site in Ontario, Canada, and lithium at the Otis Air Force field site in Cape Cod, Massachusetts. These effects were found to be negligible for both field cases considered. However, the theory is general in its treatment of the competition and interaction between intragrain processes and aquifer heterogeneities. Determining the relative importance of these processes is essentially a question of time scales. The development of this issue is the centerpiece of the discussion presented in Chapter 3.

The time scale at which the intragrain diffusion process occurs and its influence on the transient characteristics of the field scale sorption process is treated in Chapter 3. The theory developed in this Chapter provides a general framework to compare quantitatively the transient effects produced by intragrain processes and natural aquifer heterogeneities on the field scale behavior of reactive plumes. The time scale correpsonding to intragrain processes is found to be controlled by the aquifer grain size, intragrain porosity and the tortuosity of the medium. Calculations obtained for two different field contaminated sites at Cape Cod and Borden show that this time scale is much smaller than the time scale associated with aquifer heterogeneities at these sites for values of tortuosity in the range $2 - 3$. The intragrain diffusion and sorption processes explain the local, laboratory scale characteristics of the considered reactive solutes at the Cape Cod and Borden sites, but not those observed at the large spatial and time scales of the actual field contaminant plumes at these sites. Calculations of zeroth, first and second moments for the field site at Borden using a single component linear isotherm sorption assumption provide values within the range of estimates from experimental observations for four different halogenated organic compounds. However, some plume truncation apparent from these observations limits a more reliable verification of applicability of the stochastic theory to spatial moment predictions. This limitation is even more critical in comparing the third moment estimates from theory and field experiments. The importance of incorporating nonlinear isotherm effects is crucial to study field scale behavior of the lithium plume at the Cape Cod site. An approximate evaluation of the zeroth moment for this plume is presented in

support of this conclusion.

Part II is concerned with the problem of oxygen-limited biodegradation in groundwater. There has been a growing interest recently in the knowledge and applicability of biodegradation in remediation of contaminated environments. The theory developed in Chapters 4 and 5 aids in the understanding of the controlling factors affecting plume decay, oxygen utilization and microbial growth.

Chapter 4 presents an analysis of a two-component system, where the microbial mass concentration is assumed to be invariant in time, *i.e.*, at steady state. Effective transport coefficients are derived for the contaminant and dissolved oxygen, and a special emphasis is placed in the significant difference between longitudinal macrodispersivities for both components, which is a relevant finding not considered in any other modeling approach cited in the literature. Calculations were performed using parameters for field sites at Borden and Traverse City to investigate the effects of heterogeneities and nonlinear decay on the effective transport and transformation coefficients. The field scale coefficients of dispersion are found to be sensitive to the correlations between contaminant decay rate and distribution coefficient with the hydraulic conductivity field. Contaminant decay and effective retardation factor area found to be influenced by variability in the parameters to a lesser degree.

Finally, Chapter 5 introduces microbial growth dynamics to the analysis developed in Chapter 4. The influence of microbial growth on the effective transport and transformation coefficients is strong for higher values of dissolved oxygen concentrations, at which growth of the aquifer microorganisms is not limited. It is also shown through a comparison of a lumped parameter box-car model with detailed numerical simulations, that although microbial growth can take place during contaminant plume evolution, its influence on the estimated zeroth and first spatial moments of the contaminant and dissolved oxygen plumes is not significant. This suggests the assumption of using an established microbial population at steady state for modeling purposes. A simulation of biodegradation enhancement by injection of a dissolved oxygen source at a field scale, using parameters for the site at Traverse City and the analytical results provided by the stochastic theory is presented to illustrate how the

stochastic theory can be used to produce quantitative results applicable in the field.

In general, the theoretical work developed here represents a contribution to the analysis of multicomponent transport of reactive solutes in three dimensional heterogeneous porous media. The application of the spectral perturbation approach to multicomponent reactive transport in groundwater presented here helps in answering some of the questions raised related to sorption and biodegradation in heterogeneous aquifers, and poses challenging tasks that remain ahead in the fields of environmental sciences and engineering.

## 6.2 Limitations of the Approach

It is important to recognize the limitations of the theoretical analysis developed here when considering the applicability of the results in the field.

In order to apply the results of this stochastic analysis to the field situation, the ergodic hypothesis must be invoked. In essence, we try to represent the flow and transformation processes in one aquifer by an ensemble average over a large number of realizations of a stochastic process. Ergodicity requires that the averaging distance be much larger than the correlation scale of the process [Lumley and Panofsky, 1964; Gelhar and Axness, 1983]. This implies that results will only be applicable only after displacements greater than several correlation scales.

The assumption of local stationarity (statistical homogeneity) is crucial to the spectral methodology developed herein. This assumption implies that the mean concentrations are presumed to vary slowly in space. In view of this, the general developments in the previous Chapters assume that the mean concentration gradients $G_i$ and $F_i$ can be treated as only functions of time. A more rigorous justification for this assumption is presented in Appendix K. This means that mean concentrations are linear functions of the spatial coordinates. Thus, the Fickian representation for the dispersion process will strictly be valid only when the mean concentration field is relatively smooth so that a linear approximation is suitable. Consequently, the classical Fickian form is not expected to be valid near contaminant sources where large

concentration gradients will occur. This also points to the limitation of applying the results only after significant displacements.

It is also important to recognize that the macrodispersivities apply in transport equations governing ensemble mean concentrations. The degree to which these macrodispersivities represent actual mixing and dilution in a single heterogeneous aquifer depends on how well the ensemble mean approximates the actual concentration in a single aquifer. The concentration variance, which can also be evaluated from the stochastic theory, is a suitable measure of the difference between the ensemble mean and actual concentration in a single aquifer. The theory shows that the concentration variance becomes proportional to the square of the mean concentration gradient [Vomvoris and Gelhar, 1986, 1990], so that the variance (and the coefficient of variation) will become small far from the source. Consequently, the mean concentration becomes a suitable approximate of the single aquifer behavior after large plume displacement. The theory shows that the interplay between small-scale velocity variations and dissipative effects related to local dispersion play an essential role in smoothing the plume. The predicted behavior is borne out by field experiments at Borden [Sudicky, 1986] and Cape Cod [Garabedian *et al*, 1991] which show that the plumes are actually diluting (maximum concentrations have decrease by an order of magnitude), and becoming less irregular as the mean displacement increases.

The degree of dilution is also affected by the size of the plume relative to the correlation scale. Rajaram [1991] and Rajaram and Gelhar [1992] have analyzed this effect and shown that only when the transverse plume dimension is an order of magnitude larger than the correlation scale will the classical results [Gelhar and Axness, 1983, Dagan, 1984] for the macrodispersivities be appropriate. For smaller plumes the amount of dilution is reduced (the effective dispersivity is smaller).

The stochastic theory was developed under the assumption of small $\sigma_f^2$. The adequacy of the first-order approximation for a large variability of the input $lnK$ process is not warranted, as explained by Dagan [1988]; and Gelhar and Axness [1983] indicate that the theory is applicable for $\sigma_f^2 < 1$. Gutjahr *et al* [1978] show by explicit comparison with the exact solution that the second order terms have a minor influence

in the head solution when $\sigma_f^2 < 1$. More recently, the detailed numerical simulations of Tompson and Gelhar [1990] provide results with an encouraging agreement with the stochastic theory in $\sigma_f^2 \approx 1$ fields, and indicate that at higher variabilities there exist differences between the theory and the simulation results. The summary of data on $\sigma_f^2$ in Gelhar [1986] shows that $\sigma_f^2 > 1$ for some aquifers so that this can be an important limitation. Additional work needs to be done to extend the theory to large $\sigma_f^2$.

Attention has been placed here on longitudinal macrodispersion. The first order approximation in $\sigma_f^2$ does not capture higher order effects that apparently become important for the transverse macrodispersivities $A_{22}$ and $A_{33}$ [Dagan, 1988]. Also, unsteady flow effects can play an important role in transverse dispersion as suggested by Rehfeldt [1988] and Naff [1989]. Treatment of transverse dispersion for nonreactive solutes using stochastic theories is an active research area at this time. Its extension to nonreactive solutes represents a step to be taken in the future.

In spite of these limitations, the spectral approach produces results for the transient development of the macrodispersivities [Gelhar, 1987] which are identical to those found by Dagan [1984] using the small-perturbation Lagrangian approach which does not assume local stationarity of the concentration field. The agreement between these disparate methods is important because it justifies the application of the spectral approach in cases which do not yield a constant asymptotic dispersivity [Welty and Gelhar, 1991]. Note that in this work, the Eulerian spectral approach is generalized to treat two and three-component coupled transport, whereas the Lagrangian approach, which does not treat concentration explicitly, seems to be limited to passive tracers.

Also, the results for the transient development of the sorption process presented in Chapter 3 show an encouraging agreement with the numerical simulations of Burr [1992] for the time scale of variation of the effective retardation factor and the influence of intragrain sorption in the overall field scale plume sorption process.

In a wider sense, the theory needs to be tested with sorption and biodegradation field experiments and detailed numerical simulations of multi-component transport

and transformation in groundwater.

## 6.3 Recommendations

The analytical results derived using the stochastic approach presented in the previous Chapters have important practical implications. The practical aspects of the application of the results developed in this thesis are classified into two major areas: recommendations for data collection and recommendations for mathematical modeling.

In terms of data collection, this work suggests that measurements of sorption and decay/microbial growth rates should be made paired with hydraulic conductivity measurements in order to determine the actual values of the parameters themselves, and the relationship between variations of hydraulic conductivity and those of plume sorption and decay rate parameters. These correlations, in turn, will serve as an input to predict the appropriate values of the effective transport and transformation coefficients to be used in predicting the fate of groundwater contaminant plumes. Also, sorption kinetics data must be collected in order to evaluate the characteristic time scales of the intragrain processes and their influence on the overall behavior of reactive plumes using the developed stochastic theory. The effective coefficients predicted using the theory can be used as a data collection tool, helping to plan and manage soil and water quality monitoring efforts at field contaminated sites, indicating, for example, where to sample to help cover the complete extent of the plume. This would help in avoiding problems such as plume truncation that severely limit characterization and remediation of contaminated sites. Stochastic theory results have been recently used to develop methodologies for plume monitoring efforts [Graham and McLaughlin, 1989 a,b, Li and McLaughlin, 1991]. In this work, numerical modeling of the transport equations for the mean concentrations and concentration covariances have been used in a feedback loop, where the plume is monitored at locations where uncertainties are numerically predicted to be higher, and then the model is updated with the collected concentration data to start a new prediction round.

In terms of mathematical modeling of actual field scale contaminant transport in groundwater undergoing sorption and/or oxygen limited biodegradation, a number of recommendations are suggested by this work. Two basic conceptual recommendations for groundwater modeling practitioners immediately arise from the analysis developed in Chapters 2 through 5:

1. Sorption should be modeled as a one-stage process if the characteristic time scale of intragrain processes is found or expected to be much smaller than the time scale produced by natural aquifer heterogeneities. Possible nonlinearities in the sorption isotherms must be taken into consideration.

2. Microbial mass can be assumed to be at steady state for the purposes of predicting the plume migration and decay characteristics of contaminant and dissolved oxygen plumes.

Detailed numerical simulations of transport under sorption and biodegradation scenarios are necessary to test the accuracy of the results obtained using the stochastic theory. Detailed numerical simulation efforts recently considering only sorption [Burr, 1992] and sorption coupled with biodegradation [Miralles-Wilhelm *et al.*, 1992] have shown discrepancy in whether or not there is agreement with the stochastic theory. More of these efforts are needed to help elucidate this question.

More generally, numerical simulations of reactive transport using the mean equations with mean concentration dependent effective parameters, are needed to provide a more quantitative evaluation of the theory and demonstrate the application of the results derived here under realistic field conditions.

# Appendix A

# Derivation of governing equations

## A.1 Introduction

In this chapter, mass conservation statements for a contaminant solute in its aqueous phase are used to derive the equations governing the transport and transformation of the contaminant in the subsurface.

The results of the mass balances will be expressed in terms of the classical advection-dispersion equation for a non-reactive solute, modified to include each of the following transformation processes:

1. Sorption onto soil particles surface sites.
2. Diffusion into intraparticle regions of immobile water with subsequent sorption onto intraparticle surface sites.
3. First-order chemical kinetics of sorption reactions.
4. Oxygen-limited biodegradation.

## A.2 Conservation of mass statements

The conservation of contaminant mass in a control volume of aquifer material (see Figure 4.1 can be expressed in integral form as:

$$\frac{\partial}{\partial t}\int_V (nS)dV = -\int_A \vec{J}.d\vec{A} + \int_V (nr)dV \qquad (A.1)$$

Here, $S$ is the contaminant aqueous concentration (mass of contaminant per unit volume of water) and $n$ is the soil porosity (volume of water per unit volume of bulk aquifer material). The first term on the right hand side of this equation represents the net efflux of contaminant through the control volume surface, characterized by a total flux $\vec{J}$. The last term in the equation represents the sink term $r$ corresponding to the decay of the contaminant caused by a biological/chemical reaction (mass of contaminant disappearing per unit time per unit volume of water).

The total flux of the contaminant can be decomposed into advective and dispersive fluxes,

$$\vec{J} = S\vec{q} + \vec{J}_d \qquad (A.2)$$

where $\vec{q}$ is the specific discharge vector and $\vec{J}_d$ is the dispersive component of the flux. Using the divergence theorem, equation (A.1) is transformed to (in tensor notation):

$$\frac{\partial}{\partial t}(nS) + \frac{\partial}{\partial x_i}(q_i S) = -\frac{\partial J_{di}}{\partial x_i} + nr \qquad (A.3)$$

The dispersive flux is assumed to follow a Fickian form,

$$J_{di} = -nD_{ij}\frac{\partial S}{\partial x_j} \qquad (A.4)$$

Here, $D_{ij}$ is the local dispersion tensor. The governing equation may then be written in its conservative form as:

$$\frac{\partial}{\partial t}(nS) + \frac{\partial}{\partial x_i}(q_i S) = -\frac{\partial}{\partial x_i}nD_{ij}\frac{\partial S}{\partial x_j} + nr \qquad (A.5)$$

A non-conservative form of the conservation of mass equation can be obtained by introducing global continuity of the aqueous phase:

$$\frac{\partial}{\partial t}(n\rho) + \frac{\partial}{\partial x_i}(\rho q_i) = 0 \tag{A.6}$$

If water is considered an incompressible fluid, then this continuity expression reduces to:

$$\frac{\partial n}{\partial t} + \frac{\partial q_i}{\partial x_i} = 0 \tag{A.7}$$

Introducing (A.7) into (A.5) we have:

$$n\frac{\partial S}{\partial t} + q_i\frac{\partial S}{\partial x_i} = -\frac{\partial}{\partial x_i}nD_{ij}\frac{\partial S}{\partial x_j} + nr \tag{A.8}$$

Now, as it was presented above, four cases may be considered to obtain the final form of the governing equations.

### A.2.1 Sorption onto solid phase surface

Since there is additional mass of the contaminant within the control volume $V$, the first term in the mass balance, equation A.1 must be modified to include the concentration in the sorbed phase:

$$\frac{\partial}{\partial t}\int_V (nS + \rho_b\hat{S})dV$$

where $\hat{S}$ is the concentration of the contaminant in the sorbed phase (mass of sorbed contaminant per unit mass of solid aquifer material) and $\rho_b$ is the density of the bulk density of the aquifer. This leads to the modified governing equation:

$$\frac{\partial}{\partial t}(nS) + \frac{\partial}{\partial t}(\rho_b\hat{S}) + \frac{\partial}{\partial x_i}(q_iS) = -\frac{\partial}{\partial x_i}nD_{ij}\frac{\partial S}{\partial x_j} + nr \tag{A.9}$$

If the sorption process is considered to be at thermodynamic equilibrium, then the sorbed and aqueous concentrations are related by a sorption isotherm:

$$\hat{S} = \phi(S) \tag{A.10}$$

Defining a retardation function by:

$$R(S) = 1 + \frac{\rho_b}{n}\frac{\partial \phi}{\partial S} \tag{A.11}$$

the transport equation for the contaminant becomes, for constant porosity $n$:

$$R(S)\frac{\partial S}{\partial t} + v_i\frac{\partial S}{\partial x_i} = -\frac{\partial}{\partial x_i}D_{ij}\frac{\partial S}{\partial x_j} + r \tag{A.12}$$

Here, the relationship between the specific discharge and seepage velocity $\vec{q} = n\vec{v}$ has been introduced.

### A.2.2 Diffusion into immobile water phase

Once again, since there is additional contaminant mass within the control volume, the first term in the mass balance equation is modified accordingly.

$$\frac{\partial}{\partial t}\int_V (nS + \tilde{n}\Omega)dV$$

where $\tilde{n}$ and $\Omega$ are the immobile water phase counterparts of $n$ and $S$. By applying the divergence theorem, the governing equation is now:

$$\frac{\partial}{\partial t}(nS) + \frac{\partial}{\partial t}(\tilde{n}\Omega) + \frac{\partial}{\partial x_i}(q_i S) = -\frac{\partial}{\partial x_i}nD_{ij}\frac{\partial S}{\partial x_j} + nr \tag{A.13}$$

In this case, since there does not exist a direct relationship between $S$ and $\Omega$, an equation relating the two must be found to solve the problem. A mass balance equation for the contaminant in the immobile zone can be found by writing:

$$\frac{\partial}{\partial t}\int_V (\tilde{n}\Omega)dV = -\int_A \vec{J}.d\vec{A} + \int_V (\tilde{n}\tilde{r})dV \tag{A.14}$$

Here, the first term on the right hand side of (A.14) consists of the diffusive mass exchange with the contaminant in the mobile regions. Let this diffusive flux per unit bulk volume be modeled as a first-order rate process, driven by the concentration difference between the mobile and immobile groundwater zones:

$$\frac{flux}{volume} = \omega(S - \Omega) \tag{A.15}$$

Introducing the latter expression into (A.14) and using once more the divergence theorem we have,

$$\frac{\partial}{\partial t}(\tilde{n}\Omega) = \omega(S - \Omega) + \tilde{n}\tilde{r} \tag{A.16}$$

Replacing (A.16) in (A.13) yields:

$$\frac{\partial}{\partial t}(nS) + \frac{\partial}{\partial x_i}(q_i S) = -\frac{\partial}{\partial x_i} n D_{ij} \frac{\partial S}{\partial x_j} - \omega(S - \Omega) + nr \tag{A.17}$$

or, for locally constant porosities and introducing continuity,

$$\frac{\partial \Omega}{\partial t} = \frac{\omega}{\tilde{n}}(S - \Omega) + \tilde{r} \tag{A.18}$$

$$\frac{\partial S}{\partial t} + v_i \frac{\partial S}{\partial x_i} = -\frac{\partial}{\partial x_i} D_{ij} \frac{\partial S}{\partial x_j} - \frac{\omega}{n}(S - \Omega) + r \tag{A.19}$$

For reactive solutes, the source terms $r$ and $\tilde{r}$ can be used to represent the mass sorbed to the solid phase in the immobile zone.

$$r = -\frac{\rho_b}{n} K_d \frac{\partial S}{\partial t} \tag{A.20}$$

$$\tilde{r} = -\frac{\tilde{\rho}_b}{\tilde{n}} \tilde{K}_d \frac{\partial \Omega}{\partial t} \tag{A.21}$$

where linear isotherms characterized by an equilibrium distribution coefficients $K_d$ and $\tilde{K}_d$ have been assumed to model sorption onto solids in the mobile and immobile zones. The bulk density in the zones are $\rho_b$ and $\tilde{\rho}_b$. In view of this, a set of governing equations describing equilibrium linear sorption and diffusion of solute to zones of water immobilization may be written as:

$$\Gamma \frac{\partial \Omega}{\partial t} = \frac{\omega}{\tilde{n}}(S - \Omega) \tag{A.22}$$

$$R\frac{\partial S}{\partial t} + v_i\frac{\partial S}{\partial x_i} = -\frac{\partial}{\partial x_i}D_{ij}\frac{\partial S}{\partial x_j} - \frac{\omega}{n}(S - \Omega) \tag{A.23}$$

with $R$ and $\Gamma$ being the retardation factors in the mobile and immobile water zones, respectively:

$$R = 1 + \frac{\rho_b}{n}K_d \tag{A.24}$$

$$\Gamma = 1 + \frac{\tilde{\rho}_b}{\tilde{n}}\tilde{K}_d \tag{A.25}$$

### A.2.3 First-order sorption kinetics

If the sorption process itself is controlled by a first order rate process, this is:

$$\frac{\partial}{\partial t}(\rho_b\hat{S}) = k_1'S - k_2'\hat{S} \tag{A.26}$$

or, for a time invariant $\rho_b$,

$$\frac{\partial \hat{S}}{\partial t} = k_1S - k_2\hat{S} \tag{A.27}$$

This is the governing equation for the contaminant in the sorbed phase $\hat{S}$. The governing equation for the contaminant in the aqueous phase $S$ can be written by replacing (A.27) into (A.9) to obtain:

$$\frac{\partial S}{\partial t} + v_i\frac{\partial S}{\partial x_i} = -\frac{\partial}{\partial x_i}D_{ij}\frac{\partial S}{\partial x_j} - \frac{\rho_b}{n}(k_1S - k_2\hat{S}) + r \tag{A.28}$$

As with the case of diffusion into the immobile water phase, this is a set of coupled partial differential equations that must be solved simultaneously in order to obtain the concentration distributions $S$ and $\Omega$.

### A.2.4 Oxygen-limited biodegradation

The source term in the aqueous mobile phase contaminant equation $r$ needs to be expressed according to a model for microbial kinetics. For the case of oxygen-limited biodegradation, a dual Monod-type expression can be invoked. In this case, coupled governing equations are obtained for the contaminant, dissolved oxygen and microbial mass in the aquifer. These equations must also be solved simultaneously. This process is explained in detail in Chapters 4 and 5.

A governing equation that incorporates the effects of linear equilibrium sorption and biodegradation may be written as:

$$R\frac{\partial S}{\partial t} + v_i\frac{\partial S}{\partial x_i} = -\frac{\partial}{\partial x_i}D_{ij}\frac{\partial S}{\partial x_j} + r \qquad \text{(A.29)}$$

where the biodegradation source term $r$ is a function of the concentrations of the components involved: contaminant, dissolved oxygen and microbial mass.

# Appendix B

# Scaling of spectral concentration amplitudes

In large-time analyses of concentration fluctuations spectra, it is important to recognize that when the components of a system are undergoing a decay process, by biodegradation, by transfer to another phase or by any other means, the introduction of a time frame of reference that 'follows' the plume is extremely helpful. It is convenient in the same way as introducing the moving coordinate system in the analysis of retarded plume behavior [Garabedian *et al*, 1988].

Changes in original time of concentration fluctuations can never be neglected, since the mass in solution is decaying continuously. In this new frame of reference, the time concentration fluctuations (or their corresponding spectral amplitudes) can be considered to be at steady state, even though the components are undergoing a decay process at all times in the original frame of reference. So the idea of a scaling in time is to remove the influence of the decay process so that at large scaled times a steady state assumption may be invoked.

For example, take a single component system with a first order constant decay process:

$$\frac{\partial C}{\partial t} + v_i \frac{\partial C}{\partial x_i} = D_{ij} \frac{\partial^2 C}{\partial x_i \partial x_j} - \kappa C \qquad \text{(B.1)}$$

If we solve the ordinary differential equation that results from dropping the advection and dispersion processes, we have that,

$$C(t) = C_0 exp[-\kappa t] \tag{B.2}$$

Now, this solution can be used to scale the concentration as,

$$C = \hat{C} exp[-\kappa t]$$

or conversely,

$$\hat{C} = C exp[\kappa t] \tag{B.3}$$

where $\hat{C}$ is a scaled concentration obtained by replacing the value $C(0)$ which represents the initial concentration or initial mass in the system. If this expression is replaced in equation (B.1), the result is:

$$\frac{\partial C}{\partial x_i} = \frac{\partial \hat{C}}{\partial x_i} exp[-\kappa t]$$

$$\frac{\partial C}{\partial t} = \left( \frac{\partial \hat{C}}{\partial t} - \kappa \hat{C} \right) exp[-\kappa t]$$

$$\frac{\partial \hat{C}}{\partial t} + v_i \frac{\partial \hat{C}}{\partial x_i} = D_{ij} \frac{\partial^2 \hat{C}}{\partial x_i \partial x_j} \tag{B.4}$$

which is the conservation equation for a passive quantity. So this transformation yields a transport equation for a non-decaying quantity, which at large times reaches a steady state solution that can also be obtained by dropping the time derivative term in the original equation. This means that if this scaling process is done, the large time behavior of a given quantity can be obtained by dropping the time derivative term in the scaled transport equation for the corresponding quantity. In the case of the concentration fluctuations spectral amplitudes, this type of scaling allows to obtain

their large time value without having to solve sets of coupled differential equations.

Take, for example, the spectral amplitude equations for a two-zone model as described in Chapter 2, equations (2.45) and (2.46),

$$\bar{R}\frac{\partial dZ_S}{\partial t} + dZ_R\left(\frac{\partial \bar{S}}{\partial t} - \frac{v}{R_S}\frac{\partial \bar{S}}{\partial \zeta_1}\right) + ivk_1 dZ_S - \frac{\partial \bar{S}}{\partial \zeta_i}dZ_{v_i} = -D_{ij}k_i k_j dZ_S$$

$$- dZ_{\omega_1}(\bar{S} - \bar{\Omega}) - \bar{\omega}_1(dZ_S - dZ_\Omega) \tag{B.5}$$

$$\bar{\Omega}\frac{\partial dZ_\Omega}{\partial t} + dZ_\Gamma\frac{\partial \bar{\Omega}}{\partial t} = dZ_{\omega_2}(\bar{S} - \bar{\Omega}) + \bar{\omega}_2(dZ_S - dZ_\Omega) \tag{B.6}$$

Solving the first-order decay equations:

$$\bar{R}\frac{\partial dZ_S}{\partial t} = -\bar{\omega}_1(dZ_S - dZ_\Omega) \tag{B.7}$$

$$\bar{\Omega}\frac{\partial dZ_\Omega}{\partial t} = \bar{\omega}_2(dZ_S - dZ_\Omega) \tag{B.8}$$

we obtain the solutions,

$$dZ_S = dZ_{S_0}exp\left(-\int_0^t \frac{\bar{\omega}_1}{\bar{R}}dt'\right) + \int_0^t \frac{\bar{\omega}_1}{\bar{R}}dZ_\Omega exp\left(-\int_{t'}^t \frac{\bar{\omega}_1}{\bar{R}}dt''\right)dt' \tag{B.9}$$

$$dZ_\Omega = dZ_{\Omega_0}exp\left(-\int_0^t \frac{\bar{\omega}_2}{\bar{\Gamma}}dt'\right) + \int_0^t \frac{\bar{\omega}_2}{\bar{\Gamma}}dZ_S exp\left(-\int_{t'}^t \frac{\bar{\omega}_2}{\bar{\Gamma}}dt''\right)dt' \tag{B.10}$$

and the scaling equations are obtained by replacing the initial values of the spectral amplitudes by the scaled values of the spectral amplitudes into equations (2.45) and (2.46), to yield conservation equations for non-decaying spectral amplitudes $dZ_S$ and $dZ_\Omega$, equations (2.50) and (2.51), where the mean transfer factors $\bar{\omega}_1$ and $\bar{\omega}_2$ have been replaced by the effective transfer factors $\omega_{1e}$ and $\omega_{2e}$ to account for the possible heterogeneity of these parameters. Note that since,

$$dZ_S = d\bar{Z}_{\bar{S}} exp\left(-\int_0^t \frac{\omega_{1e}}{\bar{R}} dt'\right) + \int_0^t \frac{\omega_{1e}}{\bar{R}} dZ_\Omega exp\left(-\int_{t'}^t \frac{\omega_{1e}}{\bar{R}} dt''\right) dt' \qquad \text{(B.11)}$$

the time derivative of this term is:

$$\frac{\partial dZ_S}{\partial t} = [\frac{\partial dZ_{\bar{S}}}{\partial t} - \frac{\omega_{1e}}{\bar{R}} dZ_{\bar{S}} + \frac{\omega_{1e}}{\bar{R}} \int_0^t \frac{\omega_{1e}}{\bar{R}} dZ_\Omega exp\left(-\int_{t'}^t \frac{\omega_{1e}}{\bar{R}} dt''\right) dt'$$

$$- \frac{\omega_{1e}}{\bar{R}} dZ_\Omega] exp\left(-\int_0^t \frac{\omega_{1e}}{\bar{R}} dt'\right) \qquad \text{(B.12)}$$

so one can write,

$$\bar{R}\frac{\partial dZ_S}{\partial t} + \bar{\omega}_1 dZ_S = \bar{R}\frac{\partial dZ_{\bar{S}}}{\partial t} exp\left(-\int_0^t \frac{\omega_{1e}}{\bar{R}} dt'\right) + (\bar{\omega}_1 - \omega_{1e}) dZ_S + \omega_{2e} dZ_\Omega$$

Replacing the latter expression into equation (2.45) yields equation (2.50):

$$\bar{R}\frac{\partial dZ_{\bar{S}}}{\partial t} exp\left(-\int_0^t \frac{\omega_{1e}}{\bar{R}} dt'\right) + (ivk_1 + D_{ij}k_i k_j + \bar{\omega}_1 - \omega_{1e}) dZ_S + dZ_R(\frac{\partial \bar{S}}{\partial t} + \frac{v}{R_S} G_1)$$

$$- G_j dZ_{v_j} = (\bar{\omega}_1 - \omega_{1e}) dZ_\Omega - (\bar{S} - \bar{\Omega}) dZ_{\omega_1} \qquad \text{(B.13)}$$

A similar analysis applies to the spectral equation for $dZ_\Omega$ and to other transport problems like the two and three component biodegradation systems treated in Chapters 4 and 5.

# Appendix C

# A deterministic model of batch sorption experiments

A physical model of the intragrain diffusion/sorption process in a batch system, which is used in most of the laboratory experiments described in Chapter 2, is developed by considering solute mass transfer between zones of 'mobile' water (where measurements are made) and immobile water (pore water). In this model, the mass flux is driven by the concentration difference between the zones, leading to a first-order lumped formulation of the mass transfer process. Sorption is assumed to occur instantaneously at each microscale location within each zone, with the diffusional transfer being the limiting transport factor. A set of governing equations can then be written as:

$$R\frac{\partial S}{\partial t} = -\omega_1(S - \Omega) \tag{C.1}$$

$$\Gamma\frac{\partial \Omega}{\partial t} = \omega_2(S - \Omega) \tag{C.2}$$

This set of ordinary differential equations can be transformed to a set of algebraic equations by using Laplace transforms.

$$s\hat{S} - S(0) = -\frac{\omega_1}{R}\hat{S} + \frac{\omega_1}{R}\hat{\Omega} \tag{C.3}$$

$$s\hat{\Omega} - \Omega(0) = \frac{\omega_2}{\Gamma}\hat{S} - \frac{\omega_2}{\Gamma}\hat{\Omega} \tag{C.4}$$

or rewriting,

$$\left(\frac{\omega_1}{R} + s\right)\hat{S} - \frac{\omega_1}{R}\hat{\Omega} = S(0) \tag{C.5}$$

$$-\frac{\omega_2}{\Gamma}\hat{S} + \left(\frac{\omega_2}{\Gamma} + s\right)\hat{\Omega} = \Omega(0) \tag{C.6}$$

This produces a solution given by:

$$\hat{S} = \frac{S(0)(\frac{\omega_2}{\Gamma} + s) + \Omega(0)\frac{\omega_1}{R}}{s^2 + s(\frac{\omega_1}{R} + \frac{\omega_2}{\Gamma})} \tag{C.7}$$

$$\hat{\Omega} = \frac{\Omega(0)(\frac{\omega_1}{R} + s) + S(0)\frac{\omega_2}{\Gamma}}{s^2 + s(\frac{\omega_1}{R} + \frac{\omega_2}{\Gamma})} \tag{C.8}$$

With a zero initial concentration in the intragrain pore water ($\Omega(0) = 0$), a solution for the concentration in the mobile zone is found by inverting the transform $\hat{S}$:

$$\frac{S(t)}{S(0)} = \left[1 - \frac{\frac{\omega_2}{\Gamma}}{\frac{\omega_1}{R} + \frac{\omega_2}{\Gamma}}\right] exp\left[-(\frac{\omega_1}{R} + \frac{\omega_2}{\Gamma})t\right] + \frac{\frac{\omega_2}{\Gamma}}{\frac{\omega_1}{R} + \frac{\omega_2}{\Gamma}} \tag{C.9}$$

This solution gives the natural time scale of the intragrain diffusion/sorption process as:

$$\tau = \left(\frac{\omega_1}{R} + \frac{\omega_2}{\Gamma}\right)^{-1} = \frac{1}{\omega}\left(\frac{1}{nR} + \frac{1}{\tilde{n}\Gamma}\right)^{-1} \tag{C.10}$$

An example calculation using parameters for Lithium sorption onto sediments of an aquifer in Cape Cod, Massachusetts [Garabedian *et al*, 1988, Garabedian *et al*, 1991] is presented here to illustrate an application of this model. For this case, the retardation factor observed was $R_{obs} = 10$ with an intragrain porosity reported by Wood *et al* of approximately $\tilde{n} = 0.1$. Table C.1 shows the array of retardation factors in the external and internal zones that would combine to give the observed value $R_{obs}$, and the corresponding time scale $\tau$ obtained from equation (C.10).

The mass transfer factor $\omega$ is calculated as:

$$\omega = \frac{D_m}{\chi a^2} \tag{C.11}$$

where $D_m$ is the molecular diffusion coefficient, $a$ is the characteristic grain size, and $\chi$ is the tortuosity parameter that accounts for the tortuous path of the solute through the immobile zone. A value of $\chi = 2$ has been assumed for these calculations.

Table C.1: Batch scale parameters for Lithium at the Cape Cod site.

| R | $\Gamma$ | $\tau$ (min) |
|---|---|---|
| 1 | 35 | 3.2 |
| 2 | 31 | 5.0 |
| 3 | 27 | 5.6 |
| 4 | 23 | 5.4 |
| 5 | 19 | 4.6 |
| 6 | 15 | 3.4 |
| 7 | 12 | 2.4 |
| 8 | 8 | 1.2 |
| 9 | 4 | 0.3 |
| 9.7 | 1 | $<< 1$ |

# Appendix D

# Analysis of third-order derivatives

The mean transport equation (2.91) contains mixed space-time derivative, second-order time derivative and third-order spatial derivative terms. Some of these terms can be shown to contribute to the skewness observed in field plumes [Wood *et al*, 1990]. Rewriting this equation,

$$R_S \frac{\partial \bar{S}}{\partial t} = v A_{11} \frac{\partial^2 \bar{S}}{\partial \zeta_1^2} - \Phi_1 \frac{\partial^2 \bar{S}}{\partial t \partial \zeta_1} - \Phi_2 \frac{\partial \bar{S}}{\partial t^2} - \Psi_1 \frac{\partial^3 \bar{S}}{\partial \zeta_1^3} + \ldots \tag{D.1}$$

Recall the expressions for the spatial and time derivatives between the fixed and moving coordinate systems,

$$\left(\frac{\partial}{\partial x_1}\right) = \left(\frac{\partial}{\partial \zeta_1}\right) \tag{D.2}$$

$$\left(\frac{\partial}{\partial t}\right)_\zeta = \left(\frac{\partial}{\partial t}\right)_x + \frac{v}{R_S}\frac{\partial}{\partial x_1} \tag{D.3}$$

From these expressions, the derivatives above follow,

$$\frac{\partial^2 \bar{S}}{\partial t \partial \zeta_1} = \frac{\partial^2 \bar{S}}{\partial t \partial x_1} + \frac{v}{R_S}\frac{\partial^2 \bar{S}}{\partial x_1^2} \tag{D.4}$$

$$\left(\frac{\partial \bar{S}}{\partial t^2}\right)_\zeta = \left(\frac{\partial \bar{S}}{\partial t^2}\right)_x + 2\frac{v}{R_S}\frac{\partial^2 \bar{S}}{\partial t \partial x_1} + \frac{v^2}{R_S^2}\frac{\partial^2 \bar{S}}{\partial x_1^2} \tag{D.5}$$

$$\left(\frac{\partial^3 \bar{S}}{\partial \zeta_1^3}\right) = \left(\frac{\partial^3 \bar{S}}{\partial x_1^3}\right) \tag{D.6}$$

Rewriting the mean equation as,

$$\frac{\partial \bar{S}}{\partial t} = \frac{v}{R_S} A_{11} \frac{\partial^2 \bar{S}}{\partial \zeta_1^2} - \frac{\Phi_1}{R_S} \frac{\partial^2 \bar{S}}{\partial t \partial \zeta_1} - \frac{\Phi_2}{R_S} \frac{\partial \bar{S}}{\partial t^2} - \frac{\Psi_1}{R_S} \frac{\partial^3 \bar{S}}{\partial \zeta_1^3} + \ldots \tag{D.7}$$

one can expand this equation in the fixed coordinate system.

$$\frac{\partial \bar{S}}{\partial t} = -\frac{v}{R_S} \frac{\partial \bar{S}}{\partial x_1} + \frac{v}{R_S} A_{11} \frac{\partial^2 \bar{S}}{\partial x_1^2} - \frac{\Phi_1}{R_S} \frac{\partial^2 \bar{S}}{\partial t \partial x_1} - \frac{\Phi_1 v}{R_S^2} \frac{\partial^2 \bar{S}}{\partial x_1^2}$$

$$- \frac{\Phi_2}{R_S} \left( \frac{\partial \bar{S}}{\partial t^2} + 2 \frac{v}{R_S} \frac{\partial^2 \bar{S}}{\partial t \partial x_1} + \frac{v^2}{R_S^2} \frac{\partial^2 \bar{S}}{\partial x_1^2} \right) - \frac{\Psi_1}{R_S} \frac{\partial^3 \bar{S}}{\partial x_1^3} + \ldots \tag{D.8}$$

Substituting this expression for the time derivative in the mixed derivative term gives,

$$\frac{\partial^2 \bar{S}}{\partial t \partial x_1} = \frac{\partial}{\partial x_1} [ - \frac{v}{R_S} \frac{\partial \bar{S}}{\partial x_1} + \frac{v}{R_S} A_{11} \frac{\partial^2 \bar{S}}{\partial x_1^2} - \frac{\Phi_1}{R_S} \frac{\partial^2 \bar{S}}{\partial t \partial x_1} - \frac{\Phi_1 v}{R_S^2} \frac{\partial^2 \bar{S}}{\partial x_1^2}$$

$$- \frac{\Phi_2}{R_S} \left( \frac{\partial \bar{S}}{\partial t^2} + 2 \frac{v}{R_S} \frac{\partial^2 \bar{S}}{\partial t \partial x_1} + \frac{v^2}{R_S^2} \frac{\partial^2 \bar{S}}{\partial x_1^2} \right) - \frac{\Psi_1}{R_S} \frac{\partial^3 \bar{S}}{\partial x_1^3} + \ldots ] \tag{D.9}$$

Second-order derivative terms can be grouped out in the latter expression. These terms are (on the right hand side),

$$\frac{v}{R_S} A_{11} + \frac{\Phi_1 v}{R_S^2} - \frac{\Phi_1 v}{R_S^2} + 2 \frac{\Phi_2 v^2}{R_S^3} - \frac{\Phi_2 v^2}{R_S^3} - \frac{\Phi_2 v^2}{R_S^3} = \frac{v}{R_S} A_{11}$$

which results in the macrodispersivity term, as expected. Meanwhile, the third-order derivative terms that appear on the right hand side of equation (D.9) are:

$$- \frac{\Phi_1}{R_S} \left( \frac{v}{R_S} A_{11} + \frac{\Phi_1 v}{R_S^2} - \frac{\Phi_1 v}{R_S^2} - \frac{\Phi_2 v^2}{R_S^3} + 2 \frac{\Phi_2 v^2}{R_S^3} - \frac{\Phi_2 v^2}{R_S^3} \right)$$

$$- \frac{\Phi_2}{R_S} \left( - \frac{v^2}{R_S^2} A_{11} - \frac{v^2}{R_S^2} A_{11} + 2 \frac{v^2}{R_S^2} A_{11} \right) - \frac{\Psi_1}{R_S} = - \frac{\Phi_1 v}{R_S^2} A_{11} - \frac{\Psi_1}{R_S}$$

And the mean equation is the written in its final form, equations (2.95) through (2.97)

$$R_S\frac{\partial \bar{S}}{\partial t} + v\frac{\partial \bar{S}}{\partial x_1} = vA_{11}\frac{\partial^2 \bar{S}}{\partial x_1^2} - \left(\Phi\frac{v}{R_S}A_{11} + \Psi\right)\frac{\partial^3 \bar{S}}{\partial x_1^3} + \cdots \qquad \text{(D.10)}$$

with,

$$\Phi = -2I_1 + 2\frac{v}{R_S}I_3 \qquad \text{(D.11)}$$

and,

$$\Psi = \left[2(\frac{v\Gamma_e}{\omega_{2e}R_S})^2 - \frac{v\Gamma_e}{\omega_{2e}R_S}A_{11}\right]I_4 + 2\left[\frac{\Gamma e}{\omega_{2e}}(\frac{v}{R_S})^2A_{11} - (\frac{\Gamma_e}{\omega_{2e}})^2(\frac{v}{R_S})^3\right]I_5 \qquad \text{(D.12)}$$

# Appendix E

# Development of integrals for the transient sorption process

The following analysis corresponds to the integrals that appear in the calculation of effective transport parameters for the transient sorption problem developed in Chapter 3. Since all random fields are linearly related to log-hydraulic conductivity field $f = lnK$, the integrals can be calculated using the spectrum $S_{ff}$.

$$I = \frac{1}{\bar{R}} \int_{-\infty}^{\infty} \frac{1 - e^{-\beta t}}{\beta} S_{ff}(\mathbf{k}) d\mathbf{k} \tag{E.1}$$

Recalling the expression for $\beta$, equation (3.10):

$$\beta(\mathbf{k}) = \frac{ivk_1 + D_{ij}k_ik_j}{\bar{R}} \tag{E.2}$$

the integral can be written as:

$$I = \frac{\bar{R}}{v} \int_{-\infty}^{\infty} \frac{1 - e^{-\beta t}}{ik_1 + \alpha_{ij}k_ik_j} S_{ff}(\mathbf{k}) d\mathbf{k} \tag{E.3}$$

Simplifying the denominator of the integrand results in,

$$I = \frac{\bar{R}}{v} \int_{-\infty}^{\infty} (1 - e^{-\beta t}) \frac{\alpha_{ij}k_ik_j - ik_1}{k_1^2 + (\alpha_{ij}k_ik_j)^2} S_{ff}(\mathbf{k}) d\mathbf{k} \tag{E.4}$$

Introducing the change of variable $u_i = \lambda_i k_i$, with $i = 1, 2, 3$ and no summation

over $i$,

$$I = \frac{\bar{R}}{v}\int_{-\infty}^{\infty} \frac{[1 - exp(-\frac{vt}{\bar{R}}\sum_{i=1}^{3}\alpha_i\frac{u_i^2}{\lambda_i^2})(cos\frac{u_1 vt}{\lambda_1} - isin\frac{u_1 vt}{\lambda_1})](\sum_{i=1}^{3}\alpha_i\frac{u_i^2}{\lambda_i^2} - i\frac{u_1}{\lambda_1})}{\frac{u_1^2}{\lambda_1^2} + (\sum_{i=1}^{3}\alpha_i\frac{u_i^2}{\lambda_i^2})^2}\frac{S_{ff}(\mathbf{u})d\mathbf{u}}{\lambda_1\lambda_2\lambda_3} \tag{E.5}$$

For practical applications, the parameters $\epsilon = \frac{\alpha_L}{\lambda_1}$ and $r = \frac{\alpha_T\lambda_1}{\lambda_3^2}$ are small compared to unity [Gelhar and Axness, 1983], which is esentially equivalent to dropping the local dispersion terms. The integral is then simplified to:

$$I = \frac{\lambda_1\bar{R}}{v}\int_{-\infty}^{\infty}\frac{sin\frac{u_1 vt}{\lambda_1}}{u_1}\frac{S_{ff}(\mathbf{u})d\mathbf{u}}{\lambda_1\lambda_2\lambda_3} \tag{E.6}$$

Introducing the spectrum for the log-hydraulic conductivity perturbation,

$$S_{ff}(\mathbf{u}) = \frac{\sigma_f^2\lambda_1\lambda_2\lambda_3}{\pi^2(1+u^2)^2} \tag{E.7}$$

the integral is reduced to,

$$I = \frac{\sigma_f^2\lambda_1\bar{R}}{\pi^2 v}\int_{-\infty}^{\infty}\frac{sin\frac{u_1 vt}{\lambda_1}}{u_1}\frac{du_1du_2du_3}{(1+u^2)^2} \tag{E.8}$$

Integration over $u_1$ produces [Gradshteyn and Ryzhik, 1980]:

$$I = \frac{\sigma_f^2\lambda_1\bar{R}}{\pi v}\int_{-\infty}^{\infty}[1 - exp(-A\sqrt{1+u_2^2+u_3^2})(2 + A\sqrt{1+u_2^2+u_3^2})\frac{du_2du_3}{(1+u_2^2+u_3^2)^2} \tag{E.9}$$

where,

$$A = \frac{vt}{\lambda_1\bar{R}}$$

Conversion into polar coordinates yields the integral:

$$I = \frac{2\sigma_f^2\lambda_1\bar{R}}{v}\int_0^{\infty}[1 - exp(-A\sqrt{1+\rho^2})(2 + A\sqrt{1+\rho^2})\frac{\rho d\rho}{(1+\rho^2)^2} \tag{E.10}$$

Manipulation of this integral gives the final expression:

$$I = \frac{\sigma_f^2 \lambda_1 \bar{R}}{v}[1 - exp(-A)] = \frac{\sigma_f^2 \lambda_1}{v}[1 - exp(\frac{vt}{\lambda_1 \bar{R}})] \tag{E.11}$$

The integrals in Chapter 3 can be calculated by assuming the stratified aquifer approximation of Gelhar and Axness [1983], where $\delta = (\frac{\lambda_2}{\lambda_1}) << 1$. This simplification transforms these integrals into the integral form (E.1). The results are:

$$I_1 = \frac{b_2 \sigma_f^2 \lambda_1}{\gamma}[1 - exp(-\frac{vt}{\lambda_1 \bar{R}})] \tag{E.12}$$

$$I_2 = \frac{v \sigma_f^2 \lambda_1}{\gamma^2}[1 - exp(-\frac{vt}{\lambda_1 \bar{R}})] \tag{E.13}$$

$$I_3 = \frac{\sigma_R^2 \lambda_1}{v}[1 - exp(-\frac{vt}{\lambda_1 \bar{R}})] \tag{E.14}$$

and their time derivatives,

$$\frac{\partial I_1}{\partial t} = \frac{b_2 \sigma_f^2 v}{\gamma \bar{R}} exp(-\frac{vt}{\lambda_1 \bar{R}}) \tag{E.15}$$

$$\frac{\partial I_3}{\partial t} = \frac{\sigma_R^2}{\bar{R}} exp(-\frac{vt}{\lambda_1 \bar{R}}) \tag{E.16}$$

# Appendix F

# Derivation of governing equations for the spatial moments of a reactive solute plume

The governing mean transport equation under consideration is equation (3.24)

$$R_S\frac{\partial \bar{S}}{\partial t} + v\frac{\partial \bar{S}}{\partial x} = vA_{11}\frac{\partial^2 \bar{S}}{\partial x^2} - \Phi\frac{v}{R_S}A_{11}\frac{\partial^3 \bar{S}}{\partial x^3} + \ldots \tag{F.1}$$

The following analysis, using the methodology developed by Aris [1956], will result in the governing equations for the total mass in solution, center of mass displacement, longitudinal second moment and skewness coefficient.

## F.1 Zeroth moment

The zeroth moment of the plume is defined:

$$M_0 = \int_{-\infty}^{\infty} n\bar{S}(\mathbf{x},t)dxdydz \tag{F.2}$$

This moment represents the total mass of the plume in solution at a given time. The governing equation for this moment is found by invoking a conservation of mass statement:

$$\frac{\partial}{\partial t}(n\bar{S} + \rho_b \hat{S}) = \frac{\partial}{\partial t}(nR_S\bar{S}) = 0 \tag{F.3}$$

Here, $n$ is the soil porosity, $\rho_b$ is the bulk density of the aquifer material and $\hat{S}$ is the sorbed concentration of the solute. Integrating this equation,

$$R_S\frac{\partial}{\partial t}\int_{-\infty}^{\infty} n\bar{S}dxdydz + \int_{-\infty}^{\infty} n\bar{S}\frac{dR_S}{dt}dxdydz = 0 \tag{F.4}$$

or,

$$R_S\frac{dM_0}{dt} + \frac{dR_S}{dt}M_0 = 0 \tag{F.5}$$

Solving this equation with a total mass of solute in the system $M_T$ gives,

$$M_0(t) = \frac{M_T}{R_S(t)} \tag{F.6}$$

This expression is a statement of mass conservation since the total solute mass in solution at a given time is the total mass of solute in the aquifer divided by the time dependent retardation factor.

## F.2 First moment

The position of the center of mass is defined by:

$$\bar{x}(t) = \frac{1}{M_T}\int_{-\infty}^{\infty} x(nR_S\bar{S})dxdydz \tag{F.7}$$

The time derivative of the center of mass displacement is written as:

$$\frac{d\bar{x}}{dt} = \frac{1}{M_T}\int_{-\infty}^{\infty} x\frac{\partial}{\partial t}(nR_S\bar{S})dxdydz \tag{F.8}$$

The governing equation can be replaced for the integrand,

$$\frac{d\bar{x}}{dt} = \frac{1}{M_T}\int_{-\infty}^{\infty} x\left[-nv\frac{\partial\bar{S}}{\partial x} + nvA_{11}\frac{\partial^2\bar{S}}{\partial x^2} - \Phi\frac{v}{R_S}A_{11}\frac{\partial^3\bar{S}}{\partial x^3}\right]dxdydz \tag{F.9}$$

Integrating by parts and assuming zero concentration and concentration gradients at infinity,

$$\frac{d\bar{x}}{dt} = v\frac{M_0}{M_T} = \frac{v}{R_S} \tag{F.10}$$

Following this equation, the center of mass moves in time with a velocity equal to the groundwater velocity divided by the transient retardation factor. Introducing the expression for the time dependent retardation factor, equation (3.20), this equation can be integrated analytically:

$$\bar{x}(t) = v\int_0^t \frac{dt'}{R_S(t')} \tag{F.11}$$

This integration produces:

$$\bar{x}(t) = \frac{vt}{\bar{R}} + \lambda_1\left(1 - \frac{b_2\sigma_f^2}{\gamma\bar{R}CV_R^2}\right) ln\left[\frac{1 - CV_R^2 exp(-\frac{vt}{\lambda_1\bar{R}})}{1 - CV_R^2}\right] \tag{F.12}$$

## F.3 Second moment

The variance of the solute distribution is defined by:

$$\sigma_X^2 = \frac{1}{M_T}\int_{-\infty}^{\infty}(x - \bar{x})^2 nR_S\bar{S}dxdydz \tag{F.13}$$

The time derivative of this moment is given as:

$$\frac{d\sigma_X^2}{dt} = \frac{1}{M_T}\int_{-\infty}^{\infty}\frac{\partial}{\partial t}\left[(x - \bar{x})^2 nR_S\bar{S}\right]dxdydz \tag{F.14}$$

Using the chain rule of differentiation and introducing the result of equation (F.10):

$$\frac{d\sigma_X^2}{dt} = \frac{1}{M_T}\left[-2\frac{v}{R_S}\int_{-\infty}^{\infty}(x - \bar{x})nR_S\bar{S}dxdydz + \int_{-\infty}^{\infty}(x - \bar{x})^2\frac{\partial}{\partial t}(nR_S\bar{S})dxdydz\right] \tag{F.15}$$

The first integral in this expression is identically zero by the definition of the center of mass displcement $\bar{x}$. In the second integral, the governing equation may be replaced to yield,

$$\frac{d\sigma_X^2}{dt} = \frac{1}{M_T}\int_{-\infty}^{\infty} \eta^2 \left[\frac{\partial}{\partial\eta} nv A_{11} \frac{\partial \bar{S}}{\partial \eta} - nv\frac{\partial \bar{S}}{\partial \eta} - \Phi \frac{v}{R_S} A_{11} \frac{\partial^3 \bar{S}}{\partial \eta^3}\right] d\eta dy dz \qquad \text{(F.16)}$$

Developing further the integration by parts gives,

$$\frac{d\sigma_X^2}{dt} = \frac{2}{M_T} v A_{11} \int_{-\infty}^{\infty} n\bar{S} dx dy dz \qquad \text{(F.17)}$$

or,

$$\frac{d\sigma_X^2}{dt} = 2A_{11}\frac{v}{R_S} \qquad \text{(F.18)}$$

which gives the result for the longitudinal macrodispersivity:

$$\frac{d\sigma_X^2}{d\bar{x}} = 2A_{11} \qquad \text{(F.19)}$$

This result has been obtained for conservative and reactive solutes [Garabedian *et al*, 1988]. Integration of this expression with respect to time can be performed to obtain an expression for the longitudinal second moment.

$$\sigma_X^2(t) = 2v\int_0^t \frac{A_{11}(t')}{R_S(t')} dt' \qquad \text{(F.20)}$$

Introducing equations (3.20) and (3.22) and using the notation:

$$A = \frac{b_2\sigma_f^2}{\gamma \bar{R}}; \qquad B = CV_R^2$$

$$z = \frac{vt}{\lambda_1 \bar{R}}$$

it follows that,

$$\sigma_X^2(z) = 2\lambda_1^2[\frac{\sigma_f^2}{\gamma^2}\int_0^z \frac{(1-e^{-z'})(1-Ae^{-z'})}{1-Be^{-z'}}dz' - 2A\int_0^z \frac{(1-e^{-z'})(1-Ae^{-z'})^2}{(1-Be^{-z'})^2}dz'$$

$$+ 2B^2\int_0^z \frac{(1-e^{-z'})(1-Ae^{-z'})^3}{(1-Be^{-z'})^3}dz'] \qquad \text{(F.21)}$$

The integration process gives the expression sought,

$$\sigma_X^2(z) = 2\lambda_1^2\left[\frac{\sigma_f^2}{\gamma^2}T_1(z) - 2AT_2(z) + 2B^2T_3(z)\right] \qquad \text{(F.22)}$$

with,

$$T_1(z) = z + \frac{A}{B}(e^{-z}-1) - (1 - \frac{A-1}{B} + \frac{A}{B^2})ln\left[\frac{1-Be^{-z}}{1-B}\right] \qquad \text{(F.23)}$$

$$T_2(z) = z + (\frac{2A+1}{B} - 1 - \frac{2A+1}{B^2} + \frac{A^2}{B^3})\left[\frac{1}{1-Be^{-z}} - \frac{1}{1-B}\right] + \frac{A^2}{B^2}(e^{-z}-1)$$

$$+ (1 - \frac{2A+1}{B^2} + \frac{A^2}{B^3})ln\left[\frac{1-Be^{-z}}{1-B}\right] \qquad \text{(F.24)}$$

$$T_3(z) = z + \frac{A^3}{B^3}(e^{-z}-1) + \frac{(A-B)^3(B-1)}{2B^4}\left(\frac{1}{(1-Be^{-z})^2} - \frac{1}{(1-B)^2}\right)$$

$$-\frac{(A-B)^2(B^2+2AB-3A)}{B^4}\left[\frac{1}{1-Be^{-z}} - \frac{1}{1-B}\right] + \frac{3A^3-3A^2B-A^3B+B^4}{B^4}ln\left[\frac{1-Be^{-z}}{1-B}\right] \qquad \text{(F.25)}$$

## F.4 Third moment

The asymmetry of the concentration distribution is represented by the skewness coefficient,

$$S_X = \frac{1}{M_T\sigma_X^3}\int_{-\infty}^{\infty}(x-\bar{x})^3 nR_S\bar{S}dxdydz \qquad \text{(F.26)}$$

Time differentiation of the skewness coefficient produces,

$$-\frac{dS_X}{dt} = -\frac{1}{M_T}\frac{3}{2\sigma_X^5}\frac{\partial}{\partial t}\sigma_X^2\int_{-\infty}^{\infty}(x-\bar{x})^3 nR_S\bar{S}dxdydz$$

$$+\frac{1}{M_T\sigma_X^3}\left[-3\int_{-\infty}^{\infty}(x-\bar{x})^2\frac{v}{R_S}nR_S\bar{S}dxdydz+\int_{-\infty}^{\infty}(x-\bar{x})^3\frac{\partial}{\partial t}(nR_S\bar{S})dxdydz\right] \tag{F.27}$$

In the last term on the right hand side of this equation, the governing equation (F.1). Using the chain rule of differentiation along with equations (F.10) and (F.18) we have that,

$$\frac{dS_X}{dt} = -\frac{3}{\sigma_X^5 M_T}A_{11}\frac{v}{R_S}S_X\sigma_X^3 M_T - \frac{3}{\sigma_X^3 M_T}\frac{v}{R_S}\int_{-\infty}^{\infty}\eta^2 nR_S\bar{S}d\eta dydz$$

$$+\frac{1}{\sigma_X^3 M_T}\int_{-\infty}^{\infty}\eta^3\left[\frac{\partial}{\partial\eta}nvA_{11}\frac{\partial\bar{S}}{\partial\eta}-nv\frac{\partial\bar{S}}{\partial\eta}-\Phi\frac{v}{R_S}A_{11}\frac{\partial^3\bar{S}}{\partial\eta^3}\right]d\eta dydz \tag{F.28}$$

Introducing the definitions for $\sigma_X^2$ and $S_X$ on the first two terms on the right hand side of this equation, and performing integration by parts on the last term yields,

$$\frac{dS_X}{dt} = -\frac{3A_{11}}{\sigma_X^2}\frac{v}{R_S}S_X + \frac{6}{\sigma_X^3}\Phi A_{11}\frac{v}{R_S^2} \tag{F.29}$$

or,

$$\frac{dS_X}{d\bar{x}} = -\frac{3A_{11}}{\sigma_X^2}S_X + \frac{6}{\sigma_X^3}\frac{\Phi}{R_S}A_{11} \tag{F.30}$$

This ordinary differential equation can be solved if the initial conditions ($t = 0$) of the variance and skewness are known. The solution for zero skewness initially (as it would be the case for a homogeneous pulse) is:

$$S_X(\bar{x}) = \frac{3}{\sigma_X^3(\bar{x})}\frac{\Phi}{R_S}[\sigma_X^2(\bar{x}) - \sigma_X^2(0)] \tag{F.31}$$

For nonzero conditions initially,

$$S_X(\bar{x}) = S_X(0) + \frac{3}{\sigma_X^3(\bar{x})}\frac{\Phi}{R_S}[\sigma_X^2(\bar{x}) - \sigma_X^2(0)] \tag{F.32}$$

# Appendix G

# Nonlinear sorption theory and moment analysis

## G.1 Nonlinear sorption theory

For a nonlinear sorption isotherm, the sorbed concentration is a nonlinear function of the aqueous concentration:

$$\hat{S} = \Lambda F(S) \tag{G.1}$$

*e.g., Freundlich* isotherm:

$$\hat{S} = K_F S^N \tag{G.2}$$

with an associated retardation factor:

$$\phi(S) = 1 + \frac{\rho_b}{n}\Lambda\frac{\partial \hat{S}}{\partial S} \tag{G.3}$$

If heterogeneity in the retardation factor field is interpreted through randomness of the sorption constant $\Lambda$, then we can write:

$$\Lambda = \bar{\Lambda} + \Lambda' \tag{G.4}$$

$$\bar{\Lambda} = a + b\bar{f} \tag{G.5}$$

$$\Lambda' = bf' + \eta \tag{G.6}$$

and,

$$\bar{\phi}(S) = 1 + \frac{\rho_b}{n}\bar{\Lambda}\frac{\partial \hat{S}}{\partial S} \tag{G.7}$$

$$\phi'(S) = 1 + \frac{\rho_b}{n}\Lambda'\frac{\partial \hat{S}}{\partial S} \tag{G.8}$$

In a similar fashion as it was done with the nonlinear source/sink term in Chapter 4, the nonlinear source term can be linearized by expanding the retardation factor around the mean concentration,

$$\phi(S) = \phi(\bar{S}) + \phi_S(S - \bar{S}) + \phi_{SS}(S - \bar{S})^2 + ... \tag{G.9}$$

with,

$$S = \bar{S} + S' \tag{G.10}$$

$$\phi_S = \left(\frac{\partial R}{\partial S}\right)_{S=\bar{S}} = \frac{\rho_b}{n}\bar{\Lambda}\left(\frac{\partial \hat{S}}{\partial S}\right)_{S=\bar{S}} \tag{G.11}$$

$$\phi_{SS} = \left(\frac{\partial^2 R}{\partial S^2}\right)_{S=\bar{S}} = \frac{\rho_b}{n}\bar{\Lambda}\left(\frac{\partial^2 \hat{S}}{\partial S^2}\right)_{S=\bar{S}} \tag{G.12}$$

The governing equation for a reactive solute is written as,

$$\phi(S)\frac{\partial S}{\partial t} + v_i\frac{\partial S}{\partial x_i} = D_{ij}\frac{\partial^2 S}{\partial x_i \partial x_j} \tag{G.13}$$

Introducing the expansion for the retardation factor in equation (G.9), averaging and dropping higher order terms produces the mean equation:

$$[\bar{\phi} + \overline{\phi'_S S'}]\frac{\partial \bar{S}}{\partial t} + \frac{\partial}{\partial t}\overline{\phi' S'} + v\frac{\partial \bar{S}}{\partial x} + \frac{\partial}{\partial x_i}\overline{v'_i S'} = D_{ij}\frac{\partial^2 \bar{S}}{\partial x_i \partial x_j} \tag{G.14}$$

and the perturbation equation,

$$[\phi' + \bar{\phi}_S S']\frac{\partial \bar{S}}{\partial t} + \bar{\phi}\frac{\partial S'}{\partial t} + v\frac{\partial S'}{\partial x} = G_j v'_j + D_{ij}\frac{\partial^2 S'}{\partial x_i \partial x_j} \tag{G.15}$$

In this equation,the spectral perturbation in the retardation factor can be written as,

$$dZ_R = dZ_\phi + \bar{\phi}_S dZ_S \tag{G.16}$$

Replacing this expression in the spectral perturbation scaling equation for one-component transport (see Appendix B) yields the solution for the spectral amplitude of the concentration perturbation as:

$$dZ_S = \frac{1}{\Delta}\left[G_j dZ_{v_j} + \left(\frac{\partial \bar{S}}{\partial t} + \frac{v}{R_S}G_1\right)dZ_\phi\right] \tag{G.17}$$

with,

$$\Delta = ivk_1 + D_{ij}k_i k_j + \left(\frac{\partial \bar{S}}{\partial t} + \frac{v}{R_S}G_1\right)(\phi_S - \phi_{se}) \tag{G.18}$$

Here, the effective retardation factor $R_S$ and the scaling function $\phi_{se}$ are related through an effective sorption constant $\Lambda_e$:

$$R_S = 1 + \frac{\rho_b}{n}\Lambda_e \frac{\partial \hat{S}}{\partial \bar{S}} \tag{G.19}$$

$$\phi_{se} = \frac{\rho_b}{n}\Lambda_e \frac{\partial^2 \hat{S}}{\partial \bar{S}^2} \tag{G.20}$$

At large times, following the procedure described in Garabedian *et al* [1988] and Chapter 3, it can be shown that the effective retardation factor is equal to the mean. This is,

$$R_S = \bar{\phi}(\bar{S}) \tag{G.21}$$

or equivalently,

$$\Lambda_e = \bar{\Lambda} \tag{G.22}$$

$$\phi_{se} = \bar{\phi}_S \tag{G.23}$$

This last expression simplifies the expression for $\Delta$, equation (G.18) to the same expression obtained for the linear sorption case. The effective retardation factor and longitudinal macrodispersivity are then found to be:

$$R_S = 1 + \frac{\rho_b}{n}\bar{\Lambda}\frac{\partial \hat{S}}{\partial \bar{S}} \tag{G.24}$$

$$A_{11} = \frac{\sigma_f^2 \lambda_1}{\gamma^2}\left[1 - \frac{\gamma b \rho_b}{n R_S}\frac{\partial \hat{S}}{\partial \bar{S}}\right]^2 + \left[\frac{\rho_b}{n}\frac{\partial \hat{S}}{\partial \bar{S}}\right]^2 \frac{\sigma_\eta^2}{R_S^2} \tag{G.25}$$

where the concentration dependence of the retardation factor and macrodispersivity is particularly important given the results presented in Chapter 3for sorption of Lithium onto Cape Cod soil.

## G.2 Moment analysis

The method of moments can also be used in this case to obtain estimates of bulk plume characteristics like in Chapter 3. However, since the field scale coefficients are concentration dependent, some preliminary concentration distribution must be assumed to obtain a first approximation. For the zeroth moment,

$$\frac{M_T}{M_0} = \frac{\int_{-\infty}^{\infty}(n\bar{S} + \rho_b \hat{S})dxdydz}{\int_{-\infty}^{\infty} n\bar{S}dxdydz} \tag{G.26}$$

Using a *Freundlich* isotherm, this equation is rewritten as:

$$\frac{M_T}{M_0} = 1 + \frac{\rho_b K_F}{n} \frac{\int_{-\infty}^{\infty} \bar{S}^N dxdydz}{\int_{-\infty}^{\infty} \bar{S} dxdydz} \tag{G.27}$$

Conservation of mass requires,

$$\frac{dM_0}{dt} + \rho_b \bar{K}_F \frac{\partial}{\partial t} \int_{-\infty}^{\infty} \bar{S}^N dxdydz = 0 \tag{G.28}$$

An approximate solution to this equation may be found by introducing a concentration distribution to evaluate the integral term. A Gaussian curve may be used with this purpose:

$$\bar{S}(\mathbf{x},t) = \frac{M_0}{n(4\pi vt)^{\frac{3}{2}}(A_{11}A_{22}A_{33})^{\frac{1}{2}}} exp\left[-\frac{(x-vt)^2}{4vA_{11}t} - \frac{y^2}{4vA_{22}t} - \frac{z^2}{4vA_{33}t}\right] \tag{G.29}$$

using this distribution, the integral term is evaluated as:

$$\int_{-\infty}^{\infty} \bar{S}^N dxdydz = \frac{1}{N^{\frac{3}{2}}} \left(\frac{M_T}{n\bar{R}}\right)^N \left[(4\pi vA_{11}t)(4\pi vA_{22}t)(4\pi vA_{33}t)\right]^{\frac{1-N}{2}} \tag{G.30}$$

Defining,

$$B = \frac{\rho_b \bar{K}_F}{n^N N^{\frac{3}{2}}} \left[(4\pi vA_{11})(4\pi vA_{22})(4\pi vA_{33})\right]^{\frac{1-N}{2}} \tag{G.31}$$

and,

$$\xi = M_0^N \quad ; \quad \tau = t^{\frac{3(1-N)}{2}} \tag{G.32}$$

one can solve equation (G.28) exactly to obtain:

$$\frac{\xi^{\frac{1}{N}}}{1-N} + B\xi\tau = \frac{M_0}{1-N} + BM_0^N t^{\frac{3(1-N)}{2}} = constant \tag{G.33}$$

At $t = 0$, the condition is that total mass in solution is equal to the total mass $M_T$, so one can solve for the ratio between aqueous mass and total mass:

$$\frac{M_0}{M_T} + \frac{B(1-N)}{M_T^{1-N}} \left(\frac{M_0}{M_T}\right)^N t^{\frac{3(1-N)}{2}} = 1 \qquad \text{(G.34)}$$

or conversely,

$$t = \left[ \frac{1 - \frac{M_0}{M_T}}{\frac{B(1-N)}{M_T^{1-N}} \left(\frac{M_0}{M_T}\right)^N} \right]^{\frac{2}{3(1-N)}} \qquad \text{(G.35)}$$

An exact solution cannot be found for the first and higher moments using this procedure. The parameters used for the analysis of the sorption data at the Cape Cod site are listed below on Table G.1. The values for the *Freundlich* isotherm parameters $K_F$ and $N$ were taken from Garabedian *et al* [1988], and preliminary dispersivities were selected to best fit the data, although sensitivity to these parameters is weaker than that for the isotherm parameters. The results obtained for the zeroth moment are presented in Figure 3-12 along with the results using linear sorption theory. An improvement in the results is obtained, showing that treatment and consideration of nonlinear sorption effects is crutial in analyzing retardation of this kind of compounds.

Table G.1: Nonlinear sorption parameters for the Cape Cod site case.

| | |
|---|---|
| $M_T$ | $595g$ |
| $\rho_b$ | $1.7g/cm^3$ |
| $n$ | 0.39 |
| $N$ | 0.5 |
| $K_F$ | $0.3(l/mg)^{0.5}$ |
| $CV_{K_F}$ | 0.5 |
| $A_{11}$ | $10m$ |
| $A_{22}$ | $2cm$ |
| $A_{33}$ | $2mm$ |

# Appendix H

# Evaluation and listing of integrals

## H.1 Calculation of the general integral expressions

The integral expressions that appear in equations (4.67) through (4.72) are evaluated in this appendix. By using the spectral representation theorem (SRT) the spectra that appear in the numerator of these integrals can be written as:

$$S_{v_i v_j} = (\frac{v}{n\gamma})^2(\delta_{i1} - \frac{k_i k_1}{k^2})(\delta_{j1} - \frac{k_j k_1}{k^2})S_{ff} \tag{H.1}$$

$$S_{wv_j} = b_1 \frac{v}{n\gamma}(\delta_{j1} - \frac{k_j k_1}{k^2})S_{ff} \tag{H.2}$$

$$S_{ww} = b_1^2 S_{ff} + S_{\delta\delta} \tag{H.3}$$

Here, the assumption of a head gradient $J_1$ in the $x_1$ direction is introduced, with $J_2 = J_3 = 0$. Let us now take the expression for $I_1$, equation (4.67):

$$I_1 = \int_{-\infty}^{\infty} \frac{S_{v_i v_j} d\mathbf{k}}{\Delta}$$

and rewrite it including the expression for the denominator $\Delta$ (4.57).

$$I_1 = \int_{-\infty}^{\infty} \frac{S_{v_i v_j} d\mathbf{k}}{-v^2 k_1^2 + ivk_1[2D_{ij}k_i k_j + \bar{r_S} - r_{se} + W(\bar{r_C} - r_{ce})]}$$

As a first step, the local dispersion terms are neglected (later, the inclusion of these terms is presented) to produce:

$$I_1 = \int_{-\infty}^{\infty} \frac{S_{v_i v_j}(-v^2 k_1^2 - ivk_1[\bar{r_S} - r_{se} + W(\bar{r_C} - r_{ce})])d\mathbf{k}}{v^4 k_1^4 + v^2 k_1^2[\bar{r_S} - r_{se} + W(\bar{r_C} - r_{ce})]^2}$$

Since the denominator of the integrand is an even function of $k_i$, the second term in the numerator does not produce a contribution to the integral. Dividing both numerator and denominator by $v^4 k_1^2$,

$$I_1 = -\frac{1}{n^2\gamma^2} \int_{-\infty}^{\infty} \frac{(\delta_{i1} - \frac{k_i k_1}{k^2})(\delta_{j1} - \frac{k_j k_1}{k^2}) S_{ff} d\mathbf{k}}{k_1^2 + \frac{1}{v^2}[\bar{r_S} - r_{se} + W(\bar{r_C} - r_{ce})]^2}$$

The longitudinal ($i = j = 1$) component of the integral will be considered. Introducing the transformation $u_i = \lambda_i k_i$ for $i = 1, 2, 3$, and the expression for the $lnK$ spectrum $S_{ff}$, equation (4.9), and defining:

$$\chi = \frac{\lambda_1}{v}[\bar{r_S} - r_{se} + W(\bar{r_C} - r_{ce})] \tag{H.4}$$

the integral is transformed to:

$$I_1 = -\frac{\sigma_f^2 \lambda_1^2}{n^2\gamma^2\pi^2} \int_{-\infty}^{\infty} \left[ \frac{(\frac{u_2}{\lambda_2})^2 + (\frac{u_3}{\lambda_3})^2}{(\frac{u_1}{\lambda_1})^2 + (\frac{u_2}{\lambda_2})^2 + (\frac{u_3}{\lambda_3})^2} \right] \frac{d\mathbf{u}}{(1+u^2)^2(u_1^2 + \chi^2)}$$

where $u^2 = u_1^2 + u_2^2 + u_3^2$. Now, by considering the stratification of the aquifer material, with isotropy in the plane of stratification [Gelhar and Axness, 1983], we can say that $\lambda_2 = \lambda_1$ and $\lambda_3 \ll \lambda_1$, so that:

$$I_1 = -\frac{\sigma_f^2 \lambda_1^2}{n^2\gamma^2\pi^2} \int_{-\infty}^{\infty} \frac{d\mathbf{u}}{(1+u^2)^2(u_1^2 + \chi^2)}$$

This integral is evaluated in spherical coordinates, with the final result:

$$I_1 = (\frac{\lambda_1}{n\gamma})^2 \sigma_f^2 [\frac{1}{\chi+1} - \frac{1}{\chi}] \tag{H.5}$$

Because of the stratification considerations, the integrand of $I_2$ and $I_3$ is the same as for $I_1$ (except for some constant coefficients). Following through the same procedure produces the results:

$$I_2 = b_1 \frac{\lambda_1^2}{n\gamma} \sigma_f^2 [\frac{1}{\chi+1} - \frac{1}{\chi}] \tag{H.6}$$

$$I_3 = (b_1^2 \sigma_f^2 + \sigma_\delta^2)[\frac{1}{\chi+1} - \frac{1}{\chi}] \tag{H.7}$$

In the case of $I_3$, the second term inside parenthesis is produced by the autocorrelation of the residual $\delta$. For $i, j \neq 1$ the integrals $I_2$ and $I_3$ are zero.

The integrals $I_4, I_5$ and $I_6$ can be found in a similar manner. Take for example $i = j = 1$ in the expression for $I_4$.

$$I_4 = \int_{-\infty}^{\infty} ivk_1 \frac{S_{v_1 v_1} d\mathbf{k}}{-v^2 k_1^2 + ivk_1[\bar{r_S} - r_{se} + W(\bar{r_C} - r_{ce})]}$$

This can be rewritten as:

$$I_4 = \int_{-\infty}^{\infty} \frac{S_{v_i v_j}(-iv^3 k_1^3 + v^2 k_1^2[\bar{r_S} - r_{se} + W(\bar{r_C} - r_{ce})])d\mathbf{k}}{v^4 k_1^4 + v^2 k_1^2[\bar{r_S} - r_{se} + W(\bar{r_C} - r_{ce})]^2}$$

Now, it is the first term in the numerator of the integrand that produces a zero result. The integral is now transformed to:

$$I_4 = \frac{\sigma_f^2 \lambda_1^2}{n^2 \gamma^2 \pi^2} \chi \int_{-\infty}^{\infty} \frac{du}{(1+u^2)^2 (u_1^2 + \chi^2)}$$

with the result:

$$I_4 = (\frac{\lambda_1}{n\gamma})^2 \sigma_f^2 \frac{1}{\chi+1} \tag{H.8}$$

with $I_5$ and $I_6$ resulting in:

$$I_5 = b_1 \frac{\lambda_1^2}{n\gamma} \sigma_f^2 \frac{1}{\chi+1} \tag{H.9}$$

$$I_6 = (b_1^2\sigma_f^2 + \sigma_\delta^2)\frac{1}{\chi+1} \tag{H.10}$$

## H.2 Listing of integral expressions

The following is a list of the integral expressions that appear in equations (4.79) through (4.83):

$$I_7 = \int_{-\infty}^{\infty} \frac{S_{Rv_j}d\mathbf{k}}{\Delta} = b_2\frac{\lambda_1^2}{n\gamma}\sigma_f^2[\frac{1}{\chi+1} - \frac{1}{\chi}] \tag{H.11}$$

$$I_8 = \int_{-\infty}^{\infty} \frac{S_{Rv_j}d\mathbf{k}}{\Delta} = b_2\frac{\lambda_1^2}{n\gamma}\sigma_f^2\frac{1}{\chi+1} \tag{H.12}$$

$$I_9 = \int_{-\infty}^{\infty} ivk_1\frac{S_{rv_j}d\mathbf{k}}{\Delta} = b_1\frac{\bar{S}}{\bar{S}+S_0}\frac{\bar{C}}{\bar{C}+C_0}\frac{\lambda_1^2}{n\gamma}\sigma_f^2\frac{1}{\chi+1} \tag{H.13}$$

$$I_{10} = \int_{-\infty}^{\infty} \frac{S_{v_iv_j}d\mathbf{k}}{\Delta} = (\frac{\lambda_1}{n\gamma})^2\sigma_f^2[\frac{1}{\chi+1} - \frac{1}{\chi}] \tag{H.14}$$

$$I_{11} = \int_{-\infty}^{\infty} ivk_1\frac{S_{v_iv_j}d\mathbf{k}}{\Delta} = (\frac{\lambda_1}{n\gamma})^2\sigma_f^2\frac{1}{\chi+1} \tag{H.15}$$

$$I_{12} = \int_{-\infty}^{\infty} ivk_1\frac{S_{RR}d\mathbf{k}}{\Delta} = (b_2^2\sigma_f^2 + \sigma_\eta^2)\frac{1}{\chi+1} \tag{H.16}$$

$$I_{13} = \int_{-\infty}^{\infty} ivk_1\frac{S_{rR}d\mathbf{k}}{\Delta} = b_1b_2\frac{\bar{S}}{\bar{S}+S_0}\frac{\bar{C}}{\bar{C}+C_0}\sigma_f^2\frac{1}{\chi+1} \tag{H.17}$$

$$I_{14} = \int_{-\infty}^{\infty} \frac{S_{RR}d\mathbf{k}}{\Delta} = (b_2^2\sigma_f^2 + \sigma_\eta^2)[\frac{1}{\chi+1} - \frac{1}{\chi}] \tag{H.18}$$

$$I_{15} = \int_{-\infty}^{\infty} \frac{S_{rv_j}d\mathbf{k}}{\Delta} = b_1\frac{\bar{S}}{\bar{S}+S_0}\frac{\bar{C}}{\bar{C}+C_0}\frac{\lambda_1^2}{n\gamma}\sigma_f^2[\frac{1}{\chi+1} - \frac{1}{\chi}] \tag{H.19}$$

$$I_{16} = \int_{-\infty}^{\infty} \frac{S_{rR}d\mathbf{k}}{\Delta} = b_1b_2\frac{\bar{S}}{\bar{S}+S_0}\frac{\bar{C}}{\bar{C}+C_0}\sigma_f^2[\frac{1}{\chi+1} - \frac{1}{\chi}] \tag{H.20}$$

$$I_{17} = \int_{-\infty}^{\infty} \frac{S_{r_cv_j}d\mathbf{k}}{\Delta} = b_1\frac{\bar{S}}{\bar{S}+S_0}\frac{C_0}{(\bar{C}+C_0)^2}\frac{\lambda_1^2}{n\gamma}\sigma_f^2[\frac{1}{\chi+1} - \frac{1}{\chi}] \tag{H.21}$$

$$I_{18} = \int_{-\infty}^{\infty} \frac{S_{r_cr}d\mathbf{k}}{\Delta} = b_1(\frac{\bar{S}}{\bar{S}+S_0})^2\frac{\bar{C}}{\bar{C}+C_0}\frac{C_0}{(\bar{C}+C_0)^2}\frac{\lambda_1^2}{n\gamma}\sigma_f^2[\frac{1}{\chi+1} - \frac{1}{\chi}] \tag{H.22}$$

$$I_{19} = \int_{-\infty}^{\infty} ivk_1\frac{S_{r_cv_j}d\mathbf{k}}{\Delta} = b_1\frac{\bar{S}}{\bar{S}+S_0}\frac{C_0}{(\bar{C}+C_0)^2}\frac{\lambda_1^2}{n\gamma}\sigma_f^2\frac{1}{\chi+1} \tag{H.23}$$

$$I_{20} = \int_{-\infty}^{\infty} \frac{S_{r_S v_j} d\mathbf{k}}{\Delta} = b_1 \frac{S_0}{(\bar{S}+S_0)^2} \frac{\bar{C}}{\bar{C}+C_0} \frac{\lambda_1^2}{n\gamma} \sigma_f^2 [\frac{1}{\chi+1} - \frac{1}{\chi}] \tag{H.24}$$

$$I_{21} = \int_{-\infty}^{\infty} ivk_1 \frac{S_{r_C r} d\mathbf{k}}{\Delta} = b_1 (\frac{\bar{S}}{\bar{S}+S_0})^2 \frac{\bar{C}}{\bar{C}+C_0} \frac{C_0}{(\bar{C}+C_0)^2} \frac{\lambda_1^2}{n\gamma} \sigma_f^2 \frac{1}{\chi+1} \tag{H.25}$$

$$I_{22} = \int_{-\infty}^{\infty} ivk_1 \frac{S_{r_S R} d\mathbf{k}}{\Delta} = b_1 b_2 \frac{S_0}{(\bar{S}+S_0)^2} \frac{\bar{C}}{\bar{C}+C_0} \sigma_f^2 \frac{1}{\chi+1} \tag{H.26}$$

$$I_{23} = \int_{-\infty}^{\infty} \frac{S_{r_S R} d\mathbf{k}}{\Delta} = b_1 b_2 \frac{S_0}{(\bar{S}+S_0)^2} \frac{\bar{C}}{\bar{C}+C_0} \sigma_f^2 [\frac{1}{\chi+1} - \frac{1}{\chi}] \tag{H.27}$$

$$I_{24} = \int_{-\infty}^{\infty} ivk_1 \frac{S_{r_S v_j} d\mathbf{k}}{\Delta} = b_1 \frac{S_0}{(\bar{S}+S_0)^2} \frac{\bar{C}}{\bar{C}+C_0} \frac{\lambda_1^2}{n\gamma} \sigma_f^2 \frac{1}{\chi+1} \tag{H.28}$$

$$I_{25} = \int_{-\infty}^{\infty} ivk_1 \frac{S_{r_S r} d\mathbf{k}}{\Delta} = b_1 \frac{\bar{S}}{\bar{S}+S_0} \frac{S_0}{(\bar{S}+S_0)^2} (\frac{\bar{C}}{\bar{C}+C_0})^2 \frac{\lambda_1^2}{n\gamma} \sigma_f^2 \frac{1}{\chi+1} \tag{H.29}$$

$$I_{26} = \int_{-\infty}^{\infty} \frac{S_{r_C R} d\mathbf{k}}{\Delta} = b_1 b_2 \frac{\bar{S}}{\bar{S}+S_0} \frac{C_0}{(\bar{C}+C_0)^2} \sigma_f^2 [\frac{1}{\chi+1} - \frac{1}{\chi}] \tag{H.30}$$

# Appendix I

# Derivation of expressions for field-scale coefficients

## I.1 Effective decay rate

In the mean equation for the contaminant (4.37), the decay terms (*i.e.* zeroth order derivatives of concentrations) can only come from the mean decay rate term $\bar{r}$, and from the correlations $\overline{r'_S S'}$ and $\overline{r'_C C'}$. The only decay terms in these expressions are the last ones in equations (4.82) and (4.83). In this way, the decay terms can be written as:

$$\kappa_e \frac{\bar{S}}{\bar{S}+S_0}\frac{\bar{C}}{\bar{C}+C_0} = \bar{\kappa}\frac{\bar{S}}{\bar{S}+S_0}\frac{\bar{C}}{\bar{C}+C_0} - n(I_{25}+WI_{21}) \tag{I.1}$$

Introducing the expressions for $I_{21}$ and $I_{25}$ from Appendix B, and the expression for $\phi$ (4.87), results in equation (4.86). Now since $\chi$ is a function of $\kappa_e$ (4.88), this results in a quadratic equation for $\chi$:

$$\chi^2 + \chi + (\frac{\lambda_1 \phi}{v})^2(b_1^2\sigma_f^2 + \sigma_\delta^2) = 0 \tag{I.2}$$

The solution to this equation is (4.88).

## I.2 Effective retardation factor

Lets write down the advection (*i.e.* first order derivatives of concentrations) that appear in the mean equation for the contaminant (4.37). The correlations $\overline{R'S'}$ and $\overline{v_i'S'}$ do not produce any advection terms, since these correlations are differentiated in space and do not have any linear terms in the mean concentrations $\bar{S}$ and $\bar{C}$. This was also a result found by Garabedian *et al*,[1988] when analyzing the linear variable sorption case. Following this, the extra advection terms that appear come from the correlations $\overline{r_S'S'}$ and $\overline{r_C'C'}$. Since these terms must be cancelled in the moving corrdinate system for each of the species, it must hold for the contaminant:

$$\frac{\bar{R}}{R_S} - 1 \quad \frac{I_{22} + Wn\bar{r}_C I_{23}}{R_S} + I_{24} + Wn\bar{r}_C I_{20} + \frac{Wn\bar{r}_S}{R_S} I_{27} - Wn\bar{r}_S I_{28} = 0 \qquad \text{(I.3)}$$

After some manipulation, the expression above yields the result for the effective retardation factor for the contaminant $R_S$ (4.92). A similar procedure results in the effective retardation factor for the dissolved oxygen (4.93).

## I.3 Macrodispersivities

To calculate the macrodispersivities for the contaminant and dissolved oxygen we must focus on the second order derivative terms. Only the correlations $\overline{R'S'}$ and $\overline{v_i'S'}$ contribute to the contaminant macrodispersivity tensor, while the correlation $\overline{v_i'C'}$ yields the terms to calculate the dissolved oxygen macrodispersivity tensor. These terms are, in the $\bar{S}$ equation (4.37):

$$(\bar{r}_C I_{10} - \frac{nv\bar{r}_C}{R_S} I_7) \frac{\partial^2 \bar{C}}{\partial \zeta_i \partial \zeta_j} + [2\frac{v}{R_S}(I_8 + Wn\bar{r}_C I_7) - (I_{11} + Wn\bar{r}_C I_{10})$$

$$- (\frac{v}{R_S})^2 (I_{12} + Wn\bar{r}_C I_{14})] \frac{\partial^2 \bar{S}}{\partial \zeta_i \partial \zeta_j} \equiv -vA_{ij} \frac{\partial^2 \bar{S}}{\partial \zeta_i \partial \zeta_j} \qquad \text{(I.4)}$$

and in the $\bar{C}$ equation:

$$Wn\bar{r}_S(I_{10} - \frac{v}{R_C}I_7)\frac{\partial^2\bar{S}}{\partial\xi_i\partial\xi_j} - (I_{11} + Wn\bar{r}_C I_{10})\frac{\partial^2\bar{C}}{\partial\xi_i\partial\xi_j} \equiv -vB_{ij}\frac{\partial^2\bar{C}}{\partial\xi_i\partial\xi_j} \qquad (I.5)$$

Preliminary calculations for the cross-derivative terms that appear in both the $\bar{S}$ and the $\bar{C}$ equations show that these terms are small compared to the leading terms in each equation. Because of this, they can be neglected for all practical purposes.

By manipulating the equations above, one can find that the expressions for the longitudinal ($i = j = 1$) macrodispersivities can be written as:

$$A_{11} = A'_{11}\frac{1}{\chi_S + 1} \qquad (I.6)$$

$$B_{11} = B'_{11}\frac{1}{\chi_C + 1} \qquad (I.7)$$

These are equations (4.96) and (4.97). Here, $A'_{11}$ and $B'_{11}$ are given by equations (4.98) and (4.99) [Gelhar and Axness, 1983; Garabedian *et al*, 1988] and $\chi_S, \chi_C$ by equations (4.90) and (4.91).

Now, these solutions are valid when local dispersion effects have been neglected. In other words, this means that in the expression for $\Delta$ (4.57):

$$D_{ij}k_ik_j \ll [\bar{r}_S - r_{se} + W(\bar{r}_C - r_{ce})]$$

Another way to state this is:

$$\epsilon = \frac{\alpha_L}{\lambda_1} \ll \chi$$

Now, it is easily shown that the results for the macrodispersivities when the small local dispersion term ($\epsilon \ll 1$) is of the same order or larger than $\chi$, the reaction term *i.e.* $\epsilon > \chi$ should be the values $A'_{11}$ and $B'_{11}$. The question is then how to find expressions for the macrodispersivities that are valid throughout a wide range of concentrations where both of these situations may be encountered. For instance,

take the expression for $A_{11}$. If the reaction term is small, $\chi_S \ll 1$ and hence

$$A_{11} \rightarrow A'_{11}$$

and the macrodispersivity in the absence of biodegradation is recovered. The above expressions (I.6) and (I.7), which are strictly valid for the two limiting cases $\chi \gg \epsilon$ and $\chi \approx \epsilon \ll 1$, have been applied throughout all the concentration ranges.

# Appendix J

# Integral expressions in transient microbial dynamics analysis

## J.1 Evaluation of integrals

The integral expressions that appear in the analysis developed in Chapter 5 can be classified into three basic types:

$$\Pi_1 = \int_{-\infty}^{\infty} \frac{S_{ff}(\mathrm{k})}{\Delta} d\mathrm{k} \tag{J.1}$$

$$\Pi_2 = \int_{-\infty}^{\infty} \frac{ik_1 S_{ff}(\mathrm{k})}{\Delta} d\mathrm{k} \tag{J.2}$$

$$\Pi_1 = \int_{-\infty}^{\infty} \frac{k_1^2 S_{ff}(\mathrm{k})}{\Delta} d\mathrm{k} \tag{J.3}$$

Here,

$$\Delta = -\phi_1 k_1^2 + i\phi_2 k_1 \tag{J.4}$$

These integrals can be evaluated analytically as follows.

$$\Pi_1 = \int_{-\infty}^{\infty} \frac{S_{ff} d\mathrm{k}}{-\phi_1 k_1^2 + i\phi_2 k_1} = -\int_{-\infty}^{\infty} \frac{\phi_1 S_{ff} d\mathrm{k}}{\phi_1^2 k_1^2 + \phi_2^2} \tag{J.5}$$

Notice that the integrand in the above expression is an even function of the wavenumber vector $k_i$. By introducing the variable change $u_i = \lambda_i k_i$ for $i = 1,2,3$ (no summation on $i$), and,

$$\chi = \frac{\phi_2 \lambda_1}{\phi_1} \tag{J.6}$$

$$\Pi_1 = -\frac{\lambda_1^2}{\phi_1} \int_{-\infty}^{\infty} \frac{S_{ff}(\mathrm{u})}{u_1^2 + \chi^2} \frac{du}{\lambda_1 \lambda_2 \lambda_3} \tag{J.7}$$

Introducing the expression for the spectrum $S_{ff}(\mathrm{u})$:

$$\Pi_1 = -\frac{\lambda_1^2}{\phi_1} \frac{\sigma_f^2}{\pi^2} \int_{-\infty}^{\infty} \frac{du}{(u_1^2 + \chi^2)(1+u^2)^2} \tag{J.8}$$

Using cylindrical coordinates to evaluate this integral produces:

$$\Pi_1 = 2\frac{\lambda_1^2}{\phi_1} \frac{\sigma_f^2}{\pi} \int_{-\infty}^{\infty} \frac{du_1}{u_1^2 + \chi^2} \int_0^{\infty} \frac{r dr}{(1 + u_1^2 + r^2)^2} \tag{J.9}$$

with the final result,

$$\Pi_1 = -\frac{\lambda_1^2}{\phi_1} \frac{\sigma_f^2}{\chi(1+\chi)} \tag{J.10}$$

The second integral in the list is evaluated following:

$$\Pi_2 = \int_{-\infty}^{\infty} \frac{i k_1 S_{ff} d\mathrm{k}}{-\phi_1 k_1^2 + i\phi_2 k_1} = \int_{-\infty}^{\infty} \frac{\phi_2 S_{ff} d\mathrm{k}}{\phi_1^2 k_1^2 + \phi_2^2} \tag{J.11}$$

The procedure developed above yields,

$$\Pi_2 = \frac{\lambda_1^2 \phi_2}{\phi_1} \int_{-\infty}^{\infty} \frac{S_{ff}(\mathrm{u})}{u_1^2 + \chi^2} \frac{du}{\lambda_1 \lambda_2 \lambda_3} \tag{J.12}$$

Introducing the expression for the spectrum in the integrand, and rearranging:

$$\Pi_2 = \frac{\chi^2}{\phi_2} \frac{\sigma_f^2}{\pi^2} \int_{-\infty}^{\infty} \frac{du}{(u_1^2 + \chi^2)(1+u^2)^2} \tag{J.13}$$

with the final result,

$$\Pi_2 = \frac{\sigma_f^2 \lambda_1^2}{\phi_2} \frac{\chi}{1+\chi} \tag{J.14}$$

The last integral in the list above can be evaluated by the same methodology,

$$\Pi_3 = \int_{-\infty}^{\infty} \frac{k_1^2 S_{ff} d\mathbf{k}}{-\phi_1 k_1^2 + i\phi_2 k_1} = -\int_{-\infty}^{\infty} \frac{\phi_1 k_1^2 S_{ff} d\mathbf{k}}{\phi_1^2 k_1^2 + \phi_2^2} \tag{J.15}$$

$$\Pi_3 = -\frac{1}{\phi_1} \int_{-\infty}^{\infty} \frac{u_1^2 S_{ff}(\mathbf{u})}{u_1^2 + \chi^2} \frac{d\mathbf{u}}{\lambda_1 \lambda_2 \lambda_3} \tag{J.16}$$

$$\Pi_3 = -\frac{1}{\phi_1} \frac{\sigma_f^2}{\pi^2} \int_{-\infty}^{\infty} \frac{u_1^2 d\mathbf{u}}{(u_1^2 + \chi^2)(1+u^2)^2} \tag{J.17}$$

with the final result,

$$\Pi_3 = -\frac{1}{\phi_1} \frac{\sigma_f^2}{\chi(1+\chi)} \tag{J.18}$$

## J.2 Listing of integrals

The following is a list of the integrals that appear in the analysis for the effective transport and transformation coefficients in Chapter 5. Lets define,

$$T_0 = \frac{\bar{S}}{S_0 + \bar{S}} \frac{\bar{C}}{C_0 + \bar{C}} \tag{J.19}$$

$$T_1 = \bar{M} \frac{S_0}{(S_0 + \bar{S})^2} \frac{\bar{C}}{C_0 + \bar{C}} \tag{J.20}$$

$$T_2 = \bar{M} \frac{C_0}{(C_0 + \bar{C})^2} \frac{\bar{S}}{S_0 + \bar{S}} \tag{J.21}$$

$$\Pi_4 = \int_{-\infty}^{\infty} \frac{ik_1 S_{rr_S}(\mathbf{k})}{\Delta} d\mathbf{k} = T_0 T_1 \bar{M} \frac{b_1^2 \sigma_f^2 + \sigma_\delta^2}{\phi_2} \frac{\chi}{1+\chi} \tag{J.22}$$

$$\Pi_5 = \int_{-\infty}^{\infty} \frac{S_{rr_S}(\mathbf{k})}{\Delta} d\mathbf{k} = -T_0 T_1 \bar{M} \frac{(b_1^2\sigma_f^2 + \sigma_\delta^2)\lambda_1^2}{\phi_1 \chi(1+\chi)} \tag{J.23}$$

$$\Pi_6 = \int_{-\infty}^{\infty} \frac{ik_1 S_{\beta r_S}(\mathbf{k})}{\Delta} d\mathbf{k} = T_1 \frac{b_1 b_3 \sigma_f^2}{\phi_2} \frac{\chi}{1+\chi} \tag{J.24}$$

$$\Pi_7 = \int_{-\infty}^{\infty} \frac{S_{rr_C}(\mathbf{k})}{\Delta} d\mathbf{k} = -T_0 T_1 \bar{M} \frac{(b_1^2\sigma_f^2 + \sigma_\delta^2)\lambda_1^2}{\phi_1 \chi(1+\chi)} \tag{J.25}$$

$$\Pi_8 = \int_{-\infty}^{\infty} \frac{ik_1 S_{rr_C}(\mathbf{k})}{\Delta} d\mathbf{k} = T_0 T_2 \bar{M} \frac{b_1^2\sigma_f^2 + \sigma_\delta^2}{\phi_2} \frac{\chi}{1+\chi} \tag{J.26}$$

$$\Pi_9 = \int_{-\infty}^{\infty} \frac{ik_1 S_{\beta r_C}(\mathbf{k})}{\Delta} d\mathbf{k} = T_2 \frac{b_1 b_3 \sigma_f^2}{\phi_2} \frac{\chi}{1+\chi} \tag{J.27}$$

$$\Pi_{10} = \int_{-\infty}^{\infty} \frac{ik_1 S_{rr_M}(\mathbf{k})}{\Delta} d\mathbf{k} = T_0^2 \bar{M} \frac{b_1^2\sigma_f^2 + \sigma_\delta^2}{\phi_2} \frac{\chi}{1+\chi} \tag{J.28}$$

$$\Pi_{11} = \int_{-\infty}^{\infty} \frac{k_1^2 S_{rr_M}(\mathbf{k})}{\Delta} d\mathbf{k} = -T_0^2 \bar{M} \frac{b_1^2\sigma_f^2 + \sigma_\delta^2}{\phi_1 \chi(1+\chi)} \tag{J.29}$$

$$\Pi_{12} = \int_{-\infty}^{\infty} \frac{k_1^2 S_{\beta r_M}(\mathbf{k})}{\Delta} d\mathbf{k} = -T_0 \frac{b_1 b_3 \sigma_f^2}{\phi_1 \chi(1+\chi)} \tag{J.30}$$

$$\Pi_{13} = \int_{-\infty}^{\infty} \frac{ik_1 S_{\beta r_M}(\mathbf{k})}{\Delta} d\mathbf{k} = T_0 \frac{b_1 b_3 \sigma_f^2}{\phi_2} \frac{\chi}{1+\chi} \tag{J.31}$$

$$\Pi_{14} = \int_{-\infty}^{\infty} \frac{ik_1 S_{\beta r}(\mathbf{k})}{\Delta} d\mathbf{k} = T_0 \bar{M} \frac{b_1 b_3 \sigma_f^2}{\phi_2} \frac{\chi}{1+\chi} \tag{J.32}$$

$$\Pi_{15} = \int_{-\infty}^{\infty} \frac{k_1^2 S_{\beta r}(\mathbf{k})}{\Delta} d\mathbf{k} = -T_0 \bar{M} \frac{b_1 b_3 \sigma_f^2}{\phi_1 \chi(1+\chi)} \tag{J.33}$$

$$\Pi_{16} = \int_{-\infty}^{\infty} \frac{S_{\beta\beta}(\mathbf{k})}{\Delta} d\mathbf{k} = -\frac{(b_3^2\sigma_f^2 + \sigma_v^2)\lambda_1^2}{\phi_1 \chi(1+\chi)} \tag{J.34}$$

$$\Pi_{17} = \int_{-\infty}^{\infty} \frac{ik_1 S_{Rv_i}(\mathbf{k})}{\Delta} d\mathbf{k} = b_2 \frac{v}{\gamma} \frac{\sigma_f^2}{\phi_2} \frac{\chi}{1+\chi} \tag{J.35}$$

$$\Pi_{18} = \int_{-\infty}^{\infty} \frac{S_{Rv_i}(\mathbf{k})}{\Delta} d\mathbf{k} = -\frac{b_2 v \lambda_1^2}{\gamma \phi_1 \chi (1+\chi)} \tag{J.36}$$

$$\Pi_{19} = \int_{-\infty}^{\infty} \frac{ik_1 S_{RR}(\mathbf{k})}{\Delta} d\mathbf{k} = \frac{(b_2^2 \sigma_f^2 + \sigma_\eta^2)}{\phi_2} \frac{\chi}{1+\chi} \tag{J.37}$$

$$\Pi_{20} = \int_{-\infty}^{\infty} \frac{S_{RR}(\mathbf{k})}{\Delta} d\mathbf{k} = -\frac{(b_2^2 \sigma_f^2 + \sigma_\eta^2)\lambda_1^2}{\phi_1 \chi (1+\chi)} \tag{J.38}$$

$$\Pi_{21} = \int_{-\infty}^{\infty} \frac{ik_1 S_{Rr}(\mathbf{k})}{\Delta} d\mathbf{k} = T_0 \bar{M} \frac{b_1 b_2 \sigma_f^2}{\phi_2} \frac{\chi}{1+\chi} \tag{J.39}$$

$$\Pi_{22} = \int_{-\infty}^{\infty} \frac{S_{Rr}(\mathbf{k})}{\Delta} d\mathbf{k} = -T_0 \bar{M} \frac{b_1 b_2 \sigma_f^2 \lambda_1^2}{\phi_1 \chi (1+\chi)} \tag{J.40}$$

$$\Pi_{23} = \int_{-\infty}^{\infty} \frac{ik_1 S_{R\beta}(\mathbf{k})}{\Delta} d\mathbf{k} = \frac{b_2 b_3 \sigma_f^2}{\phi_2} \frac{\chi}{1+\chi} \tag{J.41}$$

$$\Pi_{24} = \int_{-\infty}^{\infty} \frac{ik_1 S_{v_i v_j}(\mathbf{k})}{\Delta} d\mathbf{k} = \frac{v^2 \sigma_f^2}{\gamma^2 \phi_2} \frac{\chi}{1+\chi} \tag{J.42}$$

$$\Pi_{25} = \int_{-\infty}^{\infty} \frac{S_{v_i v_j}(\mathbf{k})}{\Delta} d\mathbf{k} = -\frac{v^2 \sigma_f^2 \lambda_1^2}{\gamma^2 \phi_1 \chi (1+\chi)} \tag{J.43}$$

$$\Pi_{26} = \int_{-\infty}^{\infty} \frac{ik_1 S_{v_i r}(\mathbf{k})}{\Delta} d\mathbf{k} = T_0 \bar{M} \frac{b_1 v \sigma_f^2}{\gamma \phi_2} \frac{\chi}{1+\chi} \tag{J.44}$$

$$\Pi_{27} = \int_{-\infty}^{\infty} \frac{ik_1 S_{v_i \beta}(\mathbf{k})}{\Delta} d\mathbf{k} = \frac{b_3 v \sigma_f^2}{\gamma \phi_2} \frac{\chi}{1+\chi} \tag{J.45}$$

$$\Pi_{28} = \int_{-\infty}^{\infty} \frac{ik_1 S_{v_i r_s}(\mathbf{k})}{\Delta} d\mathbf{k} = T_1 \frac{b_1 v \sigma_f^2}{\gamma \phi_2} \frac{\chi}{1+\chi} \tag{J.46}$$

$$\Pi_{29} = \int_{-\infty}^{\infty} \frac{ik_1 S_{Rr_S}(\mathbf{k})}{\Delta} d\mathbf{k} = T_1 \frac{b_1 b_2 \sigma_f^2}{\phi_2} \frac{\chi}{1+\chi} \tag{J.47}$$

$$\Pi_{30} = \int_{-\infty}^{\infty} \frac{S_{v_i r_S}(\mathbf{k})}{\Delta} d\mathbf{k} = -T_1 \frac{v b_1 \sigma_f^2 \lambda_1^2}{\gamma \phi_1 \chi (1+\chi)} \tag{J.48}$$

$$\Pi_{31} = \int_{-\infty}^{\infty} \frac{S_{Rr_S}(\mathbf{k})}{\Delta} d\mathbf{k} = -T_1 \frac{b_1 b_2 \sigma_f^2 \lambda_1^2}{\phi_1 \chi (1+\chi)} \tag{J.49}$$

$$\Pi_{32} = \int_{-\infty}^{\infty} \frac{S_{v_i r_C}(\mathbf{k})}{\Delta} d\mathbf{k} = -T_2 \frac{v b_1 \sigma_f^2 \lambda_1^2}{\gamma \phi_1 \chi (1+\chi)} \tag{J.50}$$

$$\Pi_{33} = \int_{-\infty}^{\infty} \frac{S_{Rr_C}(\mathbf{k})}{\Delta} d\mathbf{k} = -T_2 \frac{b_1 b_2 \sigma_f^2 \lambda_1^2}{\phi_1 \chi (1+\chi)} \tag{J.51}$$

$$\Pi_{34} = \int_{-\infty}^{\infty} \frac{ik_1 S_{v_i r_M}(\mathbf{k})}{\Delta} d\mathbf{k} = T_0 \frac{b_1 v \sigma_f^2}{\gamma \phi_2} \frac{\chi}{1+\chi} \tag{J.52}$$

$$\Pi_{35} = \int_{-\infty}^{\infty} \frac{ik_1 S_{Rr_M}(\mathbf{k})}{\Delta} d\mathbf{k} = T_0 \frac{b_1 b_2 \sigma_f^2}{\phi_2} \frac{\chi}{1+\chi} \tag{J.53}$$

$$\Pi_{36} = \int_{-\infty}^{\infty} \frac{ik_1 S_{v_i r_C}(\mathbf{k})}{\Delta} d\mathbf{k} = T_2 \frac{b_1 v \sigma_f^2}{\gamma \phi_2} \frac{\chi}{1+\chi} \tag{J.54}$$

# Appendix K

# Evaluation of the concentration gradient stationarity condition

The theoretical developments that follow are aimed at evaluating the assumption of stationarity of the concentration gradients in the analysis of the field scale effective coefficients presented in Chapters 2 through 5. As a starting point, the transport equation for a conservative solute is considered, and then results are generalized for reactive and multicomponent transport.

The perturbation equation in the moving coordinate system is [Gelhar, 1987]:

$$\frac{\partial C'}{\partial t} = D_i \frac{\partial^2 C'}{\partial \zeta_i^2} + G_j v_j' \tag{K.1}$$

This equation will now be solved in a Green's function context, as opposed to using a spectral transformation. The Green's function solution to this partial differential equation for isotropic local dispersion $D_i = \alpha v$ is [Carslaw and Jaeger, 1959]:

$$C'(\zeta,t) = \int_0^t \int_{-\infty}^{\infty} \frac{1}{[4\pi\alpha v(t-t')]^{3/2}} exp\left[-\frac{(\zeta-\zeta')^2}{4\pi\alpha v(t-t')}\right] G_j(\zeta',t') v_j' d\zeta' dt' \tag{K.2}$$

In the mean equation, the correlation between velocity and concentration perturbation appears to define the macrodispersivity tensor. This correlation is found by multiplying the above expression by $v_i'$ and taking expectations to produce:

$$\overline{v_i' C'} = \int_0^t \frac{1}{[4\pi\alpha v(t-t')]^{3/2}} dt' \int_{-\infty}^{\infty} exp\left[-\frac{(\zeta-\zeta')^2}{4\pi\alpha v(t-t')}\right] G_j(\zeta',t')\overline{v_i' v_j'} d\zeta' \qquad \text{(K.3)}$$

An evaluation of this expression cannot be made without approximating the concentration gradient $G_j$ in some way. In order to obtain the spatial integral, the concentration gradient can be expanded in a Taylor series around the point $\zeta' = \zeta$ since this integral is the sum of exponentially weighted contributions and the greatest contribution in this sum will come from this term.

$$G_j(\zeta',t') = (\zeta,t') + \left(\frac{\partial G_j}{\partial \zeta_k'}\right)_{\zeta_k'=\zeta_k} (\zeta_k' - \zeta_k) + ... \qquad \text{(K.4)}$$

Taking the first term in this expansion into equation (K.3) produces the first integral term, and by using the convolution theorem it is found that:

$$\int_0^t \frac{1}{[4\pi\alpha v(t-t')]^{3/2}} dt' G_j(\zeta,t') \int_{-\infty}^{\infty} exp\left[-\frac{(\zeta-\zeta')^2}{4\pi\alpha v(t-t')}\right] \overline{v_i' v_j'} d\zeta' =$$

$$\int_0^t G_j(\zeta,t') \int_{-\infty}^{\infty} S_{v_i v_j} e^{-i\mathbf{k}.\mathbf{x}} e^{-(ivk_1+\alpha vk^2)(t-t')} d\mathbf{k} \qquad \text{(K.5)}$$

which yields the result of Gelhar [1987]:

$$\overline{v_i' C'} = \int_{-\infty}^{\infty} S_{v_i v_j} d\mathbf{k} \int_0^t exp[-\beta(t-t')] G_j(\zeta,t') dt' \qquad \text{(K.6)}$$

with,

$$\beta = ivk_1 + \alpha vk^2 \qquad \text{(K.7)}$$

Now, if an additional term in the Taylor expansion for the concentration gradient is retained, an evaluation of the influence of this higher order term can be calculated. The second integral term becomes after using the convolution theorem:

$$\int_0^t \frac{1}{[4\pi\alpha v(t-t')]^{3/2}} dt' \left(\frac{\partial G_j}{\partial \zeta_k}\right) \int_{-\infty}^{\infty} (\zeta-\zeta') exp\left[-\frac{(\zeta-\zeta')^2}{4\pi\alpha v(t-t')}\right] \overline{v_i' v_j'} d\zeta' =$$

$$\int_0^t \left(\frac{\partial G_j}{\partial \zeta_k}\right) \int_{-\infty}^{\infty} S_{v_i v_j} e^{-\beta(t-t')} \alpha v (t-t')(-i2k_k) d\mathbf{k} \qquad \text{(K.8)}$$

Rearranging, and assuming that the derivative of the concentration gradient is a slowly varying function of time:

$$\Delta\overline{v_i' C'} = \int_{-\infty}^{\infty} S_{v_i v_j}(\mathbf{k})(-i2k_l) \left(\frac{\partial G_j}{\partial \zeta_l}\right) d\mathbf{k} \int_0^t e^{-\beta(t-t')} \alpha v (t-t') dt' \qquad \text{(K.9)}$$

The term $\Delta\overline{v_i' C'}$ has been introduced to denote the change in the correlation $\overline{v_i' C'}$ produced by including this new term. The time integral can then be found,

$$\Delta\overline{v_i' C'} = \int_{-\infty}^{\infty} S_{v_i v_j}(\mathbf{k})(i2k_l) \left(\frac{\partial G_j}{\partial \zeta_l}\right) \frac{\alpha v}{\beta^2} d\mathbf{k} \qquad \text{(K.10)}$$

$$\Delta\overline{v_i' C'} = 2\left(\frac{\partial G_j}{\partial \zeta_l}\right) \alpha v \int_{-\infty}^{\infty} \frac{i k_l S_{v_i v_j}}{(ivk_1 + \alpha v k^2)^2} d\mathbf{k} \qquad \text{(K.11)}$$

$$\Delta\overline{v_i' C'} = 4\left(\frac{\partial G_j}{\partial \zeta_l}\right) \int_{-\infty}^{\infty} \frac{\alpha^2 v^2 k_l k_1 k^2}{[v^2 k_1^2 + (\alpha v k^2)^2]^2} S_{v_i v_j} d\mathbf{k} \qquad \text{(K.12)}$$

Upon introduction of the relationship between the flow and the log-hydraulic conductivity spectral amplitudes (4.63), the longitudinal component $i = j = 1$ can be found to be:

$$\Delta\overline{v_1' C'} = 4\frac{\partial G_1}{\partial \zeta_1} \frac{\alpha^2 v^5}{\gamma^2} \int_{-\infty}^{\infty} \frac{S_{ff} k_1^2 k^2}{[v^2 k_1^2 + \alpha^2 v^2 k^4]^2} d\mathbf{k} \qquad \text{(K.13)}$$

Introducing the changes of variables $u_i = \lambda_i k_i$ for $i = 1, 2, 3$ and no summation on the index $i$; $\epsilon = \frac{\alpha}{\lambda_1}$ ; $\delta = (\frac{\lambda_2}{\lambda_1})^2$, and the expression for the log-hydraulic conductivity spectrum (4.9):

$$\Delta\overline{v_1' C'} = 4\frac{\partial G_1}{\partial \zeta_1} \frac{\alpha^2 v}{\gamma^2} \frac{\sigma_f^2}{\pi^2} \delta^3 \int_{-\infty}^{\infty} \frac{\epsilon^2 u_1^2 (\delta u_1^2 + \delta u_2^2 + u_3^2)}{[\delta^2 u_1^2 + \epsilon^2(\delta u_1^2 + \delta u_2^2 + u_3^2)]^2} \frac{du}{(1+u^2)^2} \qquad \text{(K.14)}$$

For values of $\epsilon << 1$, the main contribution to the integral comes from the smaller values of $u_1$. This can be seen by making the change of variable, $u_1 = \epsilon V$ :

$$\Delta\overline{v_1'C'} = 4\frac{\partial G_1}{\partial \zeta_1}\frac{\alpha^2 v}{\gamma^2}\frac{\sigma_f^2}{\pi^2}\delta^3\int_{-\infty}^{\infty}\frac{\epsilon^4 V^2(\delta\epsilon^2V^2+\delta u_2^2+u_3^2)}{[\delta^2\epsilon^2V^2+\epsilon^2(\delta\epsilon^2V^2+\delta u_2^2+u_3^2)]^2}\frac{\epsilon dV du_2 du_3}{(1+\epsilon^2V^2+u_2^2+u_3^2)^2} \tag{K.15}$$

By taking the limit as $\epsilon \to 0$, and integrating over the variable $V$ yields,

$$\Delta\overline{v_1'C'} = \frac{\partial G_1}{\partial \zeta_1}\frac{\epsilon^3 v\lambda_1^2}{\gamma^2}\frac{\sigma_f^2}{\pi}\int_{-\infty}^{\infty}\frac{du_2 du_3}{(1+u_2^2+u_3^2)^2} \tag{K.16}$$

which gives the final result,

$$\Delta\overline{v_1'C'} = \frac{\partial G_1}{\partial \zeta_1}\frac{v\lambda_1^2}{\gamma^2}\sigma_f^2\epsilon^3 \tag{K.17}$$

So this term produces an influence of the order of $\epsilon^3$ which is considerably small under most practical conditions. This shows that assuming the concentration gradient as a slowly varying function of space produces results to a significant level of accuracy in field scale effective coefficient calculations. Similar analyses can be carried out for reactive solutes, where the integral terms that appear in the correlations producing field scale effects can be found to be equivalent to the one treated here.

# Bibliography


[1] Alvarez, P.J.J. and T.M. Vogel. *Substrate interactions of benzene, toluene and para-xylene during microbial degradation by pure cultures and mixed-culture aquifer studies.* App. Env. Microbiol., 57(10), 2981-2985, 1991.

[2] Aris, R. *On the dispersion of a solute in a fluid flowing through a tube.* Proc. R. Soc. London, Ser. A, 235 67-78, 1956.

[3] Baek, N.H., L.S. Clesceri, and N.L. Clesceri. *Modeling of enhanced biodegradation in unsaturated soil zone.* J. Env. Engrg, Div. ASCE, 115(1) 150-171, 1989.

[4] Baker, J.H. *Relationship between microbial activity of stream sediments determined by three different methods and abiotic variables.* Microbial Ecology, 12 193-203, 1986.

[5] Ball, W.P., C. Buehler, T.C. Harmon, D.M. Mackay, and P.V. Roberts. *Characterization of a sandy aquifer material at the grain scale.* J. Contaminant Hydrology, 5, 253-295, 1990.

[6] Ball, W.P. and P.V. Roberts. *Long-term sorption of halogenated organic chemicals by aquifer material 1. Equilibrium.* Env. Sci. Tech., 25(7) 1223-1237, 1991.

[7] Ball, W.P. and P.V. Roberts. *Long-term sorption of halogenated organic chemicals by aquifer material 2. Intraparticle diffusion.* Env. Sci. Tech., 25(7) 1237-1249, 1991.

[8] Barker, J.F., G.C. Patrick, and D. Major. *Natural attenuation of aromatic hydrocarbons in a shallow sand aquifer.* Ground Water Monitoring Rev., 7, 64-71, 1987.

[9] Berry-Spark, K., J.F. Barker, D. Major, and C.I. Mayfield. *Remediation of gasoline-contaminated groundwater - A controlled field experiment.* Proc., Conf. on Petrol. Hydrocarbons and Organic Chemicals in Groundwater: Prevention, Detection, and Restoration, Houston, spons. by Nat. Well Water Assoc. and Amer. Petrol. Inst., 127-144, 1987.

[10] Billen, G., P. Servais, and A. Fontigny. *Growth and mortality in bacterial population dynamics of aquatic environments.* Adv. Limnol., 31, 173-183, 1988.

[11] Birdwell, S.R. and C.L. McConnell. *Theoretical model of the in-situ bioreclamation process.* Proc., Conf. on Petrol. Hydrocarbons and Organic Chemicals in Groundwater: Prevention, Detection, and Restoration, Houston, spons. by Nat. Well Water Assoc. and Amer. Petrol. Inst., 687-614, 1988.

[12] Borden, R.C., P.B. Bedient, M.D. Lee, C.H. Ward, and J.T. Wilson. *Transport of dissolved hydrocarbons influenced by oxygen-limited biodegradation 2. Field application.* Water Resour. Res., 22(13), 1982-1990, 1986.

[13] Bouwer, E.J. and P.L. McCarty. *Modeling of trace organics biotransformation in the subsurface.* Groundwater, 22(4), 433-440, 1984.

[14] Boyle, M. *The Environmental Microbiology of Chlorinated Aromatic Decomposition.* J. Env. Quality, 18(4) 395-402, 1989.

[15] Brookman, G.T., M. Flanagan, and J.O. Kebe. *Literature survey: Unassisted natural mechanisms to reduce concentrations of soluble gasoline components.* TRC Project 2663-N31-00, American Petroleum Institute, 1985.

[16] Brusseau, M.K., R.E. Jessup, and P.S.C. Rao. *Modeling the transport of solutes influenced by multi-process nonequilibrium.* Water Resour. Res., 25(9), 1971-1988, 1989.

[17] Brusseau, M.L. *Application of a multiprocess nonequilibrium sorption model to solute transport in a stratified porous medium.* Water Resour. Res., 27(4) 589-595, 1991.

[18] Burr, D.T. *Numerical investigations of solute transport behaviour in three-dimensional heterogeneous porous media.* M.S. Thesis, University of Waterloo, 1992.

[19] Carslaw, H.S. and J.C. Jaeger. *Conduction of hest in solids.* Oxford Univ. Press, 1959.

[20] Chen, Y.M., L.M. Abriola, P.J.J. Alvarez, P.J. Anid, and T.M. Vogel. *Modeling transport and biodegradation of benzene and toluene in sandy aquifer material: comparisons with experimental measurements.* Water Resour. Res., 28(7), 1833-1847, 1992.

[21] Chiang, C.Y., C.N. Dawson, and M.F. Wheeler. *Modeling of in-situ biorestoration of organic compounds in groundwater.* Transp. Porous Media, 6, 667-702, 1991.

[22] Chiang, C.Y., J.P. Salanitro, E.Y. Chai, J.D. Colthart, and C.L. Klein. *Aerobic biodegradation of benzene, toluene and xylene in a sandy aquifer - Data analysis and computer modeling.* Ground Water, 27(6), 823-834, 1989.

[23] Chrysikopoulos, C.V., P.K. Kitanidis, and P.V. Roberts. *Macrodispersion of sorbing solutes in heterogeneous porous formations with spatially periodic retardation factor and velocity field.* Water Resour. Res., 28(6) 1517-1529, 1992.

[24] Curtis, G.P., P.V. Roberts, and M. Reinhard. *A natural gradient experiment on solute transport in a sand aquifer 4. Sorption of organic solutes and its influence on mobility.* Water Resour. Res., 22(13), 2059-2067, 1986.

[25] Cvetkovic, V.D. and A.M. Shapiro. *Mass arrival of a sorptive solute in heterogeneous porous media.* Water Resour. Res., 26(9), 2057-2067, 1990.

[26] Dagan, G. *Stochastic modeling of groundwater flow by unconditional and conditional probabilities 2. The solute transport.* Water Resour. Res., 18(4), 835-848, 1982.

[27] Dagan, G. *Solute transport in heterogeneous porous formations.* J. Fluid Mech., 145, 151-177, 1984.

[28] Dagan, G. *Time-dependent macrodispersion for solute transport in anisotropic heterogeneous aquifers.* Water Resour. Res., 24(90), 1491-1500, 1988.

[29] Dasinger, A. *Large scale simulations of groundwater flow and solute in an anisotropic, heterogeneous aquifer.* M.S. thesis, M.I.T, 1989.

[30] Freeze, R.A. and J.A. Cherry. *Groundwater.* Prentice Hall, New Jersey, 1979.

[31] Freyberg, D.L. *A natural gradient experiment on solute transport in a sand aquifer 2. Spatial moments and the advection and dispersion of nonreactive tracers.* Water Resour. Res., 22(13), 2031-2046, 1986.

[32] Frind, E.O., E.A. Sudicky, and J.W. Molson. *Three-dimensional simulation of organic transport with aerobic biodegradation.* Proc., IAHS Third Scientific Assembly, Baltimore, MD, 1989.

[33] Fry, J.C. *Determination of Biomass.* Methods of Aquatic Bacteriology Chap. 2, B. Austin Editor: John Wiley and Sons, 1988.

[34] Garabedian, S.P., L.W. Gelhar, and M.A. Celia. *Large-scale dispersive transport in aquifers: field experiments and reactive transport theory.* Ralph M. Parsons Laboratory Report Number 315, Dept of Civil Engineering MIT, Cambridge-Massachusetts 02139, 1988.

[35] Garabedian, S.P., D.R LeBlanc, L.W. Gelhar, and M.A. Celia. *Large-scale natural gradient tracer test in sand and gravel, Cape Cod, Massachusetts 2. Analysis of spatial moments for a nonreactive tracer.* Water Resour. Res., 27(5), 911-924, 1991.

[36] Gelhar, L.W. *Stochastic analysis of solute transport in saturated and unsaturated porous media.* Advances in Transport Phenomena in Porous Media, NATO ASI Ser., edited by J. Bear and M.Y. Corapcioglu, 657-700, 1987.

[37] Gelhar, L.W. and C.L. Axness. *Three-dimensional stochastic analysis of macrodispersion in aquifers.* Water Resour. Res., 19(1), 161-180, 1983.

[38] Gelhar, L.W., A.L. Gutjahr, and R.L. Naff. *Stochastic analysis of macrodispersion in a stratified aquifer.* Water Resour. Res., 15(6), 1387-1397, 1979.

[39] Goltz, M.N. and P.V. Roberts. *Three-dimensional solutions for solute transport in an infinite medium with mobile and immobile zones.* Water Resour. Res., 22(7) 1139-1148, 1986.

[40] Gradshteyn, I.S. and I.M. Ryzhik. *Table of integrals, series and products.* Academic Press, Inc., Second edition, 1980.

[41] Graham, W. and D. McLaughlin. *Stochastic analysis of nonstationary subsurface solute transport 1. Unconditional moments.* Water Resour. Res., 25(2), 215-232, 1989.

[42] Graham, W. and D. McLaughlin. *Stochastic analysis of nonstationary subsurface solute transport 2. Conditional moments.* Water Resour. Res., 25(11), 2331-2355, 1989.

[43] Harmon, T.C., L. Semprini, and P.V. Roberts. *Simulating solute transport using laboratory-based sorption parameters.* J. Env. Engrg., 118(5) 666-689, 1992.

[44] Harvey, R.W. and L.H. George. *Growth determinations for unattached bacteria in a contaminated aquifer.* App. Env. Microbiol., 53(12), 2992-2996, 1987.

[45] Hess, K.M., S.H. Wolf, and M.A. Celia. *Large-scale natural gradient tracer test in sand and gravel, Cape Cod, Massachusetts, 3, Hydraulic conductivity variability and calculated macrodispersivities.* Water Resour. Res., 28(8) 2011-2027, 1992.

[46] Hornberger, G.M., A.L. Mills, and J.S. Herman. *Bacterial transport in porous media: evaluation of a model using laboratory observations.* Water Resour. Res., 28(3), 915-938, 1992.

[47] Kabala, Z.J. and G. Sposito. *A stochastic model of reactive solute transport with time-varying velocity in a heterogeneous aquifer.* Water Resour. Res., 27(3), 341-350, 1991.

[48] Kindred, S., M.A. Celia, and I. Herrera. *Contaminant transport and biodegradation, 2. Conceptual model and test simulations.* Water Resour. Res., 25(6), 1149-1159, 1989.

[49] Kinzelbach, W. *The random walk method in pollutant transport simulation.* Groundwater flow and quality modeling, E. Custodio et al eds., 227-245, 1988.

[50] Kinzelbach, W., W. Schaefer, and J. Herzer. *Numerical modeling of nitrate transport in a natural aquifer.* Contaminant Transport in Groundwater, Kobus and Kinzelbach, eds., 191-198, 1989.

[51] Kobayashi, H. and B. E. Rittmann. *Microbial Removal of Hazardous Organic Compounds.* Environ. Sci. Technol., 16(2), 1989.

[52] Leahy, J.G. and R.R. Colwell. *Microbial Degradation of Hydrocarbons in the Environment.* Microbiological Reviews, 54(3) 305-315, 1990.

[53] Lee, M.D., J.M. Thomas, R.C. Borden, P.B. Bedient, C.H. Ward, and J.T. Wilson. *Biorestoration of aquifers contaminated with organic compounds.* CRC Critical Reviews in Environmental Control, 18(1), 29-89, 1988.

[54] Li, Shu-Guang and D. McLaughlin. *A nonstationary spectral method for solving stochastic groundwater problems: unconditional analysis.* Water Resour. Res., 27(7), 1589-1605, 1991.

[55] Longmuir, I.S. *Respiration rate of bacteria as a function of oxygen concentration.* Biochemistry, 57, 81-87, 1954.

[56] Lumley, J.L. and H.A. Panofsky. *The structure of atmospheric turbulence.* John Wiley, New_York, 1964.

[57] Mackay, D.M., W.P. Ball, and M.G. Durant. *Variability of aquifer sorption properties in a field experiment on groundwater transport of organic solutes: methods and preliminary results.* J. Cont. Hydrol., 1, 119-132, 1986.

[58] MacQuarrie, K.T.B. *Simulation of biodegradable organic contaminants in groundwater.* M.S. Thesis, University of Waterloo, Waterloo, Ontario, 1988.

[59] MacQuarrie, K.T.B. and E.A. Sudicky. *Simulation of biodegradable organic contaminants in groundwater, 2. Plume behavior in uniform and random flow fields.* Water Resour. Res, 26(2), 223-239, 1990.

[60] MacQuarrie, K.T.B., E.A. Sudicky, and E.O. Frind. *Simulation of biodegradable organic contaminants in groundwater, 1. Numerical formulation in principal directions.* Water Resour. Res., 26(2), 207-222, 1990.

[61] Miralles-Wilhelm, F., V. Kapoor, and L.W. Gelhar. *Modeling oxygen-transport limited biodegradation in three-dimensionally heterogeneous aquifers.* Prepared under contract API GW-14-360-8, American Petroleum Institute, 1992.

[62] Molz, F.J. and M.A. Widdowson. *Internal inconsistencies in dispersion-dominated models that incorporate chemical and microbial kinetics.* Water Resour. Res., 24(4), 615-619, 1988.

[63] Molz, F.J., M.A. Widdowson, and L.D. Benefield. *Simulation of microbial growth dynamics coupled to nutrient and oxygen transport in porous media.* Water Resour. Res., 22(8), 1207-1216, 1986.

[64] Naff, R.L. *A continuum approach to the study and determination of field longitudinal dispersion coefficients.* Ph.D. dissertation, N.M. Inst. of Mining and Technology, Socorro, New Mexico, 1978.

[65] Naff, R.L. *On the nature of the dispersive flux in saturated heterogeneous porous media.* Water Resour. Res., 26(5) 1013-1026, 1990.

[66] Naff, R.L., T.C.J. Yeh, and M.W. Kemblowski. *A note on the recent natural gradient tracer test at the Borden site.* Water Resour. Res., 24(12), 2099-2103, 1988.

[67] Patrick, G.C. and J. F. Barker. *Natural-gradient tracer study of dissolved benzene, toluene and xylenes in groundwater.* Proc. Second Annual Canadian/American Conf. Hydrogeol: Hazardous Wastes in Groundwater-A soluble dilemma, Banff, Alberta, 1986.

[68] Prickett, T.A., T.G. Naymik, and C.G. Lonnquist. *A random walk solute transport model for selected groundwater quality evaluations.* Illinois State Water Survey, Bulletin 65, Champaign, 1981.

[69] Rajaram, H. *Scale dependent dispersion in heterogeneous porous media.* Ph.D Thesis, M.I.T, 1991.

[70] Rajaram, H. and L.W. Gelhar. *3-D spatial moment analysis of the Borden tracer test.* Water Resour. Res., 27(6), 1239-1251, 1991.

[71] Rifai, H.S. and P.B. Bedient. *Comparison of biodegradation kinetics with an instantaneous reaction model for groundwater.* Water Resour. Res., 26(4), 637-645, 1990.

[72] Rifai, H.S., P.B. Bedient, J.T. Wilson, K.M. Miller, and J.M. Armstrong. *Biodegradation modeling at an aviation fuel spill site.* J. Env. Engrg, Div. ASCE, 114(5), 1007-1029, 1988.

[73] Roberts, P.V., M.N. Goltz, and D.M. Mackay. *A natural gradient experiment on solute transport in a sand aquifer 3. Retardation estimates and mass balances for organic solutes.* Water Resour. Res., 22(13), 2047-2058, 1986.

[74] Robin, M.J.L., E.A. Sudicky, R.W. Gillham, and R.G. Kachanoski. *Spatial variability of Strontium distribution coefficients and their correlation with hydraulic conductivity in the Canadian Forces Base Borden aquifer.* Water Resour. Res., 27(10) 2619-2632, 1991.

[75] Schafer, W. and W. Kinzelbach. *Numerical investigations into the effects of aquifer heterogeneity on in situ bioremediation.* Batelle Memorial Institute, pp. 196-225, 1991.

[76] Schwarzenbach, R.P. and J. Westall. *Transport of nonpolar organic compounds from surface water to groundwater. Laboratory sorption studies.* Env. Sci. Tech., 15, 1360-1367, 1981.

[77] Selroos, J.O. and V. Cvetkovic. *Modeling solute advection coupled with sorption kinetics in heterogeneous formations.* Water Resour. Res., 28(5), 1271-1278, 1992.

[78] Semprini, L., D. Grbic-Galic, P. Mc Carty, and P. Roberts. *Methodologies for evaluating in-situ bioremediation of chlorinated solvents.* EPA report EPA/600/R-92/042, Robert S. Kerr Environmental Research Laboratory, 1992.

[79] Skopp, J. and A.W. Warrick. *A two-phase model for the miscible displacement of reactive solutes in soils.* Soil Sci. Soc. Am., 38(4) 545-550, 1974.

[80] Sposito, G. and D.A. Barry. *On the Dagan model of solute transport in groundwater: Foundational aspects.* Water Resour. Res., 23(10), 1867-1875, 1987.

[81] Srinivasan, P. and J.W. Mercer. *Simulation of biodegradation and sorption processes in groundwater.* Groundwater, 26(4), 475-487, 1988.

[82] Sudicky, E.A. *A natural gradient experiment on solute transport in a sand aquifer: spatial variability of hydraulic conductivity and its role in the dispersion process.* Water Resour. Res., 22(13), 2069-2082, 1986.

[83] Sudicky, E.A. *The Laplace transform Galerkin technique for efficient time-continuous solute transport in double porosity media.* Geoderma, 46, 209-232, 1990.

[84] Sudicky, E.A. and J.A. Cherry. *Field observations of tracer dispersion under natural flow conditions in an unconfined sandy aquifer.* Water Pollut. Res. Can., 14, 1-17, 1979.

[85] Taylor, S.W. and P.R. Jaffe. *Enhanced in situ biodegradation and aquifer permeability reduction.* J. Env. Engrg., 117(1), 25-46, 1990.

[86] Tompson, A.F.B., R. Ababou, and L.W. Gelhar. *Application and use of the 3-D turning bands random field generator: Single realization problems.* Tech. Rep. 313, R.M. Parsons Lab, M.I.T., 1987.

[87] Tompson, A.F.B. and D.E. Dougherty. *Particle-grid methods for reacting flows in porous media with application to Fisher's equation.* Comp. meth. in subsurface hydrology, G. Gambolati et al eds., 393-398, 1990.

[88] Tompson, A.F.B. and L.W. Gelhar. *Numerical simulation of solute transport in three-dimensional, randomly heterogeneous porous media.* Water Resour. Res., 26(10), 2541-2562, 1990.

[89] Tompson, A.F.B., E.G. Vomvoris, and L.W. Gelhar. *Numerical simulation of solute transport in randomly heterogeneous porous media: Motivation, model development and application.* Tech. Rep. 316, R.M. Parsons Lab, M.I.T., 1988.

[90] Twenter, F.R., T.R. Cummings, and N.G. Grannemann. *Ground-water contamination in East Bay Township-Michigan.* U.S. Geological Survey, Water Resources Investigation Report 85-4064, 1985.

[91] Valocchi, A.J. *Theoretical analysis of deviations from local equilibrium during sorbing solute transport through idealized stratified aquifers.* J. Cont. Hydrol., 2, 191-207, 1988.

[92] Valocchi, A.J. *Spatial moment analysis of the transport of kinetically adsorbing solutes through stratified aquifers.* Water Resour. Res., 25(2), 273-279, 1989.

[93] Van Genuchten, M.T. and P.J. Wierenga. *Mass transfer studies in sorbing porous media I. Analytical solutions.* Soil Sci. Soc. Am., 40(4) 473-480, 1976.

[94] Welty, C. and L.W. Gelhar. *Stochastic analysis of the effects of fluid density and viscosity variability on macrodispersion in heterogeneous porous media.* Water Resour. Res., 27(8), 2061-2075, 1991.

[95] Wheeler, M.F. and C.N. Dawson. *An operator-splitting method for advection diffusion reaction problems.* MAFELAP Proceedings VI, J.R. Whiteman ed., 463-482, 1988.

[96] Wilson, J., L. Leach, J. Michalowski, S. Vandergrift, and R. Callaway. *In-situ reclamation of spills from underground storage tanks: New approaches for site characterization and project design and evaluation of performance.* Proceedings: Environmental Research Conference on Groundwater Quality and Waste Disposal, 1990.

[97] Wilson, J.T., G.B. Smith, J.W. Cochran, J.F. Barker, and P.V. Roberts. *Field evaluation of a simple microcosm simulating the behavior of volatile organic compounds in subsurface materials.* Water Resour. Res., 23(8), 1547-1553, 1987.

[98] Wu, S.C. and P.M. Gschwend. *Sorption Kinetics of Hydrophobic Organic Compounds to Natural Sediments and Soils.* Environ. Sci. Technol., 20 717-725, 1986.